Dynamic modelling of compression ring conformability in high performance engines

by

Matthew William Dickinson

A thesis in partial fulfilment for the requirements for the degree of Doctor of Philosophy at the University of Central Lancashire

October 2016

Student Declaration

Concurrent registration for two or more academic awards

I declare that while registered as a candidate for the research degree, I have not been a registered candidate or enrolled student for another award of the University or other academic or professional institution

---

Material submitted for another award

I declare that no material contained in the thesis has been used in any other submission for an academic award and is solely my own work

---

Collaboration

Where a candidate's research programme is part of a collaborative project, the thesis must indicate in addition clearly the candidate's individual contribution and the extent of the collaboration. Please state below:

No collaboration

Signature of Candidate 

Type of Award Doctor of Philosophy

School School of engineering

ABSTRACT

Internal combustion (IC) engines have been the predominant technology for sourcing or generating power for over 100 years. The fundamental function of engines has not changed since there first introduction. By combusting fuel within the chamber causes a pressure build from the expanding gasses pushing the piston assembly through the cylinder, this linear action is then translated to rotation through the crankshaft to generate work. During combustion the gasses will try to move past the piston and into the crankcase, to deter this from occurring piston rings are introduced. Thus rings are designed to be in tight contact to the cylinder wall, and is subject to friction and wear as it travels up and down the cylinder wall. When a new ring pack is introduced, a running-in process is required. This involves running the engine at a variation of speeds for set times, typically defined by the manufacturer. While this procedure is executed the compression ring will undergo a series of thermodynamic morphological stages, the material will change shape due to the heat from the combustion process and suffer material loss due to the friction wear between cylinder wall and ring face. This thesis examines the impact of the running-in method on the compression ring and its performance. The work presented shows a novel numerical method that offers the first simulated solution to compression ring rotation around the piston crown and its impact on the engine performance. This has been achieved by adopting simultaneously two modelling packages to compute dynamics and contact mechanics for a more accurate multiphysics result. Using this model a coating refinement has been developed, offering a new chamfer change to the present ISO standard ensuring a longer coating operational life.

Keywords: Rotation, deformation, dynamics, multi-physics, compression ring, friction, MoS_2, Chamfer, Piston.

TABLE OF CONTENTS

LIST OF FIGURES

LIST OF TABLES

Dedicated to

My wonderful supportive wife and both of my sons Kyle and Daniel.

ACKNOWLEDGEMENTS

I would like to first acknowledge my supervisors Dr Nathalie Renevier and Dr John Calderbank for their help, without your patience during this process I don't believe I would have learned as much as I have about the topic, research and myself.

I would also like to thank my research design tutor Professor Ian Sherrington for all the insightful discussions that we have shared.

NOMENCLATURE

$A = Compression\ ring\ wall\ thickness\ (m)$

$A_i, B_i = Fourier\ coefficients\ (N)$

$a, c = coefficent\ of\ thermal\ expansion\ directional\ change\ (°C^{-1})$

$\alpha = Angular\ acceleration\ acting\ around\ the\ piston\ groove\ \left(\frac{rad}{s^2}\right)$

$\alpha_v = volume\ coefficent\ of\ expansion\ \ (°C^{-1})$

$\alpha_l = linear\ coefficent\ of\ expansion\ (°C^{-1})$

$\alpha_a, \alpha_c = Linear\ cofficent\ of\ thermal\ expansion\ (M_o S_2)$

$B = Bulk\ modulus\ (GPa)$

$\beta = Twist\ angle\ (deg°)$

$C_L = Cylinder\ Length\ (m)$

$C_l = compression\ ring\ axial\ width\ (m)$

$C_v = isometric\ heat\ capacity\ (J\ mol^{-1}K^{-1})$

$D_n\ = radial\ dimension\ of\ compression\ ring\ (m)$

$d_g = Thermal\ degeneracy\ (°C)$

$d_s = Arc\ length\ (rads)$

$\Delta k = Change\ in\ curvatures\ (m)$

$\Delta l = Change\ in\ length\ (m)$

$\Delta r = radial\ deviation\ from\ the\ circle\ (rads)$

$\Delta T = Temperature\ change\ (°C)$

$\Delta V = Volume\ change\ in\ length\ (m^3)$

$\Delta\omega_E = Lattice\ (\ell mn)$

$\Delta\omega_A = Enharmonic\ effect\ (f)$

$\Delta\omega_M = Thermal\ expansion\ incongruity\ (°C)$

$E = Compression\ ring\ material\ modulus\ (Pa)$

$F_r = axial\ force\ (Nm)$

$\emptyset_{bn} = Phase\ angle\ (\deg°)$

$G_c = Specific\ gas\ constant\ (\frac{J}{KgK})$

$Gas_F = Compression\ ring\ gas\ force\ (N)$

$Gas_I = Compression\ ring\ gas\ moment\ (kg\ M^2)$

$\eta =\ viscosity\ (Pa^2)$

$H_{ring} = Lubrcation\ film\ height\ (m)$

$H_{min} = Minimum\ film\ thickness\ (m)$

$I = Axial\ moment\ of\ inertia\ (kg.m^2)$

$i = Order\ of\ deformation$

$i_r,\ j_r = angle\ of\ rotation\ coordinates\ (m)$

$\varphi = Angle\ from\ centre\ of\ the\ compression\ ring\ (\pi\ from\ gap)$

$K =\ Coefficent\ of\ friction$

$k = Coefficent\ of\ deformation\ (\frac{1}{K})$

$k_1 = thermal\ conductivity\ of\ material\ (\frac{W}{mK})$

$L = Connecting\ Rod\ Length\ (m)$

$L_m = Ring\ angular\ momentum\ (\frac{rad}{s^2})$

$L_1 = Compression\ ring\ height\ (m)$

$l_0 = Initial\ length\ (m)$

$\Lambda = Order\ term$

$m_r = piston\ mass\ (kg)$

$n = number\ sample\ points$

$p = pressure\ (KPa)$

$p(x) = compression\ ring\ directional\ pressure\ (Pa)$

$P_{top} = Combustion\ pressure$

$P_{bottom} = Crankcase\ pressure$

$P_a = Hardness\ of\ abrasive\ particle\ (GPa)$

$P_f = Primary\ force\ (N)$

$P_L = Piston\ Length\ (\mathrm{m})$

$P_0 = Specific\ surface\ pressure\ (Pa)$

$P_t = Piston\ ring\ hardness\ (GPa)$

$P_{bar} = thin\ film\ pressure\ (\frac{m^2}{N})$

$P_{bottom} = Pressure\ acting\ at\ the\ bottom\ of\ the\ compression\ ring\ (Pa)$

$P_{top} = Pressure\ acting\ at\ the\ top\ of\ the\ compression\ ring\ (Pa)$

$P_{back} = Pressure\ acting\ at\ the\ back\ of\ the\ compression\ ring\ (Pa)$

$q = heat\ flux\ (W/m^2)$

$\theta = Crank\ Angle\ (rads)$

$\theta_1 = Average\ roughness\ angle\ of\ the\ abrasive\ particle\ (rads)$

$R = Crank\ Radius\ (m)$

$R_a = \ Roughness\ average\ (\mu m)$

$Ring_{rad} = Ring\ contact\ profile\ difference\ (m)$

$R_{mass} = Ring\ Mass\ (Kg)$

$R_t = Maximum\ height\ of\ profile\ (\mu m)$

$R_p = Maximum\ profile\ peak\ height\ (\mu m)$

$R_q = \ Root\ mean\ square\ (RSM)$

$R_{rad} = Ring\ radius\ (m)$

$R_v = Maximum\ profile\ valley\ depth\ (\mu m)$

$R_{vel} = Ring\ angular\ velocity\ (rad\ s^1)$

$R\omega = Crank\ angular\ velocity\ (rad\ s^1)$

$S_f = Secondary\ force\ (N)$

$S_w = Ring\ stress\ during\ operation\ (Pa)$

$s_1 =$ nominal diameter of cylinder (m)

$\sigma_1 = Major\ principal\ stress\ (Pa)$

$\sigma_2 = Minor\ principal\ stress\ (Pa)$

$T = Temperature\ (K)$

$T_{cof} = Gruneisen\ parameter$

$T_f = Thermal\ stress$ (℃)

$T_{If} = Total\ inertia\ force\ (N)$

$T_{MP} = ring\ Tangential\ bending\ (N)$

$T_{MF} = ring\ Tangential\ bending\ force\ (N)$

$t_m = gap\ clearance\ in\ installed\ state\ (m)$

$t_y = free\ gap\ in\ relaxed\ state\ (m)$

$\tau = Shear\ stress\ (Pa)$

$\tau_i = Rigid\ body\ torque\ (Nm)$

$\tau_1 = torsion\ in\ the\ ring\ (Nm)$

$u_0, v_0 = ring\ displacments\ (m)$

$u_{bn} = Maximum\ cylinder\ deformation\ (m)$

$U_{max} = Maximum\ piston\ ring\ deformation\ (m)$

$V = Current\ Volume\ (m^3)$

$V_0 = original\ volume\ (m^3)$

$V_m = molar\ volume\ \left(\frac{m^3}{mole}\right)$

$v = \ velocity\ (\frac{m}{s})$

$\omega = Crank\ shaft\ angular\ velocity$

$\omega_0 = Room\ temperature\ frequency\ (Hz)$

$y_i = Height\ of\ postion\ (m)$

$x = Mass\ postion\ (m)$

CHAPTER 1 - INTRODUCTION

1.1. Background

In four-stroke internal combustion engines, fuel and air are first mixed before entering the chamber. Once in the combustion bowl, the fuel is ignited causing an increase of both pressure and temperature [1-3]. A pressure *p* acts against the cylinder wall and the piston assembly composed of piston crown (top part of b in Figure 1.1) and compression ring (h in Figure 1.1). The pressure applied causes the piston assembly to move position from top dead centre (TDC) to bottom dead centre (BDC), the move is known as the intake stage.

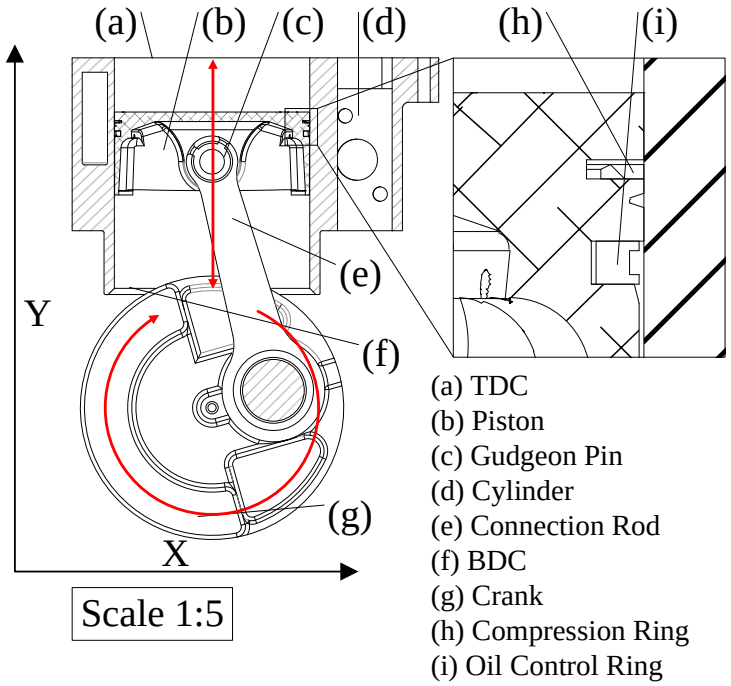

Figure 1.1 - Schematic of engine piston assembly

The piston will then travel in the reverse direction from BDC (f in Figure 1.1) to TDC (a in Figure 1.1) known as the compression stage. The process is followed by two further stages known as the combustion and exhaust.

During the intake and compression stages, some of the gas will slip down the side of the piston, into the groove and push the inside of the ring to create a seal. The piston travelling down the cylinder BDC and returning back to the TDC, known as reciprocating piston motion with displayed characteristics in Figure 1.1, will also introduce possible points in which the compression ring will rotate [4,5]. The contact between cylinder wall and piston will induce areas of material loss [6-10], hence lubrication is used to prevent this from happening [6,11-14]. The heat generated during the reciprocating process leads to thermal morphological changes [15].

Race engines used in motorsport vary from standard production engines from the automotive industry to specialist engines such as those used in Formula 1. In motor sports, operating conditions are generally very aggressive using the maximum allowable speeds 14,000 rpm [16-18], while standard production cars operate on the highways between 800 and 6,000 rpm.

Racing automotive engines differ from motor cycle engines with similar high performance power output achieved through high RPM rather than large engine size. Racing Motor cycle has been used in the thesis.

The topic of the internal combustion engine has been a huge area of research and development for the past 100 years [19,20]. Research included topics ranging from energy recovery with the incorporation of batteries for energy recovery and storage [21-23], to synthetic lubrication preventing the solidification of carbon fuel deposits [13,24-26]. Developments of new engine oils have led to revolutionary developments such as Petronas Syntium with CoolTech, which has the characteristic of increasing in viscosity as the temperature increases [27]. Alongside, surface engineering and in particular coatings have seen considerable development. The main aim of a coating is to improve the tribological performances in reducing the level of wear or friction. Coating pistons has been common in motorsport for many years, and the coating of piston skirts in particular has proven very successful commercially. The main types of piston skirt coating in general racing use are based on polymer formulations [28,29], on graphite [30] or a composite coating with a resin binder with fillers [31,32].

The most common rings found in racing are coated with traditional chromium electroplated coatings (Cr), MoS_2 or in more recent advancements with titanium nitride (TiN) or chromium nitride (CrN). MoS_2 rings typically “bed-in” faster than chrome, reaching full sealing capacity more quickly, while providing significantly higher scuff resistance [33,34].

The ‘bed-in’ or ‘running-in’ process is a key process when new components are first fitted and operated in an engine [7,26,33,35]. Piston rings play a significant role in sealing the cylinder during operation, holding all the gasses within the combustion chamber. It is well known that the initial thermal loads and forces cause changes in geometry due to wear of many components during early operation [36-38]. The recommendations from manufacturers for this initial ‘running-in’ can be vague despite being such an essential step in the engine life cycle. Poor running-in processes would reduce performance and overall life span of engines [39-42]. The focus of the thesis is to further consider the dynamical effect of the ‘running-in’ of compression rings coated with MoS_2 using computer aided simulation to accurately predict blow-by, frictional forces and deformation occurring on the piston ring as well as assembly interactions. The validation of the simulation have been done using experimental data obtained from engine tests.

1.2. Challenges and motivations

Real time dynamic simulation of 4-stroke internal combustion engines presents several challenges which require a multiphysics approach to be able to account for a variety of phenomena taking place simultaneously such as heat transfer, structural mechanics, non-linear structural material, multi-body dynamic and computational fluid dynamic.

Ring rotation during operation has been a controversial topic in the literature for many years. Some authors have found that rings are rotating [43] while others have not [5]. The work aimed to be able to further comprehend the phenomena and contribute to the current debate.

The “bed-in” or “running-in process used in racing motor cycle is not yet fully understood. There has been little information on the effectiveness of the large number of steps used by manufacturers to embed new rings. The simulation of running-in process would enable further improvement and simplification to this complex process.

MoS_2 rings typically “bed-in” faster than uncoated or chrome coated ones, reaching full sealing capacity more quickly, while providing significantly higher scuff resistance [33,34]. It has also been reported that higher performance can be obtained with uncoated ring and coatings may reduce engine performance. This should be further investigated.

1.3. Aims and Objectives

The aim of this work is to:

To investigate how running-in influences the performance of internal combustion engines in race conditions.

The objectives are to investigate:

- To develop a computer based simulation of the ring pack to predict wear during the running-in process and after the running in process when the coating has been applied. This will involve characterising mechanical, material and physical aspects of the tribo-system (i.e. the piston ring, lubricant, liner, and operating conditions) by establishing liner material deformation and ring profile changes and the importance of these effects during the running-in process.

- The extent to which the coating rings at different stages of running-in influence engine performance over time

1.4. Thesis outline

Continuing from the introduction, chapter 2 examines the present literature related to work done on race engine simulation of coated piston rings during the running-in. As simulation is discussed, the chapter then moves to simulation packages defining the operations and justifying the use of the software used for this work. The chapter then

closes by introducing the KTM 520 test engine, showing the main areas of interest for this work.

Chapter 3 provides an overview of current compression ring piston designs used in racing. The most common compression ring material and ways to reduce wear are introduced and discussed. The last area discussed is the role and type of lubrication as the compression ring is in contact with the cylinder wall.

Chapter 4 introduces the mathematical modelling of the running-in, which includes the use of a slider-crank model to calculate inertia forces and the compression ring rotation position and torques. These equations are expanded to include minimum film thickness, combustion gasses, wear and thermal shock in the mathematical model. Finally material loss and thermal expansion are considered. Completing the chapter with a methodology layout defining in detail how the simulation software works with the equations defined.

Chapter 5 examines the method of applying the theory discussed in chapter 4. The present British Standard and Love's theory [44] for the contact chamfer of coated compression ring is examined to establish the validity of the current chamfer design, Piston ring rotation during operation is investigated. The study is first based on geometry, then carried out using surface response method.

The thermal expansion of the ring and coating, examining the idea that the coating could be restricting the compression ring substrate to expand. Thus compromising the seal of the combustion chamber. Finally, bringing all this data together for a full running-in procedure by using data discussed in the next chapter and comparing the results to what is seen and the error with-in the results.

In chapter 5, also presents data found in dynamometer testing offering validation through measurements and observation in chapter 6. In this chapter the results found in simulation

and dynamometer testing are presented. Within the chapter some validation is offered in the methods of compression ring dynamics. However some additional phenomena are identified and discussed.

Chapter 7 provides a final conclusion to the presented, and considers assumptions and their impact on the engine simulation and a summary of work presented. The conclusion is then followed by recommendations for future work.

CHAPTER 2 – LITERATURE REVIEW

2.1. Introduction

The internal combustion engine is subjected to large levels of efficacy losses and the piston ring pack contributes to these losses [3,14,45]. One of the main challenges, in engine design, is to produce low friction rings that are able to maintain a good seal during their operational life. There is a greater need to improve the performance of current engines. Losses mainly occur on the top of the piston, where the compression rings are seated. The two main functions of compression piston rings in reciprocating engines are to seal the combustion/expansion chamber and to support heat transfer from the piston to the cylinder wall. The function may not be satisfied due improper compression ring installation in the piston assembly which is less common now with the development of specialist mounts and tools or improved operating conditions allowing for cylinder leakage.

Beside correct installation of the compression ring, the running-in of the rings has a major impact on the wear and friction generated during initial phase of operation. During running-in a large amount of pressure and heat are generated, resulting in both material loss due to wear and expansion due to heat. The compression ring is the closest to the combustion gases with harsh operating conditions. These rings are exposed to the greatest amount of chemical corrosion and heat.

The running-in process of engine components is still seen as a black art very simply described by five different manufacturers in their manual as reported in Table 1 or more with over 30 steps. There is currently no consensus on how it should be done experimentally.

Table 2-1 –Running-in used by five different companies with similar engines

Engine	Time hr	Distance	Coolant	Engine Load	RPM
KTM 520 [43]	3	Na	Liquid	<=50%	<=7000
Aprilla 550 [45]	3	Na	Liquid	<=75%	<=8000
Kawasaki 550 [46]	na	500 mile	Liquid	<=40%	<=5000
Suzuki GS550 [47]	na	500 mile	Liquid	na	<=4000
Honda CB550 [48]	na	600 mile	Liquid	<=60%	<=5000

To further comprehend the running-in process, simulations have been used. One method is Finite Element Method (FEM), introduced by Ritz [46] and Courant [47] to simplify and resolve calculus through approximation and provide numerical analysis of complex systems. In the 1970's, the use of FEA software was limited to only large companies as the computers needed to compute large levels of calculations were expensive. Implementations of FEM were limited by computational power and associated computing costs to large organisation like IBM, governmental organisations like Onera or NASA and universities.

With the introduction of more powerful personal computers over the past 20 years, FEM has been have expanded to areas like the simulation of engine efficiency.

Commercial and non-commercial packages are now used. They have advantages and limitations which are discussed in this chapter.

However, many of the software packages make various assumptions for example material is assumed to have an idea matrix structure, implying that clusters within the structure are not present.

2.2. Compression ring development

Ramsbottom [20] in his pioneering work from 1854 incorporated a new type of ring to the piston, known as the split ring, to create a better seal during engine operation and thus reduce the weight of the piston assembly A 381 mm cast iron piston, weighing 39.9kg was used to test the split ring and further weight gain could be obtained with wrought iron or brass. He mentioned that the split rings could be easily manufactured from wires, and later bent into position. The split rings should not contain loose parts like nuts, bolts or pins that could come away and damage the engine. Instead he proposed a design for piston rings, where the new ring should sit securely in a groove of the piston.

Further design considerations on the piston rings, included reduction of friction acting on the piston and pressure against the cylinder wall which led to further weight reduction.

The reduction in friction and fuel consumption were confirmed when fifteen engines, fitted with piston rings, operated for sixteen months reached a distance of 209,800 miles. The engine fitted with piston rings consumed 12% less of fuel than the conventional engines at the time. Split rings have been used ever since.

In 1862 Miller [48] re-examined Ramsbottom ring design and made further improvements in allowing pressure to build on the back side of the ring. Over many years several design modifications to piston rings, piston and cylinder have been made. In an effort to lower the fuel consumption, the piston was redesigned to enable the piston ring to sit closer to the crown [49].

2.3. Compression ring dynamics, wear and thermal conditions

Taylor [50] noted that ring dynamics affect the ring during operation. In-situ measurements made during operation of ring motion, piston secondary motion, piston oil

ring film thickness, piston ring friction and temperature highlighted the importance of both lubrication and piston design on the running of engines.

During the combustion cycle, the piston ring exerts a radial pressure against the cylinder wall, the shapes created by the split ring define the radial pressure distribution [51]. Most of the research on the pressure distribution aimed at the development of analytical methods of shape deformation of the ring. Brombolich [52] noted a possible analytical method for calculating the ring deformation and the structural mechanics that influence the ring during operation. However, the ring gap and back pressures were not considered. Mittler [53] noted that the ring did not easily twist during a full engine cycle. He also noted that during the engine cycle when the maximum force is acting on the ring (33% of the total operational cycle), the standard rectangular ring would make contact with both top and bottom face of the ring and wear of the compression ring was observed.

Mittler [54] further examined the effect of new designs on the axial motion of the piston assembly in modern internal combustion engines using mathematical modelling. Increaseing heat and mechanical loads in the combustion chamber have led to higher power density which has led to further development in piston ring designs and emission reductions. One of Mittler's main achievements was the development of the first mathematical model able to describe the basic dynamical effect of the piston ring assembly and predict blow-by, as well as oil consumption during engine operation. Mittler included piston ring geometry in the engine boundary operating conditions as he recognised that piston ring design depends heavily on the engine operating conditions.

Mittler's work lacked validation from real engine measurements to confirm the model predictions. Wang [29] validated the work started by Mittler, where he considered various types of engine configurations.

Baker [55] examined the role of the fitted piston ring assembly and noted that compression ring dynamics within a four stroke engine has been the direct result of inertial motion relative to the piston motion and the ring in-plane motions resulted in the creation of several elastodynamic modes. As the four stroke cycle process is quite complex procedure, a number of modes are exerted on the system. The cylinder pressure and ring tension forces are both acting outwards of the ring to the cylinder face. It was also noted in this work that there is a radial force that acting in the opposite direction which is accredited to miss conformability of the ring to cylinder wall. When studied under transient conditions, it was found that both forces acting on the ring and the cylinder do not reach an equilibrium, resulting in a small rotational inertial force acting on the compression ring. The results indicated that fitted pistons rings main benefit was to minimise compression ring blow-by due to a greater ring to cylinder conformability. Baker [55] also used a one-dimensional gas flow model to incorporate blow-by effect in the transient ring elastodynamics model which included in and out of plane's ring dynamics within the groove, gas flow and friction. Experimental data have been used to validate the model. The performance of the ring is affected by the micro-welding phenomena. This has been shown to lead to grooves and damage to both top and bottom faces of the ring.

Archard law [56], is a simple generic model used to describe abrasive wear of two sliding materials and has been adopted for many years for the estimation of piston wear. Archard law assumes that wear volume is proportional to sliding distance and load, and is inversely proportional to the hardness of the softer material which are not always met.

Rabinovich [57] developed an analytical model designed for to predict the operation of a piston ring using a fourth order ordinary inhomogeneous non-linear differential equation to calculate pressure distribution and Gintsburgs equation to predict the initial stages of piston ring wear. Rabinovich pressure distribution plot has confirmed the pear shaped

response described in [58], while no raw data was gathered to confirm any predictions made by the wear model.

Tung [4] proposed an abrasive wear model, using Rabinovich's equations instead of Archard's including temperature, load, oil degradation, surface roughness and cylinder wall material properties. Rabinovich's equations are more suited to describe piston rings running-in of the cylinder wall than Achard's laws.

New and novel methods for the study of friction have been introduced in an attempt to further study these effects [19,55,59-62]. Gore [63] noted that within the combustion engine the piston to cylinder interaction are a significant portion of losses due to friction. These losses are mainly attributed to changes in the engine operational conditions such as lubrication and geometry during the engine cycle. Gore used a novel floating-liner assembly to assess directly friction and the lubrication regime. Gore also noted that as the problem is highly complex, numerical models do not tend to replicate the work seen in actual test conditions.

Computer simulation packages are now commonly used to simulate piston ring assembly. Wannatong [64] used AVL computer package to simulate the piston ring dynamics algorithm to evaluate piston ring wear and lubricating oil consumption. Wannatong noted that the complexity of the system could not be readily simulated and a mathematical model using computer simulation packages should be used.

The solutions of Newton and Euler equations have been applied as boundary conditions for the simulation. Wannatong simulation were broken down into four processes with nodes defined using finite different methods to resolve non-linear equations calculated using parallel computing.

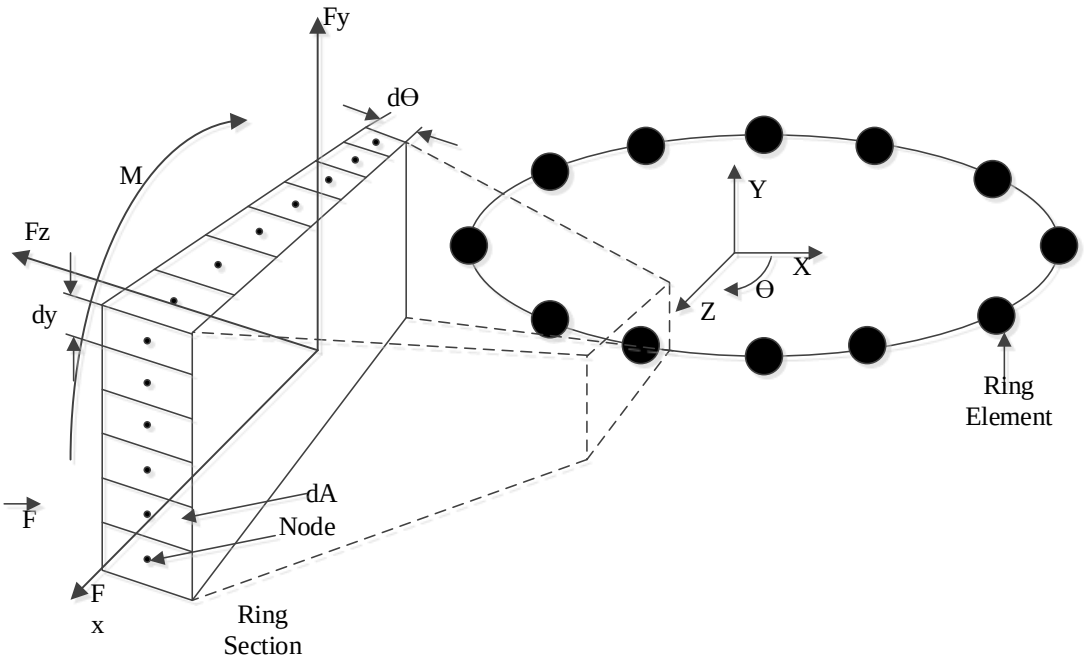

Figure 2.1 - Elements layout of piston ring simulation

The geometric reference applied to the simulation is shown in Figure 2.1. The gas flow through the rectangular piston pack and back gas flow in the piston ring pack as well as blow-by have been simulated. A good level of agreement between experiments and simulation has been found showing promise when simulating the ring motion dynamics.

Because there are no algebraic equations, the simulation is presented with the possible use of surface profile of the piston and piston rings. Unlike the work shown in [43], where the piston force solution was based on a singular force impact, this work looked at how four primary forces work on the ring during operation. However, the rings that are simulated in this model assume no coatings. The lubrication regime could also offer some indication as to how the rings move, as in this work the rings were simulated assuming the fully flooded state. Also no consideration for the wear resistant coated was given. Work done by Wang [65] shows that many profile aspects of the ring during operation are unknown. The tribological performance inside the chamber of an internal combustion

engine, the wear and lubrication can only be fully interpreted when these tribological elements are considered during operation. This work was able to predict the lubrication, dynamics and wear of the piston rings interactively during operation. It shows the results of applying a new model to a piston ring pack found in a diesel engine. The correlation between the theory and the experimental data was investigated.

Baelden [66] produced a study to present a new curved beam finite element model of piston rings. His method produced structural deformation and the contact assembly as two separate grids. He noted that he had compared his results with what has been seen in current literature and his own analytical solutions and found a strong level of accuracy. The method presented did show a good method for assembly interactions and also oil transportation. However, it was also noted that the study was based on ring conformability to the cylinder liner. It presents good foundations to continue this study as rotational behaviour and also coating and material loss were not adequately considered.

Cheng [59] examined a three-dimensional piston ring model using a hexahedral meshing finite element method. The conformability of the ring to the cylinder wall was investigated. It was also noted that alongside the contact between the piston ring face and the cylinder wall, the interaction between the ring and the groove of the piston should be studied in the axial directions. By incorporating these boundary conditions the ring twist, contact force and conformability of the ring in the groove were calculated simultaneously. As thermal loading has a significant influence on the ring pack, in the study the heat boundary condition was applied on the cylinder wall and within the piston groove. The model presented in this study considered variations found along the circumference. However, no consideration for the piston ring coating was made, as a wear resistant coating has mechanical properties that would affect the accuracy of the results.

Lam [67] presented work that studied the two stage process of expansion and compression of the internal combustion engine. In the study the work was divided into two different cycles, the first being high-pressure and the second being low-pressure. It was then possible to examine mechanical efficiencies at high and low levels simultaneously. In this work, the piston, piston ring dynamics and thermal efficiencies had low levels of consideration, many assumptions were also made in the use of the software package.

Fuel efficiency is the main goal for all research internal combustion engine, the compression ring contact-to-the cylinder liner contributes near 5% of the fuel efficiency, due to the seal between the components. When analyses are conducted on this behaviour the effect is often idealised, such as the contact faces and the isothermal conditions. Morris [68] presented a new analytical thermal solution that shows the average flow for the contact. The work presented by Morris showed simulated conditions that showed the power loss under normal driving operation. The study showed that power loss from the ring, is mainly due to the viscous shear from the lubricant when operated under cold conditions, and when the engine operates in hot conditions boundary friction dominates.

2.4. Lubrication

Many advances in engines lubricants have also been made with the introduction of synthetic oils and the incorporation of detergents/additives in lubricants. Detergent additives have maintained carbon deposits from burnt fuel in a non-solidified state to prevent carbon to react and harden around the piston ring causing the ring to stick in the groove of the piston. A noted problem over many years was the phenomenon known as

coking, this was a result of fuel burning casing carbon emissions depositing onto the piston ring [69].

Several internal combustion engine models have been developed over the years. Most of them directed towards the simulation of the ring packs for lubrication purposes [13,54,70] rather than the wear of internal combustion engine.

A study was published by Bolander [11] on the analytical model and also some experiment apparatus was developed to study the lubrication effects and also the effects of friction acting on the piston ring and the cylinder liner during operation. By incorporating Reynolds equation and film thickness equation and also taking into consideration the boundary conditions the lubrication conditions between the piston ring and cylinder liner were predicted. By employing the Green and Tripp stochastic approach the mathematical effects of boundary and mixed were simulated. The next thing that was considered to evaluate in the simulation was the effects of fluid film rupture and reformation at the TDC, this was incorporated into the mathematical model using Elrod cavitation's algorithm. It was further found that the experiment results had clear indication that the piston ring and liner experience a range of different lubrication regimes, which were hydrodynamic lubrication, mixed and finally boundary all seen during the stroke. It was further found that the experimental and analytical results were in agreement. This confirmed that the devised simulated model could in fact capture the lubrication regimes that were seen in the piston ring and liner conjunction.

Felter produced a study that examined the present technique of using Reynolds equation as a numerical method to model the lubrication of piston rings. The current method that has been used at the moment to apply the lubrication in mathematics is that of Reynolds equation which within this study is not applicable as the equation is ideal when applied in confined geometries and also in open geometries. This is of course applicable when all

of the flooding data is available. However when studying the effects of piston rings the possibility of lubrication starvation can occur. Therefore, a computational aspect was extended to include the oil film outside the piston ring to help overcome the domain.

Lee [69] studied the effects of lubrication blends and engine parameters, on engine components and oil degradation during operation. For this work a single cylinder IC engine was employed. The piston rings were run on test oil formulation and the crank was run with a fully formulated oil. While the engine was running under controlled conditions samples were taken from the sump. The samples were analysed for rheological and chemical results. With this work the methodology behind the engine experimental set up and testing was presented. The results presented showed for the sump carbonyl concentration and viscosity. The condition for the four engine components were also tested. The oil blends, engine parameters where compared.

Further work to try to understand the lubricated piston ring was shown by Tung [4,71]. In this work the focus was on engine improvements that were considered such as oil improvements, efficiency of the engine components and all coatings that have been engineered for coating material process, these processes are commonly verified with tribological experimentation. These experiments paid attention to the performance of the piston ring/cylinder bore. The main focus of the research was to develop and investigate the abrasive wear that can be found on the piston ring and liner of the bore.

During the experiment the steady state operational effect of temperature, surface roughness and also the material properties were examined. The model developed for this study was applied to theoretical modelling software in conjunction with an FEA package. From the work developed in the laboratory the wear that could be found on the cylinder bore and on the ring was simulated. This was done by using an abrasive wear model and conditions were assumed to be at steady state. By studying the load, oil deterioration, active temperature and all material properties novel aspects were located in the system.

Lotz [72] examined the present technique of using the Reynolds equation as a numerical method to model the lubrication of piston rings. The present method that has been used for applying lubrication in mathematical modelling is the use of Reynolds equation. However, in this study it was noted that the equation is not applicable as it is ideal when applied in confined geometries and also in open geometries, this is only applicable when all of the flooding data is obtainable. However, when studying the effects of piston rings these conditions become a problem as the piston ring may suffer starvation under certain running conditions. Thus the way to overcome the domain, was to apply the computational aspect that extended to include the oil film that is outside the piston ring.

The model that was created for the study had a 2D free surface code that solves the Navier Stokes equation under time dependent compression. The environment of the calculations can be seen as a mesh free moving method in which squares were using primal variables u (velocity component), r (density) and v (velocity component). During the calculations the Runge-Kutta method was applied to be used for the time integration within the system, this method was recognised as a third order method.

The density and pressure of the equation was applied by using a number of equations reported by Dowson-Higginson [73], this technique was used to close the results. The boundary conditions that were applied in this study were nonslip conditions on a surface and the stresses that were on the free surface were seen to be in equilibrium. Furthermore, during simulation if needed, a surface tension can be applied, and it was assumed that a zero viscosity of surrounding gas was apparent. When each phase solid, liquid and gas meet in an intersection the contact point was modernized based on the results from the angle that was found between the normal's of the solid, velocity of the solid and finally the free surface that was on the solid. The analytical result from the Reynolds equation

was used as a comparison for the numerical model generated and also the Reynolds equation was noted for a fixed incline slider bearing.

2.5. Coatings

Some of the first piston rings were used without surface treatment or protective coatings. However, the friction of the piston against the cylinder wall was always a research interest.

In an effort to reduce wear of the piston ring, in the 1940's Cr electroplated coatings where applied to the outside face of the ring [74] and are still in use today. Most recent developments have been to optimise the tribological systems of reciprocating engine (piston, compression ring and cylinder). There have been many developments over the past 50 years with most of the work concentrating on materials (coatings and substrates). A piston ring material is chosen to meet the demands set by the running conditions. Elasticity and corrosion resistance of the ring material is required. The ring coating, when applied should be compatible with both the material that is used for the piston ring and the cylinder liner. Grey cast iron has been used as the main material for piston rings. Due to harsh operating conditions, compression rings will sustain huge deformations due to thermal expansion and large amount of stresses will be generated on the contact by mechanical loading. Most of the degradations observed on the piston rings have been attributed to early age damage during running-in. The type of race (Formula 1, Formula Ford, motorsport GP) will dictate the tribological system arrangement for the cylinder liner, the piston and compression ring. As mentioned above, the main material for piston rings is grey cast iron.

Compression rings have also seen major coatings development where MoS_2 or some type of PVD surface treatment (titanium, chromium or ceramic) are now used [29].

Titanium nitride is widely used on high performance steel rings [75-79]. However CrN and MoS_2 have a wider range of applications due lower production costings. CrN was in use since the 40's, was replaced in the 90's by CrN (PVD), which display improved adhesive wear properties while operating[74]. Cr rings became a popular choice for off-road and dirt track engines because of their ability to resist abrasion caused by airborne contaminants. However, chrome rings can only operate up to 560^{o}c, where the coating will become less resistance to scuffing than MoS_2 coated rings. Since heat is a prime consideration in almost every performance application, MoS_2 has been the ring coating of choice for many years. MoS_2 rings typically bed-in faster than chrome, reaching full sealing capacity more quickly, while providing significantly higher scuff resistance [33]. Abrasion resistance of their MoS_2 coatings can be improved when alloyed with nickel chrome. The only disadvantages with MoS_2 is that the material can be damaged by severe engine detonation, and it may be incompatible with some bore coatings such as nickel/carbide or aluminium based alloys [61,80-82]. For such applications, a PVD coated steel ring would be the right choice.

Once the running-in process has been completed the coatings attached to the compression ring show signs of structural delamination. The piston ring is subjected to wear through forces applied during the operation. The piston ring deformation is also a result of thermal shock during combustion. Therefore, to relieve the process of running-in coating delamination, soft sacrificial coatings using materials such as MoS_2 have been applied to enable piston rings to achieve a best fit during the running-in period. The method of calculating has always been the interest of much discussion. The method that is most commonly referred to as the standard for the calculation of wear is Archard's law [56].

However, the engine problem introduces some problems to the use of this equation as pressures will change and the heat variation will also change. Becker [83] noted this problem and offered a variation of this equation that suit the problem more accurately.

Nanocomposite coatings have demonstrated levels of friction and wear under extremely high operational (sliding) in intense environmental conditions. Thin film multilayer coatings can result in hard, tough and low friction coatings. In today's research it is common practice to attempt to couple multi-layered and nanocomposite materials with surface engineering techniques to increase tribological performance.

One approach that has been talked about is the encapsulating lubricious phase in hard nanocomposites matrices. Development of an adaptive environmental coating such as adaptive environmental composites shows possible reversible adaptability to ambient humidity/temperature. It was noted by Voevodin [79], that by creating a coating [Ti/TiN]n, then applying it to cast iron piston rings in an engine the performance of the engine was increased. However, coatings such as CrN or surface treatments, such as NSS have showed similar wear performance to uncoated rings.

The plasma molybdenum was first developed as an alternate method for a wear resistant coating. It was noted by Chaika [84] that chromium-plating process was the most widely used method in industry to apply a wear resistant coating onto compression rings. However, he noted that this method will not increase engine life, it is an extremely time consuming, costly and in many cases dangerous method. Molybdenum coatings that are used extensively in other countries have been found to have one-third wear resistance to what can be seen in chromium plated piston rings. However piston rings that have had plasma spray applied with the 11Kh18MVD and 4Kh13 steel parameters show a better result. The coatings improve the performance of the engine and also cause a lower running

cost. It was found that even though the plasma molybdenum provides a lower resistance than chromium plated rings; the wear resistance was comparable to the chromium.

The use of CrN as a replacement for the standard electroplated Cr component for piston rings. Friedrich [85] noted that the CrN coating showed much promise towards the application of an alternate method of wear resistance rather than the standard electroplated Cr coating.

In the late 90's many patents were made for the use of this technology on piston rings. Many of these patents also considered the coating of the liner. A study into the properties of CrN was done by Hones [86] were he noted that the CrN nitride when compared against electroplated Cr had an atomic hexagon structure which made the coating perform with a greater abrasive wear resistance to what can be found with the standard coating.

CrN is an alternative to the standard Cr electroplated coating. Friedrich [85] examined CrN coating deposited using PVD methods for cutting tools and for automotive applications in particular the piston ring. A Cr_xN film was synthesized by use of RF magnetron sputtering and characterized for thickness, hardness, adhesion and residual stress, these factors are very important when establishing a tribological application of a substrate compound.

During engine operation the piston travels with the piston ring, both will interaction with the cylinder wall. The contact between all can be established by the changing geometry and the high mechanical loads that are active during operation. These loads are a direct result of kinematic sliding. It was found the thickness for the coatings is about 7 μm. During the operation the steel DIN 1.4112 rings tested with the bore diameter of 97.5

mm. The results were characterized by hardness, compressive residual stress and good adhesion were found to be extremely good for tribological applications.

Furthermore, it has become quite common to incorporate chromium plating applied to the contact face of the ring. Morkhov and Egorova [87] noted that by applying chrome to the contact face of the piston ring the wear could be reduced. It was noted that the ring material suffered minor material matrix deformations on an untreated ring. The experimental setup of the ring was a compression ring set with a bevelled chamfer at a 45^{o} angle, the ring coating was applied with a 135 μm thickness as it was suggested that to apply plating to any greater thickness could lead to power loss. This technology has become a common method of application for rings to reduce wear on the ring during operation.

Guermat [10] noted that by coating a compression ring with a DLC coating would indeed create a better resistance against wear when acting against the cylinder wall. However, the wear on the cylinder wall proved to be largely abrasive resulting in a large level of damage. The experiment then progressed to a comparison of two more coatings. The first being chromium nitride and the second being HVOF chromium tungsten.

When compared against the industry standard of electroplated Cr he observed that the wear resistance had increased, however the most promising coating that was found in the experiment was the HVOF CrW coating. In the work he insinuates that the DLC coating is too hard for the task, however the scenario that he created was a strange one. In the study the use of a cast iron liner was employed and the steel was used for the piston ring. As the automotive industry is now moving towards employing more advanced materials for liners, the cast iron liner has almost been dated and therefore dating any results noted in the study. Further to this little acknowledgement was offered towards the running-in period.

Braithwaite [33] presented work that offered a comparison between two similar engines which where both operated in identical conditions. However, in one of the systems molybdenum disulphide in oil suspension was used as a lubricant. For these experiments a specially designed test rig was employed. The determination of the final ring profile and the wear rates of both rings were compared along with SEM images of the final ring profiles. The results showed by using molybdenum disulphide as a modified wear mechanism is an effective addition. It was further concluded that the change in surface topography occurs mainly by plastic deformation of the material rather abrasive and adhesive wear processes.

2.6. Running-in

When the rings are first installed in the engine, they must be first run-in. The running-in is a procedure for conditioning a new compression ring by giving it an initial period of running-in. The focus of the running-in of an engine has been on the contact between the compression ring of the engine and the cylinder wall. There is no universal procedure or set of instructions to run-in an engine. Most importantly experts disagree on how running-in procedures should be done [8,88]. There will be as many procedures as engine type and operating conditions.

During the running-in process the piston ring is in contact with the cylinder liner, while the reciprocating mass (the piston) travels backwards and forwards within the cylinder. Studies have shown that the ring will twist in the positive and negative direction of 0.1 deg ± [80,86], it was also noted that any greater deformation could lead to surface fatigue on the ring. It was experimentally noted by Priest [13] that the bottom face of the compression ring will wear unevenly in the area of the thrust face compared to the opposite side of the ring. During this work observations were made with the compression ring (during the running-in) moving along the cylinder backwards and forwards in the

direction of the head of the engine, it was noted that wear was caused on both upper and lower faces of the ring.

This effect will alter the pistons contact relations between the cylinder wall, the piston ring pack and the surface of the ring. This behaviour has sparked much interest and work has been done to examine this in testing and in modelling, Taylor [25] noted that the tilt of the piston is also related to the secondary piston motion. This effect will then cause more clearance between the cylinder and the piston body. The compression ring will then be subjected to contacts of the trigonometric form. Brombolich [52] confirmed Taylor's suggestions that the piston does in fact have a secondary motion which in turn allows for the ring to rotate for a short time until the thermos-elastic changes take effect. However, Dunaevsky [5] has noted that the piston ring will continue to rotate during operation.

Ganguly [60] presented a study examining cylinder bore deformation and possible methods of reduction using computer-aided simulation. It was noted that deformation of the bore has a large influence on the engine performance and in the standard study conditions the level of deformation noted would result in engine seizure. It was also noted from the results found in the study that large levels of deformation will result in increased oil consumption, greater blowby and emissions, which will affect the overall performance of the engine to a great extent. Deformation of the cylinder was considered. However, the piston and ring pack influence from the engine cycle were represented in the forms of boundary conditions.

Tomanik [89] produced a study that examined consideration of the ring gas pressure, the ovality of the geometry which considers both piston ring and cylinder bore. The work also examined how the maximum amplitude is only ever given when using the Fourier series to describe the cylinder shape.

In his study it was noted that finite element analysis tools are normally used to create a more exact result. However, in most cases these tools are only ever used for fundamental studies. The conformance to criteria was calculated and also with the aid of an experimental measurements verification was shown. An experimental static jig was used to measure the non-contact areas of the ring, hence the deformed piston ring and bore were measured. The measurements from the experimental testing, gave basis for a semi-empirical equation to be proposed to calculate the conformability limit of the piston ring. The equation that has been proposed in this work is applicable in the initial engine design phases i.e. the running in procedure. It was noted that the deformation of the cylinder surpasses that found in the piston ring conformability. The percentage of the ring that is in contact with the cylinder is estimated, based on the linear regression empirically found during the experimental procedure.

A study was conducted by Jun [26] examined the change of surface roughness at different regions of piston rings during the running-in procedure. Also, in the work the effect of surface topography on the lubrication and all friction behaviours were considered. The work involved developing an uneven wear model, small regions of the model where allocated with a different surface roughness. To verify what was seen in the simulated models a reciprocating wear test rig was developed. The results showed that the wear that occurred during the testing has uneven wear behaviour. The results showed no indication of starvation of lubrication, at bottom dead centre and top dead centre the minimum film thickness increased while the friction force and power loss decreased. This work is an excellent study to show the wear process of the compression ring being uneven however the temperature of the engine was not considered and also rotational dynamics that occur around the compression ring were neglected.

2.7. Engineering modelling packages

Ricardo RINGPAK solvers that are provided with the software allow the user to simulate the motion of the ring pack, while assembled to the piston and contacting with the cylinder wall. The problem is solved by using a quasi-3D method where the ring is solved in a series of sections or an axi-symmetric assumption. The software is able to consider the effects of inertia, friction, lubrication and gas pressure. All sealing gas calculations are done through the method of gas flow analyses through the ring pack. The ring wear is also an option that can be added to the ring solution however the material is considered as a singular body. The software will consider two flow models one examining the compressed isothermal flow and the other an isentropic model. Each model can be selected from the user or the software will select the most appropriate solution based on the results.

AVL excite is a software package that allows for the use to size piston and piston ring assembly. The system calculates the absolute values for the ring movement, ring pressure and blow-by, this will allow for reliable trends regarding lubrication regime. However, the crown axis dynamic motion is still being developed for the system. COMSOL's graphical user interface uses a set of predefined interface tools. These tools are referred to as physics interfaces, these tools allow for modelling interfaces, allowing for variable input and interpolation tables for time dependent simulations. The software has a suite of add-on products which allow further multiphysics modelling.

Matlab/Simulink is a system which uses a block diagram interface for multi-degree of freedom simulations and model design. With this software verification of the embedded system, continuous testing and simulation, hence this software is ideal for the development of highly structured engine system simulations. The Simulink system uses a graphical programming interface which allows for editing. This system also has solvers

for simulating dynamic systems. The software is an integrated software with Matlab, this allows for all algorithms within the system to be used. Hence the results can be used for further analysis.

SimMechanics is integrated into Simulink which provides a multibody simulation model for full 3D mechanical systems. The graphical programming for multibody systems is done by using blocks representation for bodies, joints, force elements and constraints. The software will then formulate equations for the mechanical system in motion. The simulation software also has an integrated system that enables 3D CAD model to be imported. SimMechanics will also generate a visualization of the dynamic system.

2.8. Conclusion

A large percentage of the heat produced in the engine is conducted to the cylinder contact surface through the piston ring pack. The heat coming from the combusted fuels reduces the piston rings hardness and wear resistance. This in turn can lead to oil oxidation and evaporation on the cylinder wall areas.

From the combustion process vapours from the water, carbon deposit from the fuel and acidic combusted by products all contribute to the abrasive wear of the three main components (Piston, Piston rings and cylinder liner).

When the combusted by products and worn particles are mixed into the oil, the result is lubrication that has poor operating properties. The piston during operation is subjected to large amounts of pressure. The pressure that is acting on the piston has been used by engineers for some time as a method to increase contact pressure between the compression ring and the cylinder wall. This has been achieved by allowing the gas to act from the back of the piston ring during operation. All other pressures of the ring are attributed to the spring loading. The ring axial dynamics show that the ring will run in at different performances relative to the affects in the z axis.

The contact of the piston ring to liner depends on the lubrication quality, the interaction of other rings on the piston, the level of honing on the cylinder liner, the oil delivery, ring radial forces acting along all the axis, cylinder bore deformation and ring twist. The computer simulations are now at the point where complex parameters such as ones mentioned are able to be calculated where the recorded error between simulated and practical test results can be as low as 0.01 % error difference. Computer packages are now able to simulate the oil lubrication systems to a degree where issues like starvation can be accurately replicated. However, most simulation packages don't have the ability to simulate a material asperity defect. Oil film thickness is an important factor for the boundary conditions for any simulation or calculation. In the internal combustion engine the thinnest oil film thickness has been noted to be at TDC. In the piston assembly components the friction forces and coefficient of friction while acting on the cylinder wall, reflect energy consumption during oscillation, this results in a method for calculating the probability of wear. When new piston rings are installed the phase of running-in occurs. The running-in of the piston ring allows for a comfortable bedded fit, providing a steady level of mild wear. The two-body abrasion during operation is the main wear mechanism of this process, as a result of this the sliding interaction between the ring and cylinder liner lead surface asperity interaction. Hence the running-in process could have a procedure for different engine levels of performance.

The work noted in the review show complex methods of equating the problems used. Archards wear equation, has been one of the most commonly used equations throughout all engine simulations and calculations. However the nature of the equation, material loss is equated and an almost linear methodology. As the problem of the reciprocating mass introduces inertia forces in multiple directions the equation becomes obsolete when calculating the material loss of the piston ring as multiple degrees of freedom between

the contact faces need to be considered. Work that has been done by Rabinovich shows that Archards wear equation had grounds for further refinement. By introducing extra layers of variables allowing for material to be lost at certain levels dependent on the rise and fall of inertia forces.

The lubrication regime within the simulations noted tend to show the use of Reynolds equation, this equation is only successful if the surface of the piston ring is barrelled, when this problem is introduced to a flat surface as what is seen in motorcycle engines the equation has problems when both piston ring and cylinder face are parallel, to solve this problem navier-stokes [90] equation is employed. Studies have shown to calculate the pressures surrounding the piston ring during operation is a successful alternate method. The present simulations show in studies will tend represent the geometry as only basic geometry when this is not a good representation of active piston rings. Further to this most of the time the coatings are also not defined, suggesting the interface between the substrate and the cylinder wall is neglected. If the coatings are shown in the simulation only bulk material is considered. Simulation studies also note that the rotation around the piston is negligible, hence is neglected. 4 stroke motor cycle engines will tend to use only rectangular profile. The ring will have a coating applied to the contact face, the piston has also gone through many levels of development, hence creating further boundary considerations. At present there are many simulation packages on the market the sectional of the correct package used is based purely on the task at hand. The use of both mathematical models and 3D models tends to be quite a niche area. The most applicable software to solve this problem is Matlab and COMSOL system, these will allow full cross access to the system and also support equation modelling alongside there 3d systems.

CHAPTER 3 - PISTON ASSEMBLY AND SYSTEM OVERVIEW

3.1. Introduction

Over the past 100 years the compression ring has had many redesigns, in an attempt to control the output of the engine during operation. The first type of piston ring that was produced for the engine was the rectangular design which over many years has hardly deviated. This ring design is commonly found both in the petrol car and in diesel engines. This type of ring is simple, the production is easy and it acts as a good seal for standard production engines.

Designers also developed the ring with a cam like profile to encourage a greater level of ring tension/pressure when acting against the liner face, once the ring has been installed it will create a radial pressure on the liner face which will be apparent throughout the cycle. As there is a very low pressure present in the chamber during intake and the exhaust process of the four strokes a greater level of tension must be present for the states, where the ring relies on applying its own force more commonly known as the free state periods.

Mittler [54] found that the ring will not twist easily during the full cycle. He noted that during operation of the engine the maximum force acting on the range is at 33% of the operational cycle, the standard rectangular ring will contact with both top and bottom land of the piston groove. To ensure the contact seal of the ring, the tension of the ring is often increased this has an adverse effect as the increase of loading on the cylinder wall can cause a rise in the friction and wear. However, if the tension of the ring was reduced the result of blow-by was seen.

While an engine is running, inside the combustion chamber the pressure that is caused by the ignition, response forces push the piston down. However, some of the pressure against the piston will flow by the gap between the piston and the cylinder wall, which is commonly known as blow-by. The compression rings job is to stop this from occurring hence sealing the chamber.

The level of blow-by is subject to manufacturing tolerances of the compression ring and also the operational life of the component. The older the rings and the cylinder wall of an internal combustion, gives more possibilities for this phenomenon to occur.

Determination of blow-by can be for many reasons. When horsepower power is decreased in an engine, one possible explanation is that the rings have become old (wear) allowing for the bow-by to increase. Chang [91] noted that blow-by is directly proportion to that of the wear in the piston ring. However, it has been found that the incomplete combusted fuel will make its way into the oil inside the crank case, this can also lead to a build of carbon deposits in the oil which can lead to ring corking.

When blow-by occurs and begins to increase, oil can leak pass into the combustion chamber, which occurs due to the rings allowing lubrication past into the chamber. This then lowers the octane of the mixture. After this has taken effect detonation, which then results in damaged chambers and the piston. This phenomenon was recorded by Nakada [92], where it was noted that if ring tension is reduced, blow-by is increased. In work to examine this problem the dynamic motion of the rotation should be a vital factor to consider. However, in most recorded pieces dynamic motion of the ring becomes an assumption.

Masahiko [93,94] noted that to encourage better performance one needs to consider the main mechanical losses that can be found in an engine. However, designing a ring and incorporating all these factors into process can prove to be extremely difficult. Often one of the first factors considered in the design process of the ring is selecting an optimum pressure for the ring in the liner. However, too much tension can lead to power loss in the engine, the tension can then encourage a greater wear loss rate and scuffing may occur. The designer of the ring must also keep in mind the other factors.

3.2. KTM 520 Engine

3.2.1. Introduction

The KTM 520 is an off-road single cylinder 4-stroke sports motor cycle engine, a SOHC/4 valve head liquid cooled decompression internal combustion engine. The ignition process is Kokusan 4K3 Electronic, w/ Lighting Coil 12v1 10w with a timing of 5° bottom (BDC) to top dead centre (TDC) at 1000 rpm. In this work the main interest is around the assembly of the piston to cylinder relation.

A reverse engineered 3D Computer-aided design of the KTM engine has been developed so components and assembly could be further studied.

3.2.2. Crank shaft

The cranks shaft, shown in Figure 3.1, is a subassembly to the connecting rod. This removes any need for the rod needing any assembly. Each Crank plate is 128 mm diameter and both plates are made from a Carbon steel. The Crank pin has an outer radius of diameter mm and inner diameter of 15 mm with an internal chamfer of 1 mm, the component is made from a rolled steel.

Figure 3.1 Crank shaft assembly

3.2.3. Connecting rod

The connecting rod, shown in Figure 3.2, has a length measured from the two connecting points of 90 mm. The part is a single cast from a low alloyed tempered steel. The connecting rod has a bearing placed between the crank and the rod. However, to simply the relationship between the crank and piston a contact of frictionless was assumed.

Figure 3.2 KTM connecting rod

3.2.4. Piston

The piston, shown in Figure 3.3, has a 94.5 mm diameter to take into consideration thermal morphological stages caused by the heat. The piston supports a square cast iron compression ring with a slotted oil control ring. The material used is a 4032-T6 aluminium alloy. More detail is discussed on the compression ring in section 1.3.

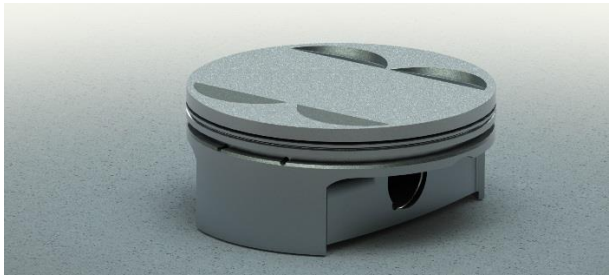

Figure 3.3 Piston

3.2.5. Cylinder

The cylinder block has a 95 mm bore (Figure 3.4) coated with Mahle grade nickel silicon carbide (NiKaSil), the cylinder is enclosed in a liquid cooling chamber.

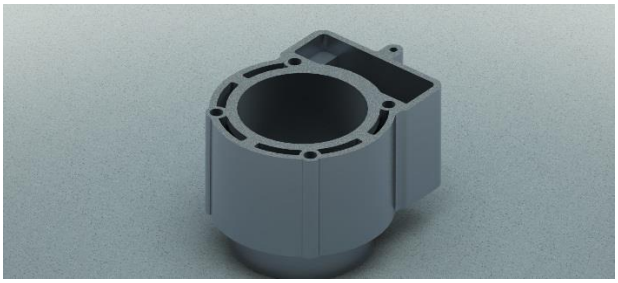

Figure 3.4 KTM 520 cylinder

The piston assembly dimensions for the KTM 520 are summarised Table 3-1.

Table 3-1 - Showing component details

Dimension (mm)	Component
0.16	Coating
95	Compression ring
94.95	Piston
95	Cylinder
115	Connecting Rod
31	Crank

3.3. Piston Design relation to the compression ring

Heat management is one of the most important factors to consider in the design considerations. The piston is moving the top compression ring from what was a common distance from the top of the crown of 7.5 – 8 mm this was then redefined 3 - 3.5 mm. This design feature was applied to the piston in the late 90's and can be found incorporated into many automobiles [95]. By making the crown to the compression ring distance smaller, the likelihood of possible miss burned fuel is minimised [2,95]. When combustion begins this dead zone area is not included in the process. This acting throughout the engine results in quite a large losses. However, by making changes to the position of the ring two major factors can alter the structural integrity of the piston. Firstly, the temperature, the ring and the top grove of the piston can be exposed to up to 500°C [2,3]. At high temperatures the possibility of material deformation and micro-welding on the lands is increased. With the material thickness of crown to groove becoming less this also introduces the possibly of cracking as there is a smaller amount of material to support the piston during operation (Figure 3.5).

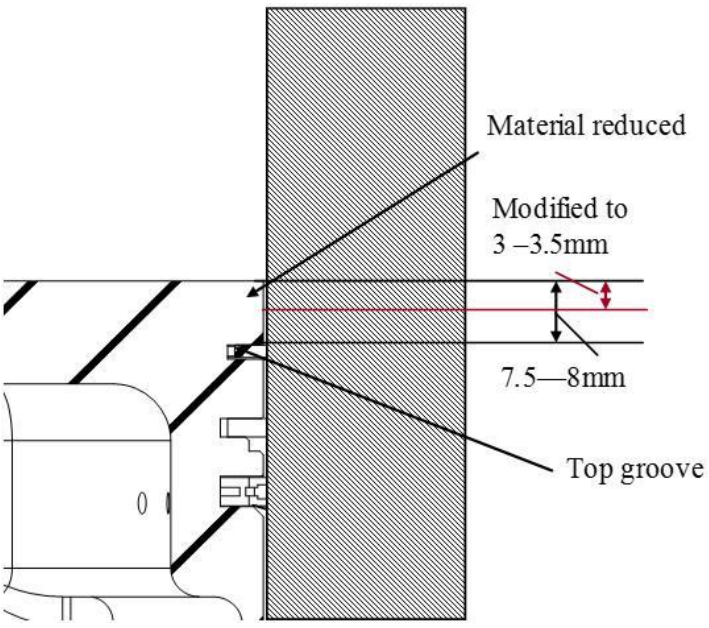

Figure 3.5 - Piston ring position changes

To counteract this, the top ring groove is anodized [96]. This incorporation can improve the durability. However, anodized profile can still fail above its optimum temperature.

Russ Hayes noted that when pistons were first designed for efficient heat transfer by creating a tapered surface on from the top of the crown down to the skirt [95]. As combustion occurs and the piston becomes gradually hotter, creating a thin worn strip profile on the piston.

Currently, elliptical profile from skirt to the oil control ring are used with CNC machining to ensure that as thermal expansion occurs the skirt is encouraged to form the round profile of the piston enabling better performance from the engine. The next design incorporation is to consider the upper section of the piston around the land area to have a smaller diameter compared with the lower half of the piston. By incorporating this into the design of the piston, this will allow the upper section of the piston to have more room for thermal expansion during operation [2,97]. These changes in the piston design allowed for the weight of a piston to be reduced from about 750 g to 600 g. With the piston redesigned the move of the gudgeon pin from 38.1/43.18 mm to 30.48/33.02 mm was allowed. Moving the pin from the present position to the new one has allowed for larger connecting rods, which in turn will improve the torque output of the engine and relieve the tension on the bearings and rings [98].

In conventional piston design the skirts would be designed with a large skirt roughly 64 mm in length. However, newer pistons now have a 38.1 mm length which can offer a number of benefits to the successful development of the piston. By lowering the length of the skirt the clearances from bore to piston are now reduced to 0.01 – 0.005 mm. Further development in super low friction coatings has now allowed for some piston manufacturers to produce what they claim to be zero clearance fit.

The final consideration in the design and development of the piston is the crown. The complex piston crown design is not produced for just one task, it is produced for controlling overall fuel immersions for the efficiency of the engine or the crown design is produced for controlling the motion of fuel to air ratio. One of the biggest problems that designers found during the engine development was the problem of detonation. However, due to the advancements of the piston developments engineers can produce fast burn crown profile which enables the engine to handle detonation at a higher level safely.

3.4. Ring ovality

This is a term that has been used for many years in the research and development of piston rings. It is a term that used to represent the distribution of contact pressure. The ring ovality is calculated by the difference between the ring gap over 180 degree and the 180 degree with a 90 degree offset. If positive ovality is found then this is an indication that a higher pressure is active around the gap (T_f), thus if negative is recorded then the opposite. This is visually represented in Figure 3.6.

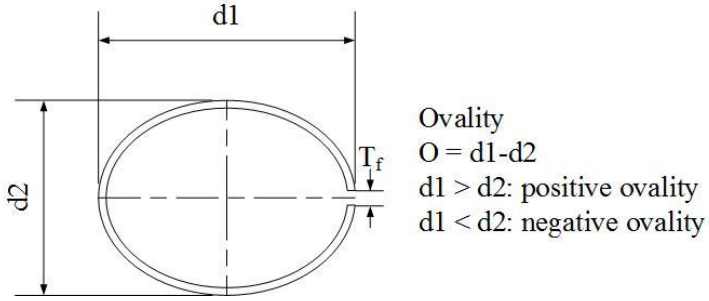

Figure 3.6 - Ring ovality

3.5. Compression ring design

3.5.1. Rectangular Ring

This design is one of the most recognised profiles of compression rings, with a rectangular cross face section, the shape will perform an adequate level of sealing under normal operating conditions. The ring is normally coated and manufactured with a parabolic face

or flat with edge chamfers (Figure 3.7) allowing for lubricating conditions to be continuous.

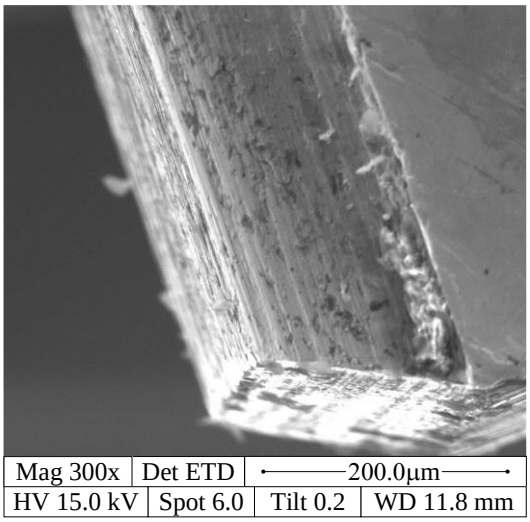

Figure 3.7 - Showing coating chamfer

These are typically applied in road production cars and motorcycle engines Figure 3.8. If the ring is manufactured with a contact chafer, the ring gap will also be chamfered, this is a design feature that is used to prevent damage to the cylinder liner. In some engines that run with a small cylinder clearance the gap chamfer can be up to 50% of the total gap area. However due to the small dimension of these chamfers the design feature will tend to go undervalued.

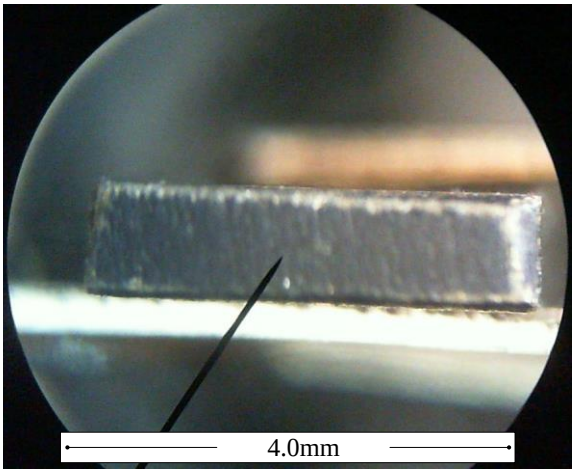

Figure 3.8 - showing the rectangular ring profile

This compression ring is what has been adopted by the KTM Company and is also seen in the test engine.

3.6. Compression ring material

The ring must seal the gap between the piston and the cylinder to ideally stop any gases passing by the piston, which transfer large amounts of heat from the crown of the piston down the cylinder liner. If there is any cavitation of the lubrication during operation there will be almost direct contact between the piston ring and the cylinder. If material to material surface contact occurs, there would be four different types of wear factors. Adhesive wear, occurs as two materials rub together with enough force to cause the less wear resistant surface to be removed. If the cylinder and ring are comparable in hardness, galling will occur where the two materials will be temporarily welded together causing material transfer between the two. Corrosive wear, is the degradation of the material when both corrosion and wear are active. The finial effect behaviour of wear on the ring is surface fatigue, where pitting and spalling will be the most contributing factors.

When considering the material compatibility there is two of the four wear noted of interest, abrasive and adhesive. When considering the compression ring, abrasive wear is the biggest factor that affects durability. Conditions where contact occurs the boundary and hydrodynamic lubrication will cease and the friction levels, will take over. However if the hardness of the cylinder and ring is the same then wear will occur on both components. Hence when selecting a compression ring for an engine there are methods that engineers can apply to lessen these effects. When the engine is first started the cylinder and ring will need to go through a running-in state, where they will both need to bed to each other, this means that there is an operational limit to the hardness. With these factors in mind studies are now done to examine the introduction of sacrificial surface

coatings designed to resist wear against the wall of the cylinder. However, the graphite element found in a cast iron cylinder liner means that wear will be much quicker than the ring, showing that engine manufacturers will also coat the cylinder liners in a Nikasil coating when cast iron is used. However, in some cases where the cylinder is assisted by a liner, the liners are coated with a ceramic nikel, which is done by the process of electrolytic deposition.

3.6.1. Cast Iron

Gray cast irons are ideal ring material for passenger cars. However, the ring must always be of a sufficient size (around 1.5-1.7 mm) to ensure performance. The rings need to be thinner and low tension to create better performance out of smaller displacement engines. This has now increased the operating loads on the rings. When placing a piston ring into a system material compatibility is important. If an uncoated grey cast iron ring is placed into a system with a gray cast iron liner the material is combatable however it is brittle. A simple way of testing for gray cast iron is if the ring is bent to the yield point the ring will snap rather than bend. Under examination the grain structure of this material reveals sharp rectangular grains in a highly dense structure Figure 3.9.

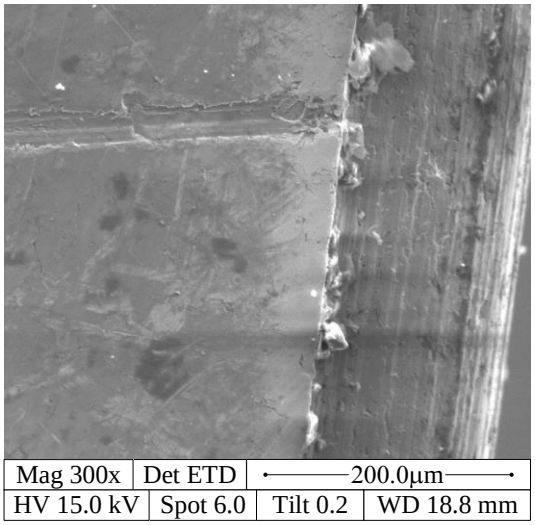

Figure 3.9 - SEM, KTM piston ring

Nakada [92] noted that rings now being designed are a narrow thickness of 1.5 mm. Gray cast iron can perform well however if the engine is subjected to heavy loads or continuous detonations the ring can lead to failure. Detail of gray cast iron piston ring grades can be seen in Figure 3.10. As large blows are delivered to the system that are produced by the colliding flames, fronts shock load the rings which can lead to the ring breaking in the engine. This damage can lead to loss of cylinder compression and oil consumption problems. Gray cast iron can be found in various grade's, intermediate this is be produced with a harder (28) HRC minimum. Rings that are made to this standard tend to be uncoated and only used for systems that use a second compression ring. However, these rings can be used for two engine compression rings. This material is used for applications such as this Chrome or MoS_2 is coated (most of the time) onto the contact face of the compression rings.

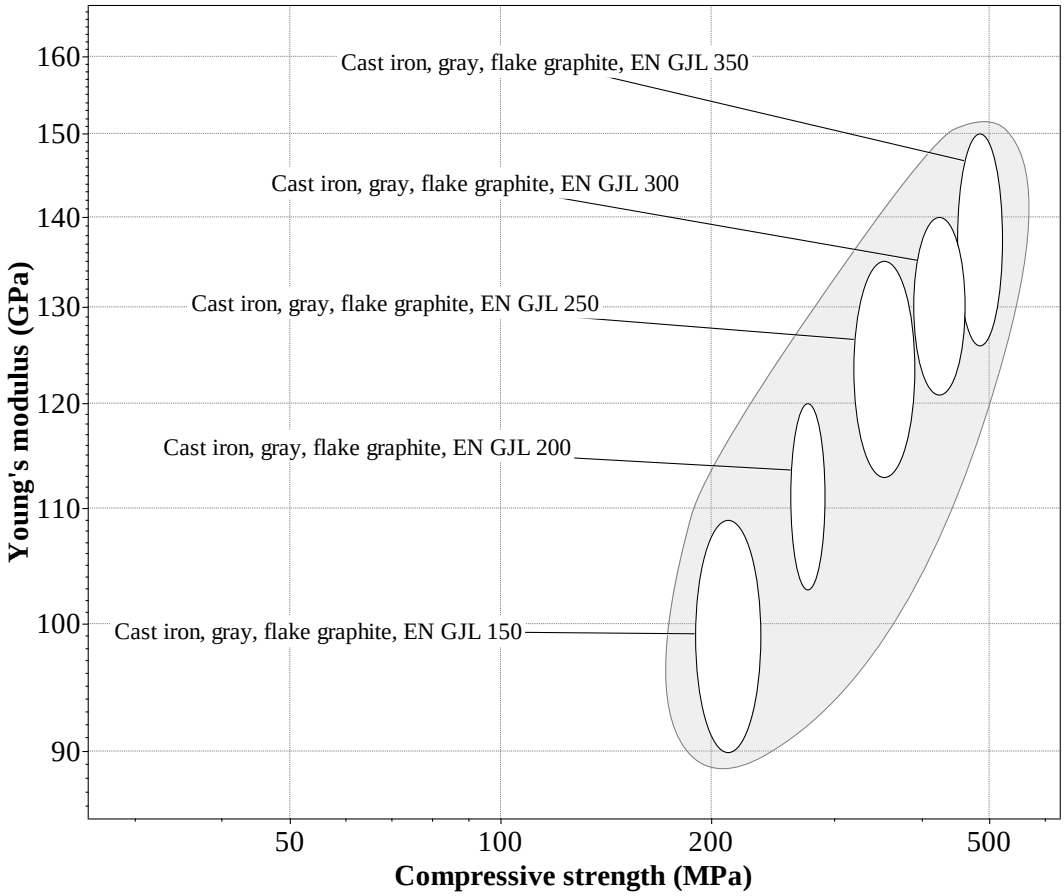

Figure 3.10 - Common gray cast irons found in compression rings [99]

Ductile iron has been in use for some time, one of its main uses for the automotive sector is in heavy duty trucks. The main reason for this is that the material possesses almost twice the strength of gray cast iron due to ductile iron's nodular microstructure. The material can bend without breaking and can withstand more stress. Hence, production car companies have used ductile iron for their compression rings for many years, cars that use a turbo-charger and high output applications tend to also use these rings for this reason. Some of these materials are shown in Figure 3.10.

Ductile iron has been a popular choice in the race industry because of its ability to perform in highly stressed environments. This material however is not easy to machine and can tend to costly to manufacturer. Also ductile iron is not 100% compatible with cast iron

cylinder walls, during operation the material will tend towards scuffing and galling. A possible solution for this has been to coat the contact face with either Cr or MoS_2.

Ductile iron is around double the strength of grey cast iron, steel is around double the strength of ductile iron. Therefore, in theory steel rings have the ability to support far greater applied forces than its predecessors. The problem with the use of steel in the piston ring is the manufacturing procedure can be quite pricey compared to the other methods noted above. However, generally speaking the use of steel rings will provide better breakage resistance, a greater heat resistance and a longer service life overall.

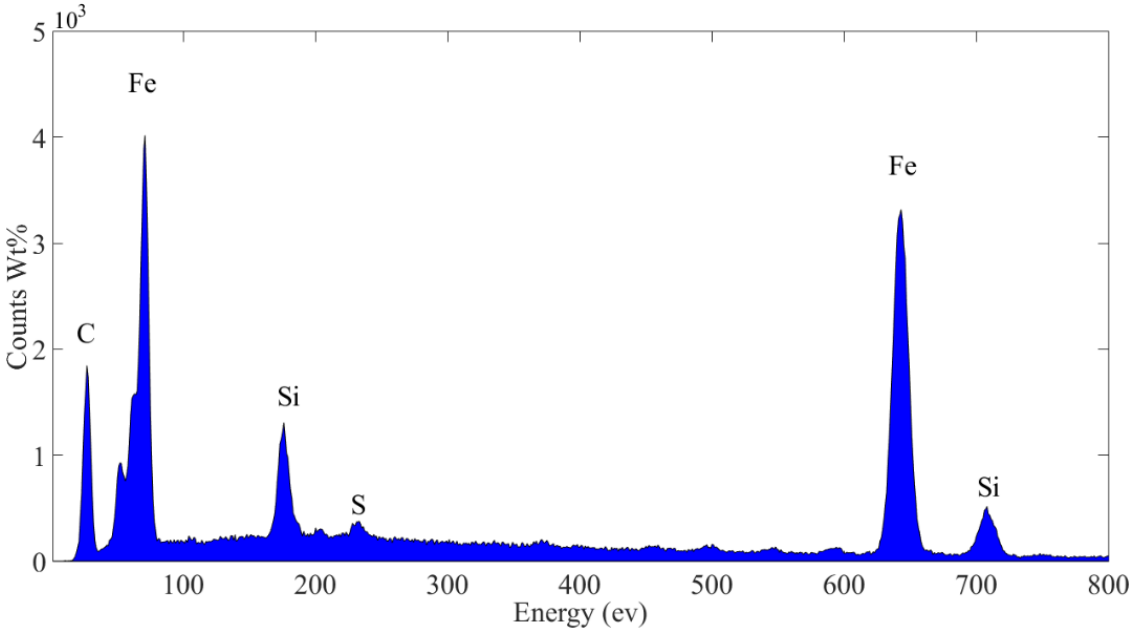

Figure 3.11 - KTM compression ring sample

Figure 3.11 shows the results from the Energy-dispersive X-ray spectroscopy (EDAX), where a sample of the ring was taken to examine the material content. These results were then cross examined with materials data bases which strongly indicated that the compression ring material was EN GJL 250 grade gray cast iron.

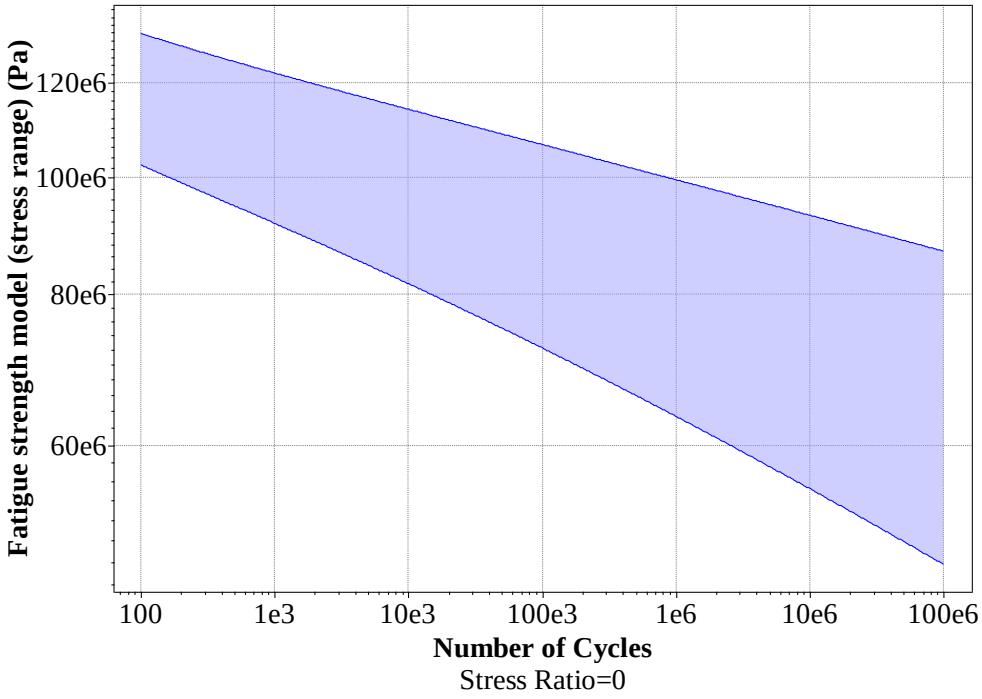

Figure 3.12 - Showing the stress ratio of ENGJL 250 unloaded[99]

Figure 3.12 shows the stress ratio against fatigue, showing the operational band of the material.

Table 3-2 - ENGJL 250 thermal and mechanical characteristics[56]

Material	Young's Modulus	Thermal conductivity	Coefficient of thermal Expansion	Poisson's Ratio	Abrasive Particle hardness
ENGJL 250	184 GPa	46 W/(mK)	11 µm/m-°C	0.26	4.904GPa

Table 3-2 shows that material properties used for modelling the KTM 520 compression ring.

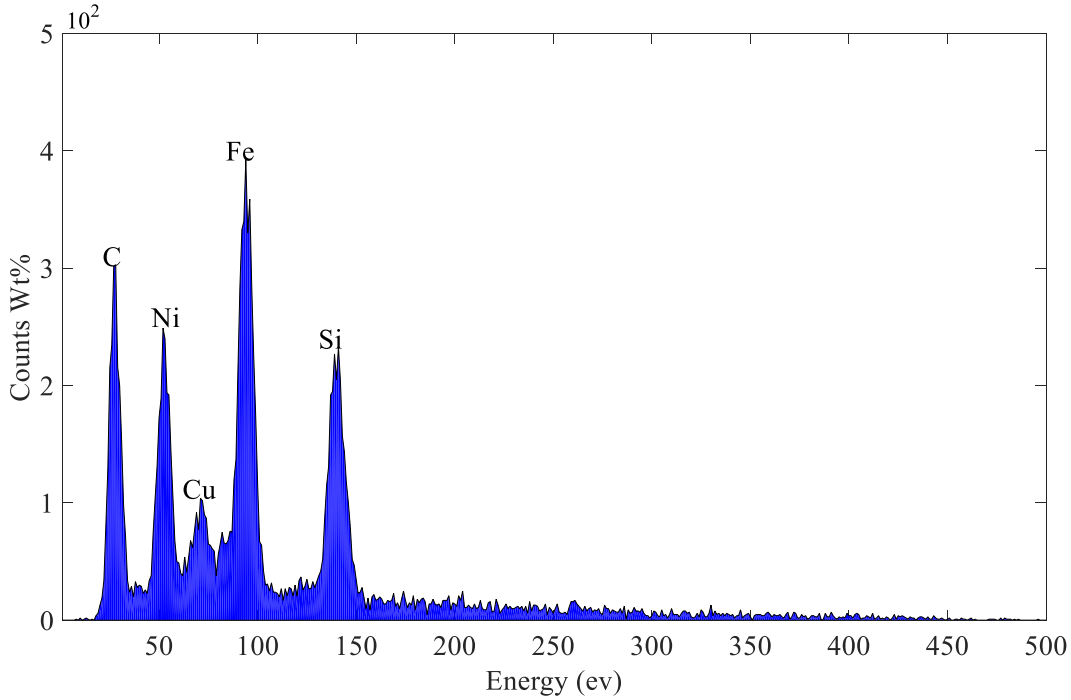

Figure 3.13 - Showing Omega compression ring surface composition

A second batch of compression ring samples where purchased from a company. Figure 3.13 shows the surface content recorded within the material with EDAX. Through further cross examination confirms the material as ENGJLA XNiCuCr15 grade of grey cast iron. However, there are slight variations with the recorded material to the purchased material.

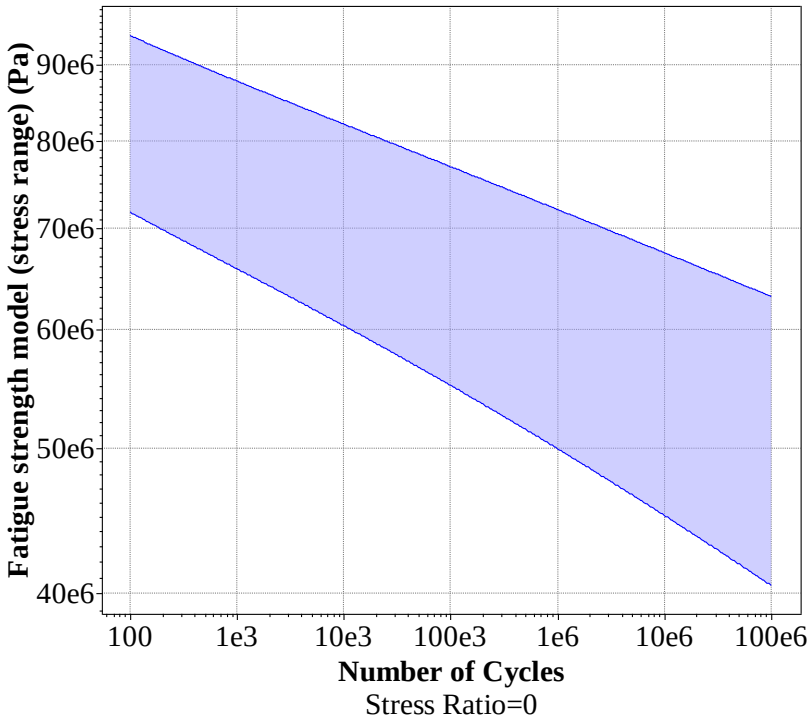

Figure 3.14 - Showing the stress ratio of ENGJLA XNiCuCr15 unloaded [99]

Figure 3.14 shows the Omega compression rings unloaded. The material is a less performance grade that what is seen from KTM standard production material.

Table 3-3 - ENGJLA XNiCuCr 15 thermal and mechanical characteristics[56]

Material	Young's Modulus	Thermal conductivity	Coefficient of thermal Expansion	Poisson's Ratio	Abrasive Particle hardness
ENGJLA XNiCuCr15	125 GPa	41 W/(mK)	10 µm/m-°C	0.27	4.74GPa

Table 3-3 shows that material properties used for modelling the Omega compression rings.

3.6.2. Steel

Steel has been the ideal choice when in need of solving problems in highly stressed engines for example high performance engines. One of the most commonly used steel samples in industry currently for the piston ring application is SAE 9254. Currently, this grade of steel has attracted significant interest for the high performance application. However, to manufacture the material for operation can be quite an expensive process. Studies have shown that bainitic ferrite plates at low temperatures are able to be manufactured. This procedure results in a material with mechanical properties that allow for increased resistance to tempering. Cruz Junior [100] conducted a study investigating the microstructure in SAE 9254 steel during heat-treatment below the martensite hardened start temperature value. Once the state was established, the same sample was tested under tempering various temperature values. Each sample was analysed using the Vickers microhardness measurements tests after quenching and tempering was applied. It was found that all the isothermally treated samples contained martensite, bainitic

characteristics. Further analyse to the study found that optimum performance of the material was found at 450°C. Some examples of these materials are shown in Figure 3.15.

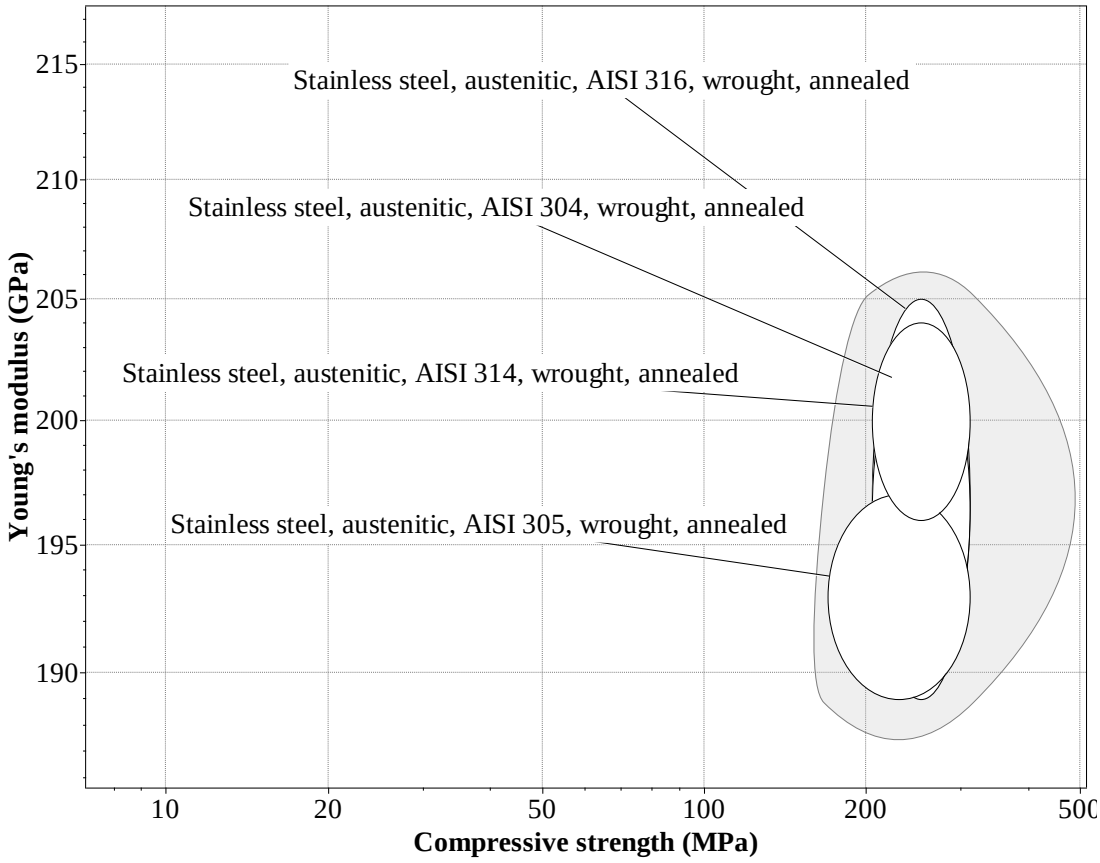

Figure 3.15 - Common steels found in compression rings [99]

Fuel efficiency is the main goal for all research internal in combustion engine, the compression ring contact to the cylinder liner contributes near 5% to the fuel efficiency, due to the seal between both components. When analyses is conducted on this behaviour the effect is often idealised, such as the contact faces and the isothermal conditions. Morris [68] presented a new analytical thermal solution that shows the average flow for the contact. The work presented showed simulated conditions that showed the power loss in normal driving operation. The study showed that power loss from the ring, is mainly due to the viscous shear from the engine when operated under cold conditions, as when the engine operates in hot conditions the boundary friction will dominate.

Table 3-4 - SAE 9254 thermal and mechanical characteristics[56]

Material	Young's Modulus	Thermal conductivity	Coefficient of thermal Expansion	Poisson's Ratio
SAE 9254	200 GPa	44.5 W/(mK)	12 µm/m-°C	0.29

Table 3-4 shows that material properties used for modelling the SAE 9254 compression ring.

3.7. Compression ring wear reduction methods

The piston ring was initially designed to create a seal between the piston and the cylinder wall. The operational design of the piston ring proved to be one of the most successful in the actual design. However, problem's began arise as performance of engines was increased the piston ring was limited in its life span. Hence, this influenced the investigation of methods to resist wear of the ring.

Coatings

Variations of engine design and operational conditions can influence the selection of coatings for the piston ring. Due to environmental legislations, Cr coatings have been abandoned to more sustainable coatings such as chromium nitride (CrN) or titanium nitride (TiN). Thin, hard coatings produced by physical vapour deposition (PVD) or chemical vapour deposition (CVD) include coating compositions like TiN, CrN that are exclusively used for small series production for competition engines and selected production engines [101]. MoS_2 based coatings deposited by a variety of plasma spraying technologies such as Atmospheric Plasma Spraying or High Velocity Oxygen Fuel Thermal Spray are also found on race engine compression rings.

In the conditions of an engine where the cylinder is coated with Nikasil and the piston ring is grey cast iron, the most compatible material of choose is MoS_2 which is used as a wear resistant coating. As reported by [82,102] due the atomic structure of MoS_2 being HCP as shown in Figure 3.16 -, when the material is placed in temperatures exceeding 400^{o}C a single layer will have possibilities of a ripple effect.

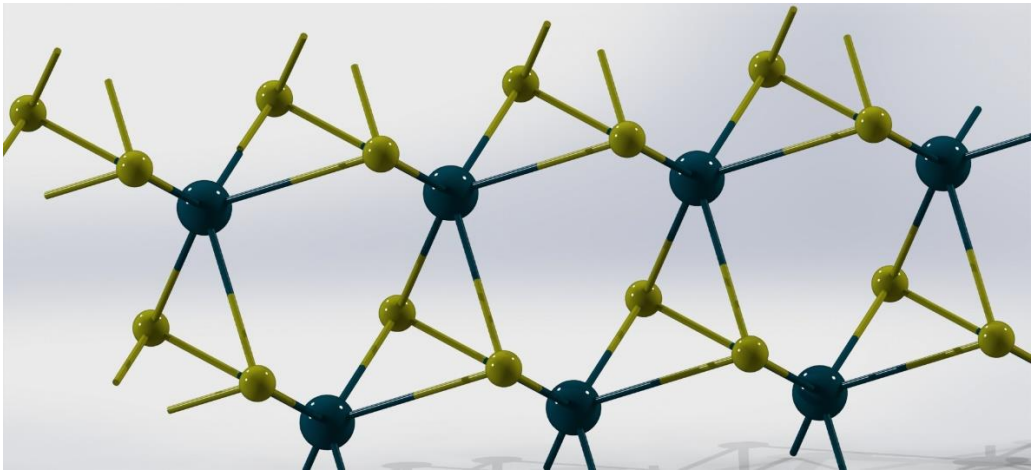

Figure 3.16 - MoS_2 atomic structure

During the running-in the high combustion temperatures cause thermal expansion of the material. Su [103] produced a study to examine the behaviour in coupling conditions and also under heat behaviour of MoS_2. It was noted that when placed into heats exceeding 400°C the single layer coating would go through thermal deformation, however will still remain in fully operational conditions. As heat is introduced the atomic bonds are drawn closer creating a much more brittle structure. However, during this operation MoS_2 will be more susceptible to shearing, or as termed by Su “ripple” or “folding” effect.

Materials in powdered form are placed into high temperature plasma flame, where they are heated at an extremely high rate. At the same time the materials are accelerated to a

high velocity. The material impacts the surface and rapidly cools forming the surface coating. This process is more commonly known as cold processing.

The plasma molybdenum was first developed as an alternate method for a wear resistant coating. It was noted by Chaika [84,104] that chromium-plating process was the most widely used method in industry to apply a wear resistant coating onto piston rings. However, this method was found not to increase engine life, and the process is extremely time consuming and costly. Molybdenum coatings that are used extensively in other countries have been found to have half/one-third wear resistance to what can be seen in chromium plated piston rings. Piston rings that have had plasma spray applied with the 11Kh18MVD and 4Kh13 steel parameters; the coatings improve the performance of the engine and also cause a lower running cost. It was found that even though the plasma molybdenum provides a lower resistance than chromium plated rings; the wear resistance was comparable to the chromium.

Table 3-5 - MoS_2 thermal and mechanical characteristics[81,99]

Material	Young's Modulus	Thermal conductivity	Coefficient of thermal Expansion	Poissons Ratio	Abrasive Particle hardness
MoS_2	124 GPa	34 W/(mK)	10.7µm/m-°C	0.125	4.916GPa

Table 3-5 shows the material characteristics of MoS_2 as recorded in two studies that examined both thermal and mechanical behaviours of the material.

3.7.1. Engine Sleeves

The engine sleeves is one of the many of parts inside the engine that has seen very little change since 1763 when James Watt created the first engine [105]. However, in 1967 a patent was produced to create a coat around the standard bore for more efficient

combustion during process. This assists the process of creating a better seal in the system [106]. In the early 1970's nickel silicon carbide (NiKaSiL) was introduced as a wear resistant coating for cylinders, the coating was designed to be compatible with grey cast iron [107].

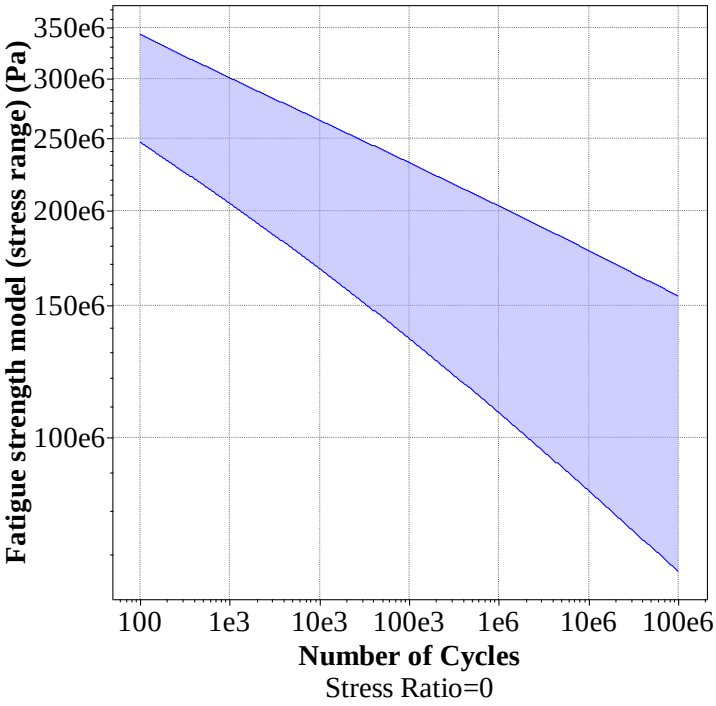

Figure 3.17 - Showing the stress ratio of Nikasil unloaded [99]

Figure 3.17 shows the material stress when unloaded, this material is typically used in area where pressure, corrosion and wear resistance is needed.

Table 3-6 - Shows the mechanical properties of Nikasil [99]

Material	Young's Modulus	Thermal conductivity	Coefficient of thermal Expansion	Poissons Ratio	Abrasive Particle hardness
NiKaSiL	165 GPa	42.1 W/(mK)	12.5µm/m-°C	0.31	6.632GPa

Table 3-6 shows that material properties used for modelling the NiKaSiL cylinder coating [108].

3.8. Lubrication

3.8.1. Lubrication purpose

First forms of lubrication for the combustion engine were vegetable oils. However, many variations could be found in use. This was common practice until the late 1800's, when the society of automobile engineers began examining the lubrication. The main purpose of the lubrication system is to reduce wear and reduce the heat at contacting surfaces. The heat and wear cannot be reduced to zero but the lubrication can lower it to levels. The lubrication system in an engine also reduces oxidation that could form during system's operation. This protects the system from rust and allows the system to transmit mechanical power in hydrodynamic fluid power. The lubrications system also creates and environment where the dirt and water are removed [109].

The lubrication removes heat and reduces wear by introducing a lower viscosity to the system. The lubrication allows two materials with a relatively high coefficient of friction to be in contact minimizing the amount of wear. The surfaces are replaced by a material that has a much more desirable coefficient of friction. Lubrication can be used in gaseous, solid and liquid forms.

When the system is un-lubricated the resistance to move is far greater and therefore greater wear occurs. However, when lubricated the system is free to move with more resistance to wear [110].

3.8.2. Liquid lubrication

The liquid lubrication is commonly produced from non-petroleum and petroleum based synthetic compounds. The thickness of this oil is often related to the thickness or viscosity. Petroleum-based oils are produced from crude oil. During early years of car manufacturing the major companies produced cars with their own type of fuel and oil

method. In the early 1900's The Society of Automotive Engineers was established and noted the need to start grading oils and fuel types. They established the SAE kinematics Viscosity of engine oil table [111] example Table 3-7.

Table 3-7 Showing the SAE viscosity rating table [111]

SAE Kinematic Viscosity of Engine Oil – Viscosity at 100^{o}C	
$mm^2 \cdot s^{-1}$	SAE Rating
16.3-21.9	50
12.5-16.3	40
9.3-12.5	30
5.6-9.3	20
Less than 5.6	10

3.8.3. Oil additive mechanisms

There are three mechanisms of oil consumption that can be found on the ring pack area. When the engine is active the oil that is still present on the liner walls and on the top of the rings evaporates into the combustion chamber and a large percentage is carried away with the exhaust gasses. The oil is also through from the piston motion inertia into the chamber. The gas that is being pushed back into the combustion chamber contains entrails of oil; again all of these factors are removed by the exhaust gasses. The evaporated oil traces that are left behind will pass between the liner and top ring. However, it has been shown that the oil amount that is present when the piston is at BDC is dependent on the scraping motion of the ring during performance [2,112]. The carbon build on the ring from the evaporated oil in the combustion chamber leads to carbon build-up on the ring and liner.

The compression ring can suffer from two operational difficulties the first being the phenomenon known as "coking". This phenomenon is where the ring is found to have

large levels of carbon deposits on it. This build leads to sticking of the ring. To counteract this phenomenon research lead to the inclusion of detergents within the oil, the detergents are present in the lubrication to neutralise the sulphur that is present in combustion gasses [113].

When calculating the steady state corrosive wear in the system this method is incorporated to determine the minimum film thicknesses. The second component that can offer performance problems in lubrication is the phenomenon known as ring blow-by. In all piston reciprocating systems with gas flow, there will always be a flow in and out of the gap clearance between the land, the ring groove land and the cylinder bore. In the gasoline engine these aspects can account for chamber volumes levels of 3%. Hence, because the engine consists of an amount of un-burned fuel this is a major source of hydrocarbons, leading to power loss in the engine. This gas can leak past the ring pack (blow-by) and the piston skirt leading to the Crank-case [1].

One of the possibility's that could be causing the blow-by phenomenon is the starvation of ring lubrication [114]. Their work suggests that to model a starved lubricated ring (Figure 3.18), a flow algorithm must be implemented in a non-axisymmetric method.

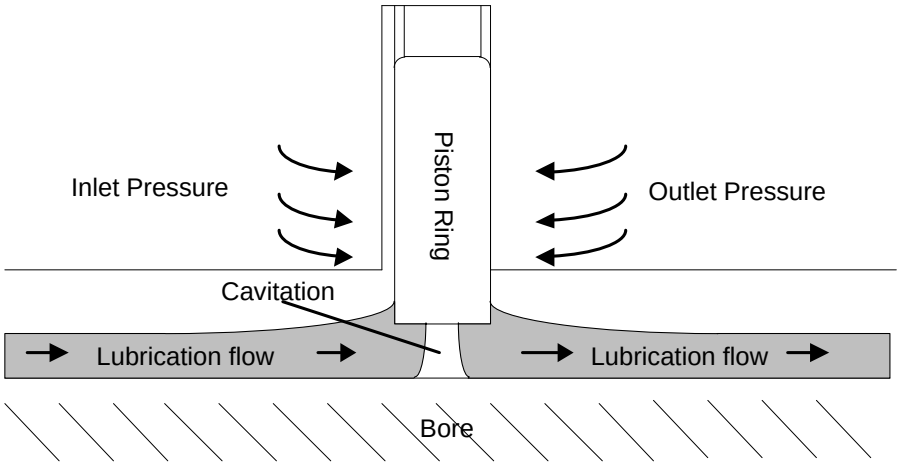

Figure 3.18: Show the lubrication creating cavitation areas

It has been suggested by Priest et al. [13] that the ring cavitation is a result of the piston ring's early life what is also known as the running-in period. It was found that the first 120 hours of the top compression ring suffers its most wear as when the ring reaches TDC the lubrication is at an extreme low. Further to this they have also suggested that to improve the running-in period of the ring would lead to a better overall performance of the engine. Oil additives are added to the base oil for better performance. This allows for unique properties of the lubrication such as the ability to hold carbon emission from the fuel to be held in stasis stop the hardening process.

3.8.4. 10W-50 Putoline oil.

This oil typically used in off-road motorcycles. As this is a 100% synthetic oil this makes it an ideal choice for use, as it is more compatible with modern engines.

Table 3-8 Lubrication characteristics [115]

Density at 15 °C, kg/l	0.860
Viscosity -25 °C, mPa.s	4610
Viscosity 40 °C, mm^2/s	116,40
Viscosity 100 °C, mm^2/s	17,50
Viscosity Index	171
Flash Point COC, °C	230
Pour Point, °C	-39
Total base number, mgKOH/g	8.3

Table 3-8 details the operational characteristics of the engine lubrication used in this work.

3.9. Conclusion

There are two paths that can be taken when designing the engine for operation, steel or cast iron. From examining the work shown the SAE 9254 grade steel is an ideal choice for said tasks, however the material does not prove cost effective for manufacture and only high end companies will tend to use them. Also the development of new ductile cast irons are proving to be an adequate replacement for the steel.

The two main compression rings that are most in active use in the 4 stroke motorcycle engine is the torsional twist ring and the same geometry as defined by Ramsbottom, the rectangle cross profile. The studies shown do also note that the coating MoS_2 will go through morphological stages which indicates that during running in, the coating will go through a hardening process.

Further work should consider the compression ring in the running-in state. The ring will be based on standard ISO standard [116] geometry. As the piston ring will also be subjected to a heat rise, which will lead to heat deformation due to the coefficient of thermal expansion. To model these elements a mathematical model methodology is used and then a flow is needed. However a full definition of the piston ring and operation will give geometry consideration and assist in the development of the flow chart.

CHAPTER 4 - MATHEMATICAL MODELLING OF THE PISTON ASSEMBLY DYNAMICS AND TRIBOLOGICAL INTERFACES

4.1. Introduction

The methods used to calculate the dynamics of the cylinder, piston, piston rings, connecting rod and crank are presented in this chapter. In order to examine the performance of an engine during the running-in, a virtual representation of a full engine has been developed. The developed system was able to simulate all working components directly connected to the compression ring. The ring twist, radial and axial motion, lubricant and friction between the ring and cylinder liner affect the ring running-in and performance [3,9,14,53,54,58,117]. Each equation to support the fundamental operation of the internal combustion engine are found in [2,3,115].

The combustion process is complex, the description of this process has been segmented as described in Figure 4.1. Engine dynamics have been first considered, while forces and torque where later added on the system. Pressure was also considered with lubrication leading to the finial parts were heat and also wear are added to the model to build a good representation of the engine cycle process, this is reflected in Figure 4.1. In this chapter each area from this process is represented by a mathematical equivalent.

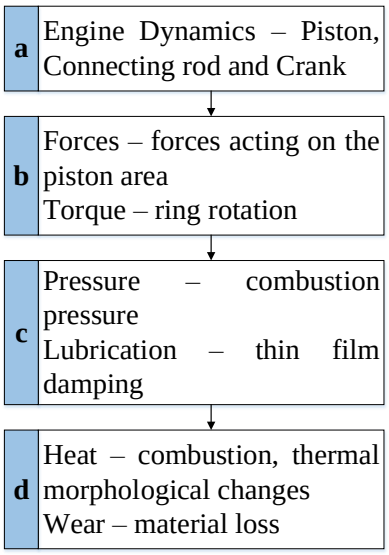

Figure 4.1 - Model complication process

4.2. Engine Dynamic Modelling

4.2.1. Mathematics of reciprocating mass and inertia forces

The reciprocating mass problem can simply be calculated with lubrication film thickness added to the model. By deriving the method of calculating the reciprocating mass, inertia forces are formulated which is typically denoted in the form of a system diagram.

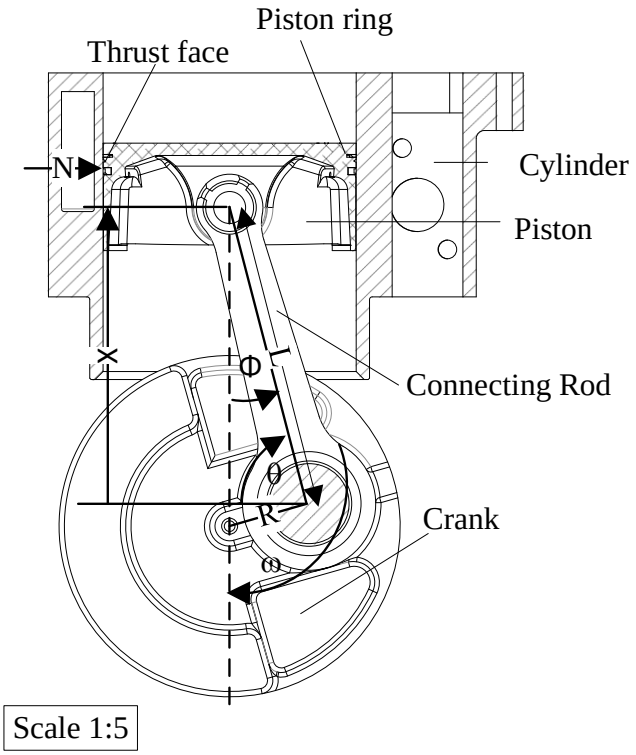

Figure 4.2 - KTM 525 engine, labelled for the crank-slider mechanism

The action of travelling from TDC to BDC (see chapter 1) and back is known as the reciprocating mass problem reflected in Figure 4.2.

$$x \approx R\left\{cos\theta + \frac{L}{R}\left[1 - \frac{1}{2}\left(\frac{R}{L}\right)^2\left(\frac{1}{2} - \frac{1}{2}cos2\theta\right)\right]\right\} \quad \textbf{(4.1)}$$

(4.1) shows the calculation to predict the position of the reciprocating mass where R, L, x and θ are the crank radius, connecting rod length, piston mas position and crank rotation by time respectively. The equation can be differentiated to give the velocity of the mass. The velocity is a function of crank angle and is given by:

$$\frac{dx}{dt} \approx -R\omega\left[sin\theta + \frac{1}{2}\left(\frac{R}{L}\right)sin2\theta\right] \quad \textbf{(4.2)}$$

The acceleration of the reciprocating mass $\frac{d^2x}{dt^2}$ calculated in (4.3) is differentiated from (4.2)) to calculate the acceleration as:

$$\frac{d^2x}{dt^2} \approx -R\omega^2\left[cos\theta + \left(\frac{R}{L}\right)cos2\theta\right] \quad \textbf{(4.3)}$$

These equations are used to calculate position, velocity and acceleration. Boundary conditions are determined using Stone method, reciprocating mass axial force (F_r) is mathematically expressed in (4.4)) as:

$$F_r \approx m_r R\omega^2\left[cos\theta + \left(\frac{R}{L}\right)cos2\theta\right] \quad \textbf{(4.4)}$$

$F_r, m_r, \omega, R, L, cos\theta$ and $cos2\theta$ are respectively the axial force of the reciprocating mass, piston mass, angular velocity, crankshaft throw, con-rod length, primary term and secondary term. The primary inertia force (P_f), secondary inertial force (S_f) and total inertia force (T_{If}) are calculated as

$$P_f = m_r R\omega^2 cos\theta \quad \textbf{(4.5)}$$

$$S_f = m_r R\omega^2 \cos(2\theta)\left(\frac{R}{L}\right) \quad \textbf{(4.6)}$$

$$T_{If} = P_f + S_f \quad \textbf{(4.7)}$$

As pistons are manufactured to have a clearance of 50 μm and during operation [45] a presumption is made that the piston will be an almost cylindrical shape, this will give the component the ability to tilt.

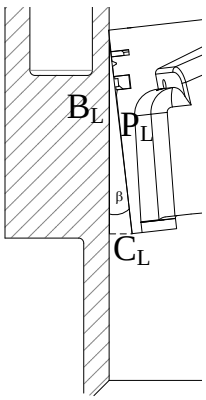

Figure 4.3 - Schematic representation of the piston tilt

A schematic representation of the tilting effect is shown in Figure 4.3, where β is the contact angle between the piston and the cylinder wall. Pythagoras's theorem was used to give possible contact angle expressed as:

$$\sin(\beta) = \frac{C_L}{P_L} \tag{4.8}$$

Where C_L and P_L are the piston cylinder clearance and piston length respectively.

4.2.2. Compression ring rotation and torque

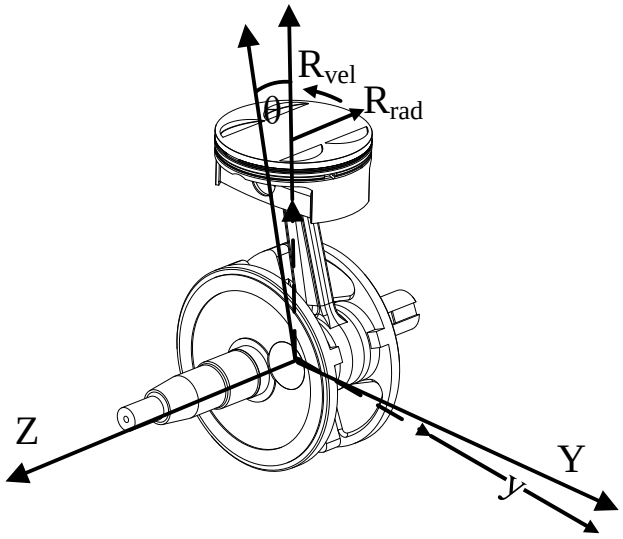

Figure 4.4 - KTM 525 with Euler rotation and angular momentum variables

The vector forces (F_r) generated by the reciprocating motion will travel along the connecting arm and through the piston as shown in Figure 4.4. The force is then projected to the compression ring geometry where conservation of angular momentum takes effect

[118]. Currently there is no consensus on the projected vector making contact or not with the compression ring encouraging rotational behaviour on the mass, this is calculated as:

$$L_m = R_{rad}R_{vel}R_{mass} \quad \textbf{(4.9)}$$

Where L_m, R_{rad}, R_{vel}, and R_{mass} are respectively the angular momentum acting on the mass, the ring radius, the ring velocity and ring mass [118]. However rotational axis due to the torque acting on the system will produce a torque that acts upon the ring, indicating that the compression ring will wear within a four degrees of freedom. The torsional aspect of this effect is represented by:

$$\sum \tau_i = L_m \alpha \quad \textbf{(4.10)}$$

Where α is the angular acceleration acting on the system. Each equation will allow for the dynamic prediction of the ring rotation.

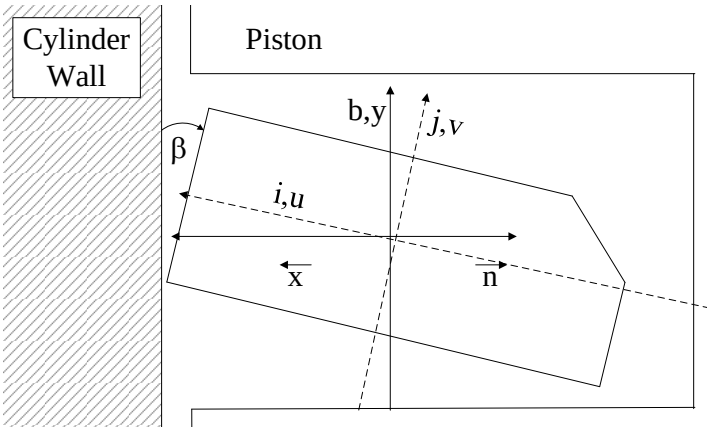

Figure 4.5 – Torsional axis

To consider the effect of torsional twist and rotation of the ring, Euler rotation and Love theorems were defined in three equations[54]. Federhofer [119] defined a single plane were (i) and (j) define the geometry coordinates and by equating both coordinates τ_1 is the torsion displayed in Figure 4.5. These equations are expressed as:

$$\Delta k_{i_r} = -\beta k_{j_r} - \frac{d^2 v}{ds^2} \quad \textbf{(4.11)}$$

$$\Delta k_{j_r} = +\beta k_{i_r} + \frac{d^2 v}{ds^2} \quad \textbf{(4.12)}$$

$$\tau_1 = \frac{d\left(-\beta + k_{j_r} u_o + k_{i_r} v_o\right)}{ds} \quad \textbf{(4.13)}$$

Where coordinates (u_0, v_0) are obtained by the twist angle β, of the coordinates (i_r, j_r) as shown in Figure 4.3 and Δk and τ_1 are respectively the change of the curvatures and torsion in the ring.

4.3. Pressure & thin film

Pressures will build during the combustion process in the cylinder bowl and around the compression ring, pressure variations depend on the stroke of the engine. To assist in the freedom of movement, lubrication is introduced to allow the piston to move smoothly throughout the combustion process.

Previous work done by Chittenden [120] examined gas pressure forming during the engine combustion cycle, who concluded that gas are acting on the piston ring pack throughout the whole cycle. . These pressures were only noted to be significant during a minimum proportion of the engine operation.

4.3.1. Minimum film thickness and distribution

The most recognised method for simulating thin films lubrication is Reynolds equation. The cylinder is fixed with respects to the piston ring surface, but height and changes can change in the position. Lubricated film shape (H_{ring}) and pressure (P_{bar}) can be calculated as follow:

$$H_{ring} = h_{min} + \left(\frac{1}{Ring_{rad}}\right)\left(x - \frac{L_1}{2}\right)^2 \quad \textbf{(4.14)}$$

Where h_{min}, $Ring_{rad}$, and L_1 are respectively minimum film thickness, ring radius of the curvature and compression ring height. The film pressure is calculated as:

$$P_{bar} = \frac{{H_{ring}}^2}{\eta v L_1} \quad \textbf{(4.15)}$$

Where η, v are respectively viscosity and velocity. While the piston moves from BDC to TDC, it is assumed that the compression ring will twist, creating a scraping effect. The average roughness was calculated as:

$$R_a = \frac{1}{n}\sum_{i=1}^{n}|y_i| \quad \textbf{(4.16)}$$

The roughness is equated and also the root mean square of the surface using

$$R_q = \sqrt{\frac{1}{n}\sum_{i=1}^{n} y_i^2} \quad \textbf{(4.17)}$$

Where in both equations n and y_i are respectively the number of points and the height of the position. The maximum profile peak height (R_p), maximum profile valley depth (R_v) and maximum height profile (R_t) have been measured as shown in Figure 4.6.

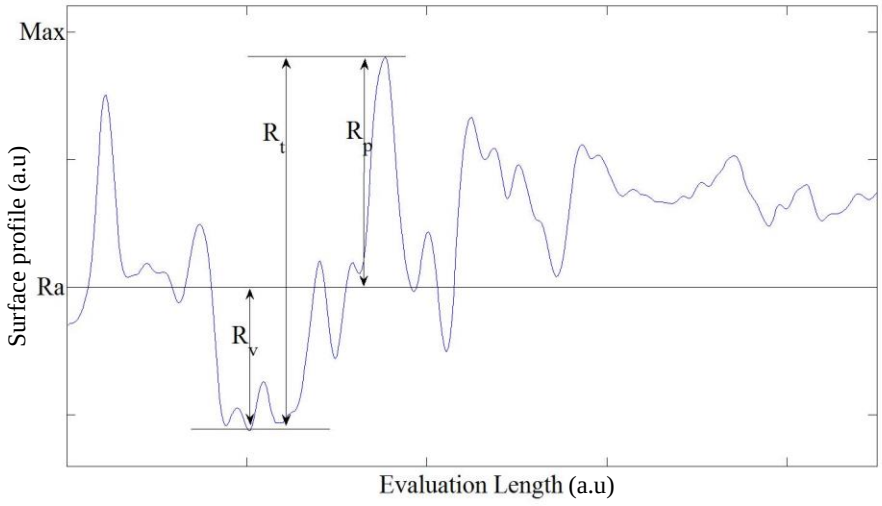

Figure 4.6 - Schematic of maximum peak, valley and height profiles

4.3.2. Combustion and ring pressure

The compression ring used in this work, is the standard KTM design, uses the common rectangular profile with a contact chamfer applied to the top of the contact face. When the ring rests in a perpendicular position of the cylinder liner, Reynolds equation becomes unstable leading to instability in the simulation work. A possible method to resolve the instability is to use the gas pressures calculation method [54].

A common method used to calculate the pressure within the combustion bowl is to consider the ideal gas equation [5,53,70].

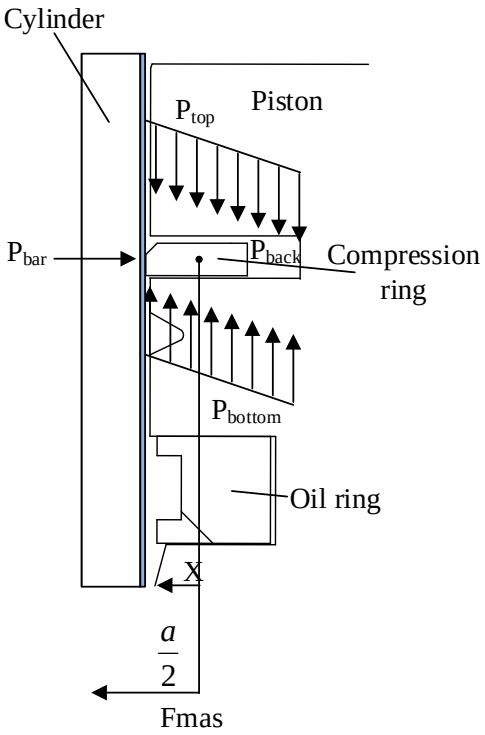

Figure 4.7 -Typical pressure distribution during engine cycle

The ideal gas equation was used to predict the pressure output from the piston within the combustion bowl using (4.18)).

$$p = \frac{m_r}{V} G_c T \quad \textbf{(4.18)}$$

Where p, m_r, V, G_c and T are respectively pressure, mass, current volume, and specific gas constant and temperature. The gas force (Gas_F) and the gas moment (Gas_I), which are independent of the pressure build from behind the ring P_{back}. A linear formulation of pressure that builds in the top clearance of the ring is equated with the following equations [53].

$$p(x) = -\frac{1}{2}(P_{bottom} + P_{back}) - \frac{x}{A}(P_{bottom} - P_{back}) \quad \textbf{(4.19)}$$

When the reciprocating mass forces are positive, acting towards TDC the pressure acting from the chamber will act negative as shown in (4.19), hence when the mass travels from TDC to BDC the pressure equation becomes positive as shown in (4.20). The bottom pressure of the ring (P_{bottom}) is the crank case pressure.

$$p(x) = +\frac{1}{2}\left(P_{top} + P_{back}\right) + \frac{x}{A}\left(P_{top} - P_{back}\right) \quad \textbf{(4.20)}$$

The resulting gas pressure can be calculated by summing (4.19), (4.20) as:

$$p(x) = -\frac{1}{2}\left(P_{top} - P_{bottom}\right) - \frac{x}{A}\left(P_{top} - P_{bottom}\right) \quad \textbf{(4.21)}$$

Fully flooded conditions have been applied, it is assumed that the lubrication regime is hydrodynamic and the radial ring forces are acting on the ring face. The pressure from the top, bottom and back of the ring are calculated, the positions where Reynold's equation becomes unstable are therefore resolved.

$$Gas_F = -\frac{1}{2}A\left(P_{top} - P_{bottom}\right) \quad \textbf{(4.22)}$$

(4.22) shows the equivalent method of calculating the acting gas force of the compression ring.

$$Gas_I = -\frac{1}{12}A^2\left(P_{top} - P_{bottom}\right) \quad \textbf{(4.23)}$$

(4.23) shows the equivalent method for calculating the acting gas moment on the compression ring.

Pressure is has been represented by the letter *p* as shown above. The tangent force acting on the ring gap after installation is represented as (T_f). When the ring is installed it is in compression and placed within the cylinder causing a large compressive force.

By relating the forces and pressure equations noted above, the bending moment of the ring is calculated as follows:

$$T_{MP} = p(x)C_l R_r^2(1 + cos\varphi) \quad \textbf{(4.24)}$$

(4.24) notes the method used to calculate the bending moment acting on the system due to the pressure, where C_l is the axial width. As there will be force acting on the ring also due to installation compression this is calculated by adopting the same method as is represented as follows:

$$T_{MF} = T_F R_r(1 + cos\varphi) \quad \textbf{(4.25)}$$

(4.25) is the method used to calculate the bending moments of the system due to the ring gap installation force. T_f is the thermal stress and is defined in (4.42). Results found in (4.24) and (4.25) when compared show a relationship which is noted further in (4.33).

When the piston ring is first installed the contact between the cylinder wall and the ring will not match. This is due to the machining tolerances and wear causing differences in the two circular shapes. Thus the ring is able to deform into to meet the differences, these lacks in contacts will over time lead to a greater level of oil consumption and increased engine blow-by.

During the operation of the engine piston rings are placed under large levels of stress. The stress that arises during operation can be calculated as:

$$S_w = \frac{8}{3\pi}\frac{E t_y (t_m - s_1)}{{D_n}^2} \quad \textbf{(4.26)}$$

This is where S_w, E, t_y, t_m, $s_1$and D_n are the stress during the engine operation, piston ring material young's modulus, free gap in relaxed state, gap clearance installed state, nominal diameter of cylinder and radial dimension of piston ring respectively [52]. From calculated stress levels shear stress is represented as:

$$\tau = \frac{\sigma_1 - \sigma_2}{2} \quad \textbf{(4.27)}$$

Where σ_1 and σ_2 are the major and minor principal stresses respectively.

4.4. Thermodynamics and tribological effects

In the combustion cycle, heat is generated which affect the cylinder, piston and piston will ring. The heat that affects the components will cause varying distortion in the cylinder surface. The piston ring needs to distort with the cylinder liner. The piston ring needs to adjust to meet the new cylinder wall profile, to restrict blow-by and low oil consumption. The deformation of the piston ring can be calculated as follows:

$$k = \frac{T_{mp} {D_n}^2}{4EI} \quad \textbf{(4.28)}$$

(4.28) notes the calculation of deformation of the piston ring during operation as noted in Tomanik's work [89]. Where k and I are the coefficient of deformation and axial moment of inertia of the piston ring cross section respectively. Tomanik's work suggests that when there is a greater coefficient of deformation the better the ring will match the cylinder profile.

He also noted that if α is the angular position, Δr is the radial change from the cylinder, A_i, B_i are the Fourier co-efficient's and i is the order of deformation which can be mathematically represented as a Fourier series.

$$\Delta r = A_0 + A_1\cos(\alpha) + A_2\cos(2\alpha) + \cdots + A_i\cos(i\alpha) + B_1\sin(\alpha).. \\ + B_2\sin(2\alpha) + \cdots + B_i\sin(i\alpha) \quad \textbf{(4.29)}$$

At each phase angle $\emptyset_{bn}$ and each n[th] order term the maximum cylinder deformation U_{bn} where calculated using (4.31) and are represented as:

$$\emptyset_{bn} = \left(\frac{1}{n}\right) tan^{-1}\left(\frac{B_n}{A_n}\right) \quad \textbf{(4.30)}$$

$$U_{bn} = 2\sqrt{(A_n^2 + B_n^2)} \quad \textbf{(4.31)}$$

The work also notes that the ability of the piston ring to make contact with the cylinder wall surface can be estimated as follows:

$$U_{max} = \frac{2\ kR_{rad}}{3(i^2 - 1)^2} \quad \textbf{(4.32)}$$

Where U_{max} and i are Maximum piston ring deformation possible and order of deformation (i = 1,2,3,4…) respectively.

When calculating the surface pressure acting on the ring, the specific pressure is one of the most important parameters to be considered. The specific surface pressure can be derived by the following equation:

$$P_0 = \frac{2F_t}{kR_{rad}h_1} \quad \textbf{(4.33)}$$

This is where P_0 and h_1 is the specific surface pressure and the width of the piston ring.

Archards [56] equation of wear is one of the most respected methods of predicting wear in literature at the present. Taking the a dimensionless constant, total normal load, sliding distance all over the hardness of the least hard surface, the equation is noted as respectively:

$$V_{Wear-abrasive} = \frac{C_L P_f tan\theta}{3P_t} \quad \textbf{(4.34)}$$

Furthering this work Tung [4] offers further refinement into the use of this equation. In this refinement the hardness of the piston ring (P_t) and the hardness of the abrasive particle (P_a) are over each other giving a hardness ratio.

$$V_{Wear-abrasive} = \frac{C_L P_f tan\theta}{3P_t} \; for \; \frac{P_t}{P_a} < 0.8$$

$$V_{Wear-abrasive} = \frac{C_L P_f tan\theta}{5.3P_t} \left(\frac{P_t}{P_a}\right)^{-2.5} for \; 1.25 > \frac{P_t}{P_a} > 0.8$$

$$V_{Wear-abrasive} = \frac{C_L P_f tan\theta}{2.43P_t} \left(\frac{P_t}{P_a}\right)^{-6.0} for \; \frac{P_t}{P_a} > 1.25 \quad \textbf{(4.35)}$$

The wear abrasive model equations are then simplified to the following:

$$V_{Wear-abrasive} = K\left(\frac{P_a^{n-1}}{P_t^n}\right) C_L P_f tan\theta \quad \textbf{(4.36)}$$

Where K is the wear coefficient constant as is a function of $\frac{P_t}{P_a}$ and is defined as:

$$\begin{aligned} \frac{P_t}{P_a} < 0.8 \quad & K = 0.333 \\ 1.25 > \frac{P_t}{P_a} > 0.8 \quad & K = 0.189 \\ \frac{P_t}{P_a} < 1.25 \quad & K = 0.416 \end{aligned} \quad \textbf{(4.37)}$$

This method for predicting the wear in the reciprocating mass problem has shown to be much more efficient for this area. To establish the fully working model with all boundary shown the heat of the system must also be defined. During the bedding in of the system, thermal changes of the components will play a huge role in the further operation of the system. The compression ring is subjected to combustion gasses hence transient temperature variations occur.

During operation at MoS_2 is a composite of atomic materials validating the equation is vital. Raman shifts are noted in wavenumbers, with units of inverse length. For the use of this in the material, the thermal expansion of the lattice is divided by the Raman shift, the enharmonic effect is also considered as it will be the main cause for change of phonon self-energy.

The lattice and the enharmonic effect are written as $(\Delta\omega_E)$ and $(\Delta\omega_A)$ respectively. As in the coating both Molybdenum and also sulphur have thermal expansion incongruity, written as $(\Delta\omega_M)$. The temperature change of the relation between the piston ring and coating can be written as:

$$\Delta\omega(T) = \Delta\omega_E(T) + \Delta\omega_A(T) + \Delta\omega_M(T) \quad \textbf{(4.38)}$$

The lattice of MoS_2 structure will increase due to thermal expansion, hence leading to the Raman shift being expressed in its most common form of:

$$\Delta\omega_E(T) = \omega_0 exp\left(-d_g T_{cof} \int_{25^oC}^{T} T_{cof} dT\right) - \omega_0 \quad \textbf{(4.39)}$$

Where the room temperature frequency, degeneracy, Gruneisen parameter and the thermal coefficient of the material are noted as ω_0, d_g, y and T_{cof} respectively.

In heat generation and cooling most solid materials will expand when heated and contract when cooled. During the engine operation the combustion bowl is subjected to heats as high as 600^{o}C after running the engine will cool hence heat will play a large role in the system. The change in length with temperature of the material is expressed as:

$$\frac{\Delta l}{l_0} = \alpha_l \Delta T \quad \textbf{(4.40)}$$

(4.40) notes the change in length of a material due to temperature change, where Δl, l_0, α_l and ΔT are the change in length, initial length, linear coefficient of

expansion and the temperature change. However, the heat will affect the dimensions of the body, hence a resulting change in the volume. This change is represented in (4.41).

$$\frac{\Delta V}{V_0} = \alpha_v \Delta T \tag{4.41}$$

(4.41) notes the method for calculating the volume change within a body due to temperature changes, whereΔV, V_0 and α_v are the volume change, original volume and volume coefficient of thermal expansion respectively. However as MoS_2 is by definition one part Molybdenum and two parts sulphur the coefficient of thermal expansion is calculated in a different method.

In the results published by El-Mahalawy [118], the in-plane and out-plane of the thermal coefficient of MoS_2 can be derived as:

$$\alpha_a(Temp) = (0.6007 \times 10^{-5} + 0.6958 \times 10^{-7} Temp)\frac{1}{a℃}$$
$$\alpha_c(Temp) = (0.1064 \times 10^{-3} + 1.5475 \times 10^{-7} Temp)\frac{1}{c℃} \tag{4.42}$$

(4.42) notes the method used to calculate the coefficient of thermal expansion for MoS_2. Where a and c are the directional change. The heat that cause's the material to expand also will have a level of conductivity. Thermal condition is a process in which heat is transported from high to low temperature areas of a material. The property of the material that defines it ability to do this is called the thermal conductivity.

$$q = -k_1 \frac{dT}{dx} \tag{4.43}$$

(4.43) denotes the formula for calculating the heat flux/heat flow of a material as per unit time per unit area, where k_1 and $\frac{dT}{dx}$ are the thermal conductivity and thermal gradient through condition respectively. As the strain of the material can be calculated by using (4.40) the thermal stress is defined as:

$$T_f = \alpha_v \Delta T E \tag{4.44}$$

(4.44) show the method for calculating the thermal stress and E is the elastic modulus.

4.5. Methodology

To define a method of application for the boundary conditions, pressure, inertia force and heat is defined in a flow method.

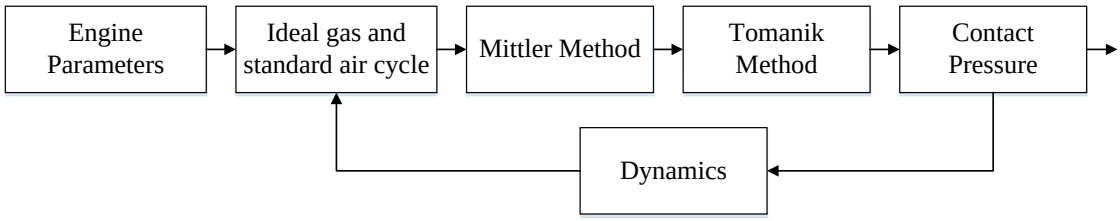

Figure 4.8 - Pressure flow method

Figure 4.8 shows the method adopted for the calculation of the pressure during operation. The engine parameters are defined as the component geometry. The ideal gas and standard air cycle is calculated using the parameters from the geometry, with the use of Mittlers [53,54] method for calculating pressure around the ring during operation Tomanik's [89] techniques for calculating cylinder deformation and ring expansion are used overall defining the contact pressure, finial the engine will then move to a new position.

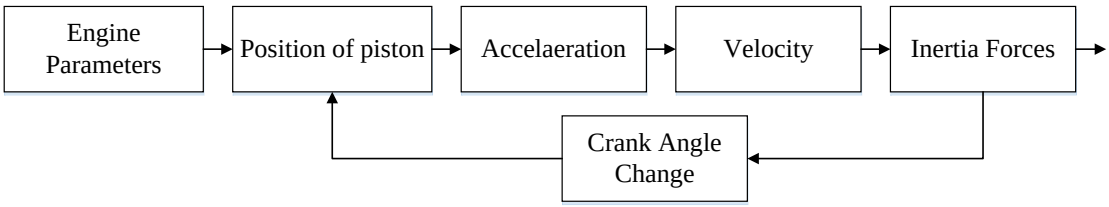

Figure 4.9 - Inertia force method

Figure 4.9 shows the same method adopted for the pressure calculation, by Stone's method [3] for calculating force the condition is applied. Each component was modelled

matching geometry and material. These values where then used to calculate the position of the piston during operation. Binomial method noted by Stone has been used to calculate the position, hence by numerical integration, acceleration and velocity were calculated. These values allowed for inertia forces to be calculated.

Important factors such as wear were also considered in the modelling. The most common method for calculating abrasive wear is through Archards wear equation [56]. This method has been adopted over many years for many applications. In the case of reciprocating mass system the Rabinovich [57] equation appears to be a better fit to the current problem. The validity of the methodology has been discussed by Tung [4] equation. The methodology used in this project is reported in Figure 4.10.

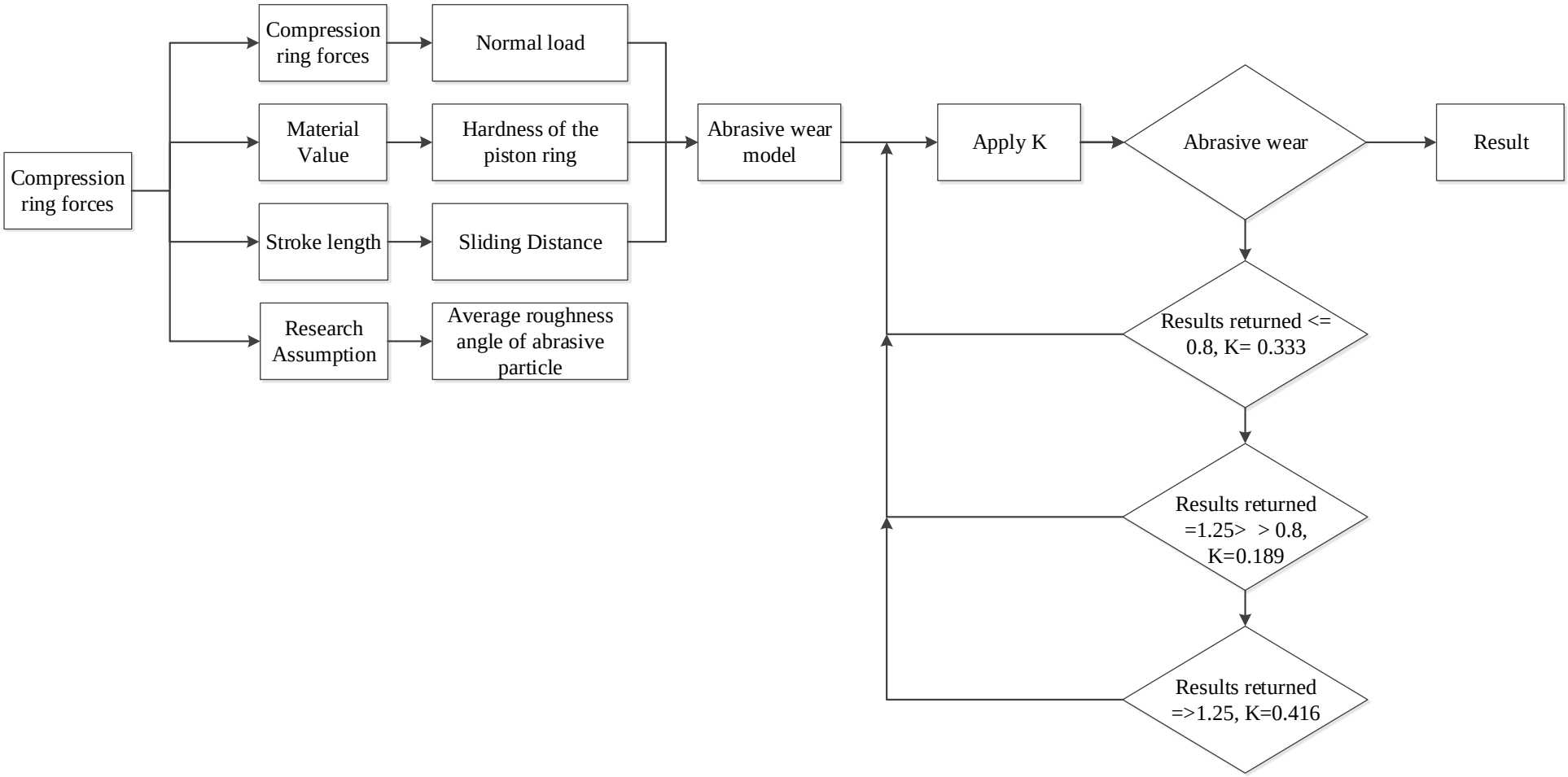

Figure 4.10 - Abrasive wear methodology

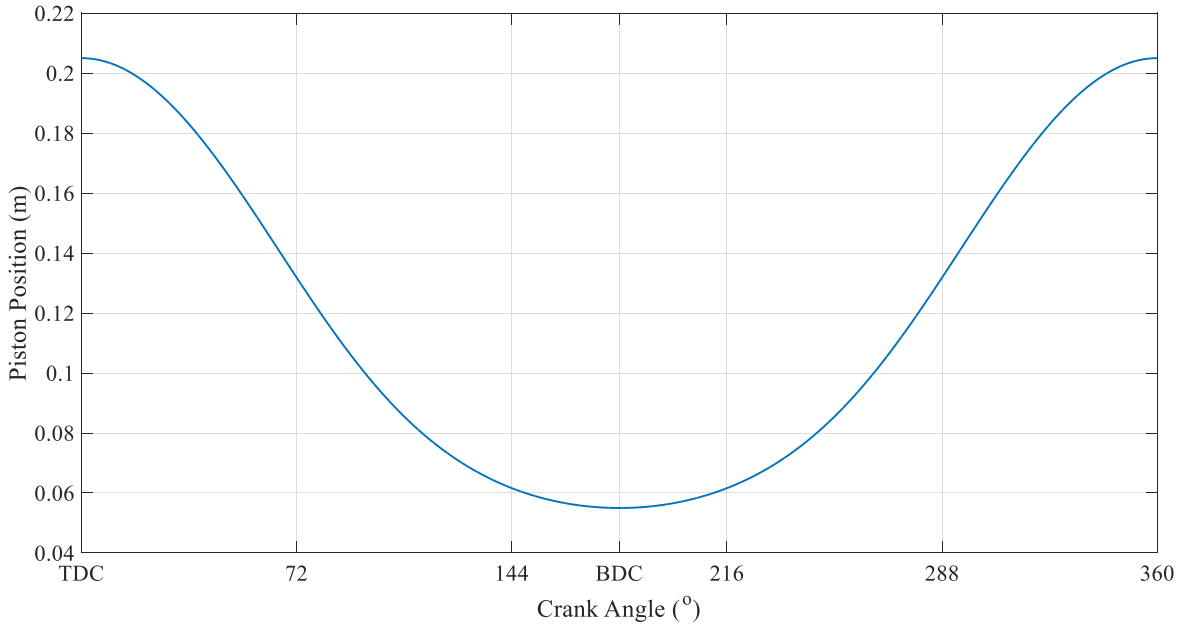

Figure 4.11 – Piston Position at 6000rpm

The dynamic equations noted in chapter four where used to model the reciprocating mass problem. The KTM engine dimensions were used along with the mass of the assembly to produce the positional plot shown in Figure 4.11, which show the displacement of the piston in metres over 1 crankshaft rotation.

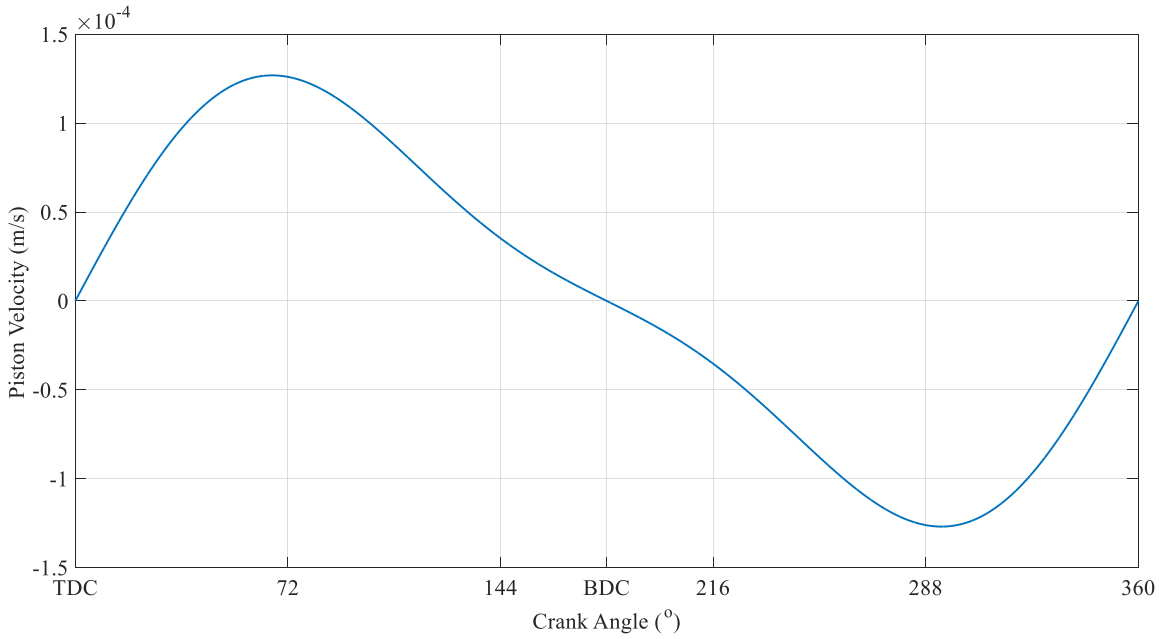

Figure 4.12 - Piston velocity at 6000 rpm

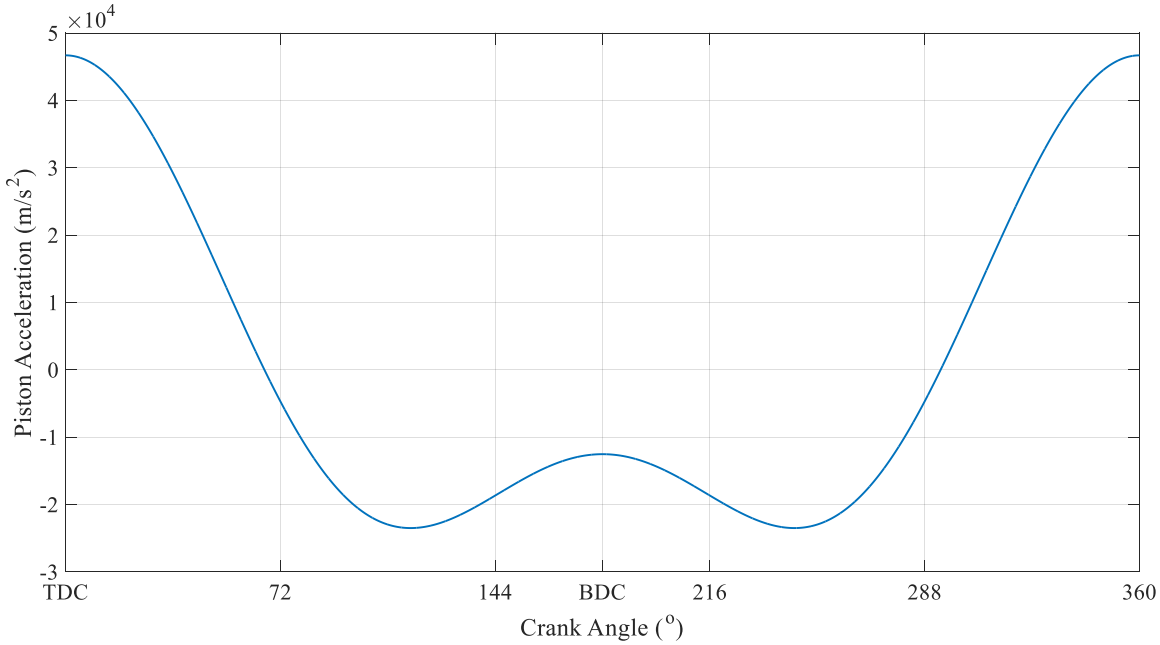

Figure 4.13 - Piston acceleration at 6000 rpm

Figure 4.12 and Figure 4.13 show the velocity and acceleration respectively, based on KTM geometry.

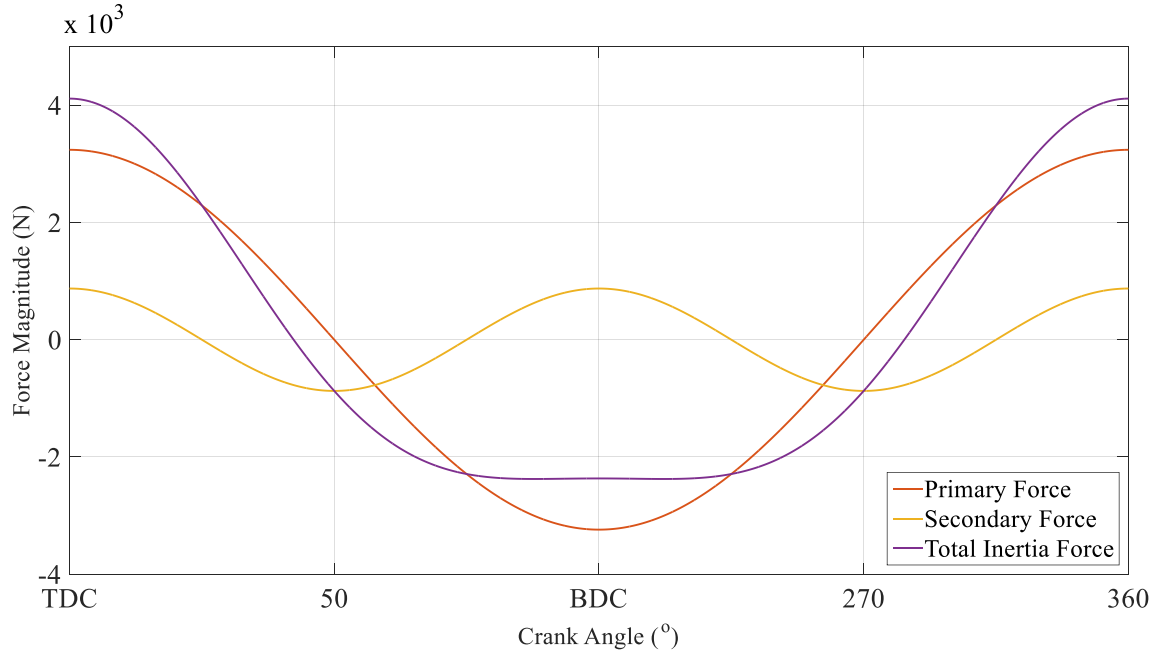

Figure 4.14 - Inertia Forces displayed based on the KTM 525

Figure 4.14 shows the primary, secondary and total inertia force plotted. Within the plot the primary force is varying with amplitude with the crankshaft rotation, and the secondary force is twice the RPM. Both forces act along the cylinder axis while in use.

As the test engine is a single cylinder engine it is vital to calculate all forces that act in the system as boundary conditions for the simulation. During each cycle of the engine the ring will be pushed by the travelling piston, the calculated force are interpolated into a boundary condition for use in further simulations.

Under the assumption that the piston skirt will deform to create a cylindrical profile, the reciprocating mass axis will offset based on the piston to cylinder clearance. This clearance will give the distance that allows for R_f shown in Figure 4.4.

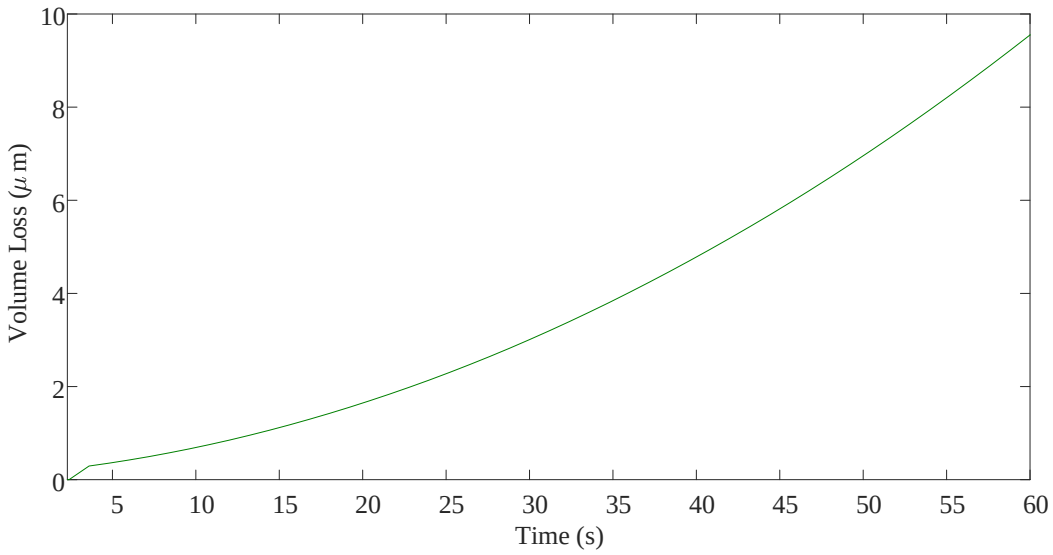

Figure 4.15 - Wear depth progression of the iron cylinder

Figure 4.15 shows the wear profile of gray cast iron, during 60 seconds of use. In the first few hours of operation the material has a large climb-in material loss. As the fiction occurs, the asperities will begin to grind down to a smooth surface. However, during the running process Figure 4.15 does not consider the cylinder deformation. As it is logical to assume if the ring goes through a deformation process then also must the cylinder. By using the KTM geometry and operational parameters of the engine, the simulated results shown in Figure 4.14, show that wear depth on a cylinder liner is the same as what was noted by Tung, the work produced in this study was validated with lab testing hence

supporting the model produced for these studies. However, the RPM within the race engine is far higher that what is shown in this study. Hence, the depth on the cylinder is increased.

To model the equations in the basic form Matlab was used, with the Simulink package. Simulink is a block diagram system that allows the user to create multi-domain simulations. By looking at the mass and inertia of the geometry produced the system is able to build an accurate representation of the engine.

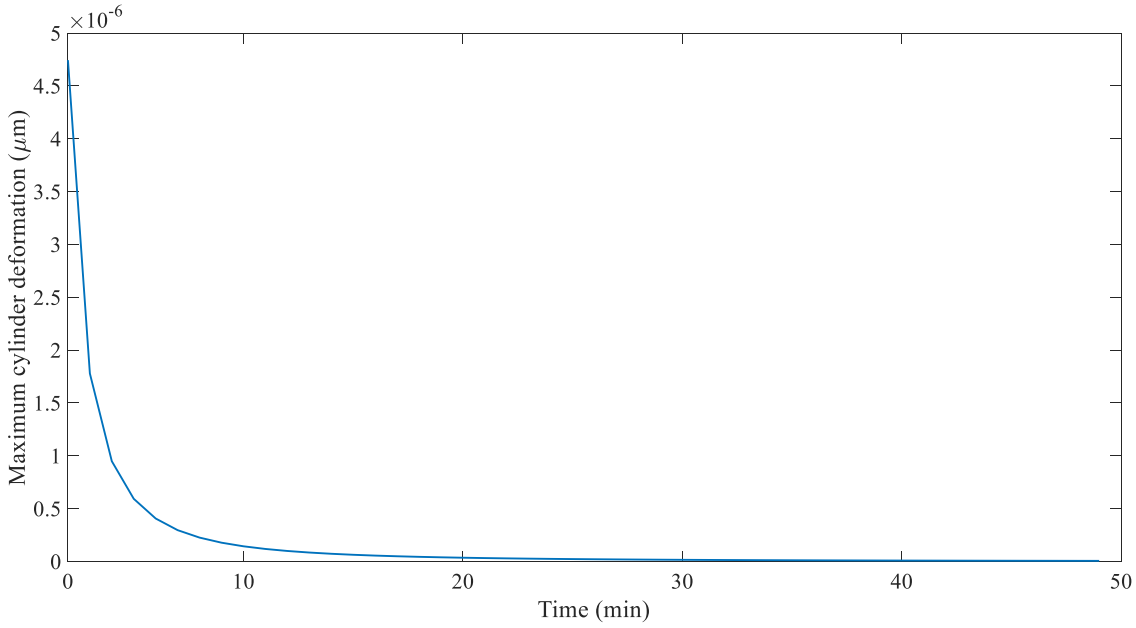

Figure 4.16 - Maximum cylinder deformation

Continuing from Tungs work, Figure 4.16 shows the maximum level of deformation in the cylinder that the piston ring can deform during operation of the KTM, the graph shows the deformation time taken for the cylinder to settle in its new deformed position. By combining work from both Tung and Tomanik, a model boundary can be built which takes into consideration that the cylinder will go through changes during this process.

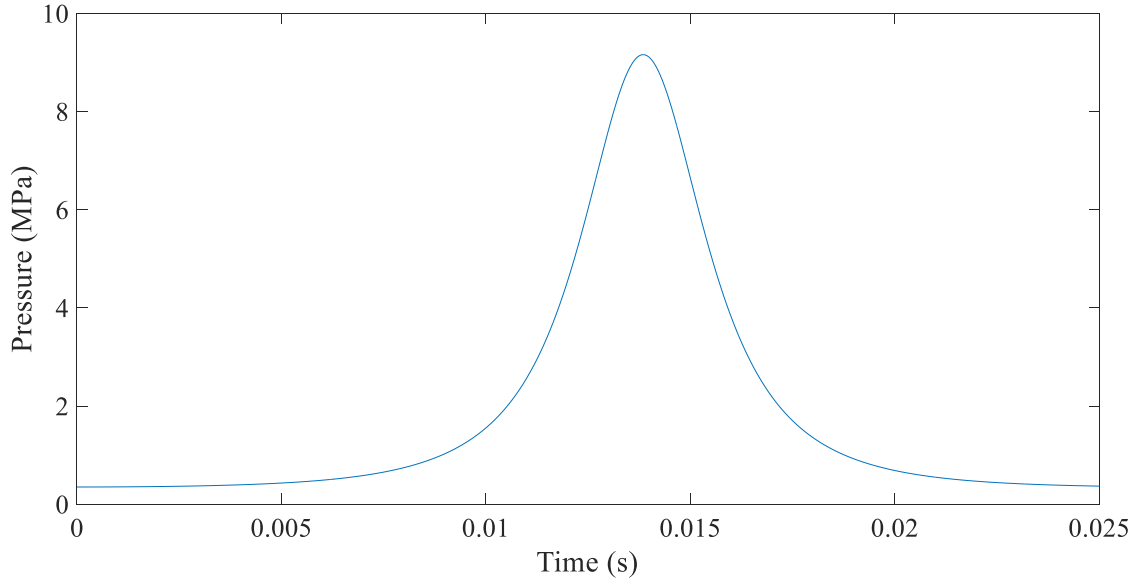

Figure 4.17 predicted cylinder pressure

By using ideal gas with standard air cycle to prediction of the pressure output from the piston, the cylinder pressure (shown in Figure 4.17) can be predicted and defined as a boundary in further simulations.

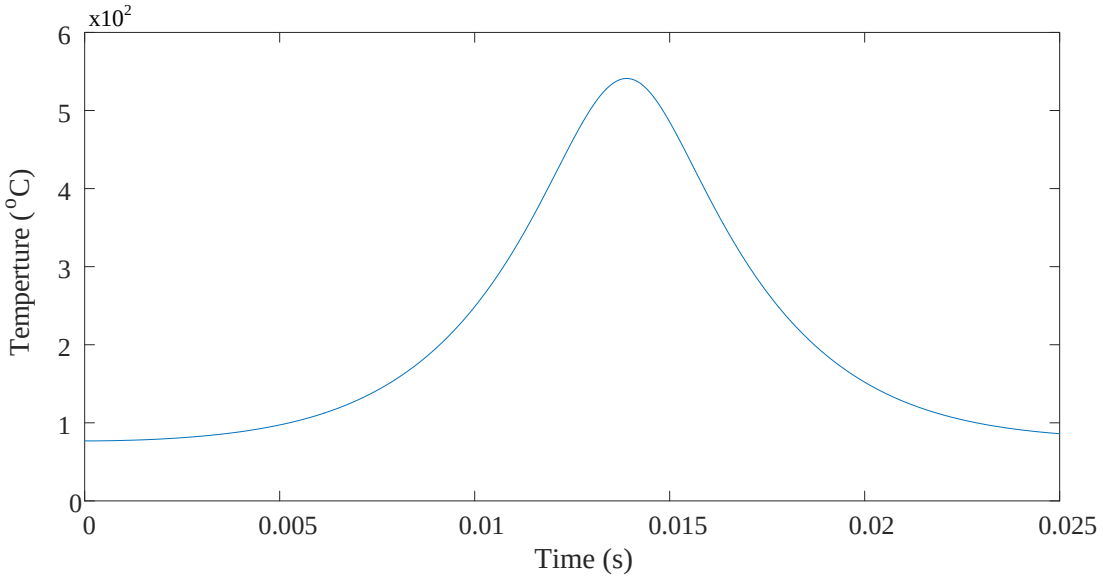

Figure 4.18 predicted cylinder temp

Based on the simulated results of the KTM, Figure 4.18 shows the predicted cylinder temperature of one cycle of the engine. With these boundary the system for the simulation of the internal combustion engine and further studies are able to be done.

4.6. Conclusions

In this chapter the method for applying mathematical representation for each boundary area of the reciprocating mass has been examined, methods for modelling the dynamics have been shown. As described in the introduction of the internal combustion engine will go through two cycles with in the four stroke process. By calculating the position of the piston during each cycle, acceleration and velocity could be extrapolated. From these set of results and knowing the mass of the piston the inertia forces were also calculated. By deriving the inertia forces equation, the use of the conservation of angular momentum was used allowing for changes in the rotation around the crown possible. Considering the heat, as the ring goes through the running-in process the heat acting inside of the engine lead to thermal changes in both the piston and rings. These conditions can possibly act on the ring and lead to possible dynamic reduction in the ring's freedom to move. A loss on the system will also be material loss and surface changes, which have also been considered in this equation listing, validation of the theory was then produced to look at an ideal output and also to ensure the equation validity before adding it to the complex model.

CHAPTER 5 - EXPERIMENTAL AND MODELING METHOD

5.1. Introduction

This chapter describes the experimental methods applied to the physical testing and simulation of the KTM 520 engine. As the combustion engine is a highly complex system the process for developing the model has been done in a phased process.

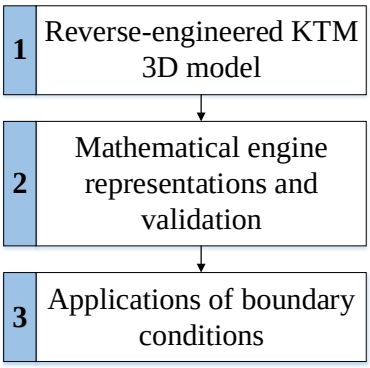

Figure 5.1 - Showing the modelling phase process

Phase one (Figure 5.1) was to establish a base line model, as the project is about race condition's a motorcycle engine was selected as these engine are often high RPM systems. By using the design software package SolidWorks the engine was reverse-engineered to produce an accurate model for simulation testing. Phase two (Figure 5.1) examine the present methods of engine calculation representation, in inputs from the heat, pressure, wear and dynamics. To validate these equations each was placed into the mathematical modelling system Matlab to ensure that the results shown are similar to previous work [3,4,44,53,54,57,71,118]. Following the validation of the system equations an application methodology was developed to organise the inputs of the system.

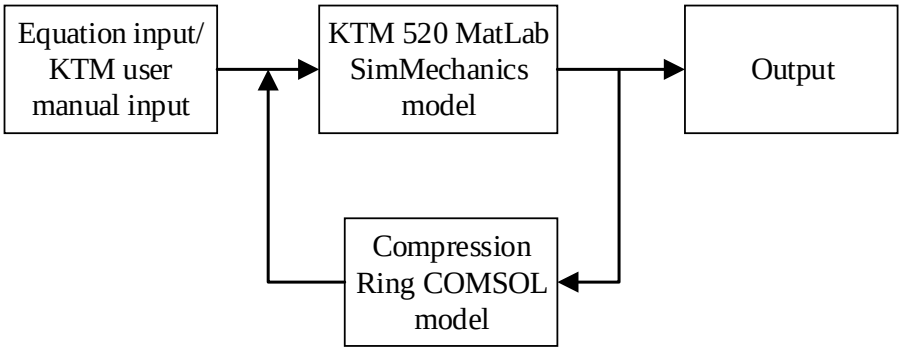

Figure 5.2 - Software package interrelation for engine simulation

Phase three (Figure 5.1) was then to apply the boundary conditions found in the equations and in the engine specifications and place them into two simulation software packages. After the SolidWorks 3D model was produced the components of the engine were imported into the MatLab SimMechanics simulation software package. To build a basic working model only the dynamics of the reciprocating mass were considered. Equations noted were used to validate any results generated. This method was repeated until all the noted dynamic equations were incorporated into the system. Results generated from the output of the dynamic simulation were used as boundary conditions for the FEA analysis. To achieve this the simulation software package COMSOL was used, within which the model values such as pressure and heat value could be imported. The thermal changes in the compression ring were then passed back into the dynamic model allowing for phenomena such as thermal change to be accurately represented. This process is summarised in four process blocks in (Figure 5.2).

Within this chapter the experimental set-up of the physical testing is also defined.

The combustion engine has more than 300 parts working together to produce the output.

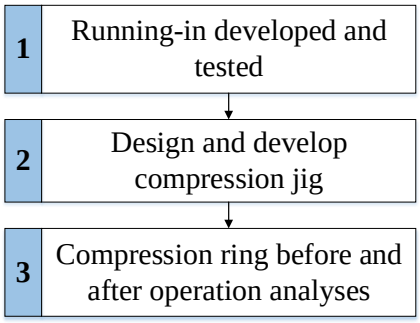

Figure 5.3 - Showing physical testing phase process

Examining the effect of the engine on the compression ring has been done in three phases. These phase are as follows: phase one: using the KTM 520 user manual develop a running-in procedure, the time ratio is defined by KTM's recommendation within the manual. The running-in schedule was used studying two main factors that relate to the work presented, the first being the temperate of the engine and the second torque produced during the procedure. Phase two was too develop a system which would allow for a complete ring to be tested on a Talysurf PGI 400.

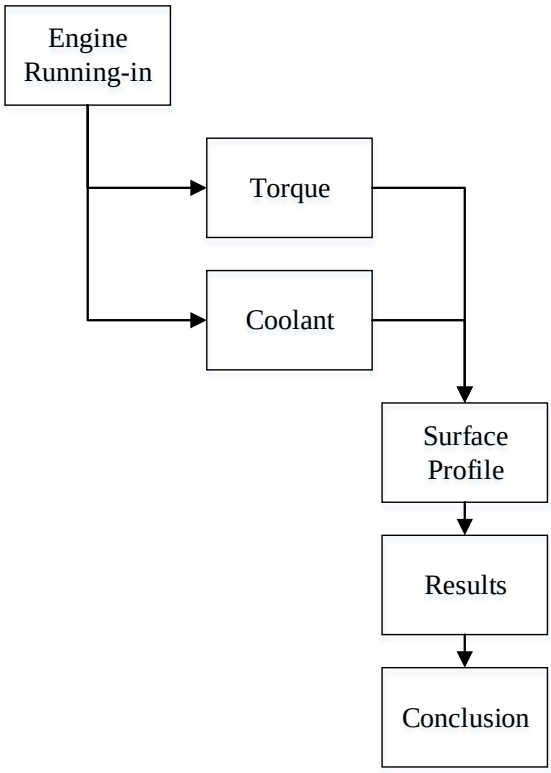

Figure 5.4 - Physical testing phase process

Phase three was to examine the profile of the compression ring before and after use. With the use of the system developed in phase two, the compression ring was checked for the wear and geometry changes. These phases are reflected in the Figure 5.4.

5.2. Experimental Methods

5.2.1. Dynamometer running-in tests

The following work is to examine the results found in the KTM 520 motorcycle engine. This engine is a single cylinder engine and is typically found in applications for motorcycles, hence making this engine ideal for race application study. The lubrication used on the engine for experiment was 10W-50 Putoline^{TM} oil.

5.2.2. Dynamometer set-up

For the testing of the engine a Ricardo Test Automation S3000 controller (Figure 5.5 (a)) was used with a Heenan – Dynamatic Mk 1 dynamoeter (Figure 5.5 (b)).

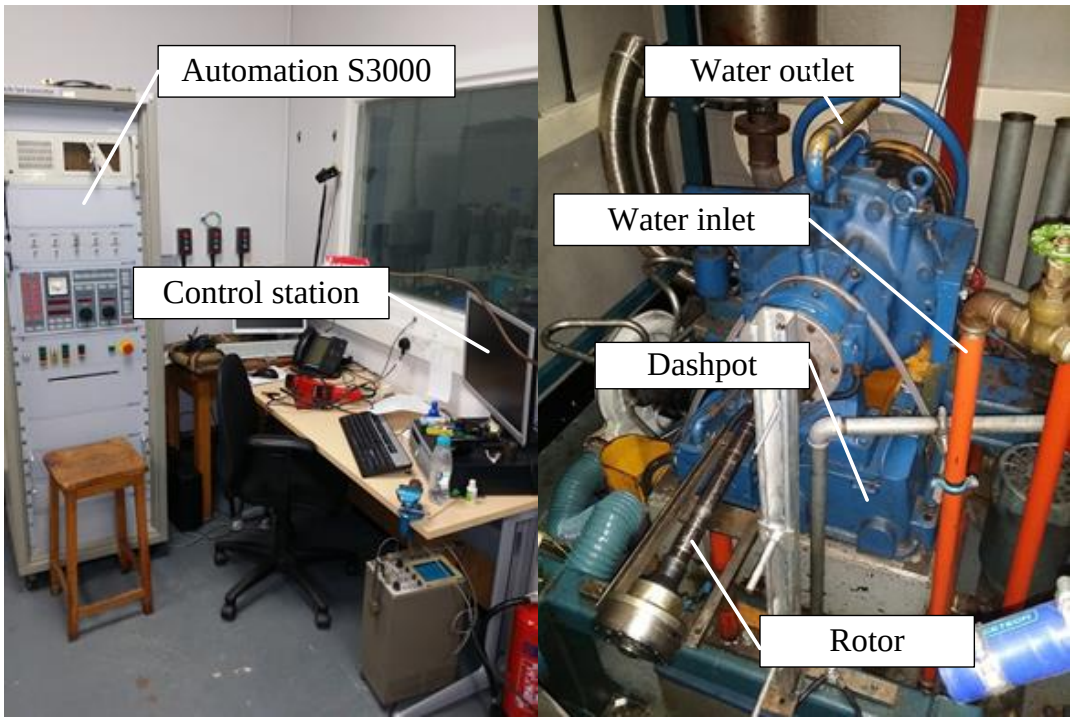

Figure 5.5 - (a) Ricardo test Automation S3000 (b) Heenan - Dynamatic MK 1

When purchasing a new engine, each company will offer a recommendation for a running-in [39-42,45,121], therefore a running-in schedule was selected based on the manufacturer's recommendations [42].

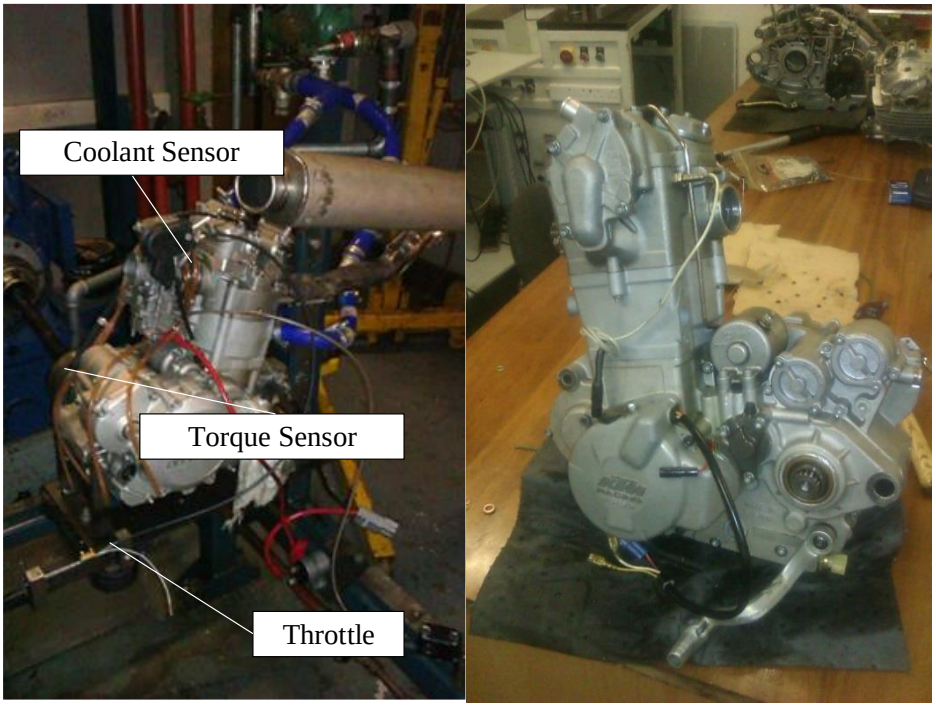

Figure 5.6 - a. KTM 520 fitted on the dynamometer b. KTM 520

Figure 5.6 a shows the KTM 520 engine mounted Ricardo dynamometer system. Figure 5.6 b shows the KTM after compression ring change.

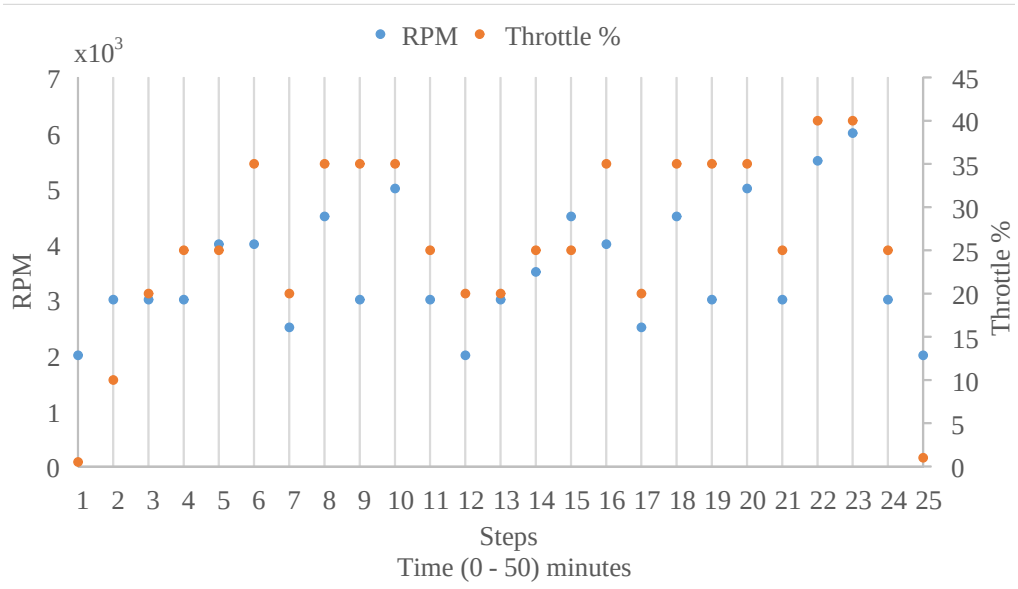

Figure 5.7 - KTM 520 running-in schedule

Figure 5.7 shows the full break down of steps for the running-in procedure that was used for the KTM test engine.

5.2.3. Development of profile piston ring fixture

Surface profilometry is a common method used in the analysis of surface roughness, shape and waviness of engineering components [122,123]. The analysis involves measurement in high resolution along the lateral and vertical axes. It is well known that the performance and life of engineering components is highly dependent on the surface properties [124]. For example, wear rates are considerably greater in rough surface compared with a smooth surface and components engineered to have a smooth surface have longer lifetimes [125]. There are a number of methods for measuring the surface roughness of components including optical techniques such as classical interferometry, holographic interferometry, speckle techniques and white light interferometry [126-128] as well as mechanical techniques [129]. This work we focuses on employing the Taylor Hobson Talysurf for measuring surface roughness [129-132]. This instrument employs a mechanical transducer known as the stylus which moves across the x-axis of the surface of a component and its vertical movement is recorded to obtain the surface profile. One of the major disadvantages of this method is that it is restricted to horizontal substrates and therefore to obtain profiles of 3-D components such as piston liner to ring contact face is problematic. In the work presented a design, manufacture and application of a new piston ring mounting system for use in the analysis of surface profiles of the complete piston ring component. The new system is employed in conjunction with the Taylor Hobson Surface Profilometer in order to ease the measurement of 3-D components which are ring shaped. The data obtained will give a greater insight into the causes of wear and performance of piston rings in racing engine.

5.2.4. Profilometer System

The Taylor Hobson instrument employs the movement of a 90º conical diamond stylus with a spherical tip in the range of 6 mm which is carried at one end of a beam pivoted at the fulcrum on knife edges. The remote end carries an armature which moves between a pair of coils altering their relative inductance. Special gauges are employed to amplify the signal increasing the resolution ratio from 1000:1 to 64000:1 allowing a 0.6 nm resolution to be reached for a range of 0.03 mm in the z-direction with a maximum nominal measuring range of 0.8 mm. The instrument has a length interval of 120 mm/0.1 mm (x_{max}/x_{min}). The data sampling interval is 0.25 mm for traverse length to 30 mm and 1 mm for length over 30 mm. The instrument is controlled by Ultra software incorporating calibration and measurement functions. For the roundness of a surface device, the Talyrond could be employed. This instrument provides the operator with a spindle provided by the company. This allows for the precision profile testing having a large accuracy of less than 0.02 µm radial axial. The device also has a coning error of 0.0003 µm/mm [133]. The data points gathered from the instrument sample at an extremely high level of 18000 points. However, the problem still with this device is how can the piston ring be mounted and profile in its circular profile? Each roundness profilometer offer the same problem of "how can the piston ring be mounted into a position where the contact face can be checked".

The standard sample stage system comprises of a three base plates where the lower base plate is incorporated to allow for fixing to the machine. Figure 5.8 shows a schematic of all the components and a photograph of the system. The mid plate is used to allow the adjustment plate the movement range of 20 mm in the Y axis. The adjustment plate is positioned by a micrometre which is mounted to the front of the base plate. Between the two plates an inner rail and outer rail is mounted these rails allow the adjustment plate to be moved with ease. To allow for precession movements of the adjustment plate, two

springs at each side of the adjustment plate are placed parallel with the micrometres which are held by two locator spring pins. For special project mounting holes are placed in the adjustment plate to allow for fixing into position.

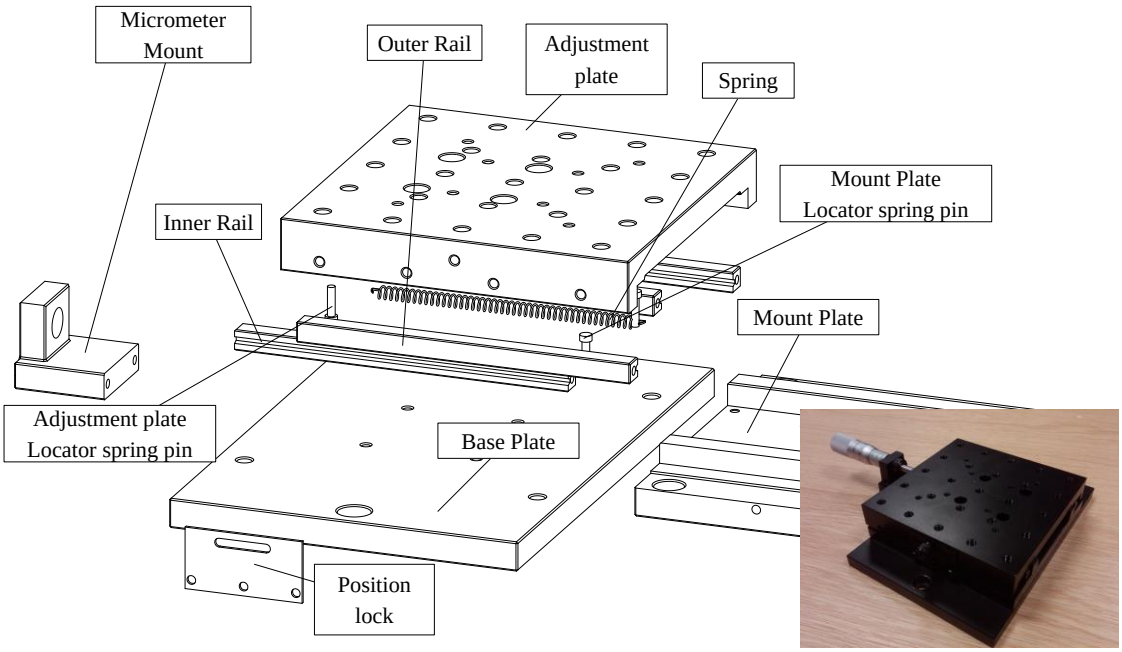

Figure 5.8 - Exploded view and photograph of the mount stage

New Piston Ring Mount System

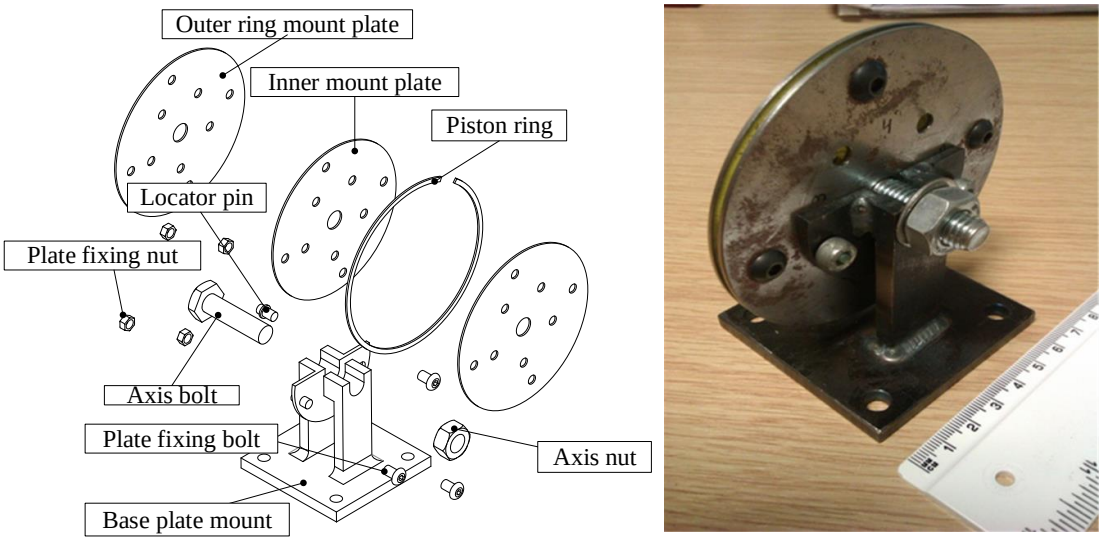

Figure 5.9 - Exploded view and photograph of the Dickinson rotating ring profiler

To overcome the disadvantages of the standard sample holder system (Figure 5.8), a new piston ring mount system was designed, manufactured and tested in our research laboratories at the University of Central Lancashire (Figure 5.9). This sample holder will

be hereafter referred to as the Dickinson Rotating Ring Contact Profile system. The system consists of three fixing plates made from aluminium held together by four fixing bolts positioned at 90° relative to the base plate mount assembly. The plates can be rotated manually at intervals of 72° for complete analysis of the entire piston ring. The inner mount plate is made from neoprene foam material which enables a soft contact with the piston ring to prevent damage to nano-engineered surfaces of the piston ring. This assembly is mounted to the standard system base plate and the screw is tightened to keep the assembly in the correct position.

5.2.5. A study into compression ring surface profile prior to operation

During operation the compression ring will be subjected to material damage in three different areas, the contact face which is between the cylinder and ring face, the top face of the ring (top land) which will have contact with the piston groove and the bottom face (bottom land) which will also contact against the groove of the piston. These contacts play a vital role in creating a seal against the combustion gasses during operation. In this study a KTM 520 four stroke engine was used. This engine's primary use is for a motorcycle, hence it is able to produce high RPM making it an ideal choice for racing condition research. The running-in procedure used was defined using the KTM user manual [42]. Two sample sets where KTM BS-grade compression rings with MoS_2 coatings. The other two sets were the BS-grade compression ring the material characteristics were defined using energy-dispersive X-ray Spectroscopy (EDAX). The ring circumference was broken down into 8 areas examining four profile points Figure 5.10.

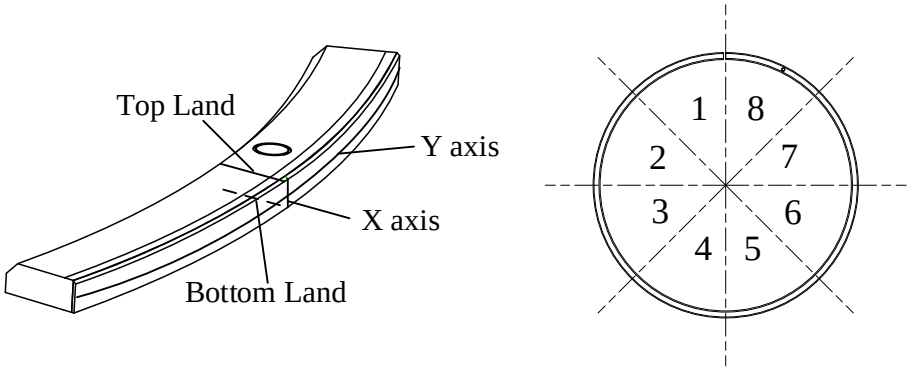

Figure 5.10 - Sample area

Also in Figure 5.11 the installation position of the ring and finishing position was noted at around 15 degrees adhering to studies that suggest a slight movement in the ring [4,9,13,134,135].

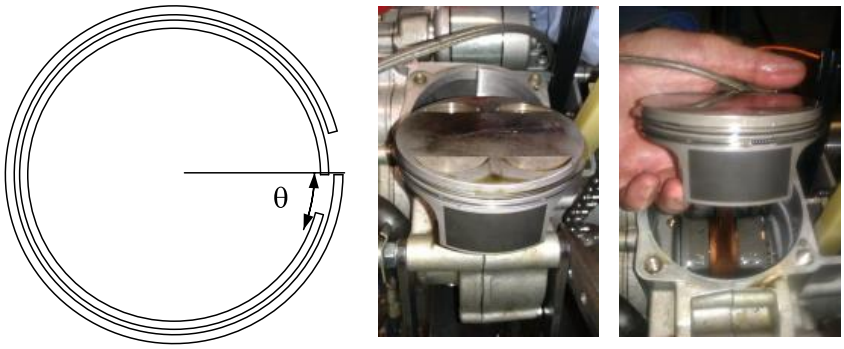

Figure 5.11 - Ring position before and after running

The main focus of work is to examine the contact between the cylinder and contact face of the ring, the x and y axis are both studied. The samples areas where measured with Table 5-1.

Table 5-1 - data length of the sample

Sample name	Length mm
Top Land	2.59
Bottom Land	2.59
X axis	1
Y axis	30

To establish the coating hardness on the material before and after operation nano-indentation tests were used.

5.2.6. Experimental set-up

As the engine operates, the piston reciprocates in the cylinder. During this process the ring comes into contact with the cylinder wall. This interaction leads to ring wear. However, the cylinder wall is lubricated along with the piston ring pack. Simulations have shown that the compression ring will be subjected to large levels of heat allowing for thermal deformation and also the contact geometry plays a large role on the ring wear [9,13,14,96,134,135].

As this study is to examine the interaction between the cylinder wall and the compression ring, the hardness of the ring before operation and after is vital. This is to enable a greater conclusion as to how the compression rings perform. The nano-indentation test definition is defined in Table 5-2.

Table 5-2 - Nano indentation calibration data

Original Experiment Definition	
Maximum Depth (nm)	2000
Minimum Depth (nm)	2000
Limit stop load (mN)	0.1
Initial load (mN)	0.05
Loading rate (mN/s)	15
Unloading rate (mN/s)	15

To study the surface profile of the compression ring a Taylor Hobson Talysurf PGI 1240 was used. 6 sets where studied, 3 sets of Omega and 3 sets of KTM.

5.3. Compression ring modelling

5.3.1. Modelling the compression ring geometry

The compression ring has factors that affect the performance of the ring. Millers work on the split compression ring, notes that there needs to be enough space between the compression ring and piston groove thus to enable assisting gases to come from behind the ring to enable a greater seal [48]. Hence, this dimension will be dictated by the piston designers.

New design features have appeared on the piston ring pack for many years. On the compression ring, in particular, the internal bevel, has been adopted for most race engines over many years, this design feature is more commonly known as the torsional twist compression ring. The compression ring's main function is to relieve stress during operation. In theory this allows for bending during the BDC to TDC part of the cycle. However, still keeping a ridged seal. The kinematics of bending and also torsional behaviour were first introduced by A.E.H. Love [44]. This work was then extended by Federhofer [119]. Some of the first piston rings were used without surface treatment or protective coatings. In an effort to reduce wear in the piston ring, in the 1940's Cr coatings were applied to the contact face of the ring [136].

The design of the piston ring has been the main focus of many studies over decades; the aim of this work is to focus on a relatively new design features of the piston ring, the piston ring contact chamfer. The piston act as a reciprocating mass moving from the bottom dead centre position (BDC) to the top dead centre (TDC), the piston ring achieves optimal performance when the ring contact is perpendicular to the cylinder. The contact chamfer also serves as a method to induce increased pressure in the lubrications aiding the seal between rings to cylinder.

The compression ring being the closest ring to combustion gases, is therefore exposed to the highest operating temperatures. The compression ring transfers 70% of the combustion chamber heat from the piston to the cylinder wall, where heat transfer and thermal elastic deformation occur. Cylinder liners have a higher coefficient of expansion than the compression ring and therefore increased clearances must be allowed for, so the piston skirt clearance in the liner is greater than that for piston ring. The skirt transmits the side thrust, caused by the varying angularity of the connecting rod, to the liner. Excessive clearance will cause the piston to tilt.

The tilt can cause large levels of stress centred on the ring top edge of the contact face. In an attempt to relieve the concentrated levels of stress, companies have incorporated a small chamfer on the top of the contact face. This work examines the internal bevel design feature and suggests an optimal geometrical size.

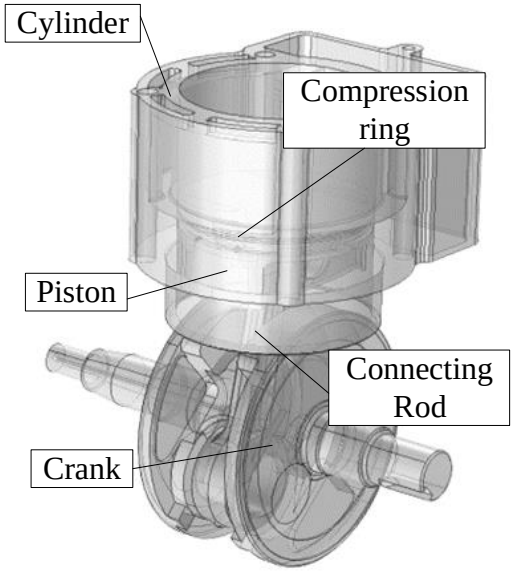

Figure 5.12 - Reversed engineered KTM 520

Reverse Engineering of a KTM 520 engine has been used to develop a 3D Computer Aided Design (CAD) model using SolidWorks that has been further analysed by Finite

Element Analysis (FEA) using COMSOL to determine the piston tilt effect on the chamfer stresses (Figure 5.12).

Over the past 200 years, the piston ring geometric cross section has remained rectangular. In the past 50 years the piston ring has been altered [119,137] to incorporate in the ring a torsional twist feature in a form of a contact chamfer on the piston ring contact face.

5.3.2. Engine Operating Boundary Conditions

In this study, both primary inertia force and secondary inertia force acting on the pistons during operation have been considered, crank radius, rod to crank length ratio $\frac{1}{n} = \frac{R}{L}$ and the crankshaft rotation measured from top dead centre.

When calculating the engine cycle, the equation assumes that there is a zero offset from the centre of the crank. In a standard four stroke internal combustion engine, in the cooled state, the piston has a cylindrical profile from crown to the bottom of the oil ring. The bottom of the oil ring to the bottom of the skirt is elliptical.

Once the piston is in operation it is assumed that the geometry becomes an almost perfect cylindrical shape. Boundary conditions of continuity in motion and torque in all directions were used and piston thermally deformed shape was assumed to be cylindrical over the whole cycle. Using Love's principles [44], stress generated through torsional twist can be calculated using Euler rotational principles [138]. Finally, the pressures acting on the piston rings have to be considered. These pressures are calculated using the equations noted in Chapter 3.

The presented work assumes the ring to be fully flooded with lubricant and R.Mittler & al. approach [54] have been used, where the effects of blow-by were studied, while considering the geometry of the piston. The lubrication distribution throughout the

system has been calculated using Reynolds equation. To calculate the forces applied to the ring, a simple equation is used, $F = pA$ where F, p and A are respectively the force, pressure and area.

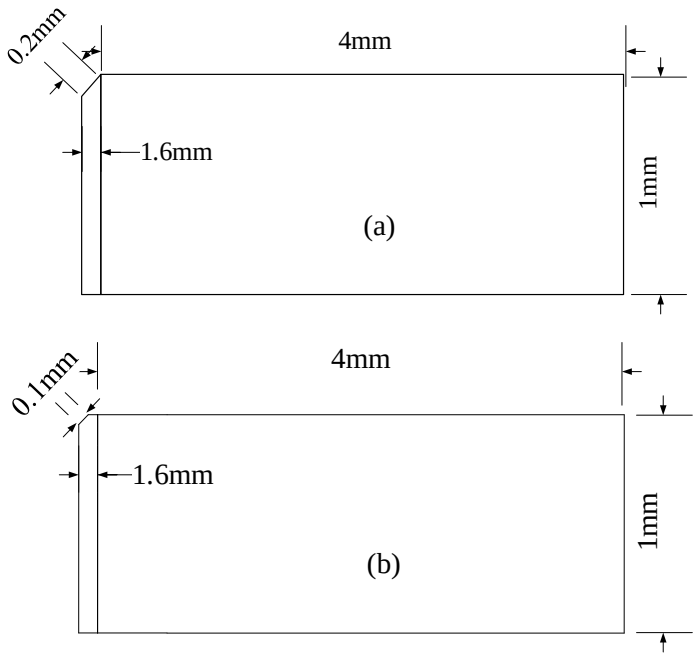

Figure 5.13 - (a) ISO 6622-1 internal combustion engines cast iron standard ring dimensions based on 90 mm diameter. (b) New Dickinson proposed design

To construct an accurate simulation of the ring, the dimensions were taken from the ISO 6622-1 [139] for a ϕ90 mm compression ring as shown on Figure 5.13 (a) close enough to the ϕ95 mm KTN rings used in the study. The proposed design of the ring coated chamfer is shown on Figure 5.13 (b) with a 0.1 mm contact chamfer machined to the upper outside face corner of the piston ring. The operational engine speed range for the KTM 520 engine was between 6,000-10,000 RPM. The boundary conditions incorporated into the simulation allowed for forces, pressures and inertias to be considered. It should be noted that in this work the description of radial forces and hydrodynamic lubrication of the ring face are not discussed.

5.3.3. Compression ring rotation modelling

As the piston travels to TDC the ring is subjected to a force projected from the vector which is produced by the connecting arm. Noether [118] and Euler [138] both noted in their work, that a vector direction that is produced by a connected rotational body will be subject to rotational forces. Therefore, as the crank rotates, torque is produced, with the connecting rod to the piston. The vector that is produced from this action results in rotational moments.

To simulate the environment of running condition, the engine speed of 9,000 RPM was selected [42]. This study presents simulation results from COMSOL to show how the compression ring performs. In this work the standard air cycle was employed, hence the ideal gas law was used, which allowed for a cycle pressure plot. A thermal and dynamic analysis was carried out to enable an accurate behaviour to represent the ring during operation.

5.3.4. Boundary Dynamics

The KTM 520 engine dimensions and material features (defined as typical KTM Spec) have been reported in chapter 3. As in the former study the ideal gas method was used to predict the pressure output from the piston. The air standard Otto cycle was applied, to generate a pressure output, which in turn created a pressure output. By using both methods for pressure prediction calculation a ‘look up’ table containing pressures at different positions for use within simulations is used.

Using numerical differentiation produces the piston velocity and, once again, to produce the piston acceleration [3]. The primary inertia force and the secondary inertia force acting on the piston have been considered.

By using Euler and Noether methods, the rotation of the piston ring is calculated [118,138].

This will now allow for the ring to fully rotate around the cylinder during operation. The final factor in the system is heat, as the engine operates the heat will cause the ring to deform. A method to represent the thermal expansion of the ring is to calculate the thermal strain defined in chapter 3.

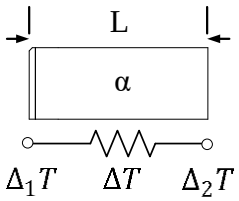

Figure 5.14 - Thermal expansion diagram

By including the thermal expansion the ring shown in Figure 5.14, will begin to oscillate and after expansion come to almost rest position.

In the four stroke internal combustion engine in the cooled state, the piston has a cylindrical profile from the crown to the bottom of the oil ring. The piston shape is elliptical from the bottom of the oil ring to the bottom of the skirt. Once the piston is in operation it is assumed that the geometry becomes almost cylindrical [36,140]. In this work it was assumed that the piston is of cylindrical profile. To develop the model further a response surface methodology was used.

5.3.5. Introduction of response surface methodology

Matlab SimMechanics was adopted to develop the KTM model in this system. To offer validation 3 sample sets of KTM BS-grade compression rings with MoS_2 coatings were

analysed after 60mins of operation. Each ring was checked using an SEM. Each image was cross-analysed using the free software Gwyddion.

Each engine component was re-engineered and defined accurately within the SimMechanics software package. Within the package all mathematical factors and Comsol simulated results are used. SimMechnics is a G-Programming method, where component blocks are used to represent each engine part (Figure 5.15).

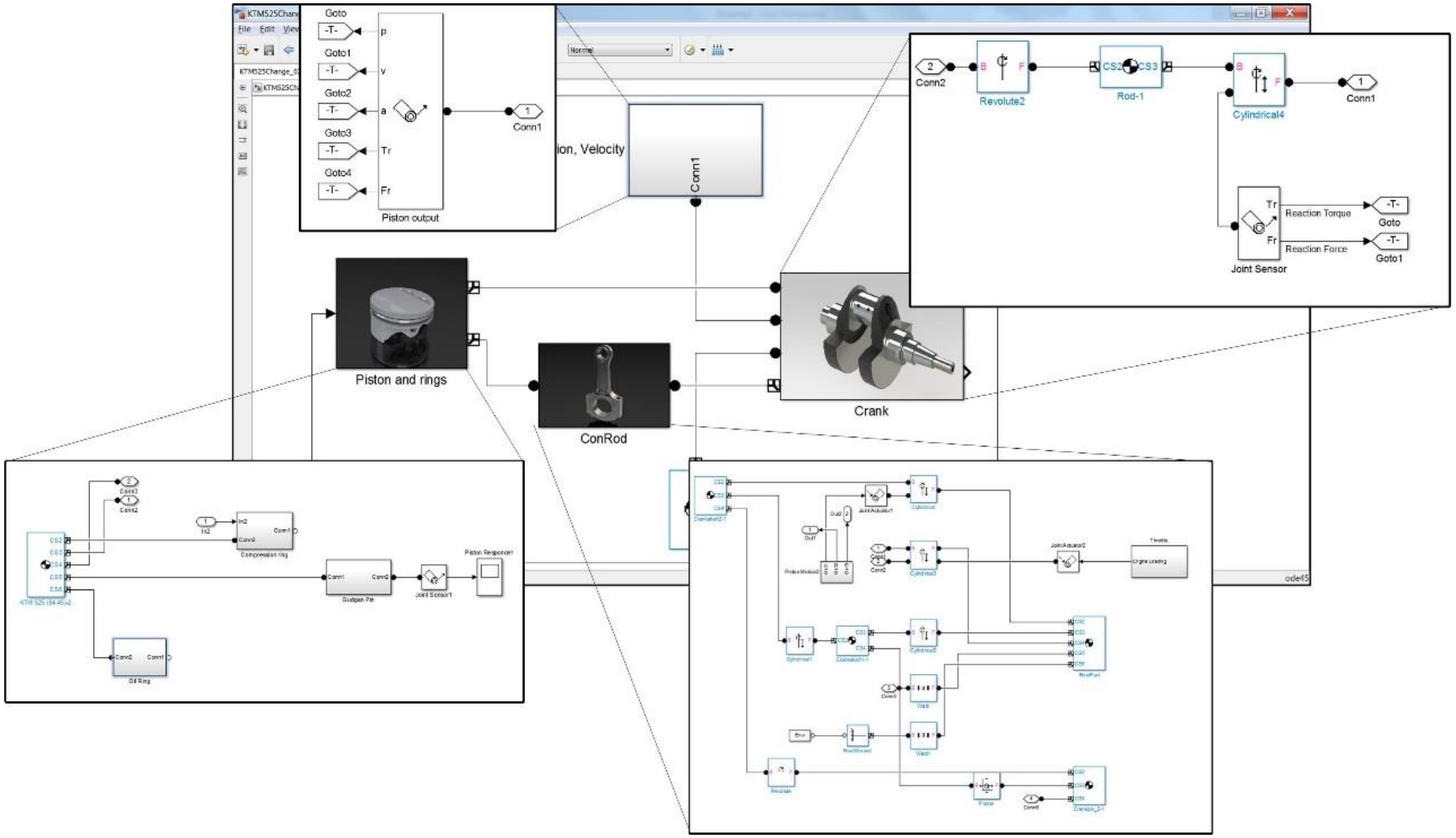

Figure 5.15 - Matlab/SimMechanics model

To examine the results further the design of experiments was adopted to optimize the compression ring geometry. More specifically the response surface methodology (RSM) is used. This methodology is a statistical technique that in the design of experiments allows for the user to explore the relationship between several experimental variables and response variables noted in Table 5-3. By using RSM the optimal response can be obtained through use of a sequence of deigned experiments. The variables are set by the topic of interest for the experiment.

Table 5-3 - Range of compression ring variables

Variable	Lower	Upper
Ring Width (mm)	1	5
Ring Mass (g)	0.7	1.2
Ring Radius (mm)	50	30

By applying RSM methods the variables range is defined and then calculated by

$$y = f(x_1, x_2, x_3) + \varepsilon$$

This is where $f(x_1, x_2, x_3)$, ε and y is the represented response surface, represents the noise and error observed respectively.

Table 5-4 - DOE response surface running order

Number Test	Ring Width (mm)	Ring Radius (mm)	Ring Mass (g)
1	5	30	1.2
2	3	40	0.7
3	5	50	1.2
4	3	40	0.7

5	1	30	0.2
6	1	50	0.2
7	3	40	0.7
8	1	30	1.2
9	5	50	0.2
10	3	40	0.7
11	1	50	1.2
12	5	30	0.2
13	5	40	0.7
14	3	40	0.2
15	3	40	0.7
16	1	40	0.7
17	3	40	1.2
18	3	30	0.7
19	3	40	0.7
20	3	50	0.7
21	1	37	0.69

Table 5-4 shows the defined design of experiments for the compression ring running order. With the use of RSM the system enables for the total runs to be optimised. This process generates the response (surface results show in Figure 5.16).

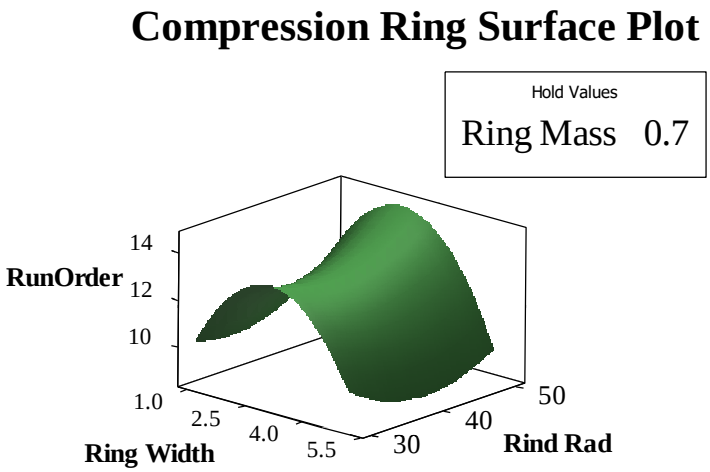

Figure 5.16 - Shows RSM for the compression ring

The RSM method defined a total of 21 runs to find the optimal performance of the piston ring. These 21 were placed into a variables list in Matlab. To run the simulation in SimMechanics with 21 runs, a piece of code was developed to automate this process.

5.3.6. Modelling of compression ring thermal behaviours

A thermal and dynamic analysis was carried out to enable an accurate behaviour to represent the ring during operation. By using the interpolation tool within COMSOL, heat and pressure predictions have been applied. A standard air cycle was used to generate a cycle pressure plot for the simulations. The KTM 520 engine has been used in this study as it is a high speed a four stroke internal combustion engine used in motor cycles.

5.3.7. Thermal and dynamic boundary's

As the piston rises from bottom dead centre to top dead centre the interaction on the piston ring comes from the lower contact of the groove where the ring sits and also the cylinder wall. However, during operation the cylinder wall will also be lubricated allowing the ring to travel more smoothly. Also during this time the piston ring will be

inclined to twist eliminating the linear continuous contact. Therefore in the simulation the pressure acting on the ring caused by the piston has been calculated and is applied as a boundary condition.

The KTM 520 engine dimensions and material features (defined as typical KTM Spec) have been reported in chapter 3. As this is a study to examine the performance of two materials for a piston ring is under coated and uncoated conditions.

To compensate for the pressure acting on the ring during operation an air standard Otto cycle was used to generate a pressure characteristic. This was achieved by modelling half of the cylinder, Piston and Piston ring. The variables such as the radius of the crank and the length of the connecting arm where added. The heat was defined from testing discussed in chapter 5. The internal cylinder area was used for the ideal gas, the model is displayed in Figure 5.17.

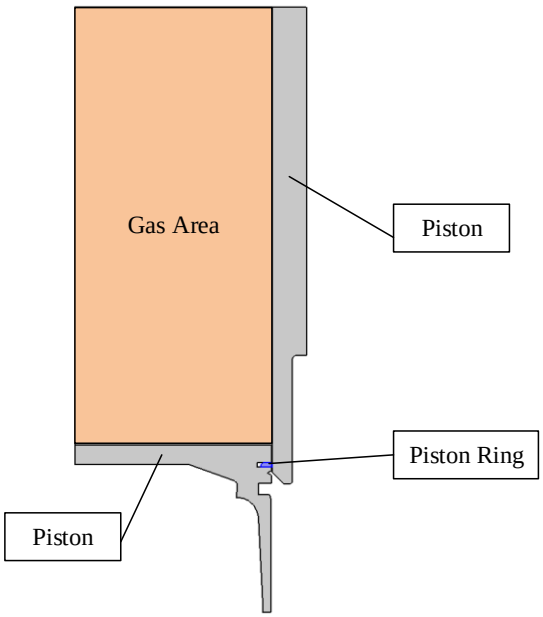

Figure 5.17 - Ideal gas model for the KTM 520

To calculate the displacement of the piston during one cycle equation (4.1) was used.

Pressure was calculated as using pressure equations noted in chapter 3. The gas force in the system can be determined from the pressure of the top and bottom, based on the circumference of the ring thickness.

The approach used by R.Mittler & al.[54] has been used to establish the pressure boundary conditions. In this study it is assumed that the ring is fully flooded. The Rabinowicz friction model was used to account for the abrasive wear occurring on the compression ring. The model also includes the thermal expansion of the ring is to calculate through use of the thermal strain which is equated by using the expression noted in chapter 5. The thermal deformation of the material have been considered in both coated and uncoated conditions.

Piston ring geometry used in this study is defined by the ISO standard [116]. In this work it is assumed that the piston is of cylindrical profile. As COMSOL has the ability to allow for work with variables and parameters, the use of equations on the simulation become easily applied. To simplify the process of the compression ring analyses the component was sub-dived into four, this is visually displayed in Figure 5.18. The data obtained from the pressure simulation was used as a variable and the inertia force calculated from the former study was defined as a positional variable over time. Thus, as the simulation when the simulation was calculating the rise from BDC to TDC the inertia force would be applied from the bottom land of the ring, the opposite options where used when the piston was travelling from TDC to BDC.

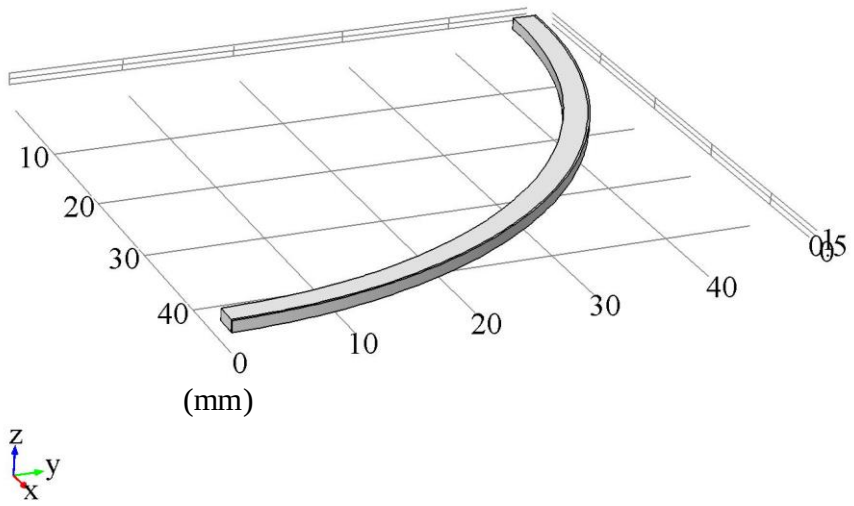

Figure 5.18 - Compression ring sample

5.3.8. Modelling standard and constrained dynamics

The main role of the compression ring is to seal the combustion area during operation. This has been the centre of much debate and advancements for the past two hundred years. During operation many factors will affect the way a compression ring will run-in to the cylinder wall, from the material of the ring to the wear reductive coating applied to the contact face. For this work a KTM 520 four stroke engine has been used. To running-in procedure used for this testing was defined using the KTM user manual. This study examines simulated results from MatLab to display the behaviours of the compression ring. In this study ideal gas was used, a dynamic and thermal analysis was completed to allow an accurate behaviour representation. The compression ring was studied as coated and uncoated conditions. The compression ring was simulated in two separate states, where the ring was fixed in position within the groove of the piston and free to move around the piston groove (Figure 5.19).

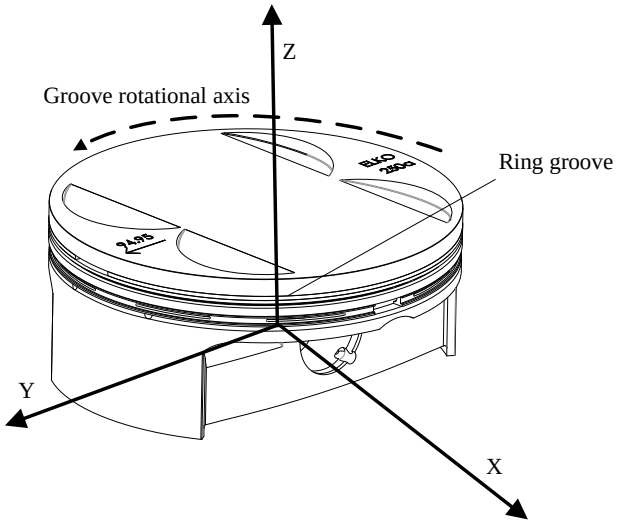

Figure 5.19 - Piston, compression ring and oil ring assembly

5.3.9. Simulated running condtions

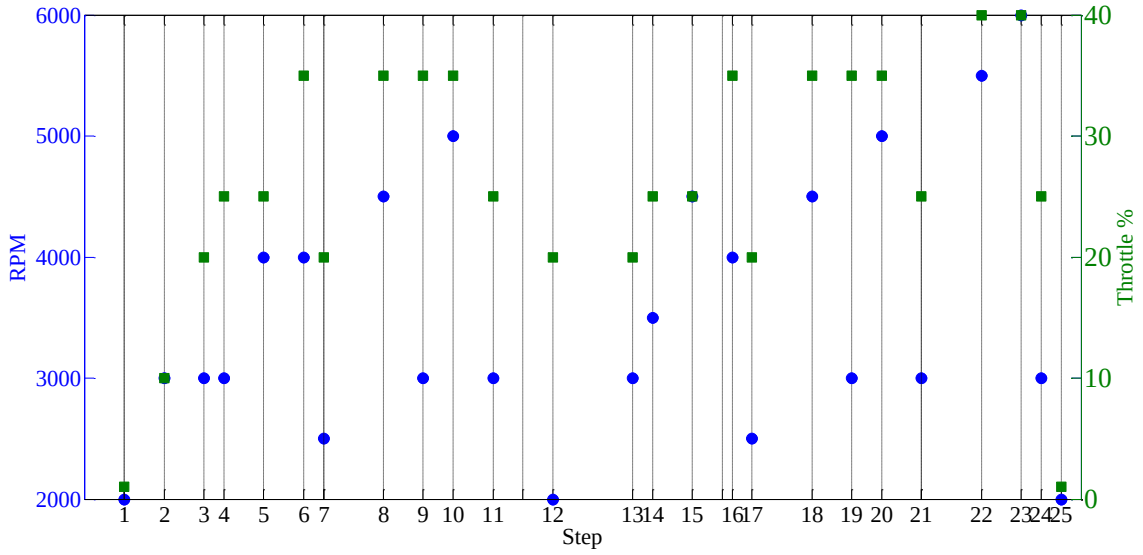

Figure 5.20 - RPM and Throttle position used in each of the 25 steps of the Running-in process

Figure 5.20 shows the running-in procedure based on the KTM manual recommended method for running a new engine has been developed to study both simulated and dynamometer work. The factors considered for this study was RPM, throttle position and time intervals as shown in Figure 5.20. The method used to calculate pressure and displacement of the piston during operation has been previously presented [9,134,135,141,142]. Cylinder conformability has been added in this study using Tomanik work [89]. To simulate the response of the system, the variables were placed into a Matlab/SimMechanics model.

CHAPTER 6 - RESULTS

6.1. Introduction

The main focus here is to examine the results found from the dynamometer testing and then continue simulation of the KTM 520 with the intention to provide validation. This chapter also discusses the development of a new profiling fixture.

6.2. Experimental results

6.2.1. Dynamometer running-in test results

Figure 6.1 shows the results from measured engine torque on coated (red) and uncoated (blue) compression rings for the KTM 520.

It can be seen from the results that the behaviour for both sets of compression rings follow the same trend. Within the first 10 minutes of operation (step 5) the torque reduces to 30Nm. This is then followed by torque of 45Nm. However, between 18 to 25 minutes the results show the material beginning to settle as the torque reduces and becomes smaller. During the running-in process the ring must run with the cylinder and through wear and thermal change, a seal will be generated. The uncoated rings will reach a maximum Torque output of 60Nm.

The coated compression rings during running display groupings around 30 – 40 Nm, however the uncoated rings display a larger torque of 60 Nm. This could indicate that the coated rings have a less aggressive and more controlled running-in process.

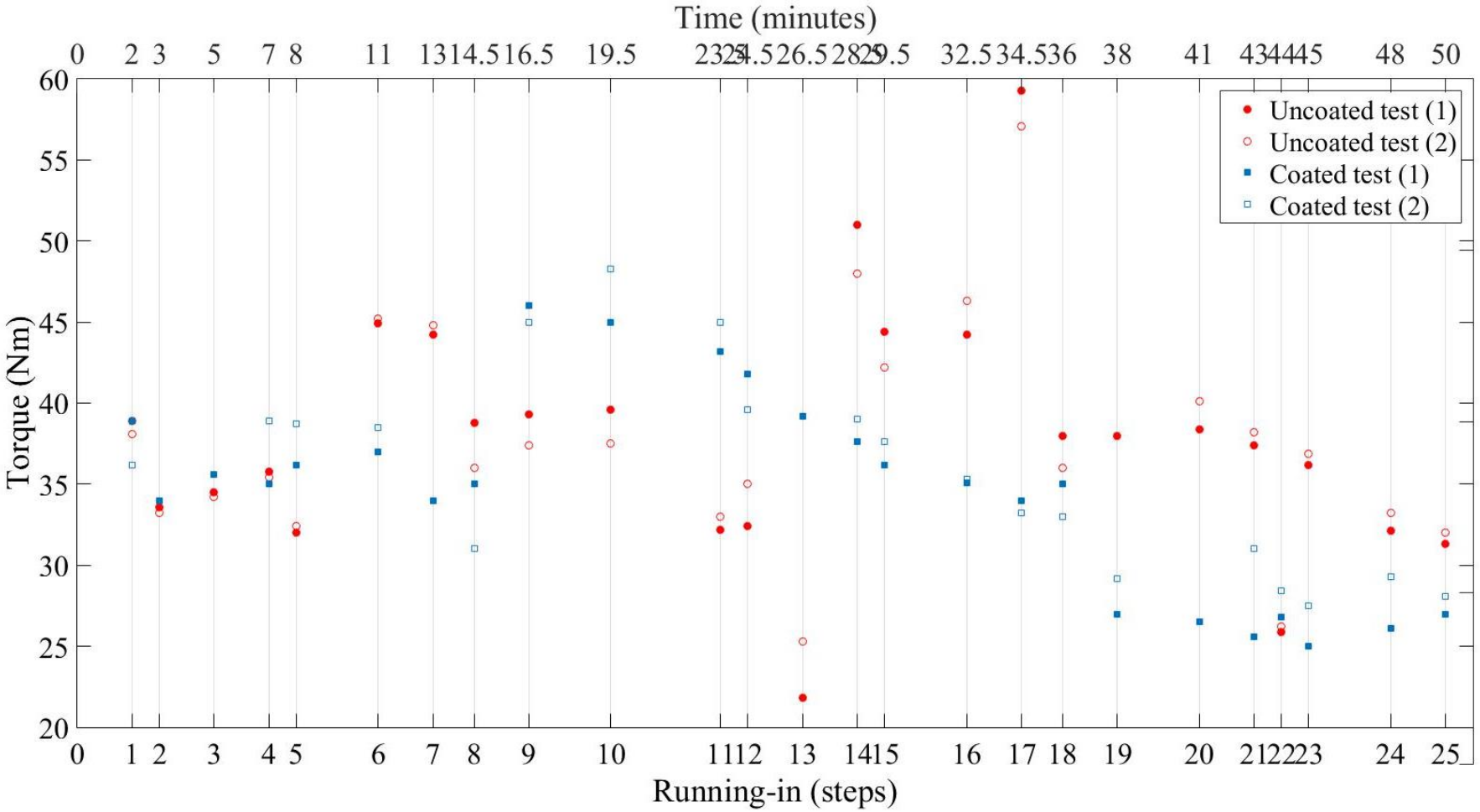

Figure 6.1 - Results of the torque output from the running-in with uncoated and coated compression rings

It was documented (Figure 6.2) that the highest Torque values and means reached from the running-in were generated by the compression rings that had no coatings applied. Throughout the running-in the average torque measurements for the respectively uncoated and coated compression rings respectively were 36.56 Nm and 31.32 Nm. As the torque variation for the coated compression ring is lower than that of the uncoated. The results suggest that having a coated compression ring reduces the overall torque output of the engine during the running-in procedure. On the KTM compression rings the most common coating found is MoS_2. This coating's sole purpose is to reduce wear loss during the operation, but also to fill asperities that can be found on the material during the wearing process. This is an effort to ensure a uniform surface is in operation.

The uncoated compression ring in the results shows an increased torque value. This could be as the result of the compression ring deforming through both wear and thermal dynamic behaviour to create an almost ideal contact relationship between the piston ring face and the cylinder wall shape. In the race application high torque values will typically indicate a greater power output of the engine and in industry are in large demand. However, to ensure a greater operational use and also ensure performance lower torque values may be needed during the running-in procedure in order to reduce the damage generated during this process. The effect of the running-in process plan will be further investigated within this work. The distribution profile of the coated and uncoated compression rings have a similar distribution profile which can be directly related to the range of parameters examined during the running-in process.

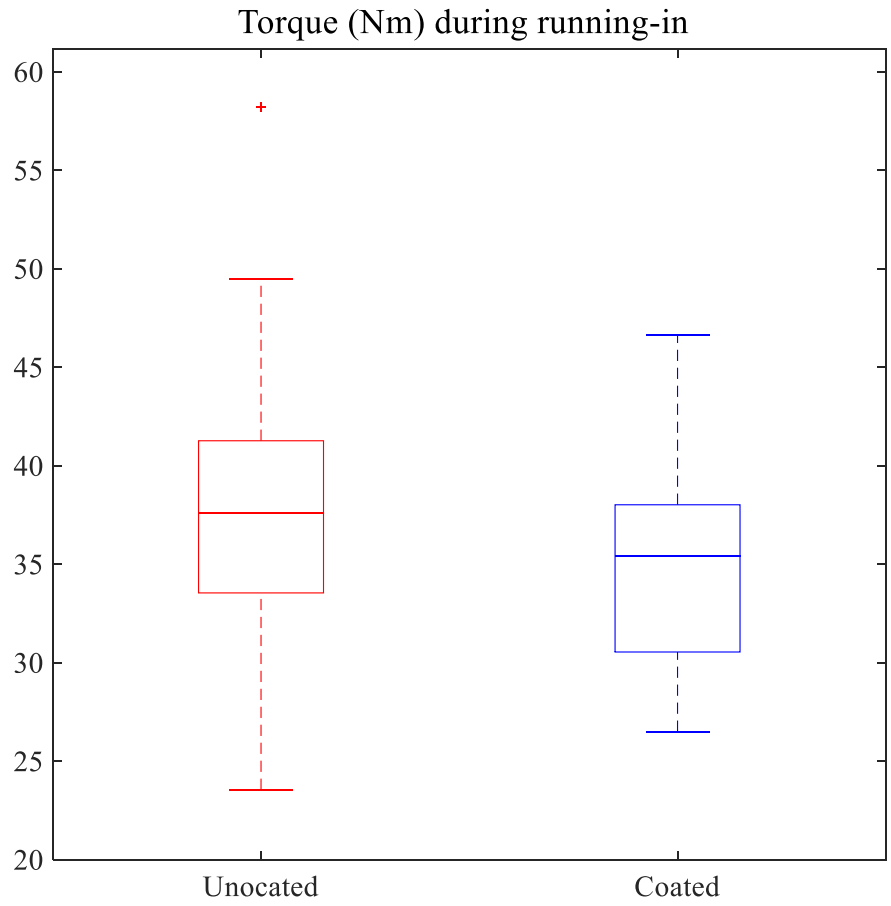

Figure 6.2 - Torque variation during running-in procedure with coated and uncoated compression rings

Table 6-1 - Mean and Std of Dyno Running-in Torque Output

	Coated	Uncoated
Mean Average Value Nm	34.898	37.718
Standard Deviation	5.885	7.424

The coolant temperature measured during the running in (Figure 6.3) shows the stabilised temperature is reached around 70 - 80° C. However, at step 21 the uncoated ring begins to have an influence on the temperature as an increase of around 3° or 4° is observed (Figure 6.3), indicating that higher temperatures are reached when using uncoated compression rings. The average coolant temperature measured during running in procedure was recorded at 73.41°C and 72.45°C for the uncoated and coated compression rings respectively (Figure 6.4).

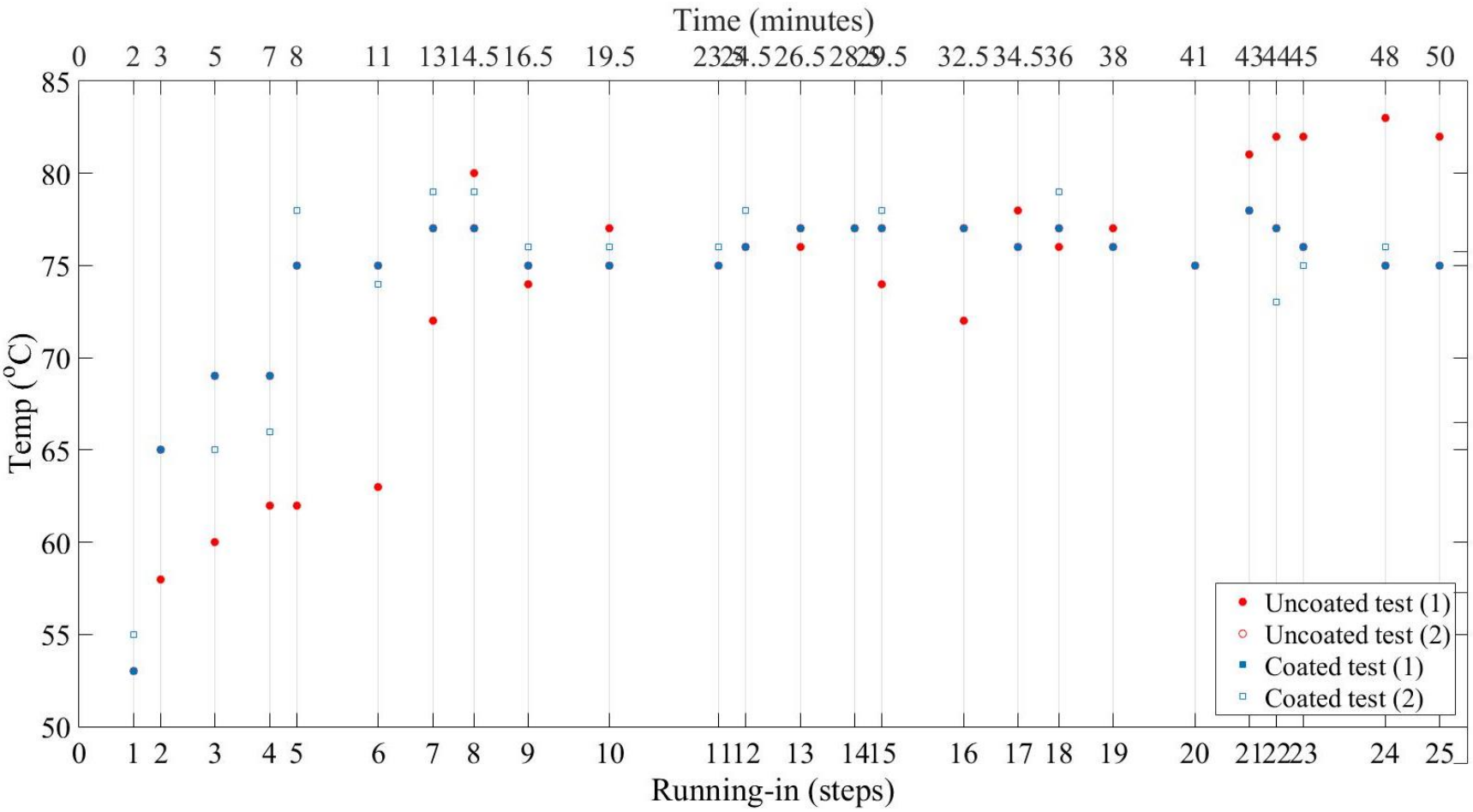

Figure 6.3 - Temperature of coolant of Coated and Uncoated compression rings during running-in

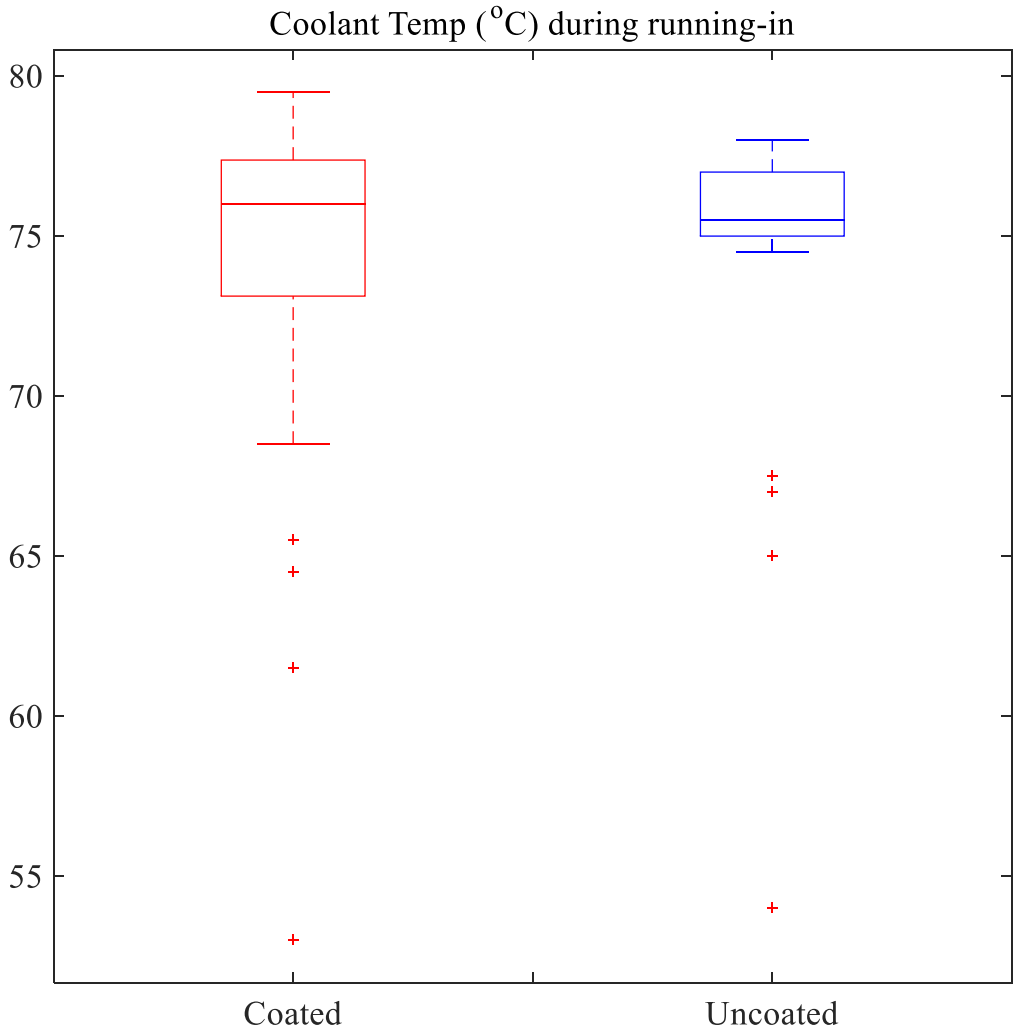

Figure 6.4 - Coolant temp output for coated and uncoated compression rings during running-in

Table 6-2 Mean and Std of Dyno Running-in Coolant Temp Output

	Coated	Uncoated
Mean Average Value Nm	72.45	73.42
Standard Deviation	8.1	6.7818

When the engine is installed with MoS_2 coated compression rings the engine output temperature is recorded to be lower than what is seen when uncoated rings are used. As MoS_2 has a much lower coefficient of friction compared with the uncoated ring in either dry or lubricated states, it is rational to consider that by having a coating present on the compression ring heat generation through friction will be lower thus lower heat. Similar examinations have been observed with the use of MoS_2 on cutting tools and in gear boxes [80,143,144].

At step 5 of the running-in procedure the throttle position is increased. With this increase a rise in temperature is also observed instantaneously (Figure 6.3) for the uncoated compression ring. The coated compression ring is noted to have a progressive increase to the same temperature confirming what has been seen in former studies [80,143,144].

When uncoated ring reaches step 9 to 12 in the running-in procedure, the results show a large fluctuation of temperature as the engine is placed into the top gear and throttle is adjusted accordingly, the uncoated grey cast iron ring has a greater coefficient of friction than what can be found on the MoS_2, hence this could be a possible cause of the heat changes in both rings.

6.2.2. Development of profile piston ring fixture

Figure 6.5 (a) shows the piston ring used in race engines. It explains the terminologies commonly used including top ring, land, bottom ring land, ring gap and contact face. Figure 6.5 (b) shows the North, East, South and West directions of the measurements made using the Dickinson Rotating Ring Contact Profiler. Measurements were repeated 10 times to determine the statistical errors in the measurements using the Taylor Hobson Talysurf. The North direction has been specific at the gap in the piston ring which was rotated 5 times for each position.

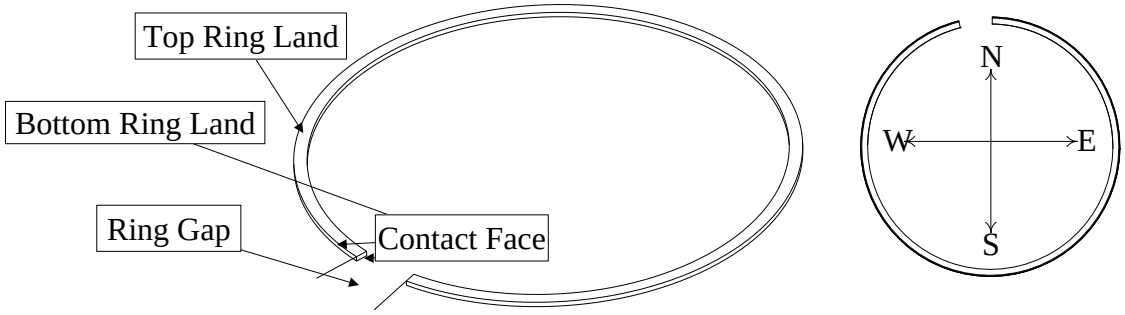

Figure 6.5 - (a) Race piston ring terminologies, (b) test regions

The measurements of R_a values is one of the most common profile parameters, this parameter gives the average roughness. R_a is typically expressed in μm for engineering

components in engines. The average roughness has a significant influence on the performance and lifetime of engine wear parts. In general the lower the R_a values the lower the coefficient of friction determining wear rates, life and performance. This parameter refers to profiles exceeding the roughness profile mean line. The parameter R_z however refers to the average maximum height of profile. The R_p parameter refers to the maximum profile peak height of the surface. These three parameters allow for a good understanding of the surface profile during analysis hence the reason for selecting these three profiles for comparison.

Table 6-3 - Flat ring profiles measurements repeated 10 times on the top land of the ring with mean and standard deviations calculated.

Flat repeat					
User 1	**Test No.**	**R_a (μm)**	**R_p (μm)**	**R_z (μm)**	**Repeat 10**
	Mean (σ)	0.3017	0.6712	2.0037	
	Standard deviation $\sqrt{(\sigma^2)}$	0.0035	0.0038	0.0202	

Table 6-3 shows the 10 measurements made with R_a, R_p and R_z values. The mean and standard deviations were calculated for R_a, R_p and R_z which gave values of 0.3017 and 0.0035; 0.6712 and 0.0038; and 2.0037 and 0.0202 respectively. These values will be used as baseline standard reference to compare subsequent results using the new Dickinson Rotating Ring Contact Profiler.

Table 6-4 - Surface profile measurements in four directions repeated five times with associated mean and standard deviations.

Rotation flat repeat					
User 1	**Test No.**	**R_a (μm)**	**R_p (μm)**	**R_z (μm)**	
	Mean (σ)	0.2789	0.6113	1.6155	**North**
	Standard deviation $\sqrt{\sigma^2}$	0.0285	0.0181	0.1106	
	Mean (σ)	0.3424	0.9863 (0.6767)	2.0431	**East**
	Standard deviation $\sqrt{\sigma^2}$	0.0986	0.6207	0.6872	

	Mean (σ)	0.3177	0.6955	2.0321	**South**
	Standard deviation $\sqrt{\sigma^2}$	0.0975	0.1078	0.7311	
	Mean (σ)	0.6623	1.2671 (0.7931)	2.7271	**West**
	Standard deviation $\sqrt{\sigma^2}$	0.3791	0.9606	0.9667	

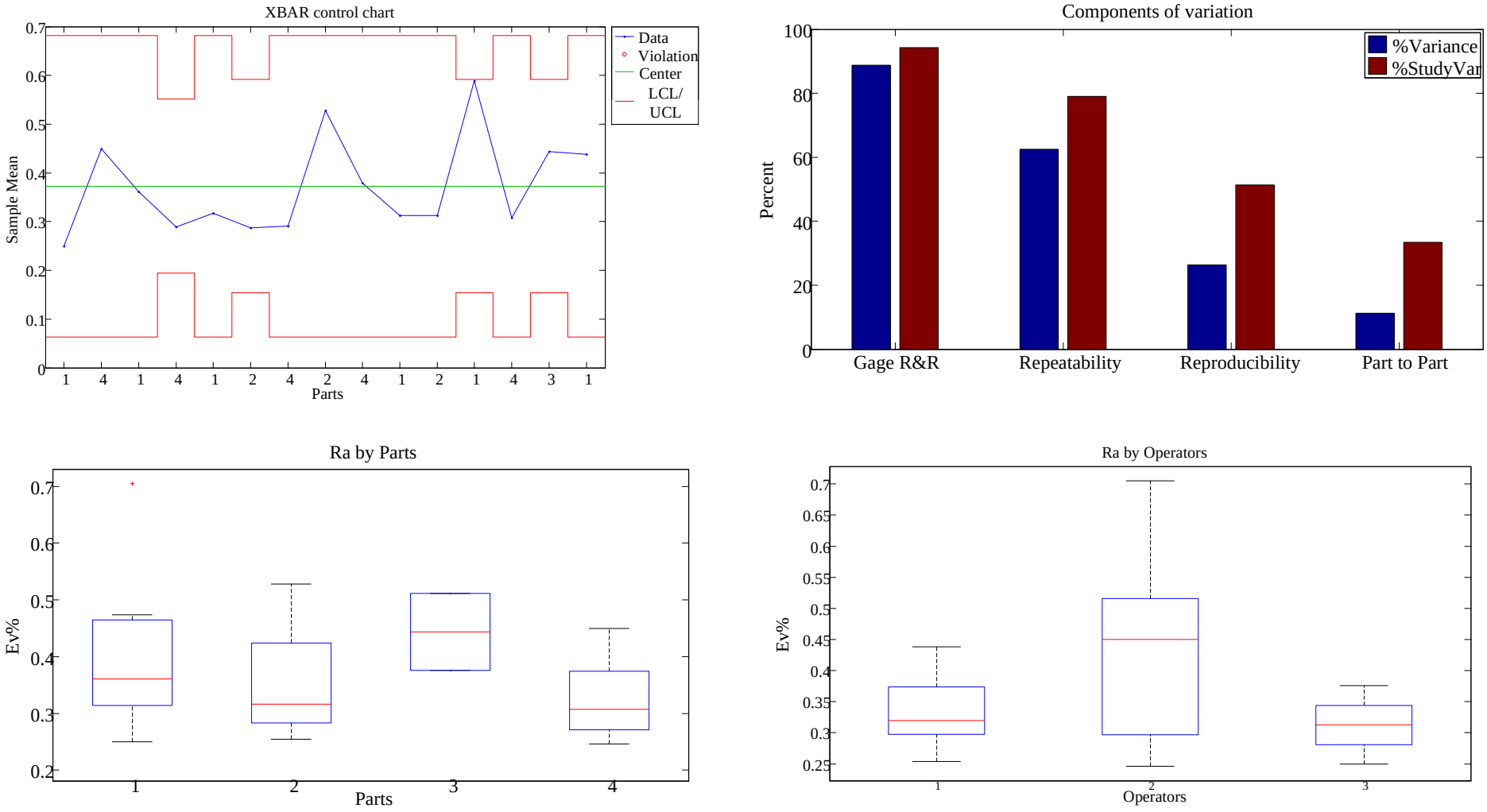

Figure 6.6 - Showing the GR&R (Ra) for the standard stage

In Table 6-4 (in each R&R test the North, East, South and west have been replaced with 1,2,3,4 respectively) the standard system has been employed using flat profile in the four principle directions. Measurements in the North and South gave means and standard deviations for R_a, R_p and R_z which are similar to those used as baseline from repeated tests shown in table 1. However, the East and West measurements for the mean and standard deviation R_p are higher than expected i.e. 0.9863 and 1.2671 for the means and 0.6207 and 0.9606 for the standard deviation respectively. There are several possible reasons for these anomalies. Firstly, they may be as a result of surface defects present in the piston ring and particulates embedded in its surface.

There are limitations of this current system. Each set of results were only able to be obtained on the flat profile, therefore, to obtain corner profiles of the piston ring and with zero movement the compression ring would need to be divided. In a situation in which ring profiles are needed however dividing the ring into smaller pieces is not an option the standard system is unable to achieve this.

The surface profile measurements were repeated using the Dickinson Rotating Ring Contact Profiler following the same procedures used for the standard system.

Table 6-5 - Ring profiles measurements repeated 10 times on the top land of the ring with mean and standard deviations calculated using the Dickinson Rotating Ring Contact Profiler.

Repeat (DRRCP)					
User 1	**Test No.**	**R_a (μm)**	**R_p (μm)**	**R_z (μm)**	**Repeat 10**
	Mean (σ)	0.3167	1.2053	2.3036	
	Standard deviation $\sqrt{(\sigma^2)}$	0.0031	0.0426	0.0476	

When the mean and standards deviations of the R_a, R_p and R_z were compared with standard systems the new system gave similar values to the standard system for R_a and

R_z. However, the mean R_p values and standard deviation were significantly higher than those obtained for the standard system. The new system mean R_p of 1.2053 and standard deviation of 0.0426 compared to the values obtained from the standard system mean R_p of 0.67118 and standard deviation of 0.0038. An examination of these means demonstrates that the mean acquired by the DRRCP is almost twice that obtained by the standard values. This suggests that the R_p values are not good indicates of surface roughness in this case possibly because the surface is curved. Table 6-5 and Table 6-6 results were obtained by placing the ring into the Dickinson Rotating Ring Contact Profiler to analyse the contact face relative to the stylus.

Table 6-6 - Surface profile measurements in four directions repeated five times with associated mean and standard deviations using the Dickinson Rotating Ring Contact Profiler.

	User 1							
	North		**East**		**South**		**West**	
	Mean (σ)	*Standard deviation* $\sqrt{\sigma^2}$	*Mean (σ)*	*Standard deviation* $\sqrt{\sigma^2}$	*Mean (σ)*	*Standard deviation* $\sqrt{\sigma^2}$	*Mean (σ)*	*Standard deviation* $\sqrt{\sigma^2}$
R_a (μm)	0.3048	0.0744	0.3573	0.0553	0.4382	0.084	0.4177	0.1573
R_p (μm)	0.9615 (0.5615)	0.1399	1.2533 (0.611)	0.2234	1.2671 (0.66714)	0.1574	1.5351 (0.7351)	0.8673
R_z (μm)	1.9869	0.2521	2.455	0.3025	2.6503	0.3799	2.8076	0.8867
	User 2							
	North		**East**		**South**		**West**	
	Mean (σ)	*Standard deviation* $\sqrt{\sigma^2}$	*Mean (σ)*	*Standard deviation* $\sqrt{\sigma^2}$	*Mean (σ)*	*Standard deviation* $\sqrt{\sigma^2}$	*Mean (σ)*	*Standard deviation* $\sqrt{\sigma^2}$
R_a (μm)	0.3097	0.0913	0.3232	0.0601	0.4382	0.0840	0.4119	0.0976
R_p (μm)	0.5830	0.2113	0.5157	0.1966	0.6671	0.5288	0.7158	0.5219
R_z (μm)	2.0049	0.4455	2.2092	0.2040	2.6503	0.3799	2.5127	0.6817
	User 3							
	North		**East**		**South**		**West**	
	Mean (σ)	*Standard deviation* $\sqrt{\sigma^2}$	*Mean (σ)*	*Standard deviation* $\sqrt{\sigma^2}$	*Mean (σ)*	*Standard deviation* $\sqrt{\sigma^2}$	*Mean (σ)*	*Standard deviation* $\sqrt{\sigma^2}$
R_a (μm)	0.3079	0.0336	0.2971	0.0551	0.3706	0.1444	0.4398	0.1347
R_p (μm)	0.67246	0.266213	0.51756	0.2260	0.5851	0.4998	0.9199	0.5077
R_z (μm)	1.9853	0.266884	2.1865	0.184299	2.4779	0.6544	2.5611	0.7682

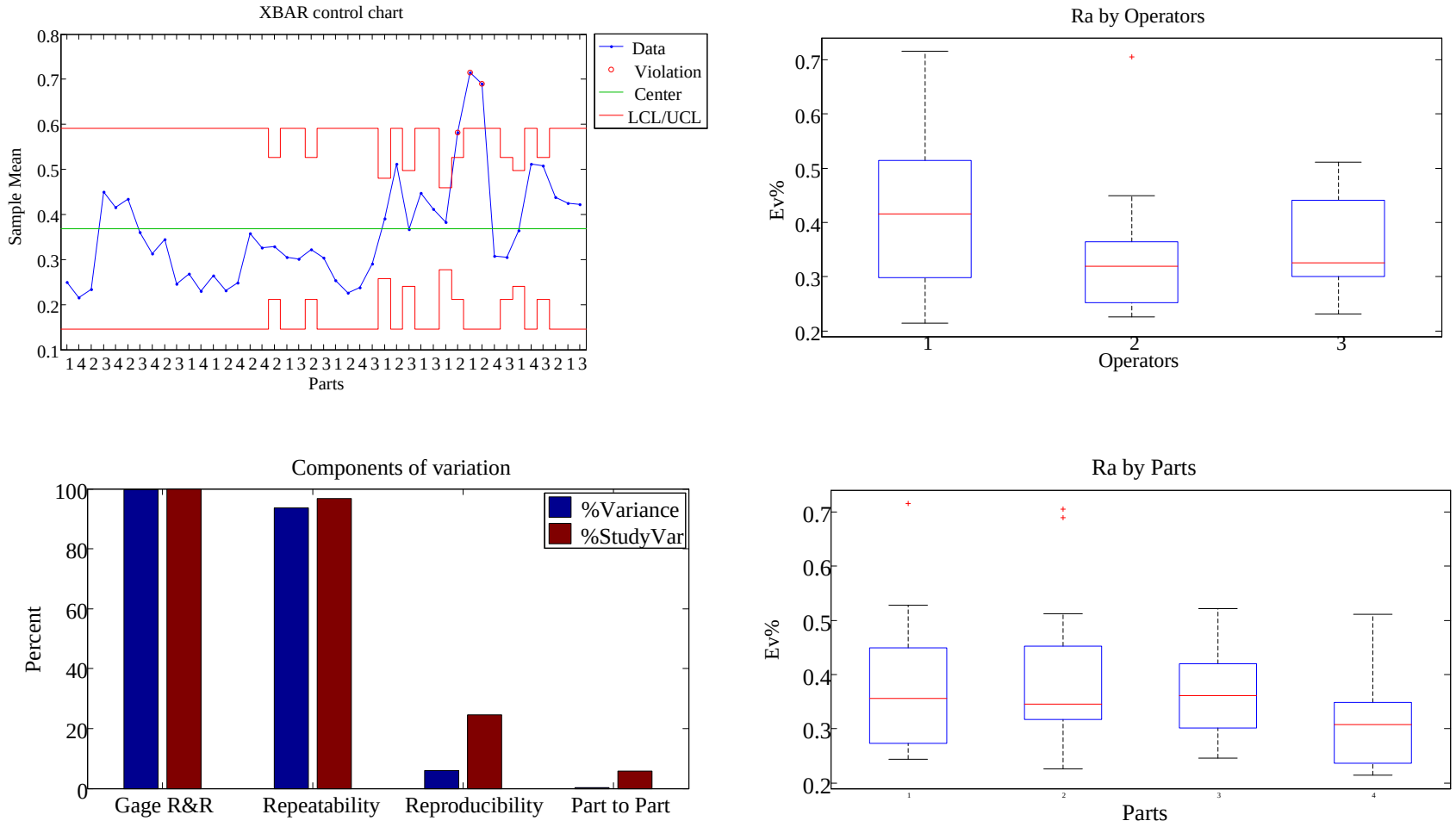

Figure 6.7 - Showing the GR&R (Ra) for the (DRRCP)

The new DRRCP has been used to measure the surface roughness profiles in four different directions north, south, west and east.

As expected the mean values are in the range 0.3 and standard deviation of 0.07 and this compares favourably with measurements taken using the standard system. There are deviations in the East and West directions similar to those obtained in the standard system. This indicates the presence of surface defects or particles. Including myself and 3 operators where used to gauge reproducibility and repeatability shown in Figure 6.7 for Ra. Figure 6.6 shows the R&R attached to the Ra value the repeatability of the this test which results in 88.35% which suggests that there is a 11.65% error in the system, this confirms that the device is in the range of acceptability based on the importance of the product.

6.2.3. A study into compression ring surface profile prior to operation

The rings where placed in with ring gap facing intake of the engine. Once the run-in was completed the rings where removed. Before and after the compression ring hardness of the rings where taken shown in Table 6-7.

Table 6-7 - Sample sets

	Omega		**KTM + MoS_2**	
Sample 8	50 min	0 min	50 min	0 min
average Er(Gpa)	133.18	125.37	197.61	184.17
υa	0.26	0.26	0.26	0.26
υb	0.2	0.2	0.2	0.2
Modulus(Gpa)	124	117	184	165

The location in which the test was conducted was located on Y Axis face for both compression ring samples.

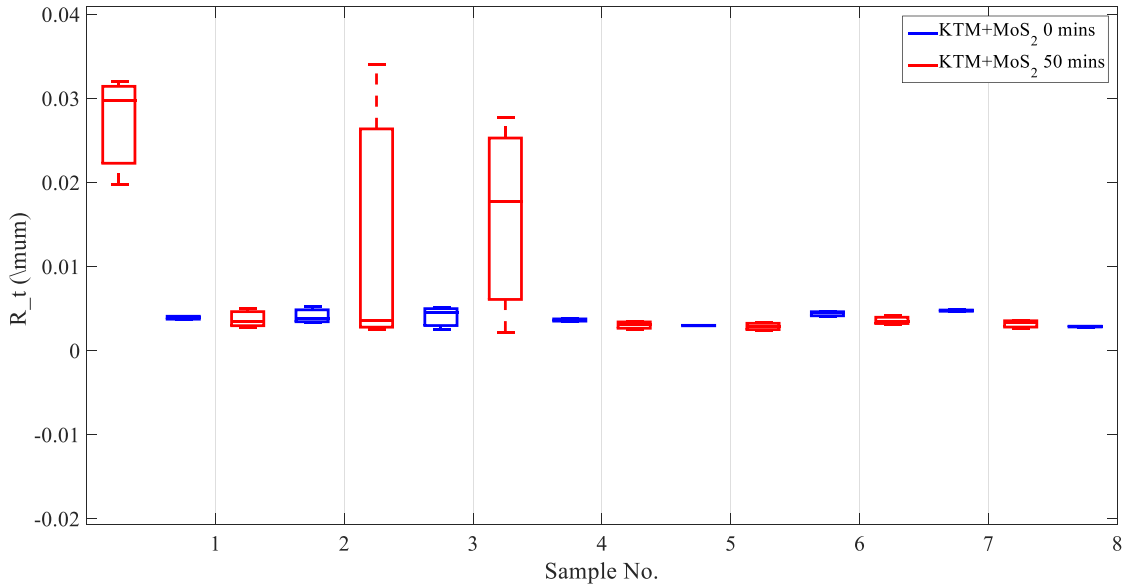

Figure 6.8 - Maximum height profile for KTM

Figure 6.8 shows the KTM compression ring samples before and after running-in. Before running the ring at sample 1 and 4 suggests large profile heights, these could be linked to the manufacturing process. As a function of the coating is to attempt to fill asperities on the material before hardening to do its main task of being a wear resistant coating.

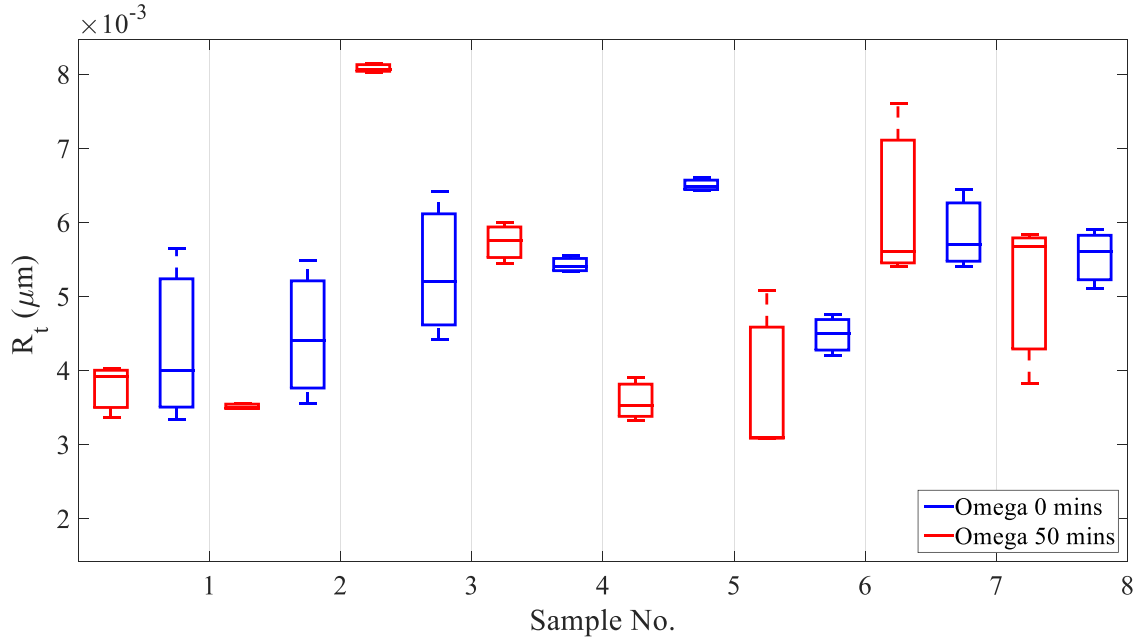

Figure 6.9- Maximum height profile for Omega samples

Figure 6.9 shows the Omega compression ring samples before and after running-in. Before operation the ring is smoother that the KTM. However, this ring is uncoated, hence post coating has not been done. After 50 min operation the uncoated ring seems to wear almost linear.

Table 6-8 - Standard Deviation of R_t

	0 minutes	50 minutes
KTM+MoS_2	8.95×10^{-3}	6.55×10^{-3}
Omega	1.60×10^{-3}	7.64×10^{-4}

Table 6-8 shows the standard deviation between samples before and after running. The second set of data is to examine the X-axis position of the results.

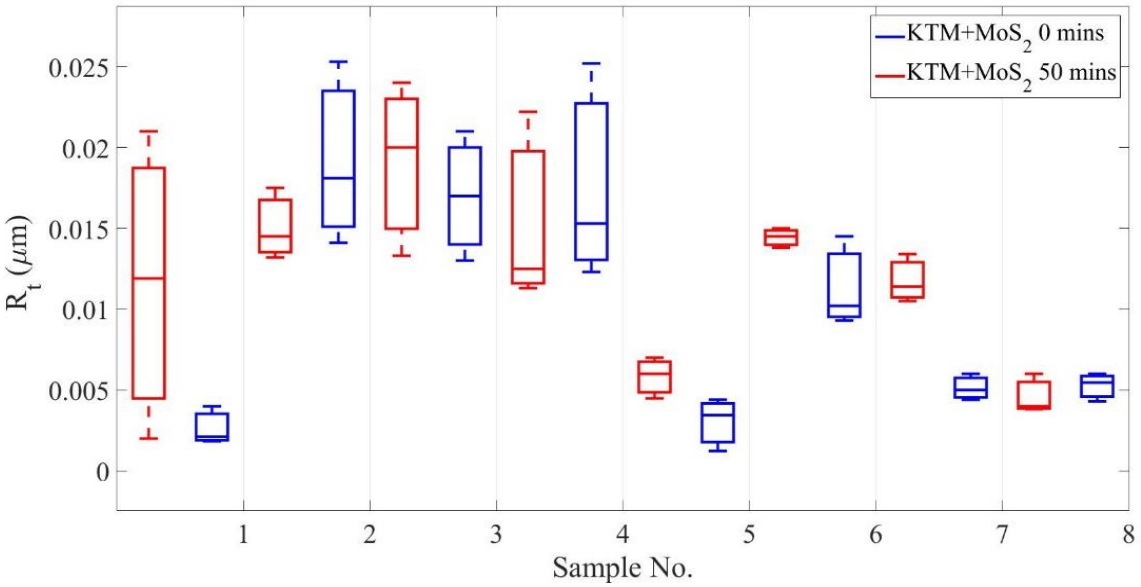

Figure 6.10 - Maximum height profile KTM X-axis

Figure 6.10 shows the X-axis of the compression ring face before and after the running-in. The results show that after 50 mins of use at samples 1, 7 and 8 the height of the surface is low. This could suggest that as the ring is place at the front (inlet) of the engine and while in use the ring will wear unevenly.

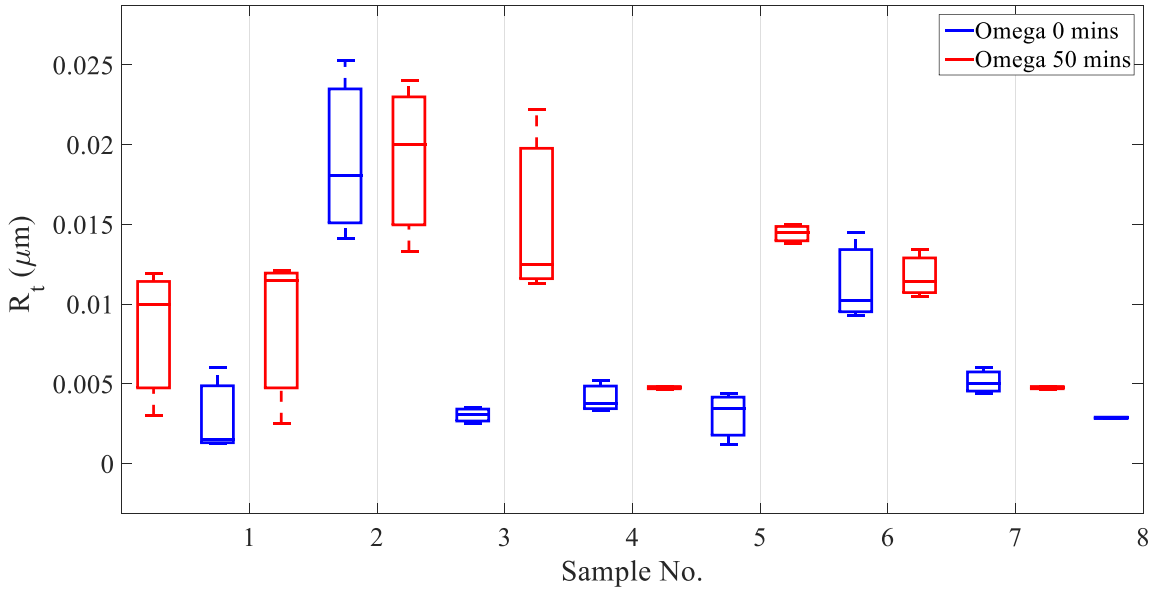

Figure 6.11 - Maximum height profile Omega

Figure 6.11 shows the x-axis of the Omega compression ring face before and after the running-in procedure. The results show that the compression ring still has high asperity areas after operation. As expected the compression ring is not coated thus surface damage and material loss will be greater.

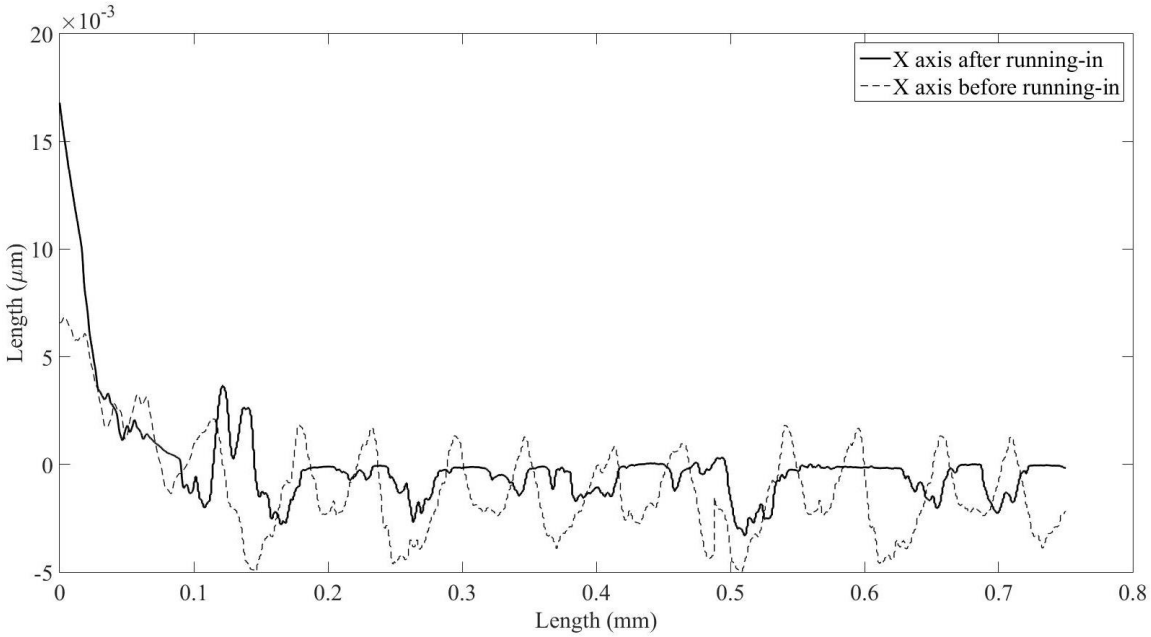

Figure 6.12 - KTM 520 X-axis ring profile before and after running-in

Figure 6.12 shows the KTM 520 contact profile before and after the running-in procedure. The surface of the compression ring profile before operation shows multiple asperity

profile which is more commonly known as “waviness”. The results presented post operation, the ring profile has less asperities and has a much more smooth profile.

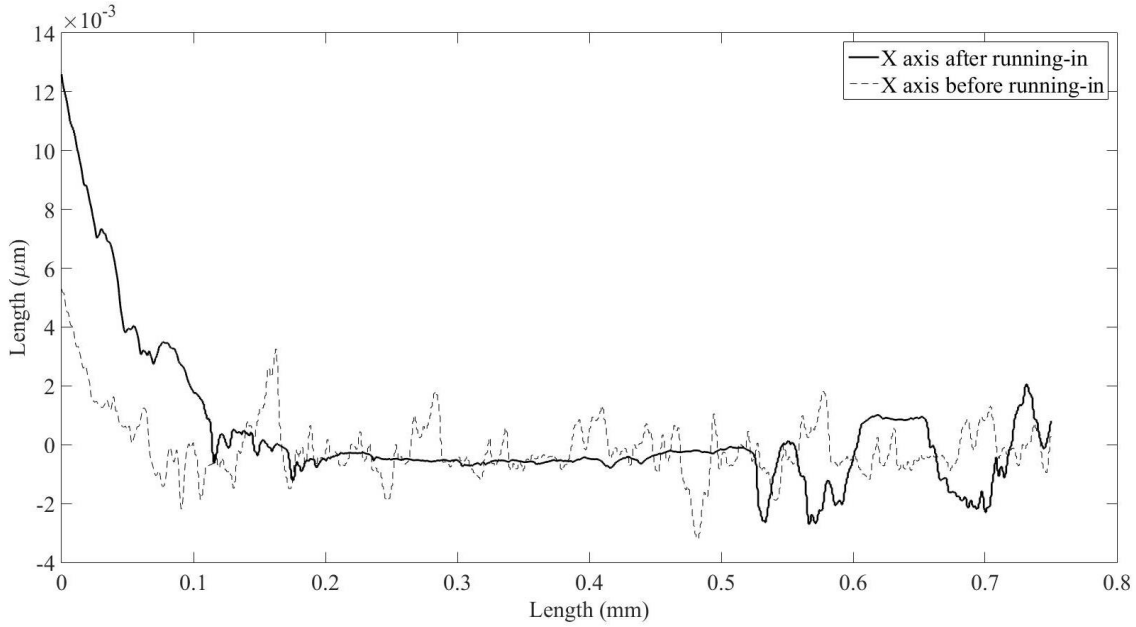

Figure 6.13 - Omega X-axis ring profile before and after running-in

Figure 6.13 shows the results from running the Omega compression ring before and after the running-in procedure has been executed. Before operation the compression ring has amounts of asperities that resemble peaks and valleys that where seen with the coated ring. After the procedure, around the chamfered area the ring has suffered a large amount of material loss, however from the surface profile it is clear to seen that the mid area of the x-axis has been the most on contact due the smooth surface.

Before the running of the KTM ring, the surface is quite rough due to the manufacturing process, hence an uncoated ring will tend to have a smoother face. After the rings had been run-in the profile heights are very close in value. However, calculating the standard deviation (Table 6-8) of both samples shows that the uncoated ring will wear more evenly that the coated ring these findings correlate to what was reported [13,136]. Sample 1 in all directions has the lowest height profile after running which from studying the original position of the ring during installation and the positon after, could suggest that the ring

will move and then stop. The results from the X-axis profiles shows ring waviness present, this profile correlates to what was suggested in [18,19], where it was suggested that by incorporating waviness into the coating profile would assist the process of running-in. However after operation some asperities how clearly grown, this could suggest material transfer during the operation, as MoS_2 will go through a morphological stage which allows the atoms of the material to move more freely hence results in the material being temporally susceptible to contamination. The uncoated compression ring however indicates some interesting insights to the dynamics, after operation the profile has a low roughness to the mid area of the ring. It is presumed that this is the result of the torsional twist as to the lower end of the face there is large amounts of material loss and also what appears to be material transfer.

6.2.4. Compression ring surface profile pre and post operation

As the compression ring is subjected to many manufacturing processes, often scuff marks can be found on the surface, the aim of this study was to examine the compression ring pre and post operation. A particular interest was placed on the lands of the ring as they will not only display the material loss but they will also show signs of scuffing where motion could occur.

Figure 6.14 a. shows the compression ring after the running-in procedure was executed, b. shows the same however before running-in, and both images have been taken at a resolution of 200µm. The image shown in b. shows the material after manufacturing. There are surface scratches and some small markings, and these are presumed to be the results of post-processing of the ring while the coating was thermally sprayed. Figure 6.14 b shows small collections of MoS_2, this is a results of the post-processing of thermal spray application. To the lower right side of the image the MoS_2 coating note the small collections of coating material as a results of the thermal spraying application.

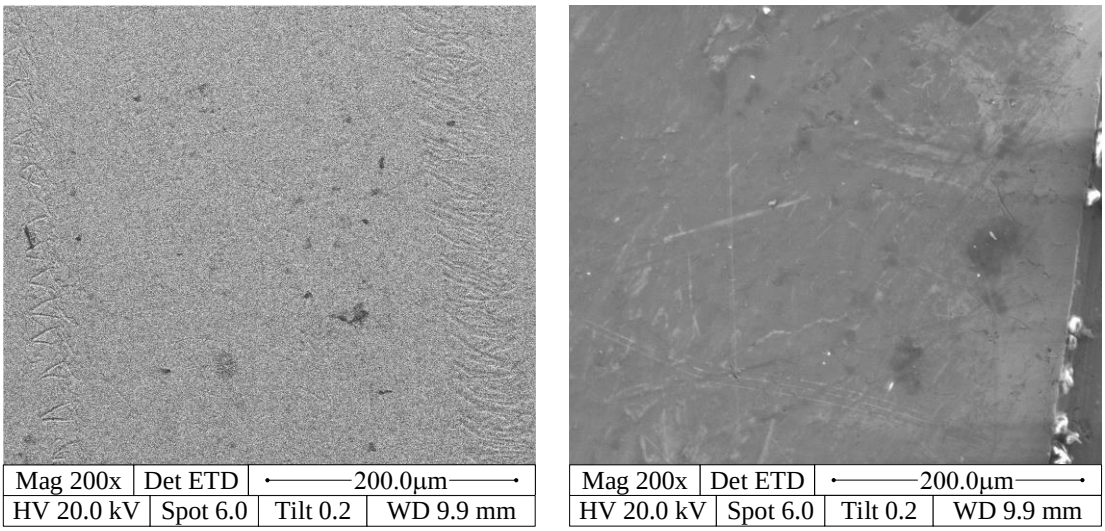

Figure 6.14 - a. surface profile after use, b. surface profile before use

In Figure 6.14 a. the image shows the surface after the running-in procedure. The image shows two track marks that are clearly defined in the surface. It is presumed that the track to the right of the image is at a point where the ring as has been twisting and the track to the right close to the piston groove lip. The markings only exists within the thrust face operation area.

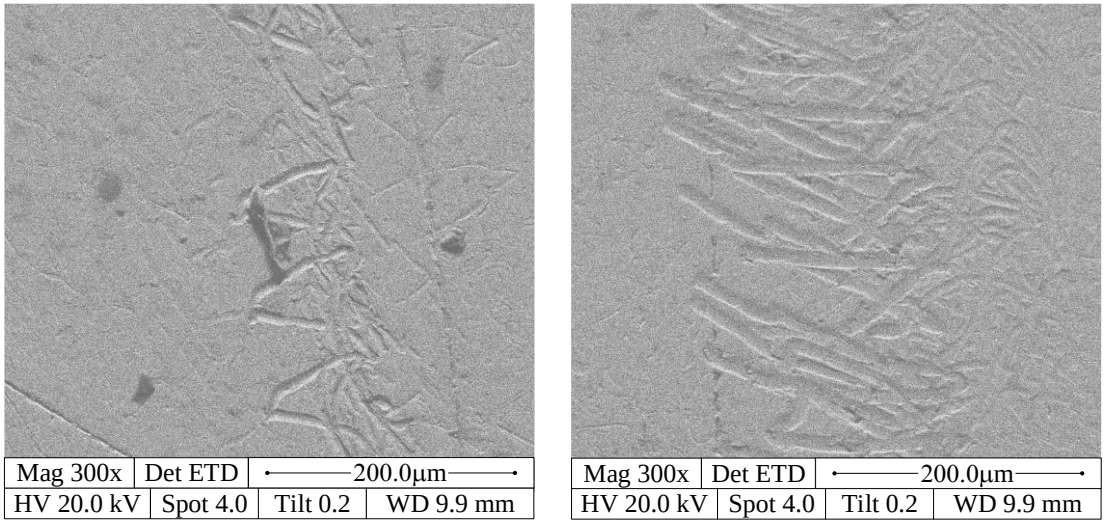

Figure 6.15 - a. inner wear track, b. outer wear track

Figure 6.15 shows a SEM image taken at the resolution of 50µm from what has been seen in Figure 6.14. a. is of the inner track here shows less of contact due to the level of

scratches seen. b. shows the outer area. Here it is clear that the rotational action has occurred causing the markings seen.

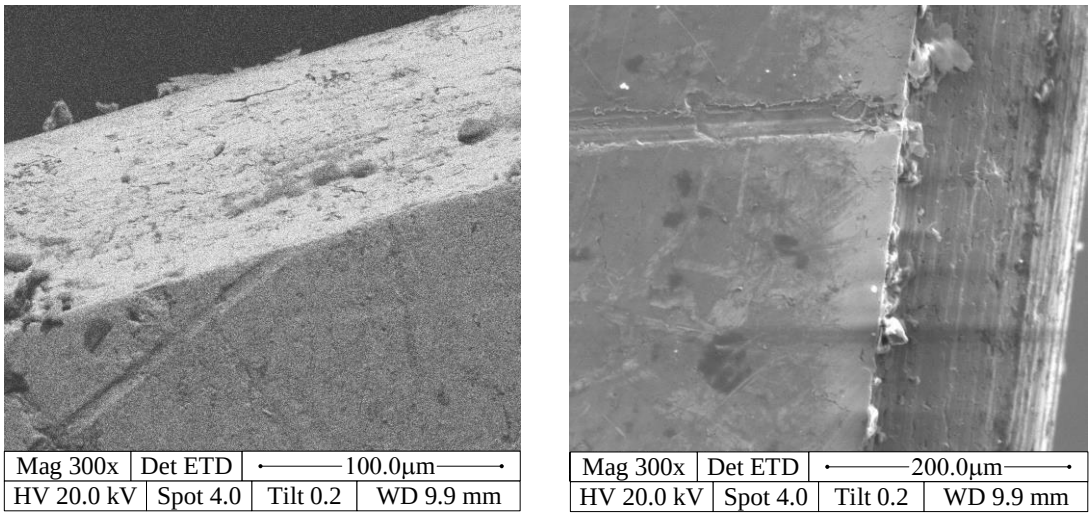

Figure 6.16 - a. Piston ring after 50 minute operation b. piston ring before operation

Figure 6.16 a. shows the compression ring after the running-in procedure and b. shows the compression ring before operation. b. shows the compression ring before the running-in is executed the cast iron is of smooth appearance, to the right of the image is the coating, the small collections of material to the face are a result of post processing thermal spray to apply the coating. a. shows the compression ring post running-in procedure, the coating appears in a streak like condition this confirms results seen by Renevier [80] which note that MoS_2 in thermal states will attempt to shear, hence the material producing a result in a fold-like fashion. Also on the coating, there are small surface cracks.

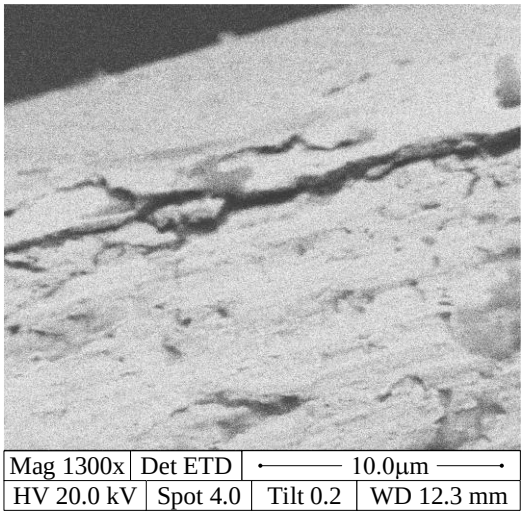

Figure 6.17 - Compression ring after operation surface damage

Figure 6.17 shows a closer area of the crack seen in Figure 6.16 a. The image shows a crack in the coating.

The results show that before operation the compression ring has miner surface markings, the material has a smooth appearance. The results from the ring after the running-in has been executed show scratches that indicate rotational behaviour. These scratches do not cover the full circumference of the ring and also do not have mass levels of scratches, indicating that the ring will rotate however after a fixed amount of time come to rest. This supporting work seen in chapter 4 where it has been noted that the ring will oscillate until the thermal-morphological stages have occurred and the ring has been bed-in to positon.

Chapter 4 examined the ring performance influence on the engine however the results noted that at certain steps the engine test results matched the simulated fixed results. This could be an indication that during running the ring could become temporarily fixed in the piston groove. However, due to the rotational force around the crown and the profile not as yet bedded into position with the cylinder, moments around the mass will continue, resulting in surface damage as displayed in Figure 6.17.

6.3. Modelling results

6.3.1. A study into ring coating geometry

Figure 6.18 shows a COMSOL simulation result. After each engine simulation test the piston ring had a probe attached to record the highest stress on the contact face. As the piston was assumed to be in an almost cylindrical shape, contacts between the cylinder face, compression ring and piston were used. This allowed for the piston tilt phenomenon to occur.

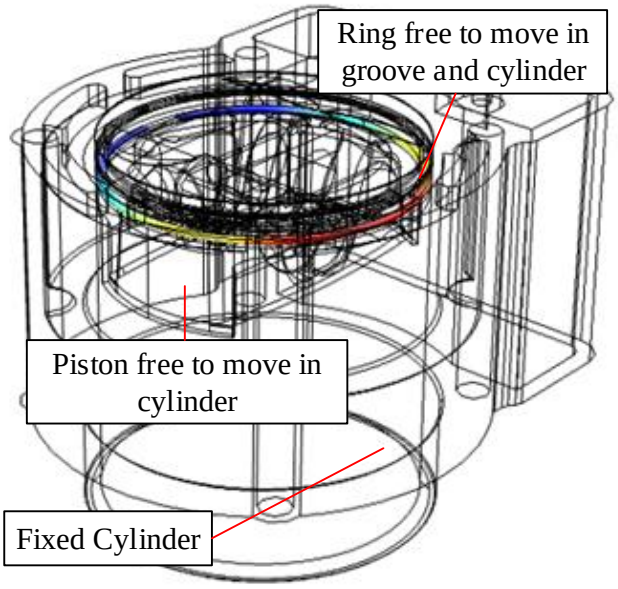

Figure 6.18 - Compression ring simulation with assembly present

Accumulated stresses have been generated during the upward dynamic displacement of the piston (BDC to TDC). This confirms the behaviour previously noted by R.Mittler & al. [43]. The problem investigated in this work refers to the piston ring chamfer concentration stresses found on the contact face of the ring (shown in Figure 5.13).

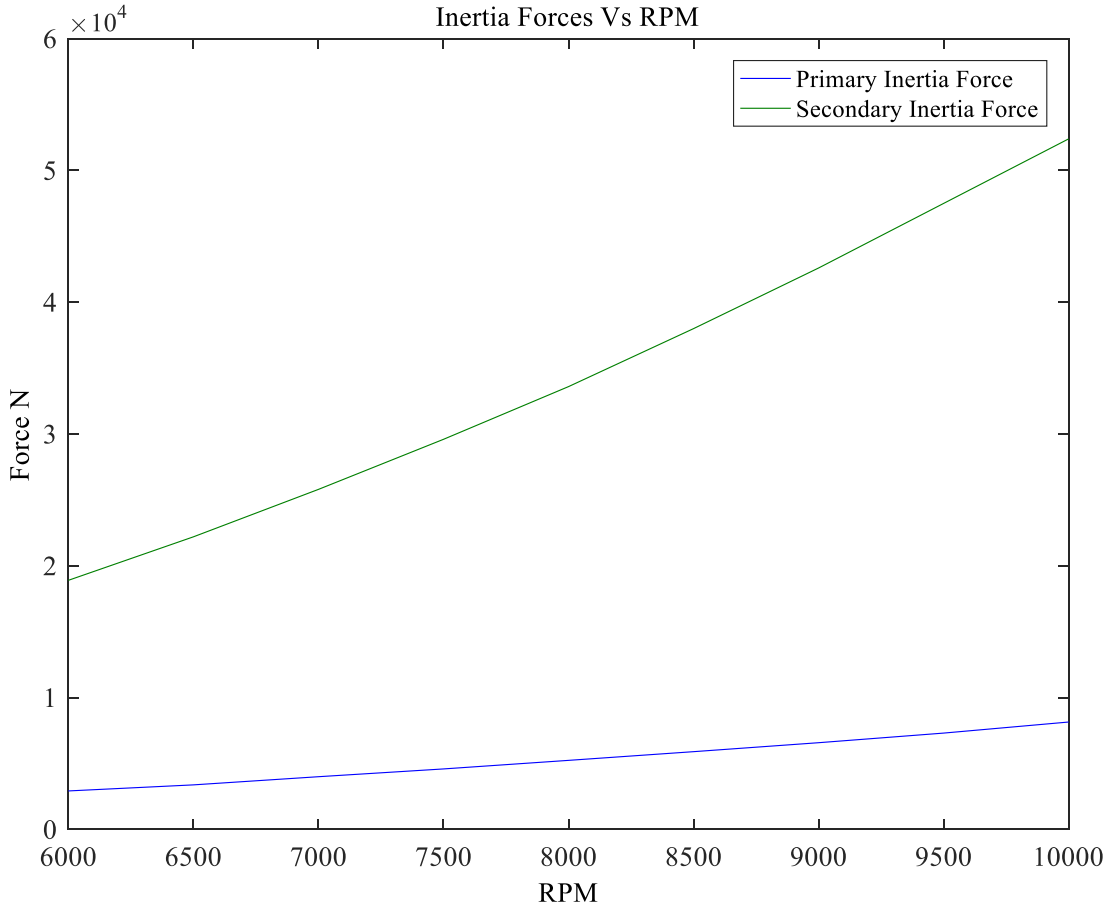

Figure 6.19 - Inertia forces and RPM rise

Inertia forces as a function of RPM have been shown in Figure 6.19. Figure 6.20 details both the chamfer configurations in the operation range of 6000-10000 rpm. Simple square ring geometry has been used for the simulation to focus the investigation on the stress concentration created near P2 when the engine operates in sector 1 (Figure 6.20).

When the engine operates in sector 1 as shown in Figure 6.20, where the piston inertia forces will not exert a stress great enough to induce a large level of structural damages, grey cast iron rings can resist against the stress being applied. Studies done on the elastic properties of uncoated piston ring [44,119,137] have shown that a chamfer can relieve some of the concentrated stresses present in the grey cast iron. While the ISO standard [116,139] recommends for the chamfer to reach the grey cast iron substrate, this has been contradicted by Love [44] works suggesting that the chamfer should remain within the

coating thickness, as excessive stresses would be generated at the grey cast iron/MoS_2 interface causing severe damages to both coating and grey cast iron substrate.

As the engine speed rises in excess of 9,500 rpm and enters Sector 2 as shown in Figure 6.20, the contact point between the grey cast iron ring and the cylinder wall begins to shear (Sector 2 in Figure 6.20).

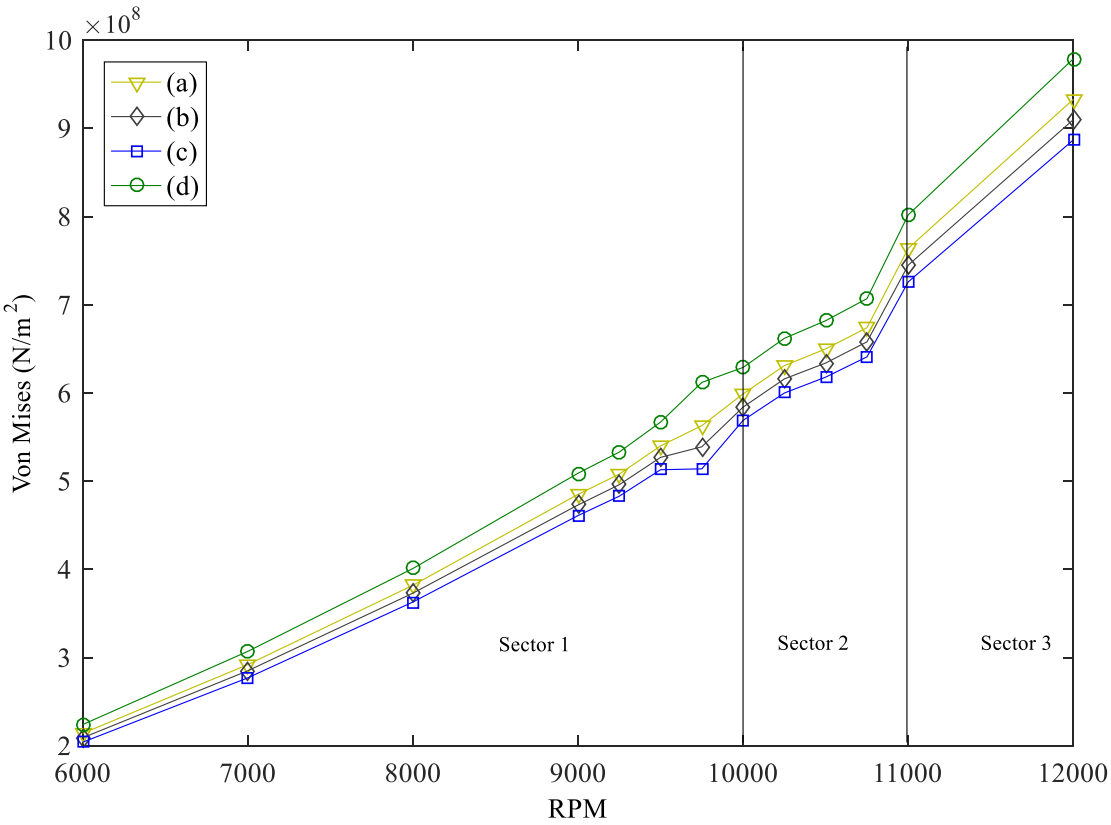

Figure 6.20 - Effect of Shearing as a function of chamfer length (a) 0.2 mm recommended in ISO standard, (b) 0.175 mm, (c) 0.15 mm and (d) 0.1 mm

The grey cast iron ring begins to shear between the operational rpm values of 10,000 – 11,000 rpm (sector 2 of Figure 6.20), hence it is suggested that engine should refrain from operating in this range.

The contact chamfer on the ring was reduced from the standard size from 0.2 mm to a new size of 0.1 mm, and results are conformed with Love's [44] elasticity principles. Both ring designs were simulated in the same operating conditions. Shearing (Figure

6.20) present during operation in section 2 can be reduced with the new design (b), this would increase life expectancy and failure to fatigue.

When Love's [44] principles are used to optimise the design and manufacture of the chamfer, reduced stress and improved performances can be obtained. As the rpm increases, the inertia forces also increases when both inertia forces and pressure forces are incorporated in the calculation.

When the engine operates in the rpm range of 10,000 to 11,000 shearing becomes especially greater around the operational value of 10,750rpm. During a full cycle of the engine, the piston will move from bottom dead centre to top dead centre, at this point the piston will tilt, the ring contact face will also be set at β, hence shearing may occur.

This work has examined only race car conditions; hence the combustion pressures that have been given are extremely high compared to what is seen in normal engine output pressures. The work completed references [44,119,137], indicates that by placing a chamfer on the material in such a way will allow the material to deform and have a more even stress distribution during the operation.

By taking the material thickness and then dividing the dimension by two, a stress reduction has been recorded [44,53,137]. If a change to the contact chamfer is made, the shear force acting in sector 2 will be reduced as shown in Figure 6.20. If the engine speed increases, the stress (sector 3 in Figure 6.20) continues to climb exponentially, however with the geometrical modifications, stress levels can be further reduced.

6.3.2. A study into compression ring thermodynamic material system

With the use of the standard air cycle, piston inertia force and cylinder pressure output was simulated shown in Figure 4.11, Figure 4.18 and Figure 4.17. Two materials were

used for the running-in of this compression ring. All simulations were calculated around the operational value of 8,000 RPM. All ring geometry is from the 6622 ISO standard.

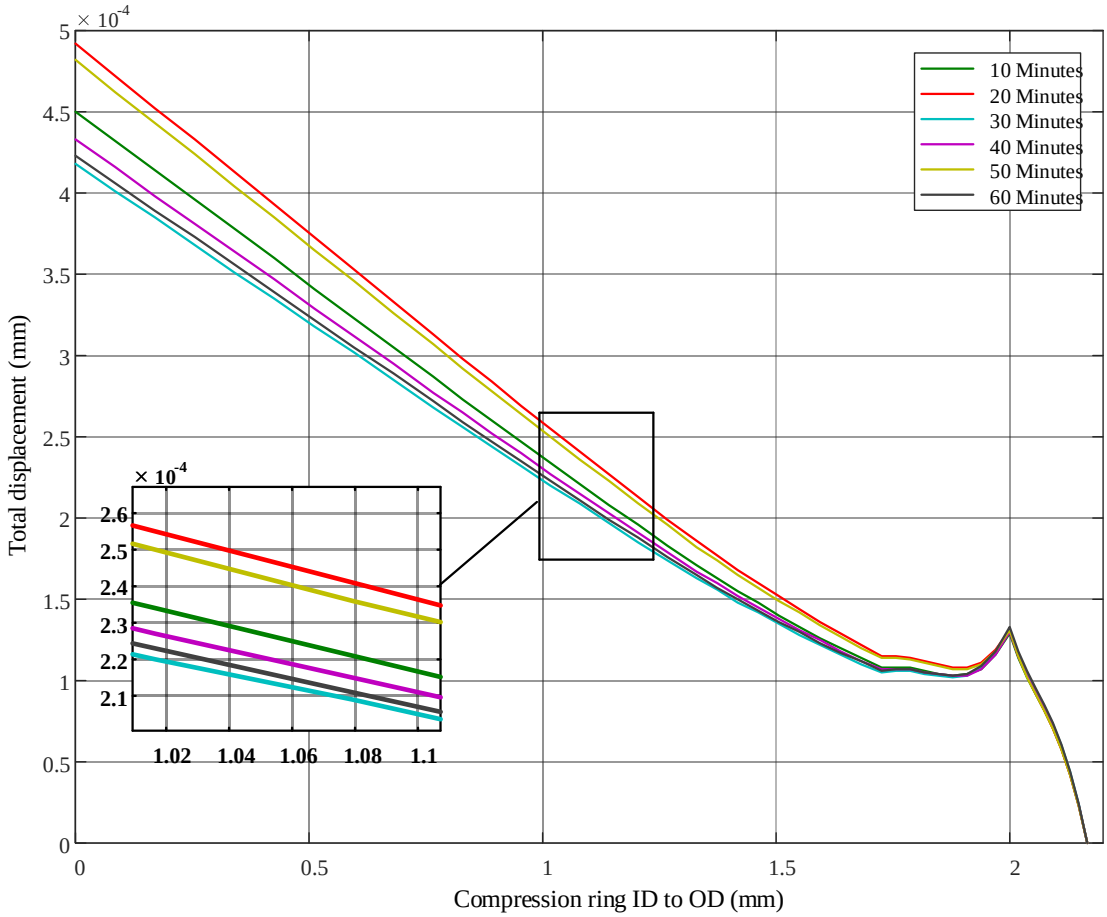

Figure 6.21 - SAE 9254+MoS_2 after 30 mins running-in

During the simulation time step iterations of 0.01s were used. In these results the cross sectional distance 2.2 mm of the ring is considered. Also both x and y planes where considered for deformation to also incorporate torsional twist noted by [14].

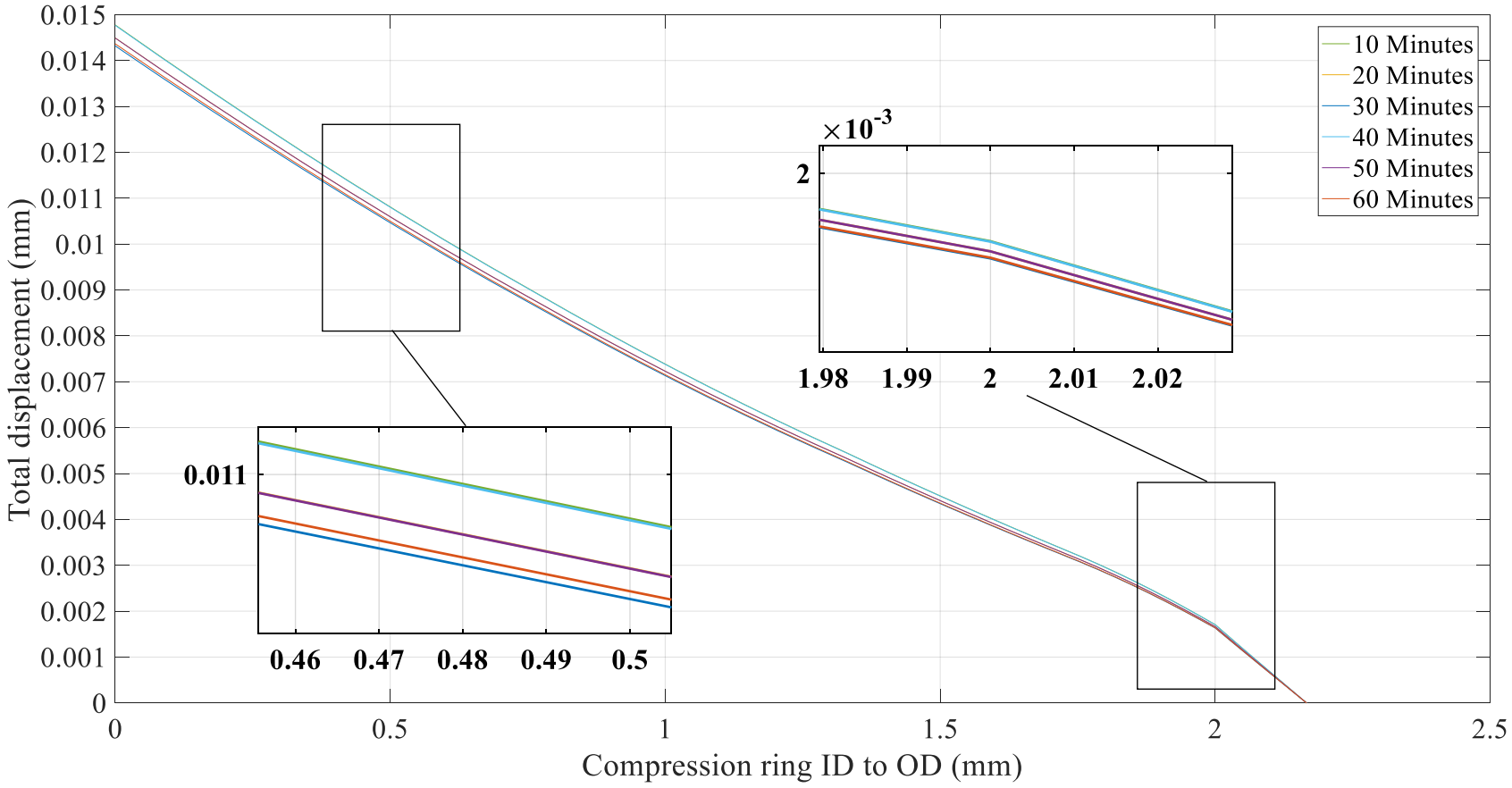

Figure 6.22 - EN GJL 250 +MoS_2 after 30 mins running-in

In both sets of results the thermal deformation and applied pressure are considered. As the heat and pressure begin to build during operation, as to be expected the back face of the ring will deform the greatest over time. The ENGJL 250 will deform to a maximum of 0.018 mm over the 30 mins of running. As for the SAE 9254 will have minor deformation up to 50 um during the same operation time. However in both sets of results the substrate material is restricted in fully deforming by the MoS_2 coating. It has been noted by [14,112] that during the running-in it is vital to the engine performance that the ring will run-in wearing down to suit the cylinder wall.

6.3.3. A study into the compression ring rotation based on geometry

The inertia forces were simulated for a range of speeds from 6000 to 12000 rpm. The values of the forces used in the simulation are shown in Figure 4.14. The compression ring abrasive wear is defined using the Rabinowicz[58] wear equation.

Several ring widths were used to show displacement of the rings while operating at 9,000rpm. Figure 5 shows the oscillation output obtained with several ring widths including the recommended 1 mm from the 6622 ISO standard. A further 3 more variations have been examined.

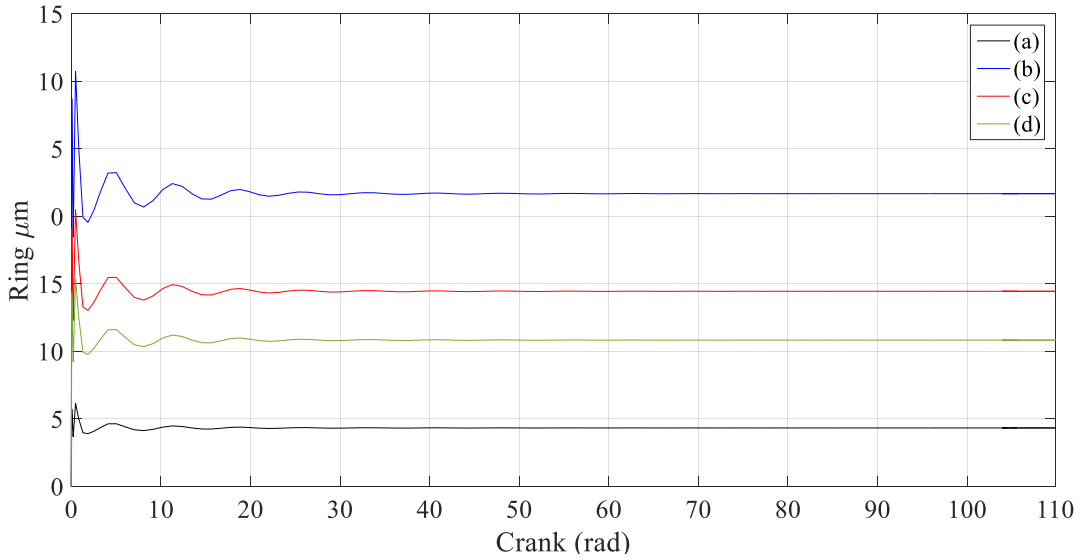

Figure 6.23 – total ring displacement around the z axis using COMSOL (a) 1 mm recommended in ISO standard, (b) 1.8 mm, (c) 1.6 mm and (d) 1.2 mm

Figure 6.23 with a number of ring thicknesses and indicates increased steady state offset with ring thickness. The values presented are for the dimensions of a KTM engine running at 9000rpm. The piston rings have a low cross-sectional dimensions.

As the rotational momentum builds during operation, each width change shows a great distance move from the origin, indicating mass of the ring is one of the significant parameters during this process. It has been noted [4,52,53] that pistons rings might exhibit a continuous motion. Other work [5,97,145] indicates little or no motion. The increasing steady-state offset in the rotation around the z-axis indicates that the system is dependent on the bedding-in process The simulation indicate motion is dependent upon the geometry and radius of curvature of a piston ring.

6.3.4. A study into compression ring dynamics using RSM

All results where run at 7,000 rpm with all 21 range values.

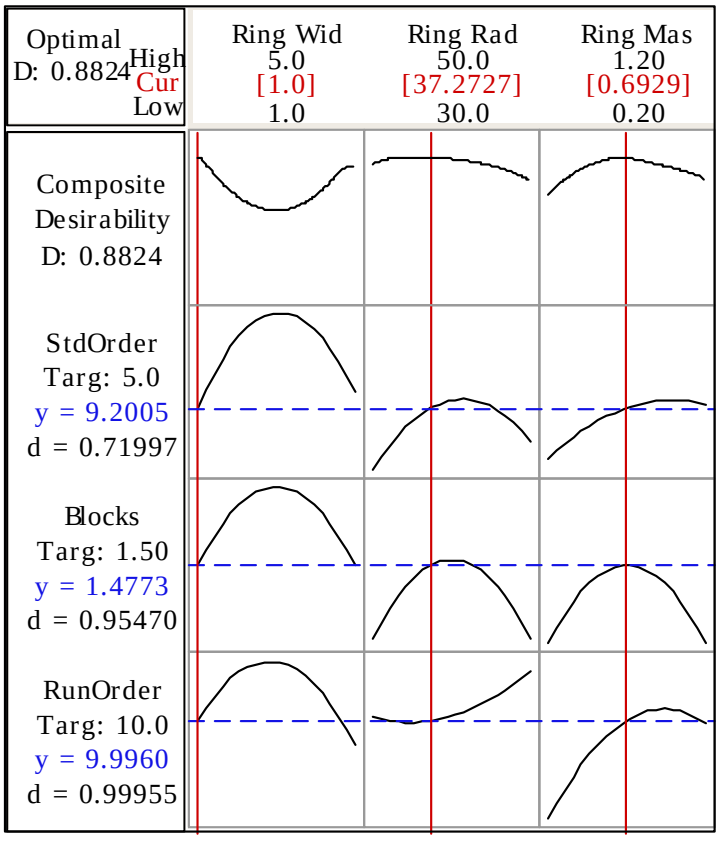

Figure 6.24 - Running order optimised surface

The running order of the optimised solution (Table 6-9) is presented in Figure 6.24.

Table 6-9 - Optimised solution

Ring Width (RW) mm	Ring Rad (RR) mm	Ring Mass (RM) g
1	37.27	0.69239

Each goal for the StdOrder = 5, Blocks = 1.5 and Runorder = 10. The composite desirability is 0.88239.

These results include abrasive wear, thermal coefficient of expansion and ring pressures. Large oscillations are found below 10 radians of the crank rotation, with the factors defined, a second order system behaviour is seen. For the optimised solution (Table 6-9), the ring will rotate by a maximum of 0.005 rads. The result also indicates a resting time reached after 50 rads.

To validate the model SEM images have been taken. By measuring the length of the wear track, and using Figure 6.25.

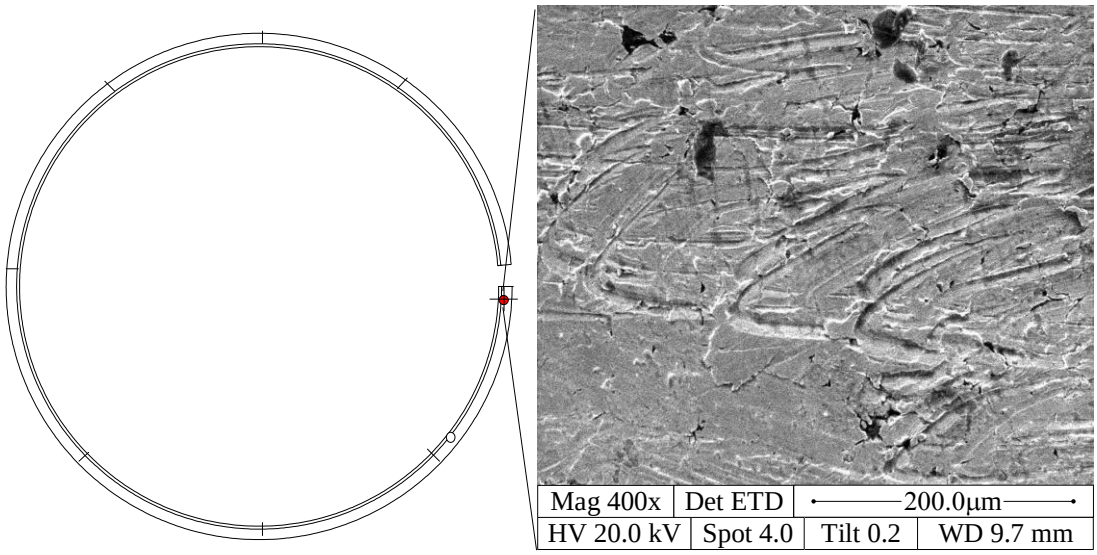

Figure 6.25 - KTM 520 sample 1 top face

Figure 6.25 shows one of three samples images taken of the run-in KTM piston rings.

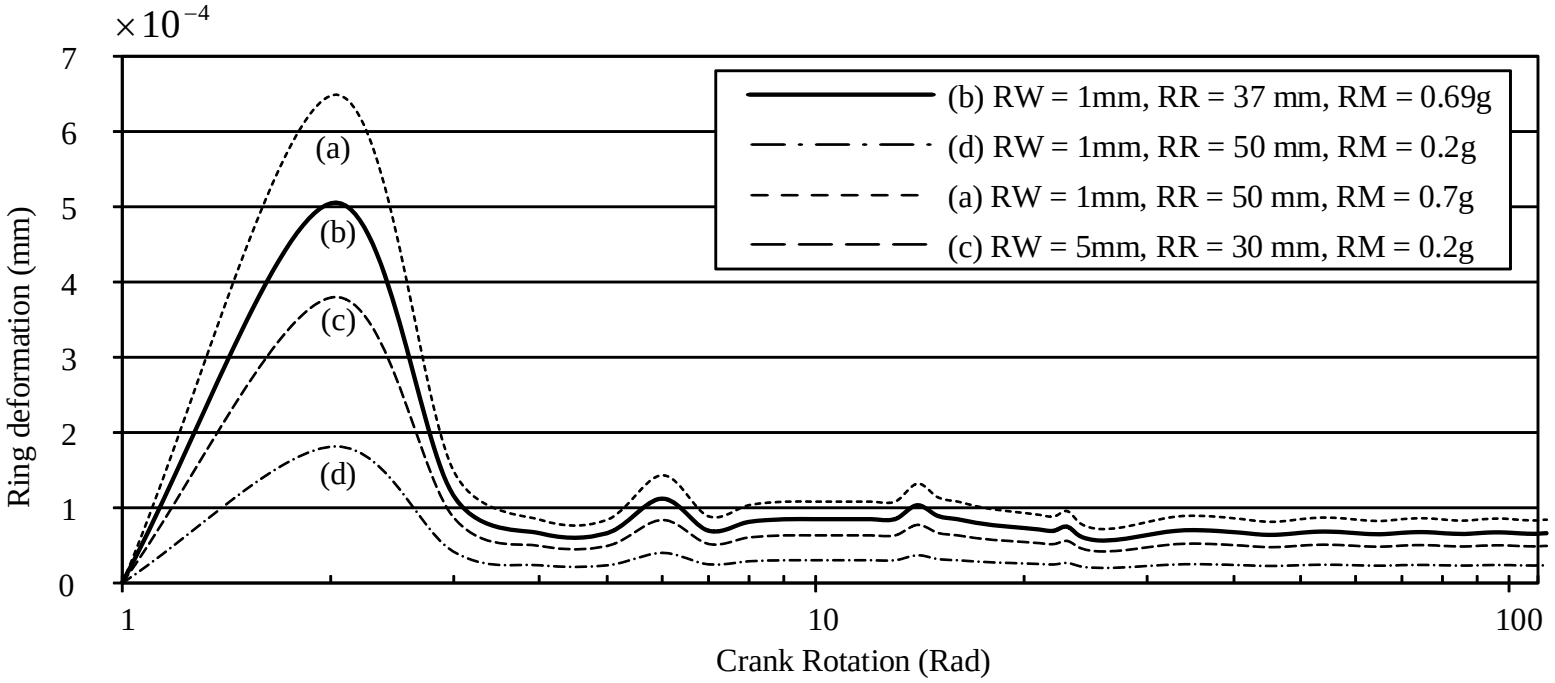

Figure 6.26 - Ring deformation radius

Figure 6.26 shows four representatives RS ring displacement radius outputs were (a), (b), (c) and (d) are test number 11, 21, 12 and 6 respectively of values from Table 5-4.

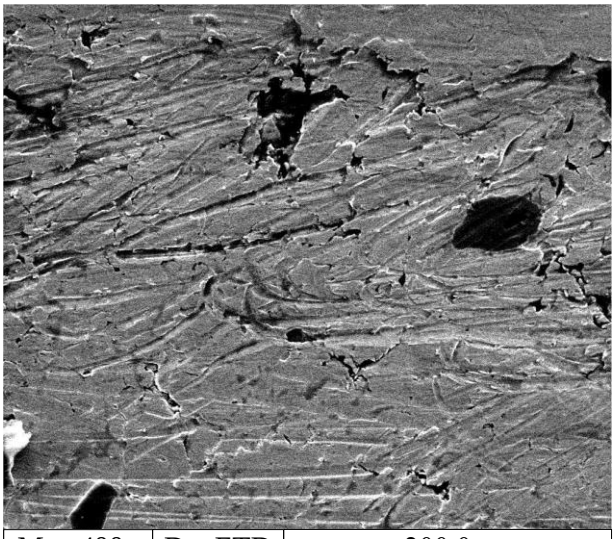

Mag 400x	Det ETD	•———200.0µm———•	
HV 20.0 kV	Spot 4.0	Tilt 0.2	WD 9.7 mm

Figure 6.27 - KTM 520 sample 3 top face

Figure 6.27 shows the sample 3 SEM that was measured and compared with the simulated results. Each image was measured for the maximum arc size relative to the ring radius. Once identified the (6.1) was employed.

$$x = tan^{-1}\left(\frac{L}{R_{rad}}\right) \quad \textbf{(6.1)}$$

Where L and R_{rad} are the length of the recorded grove and compression ring radius respectively.

Table 6-10 - Simulated against sample results

Sample No.	Sample length (mm)	Measured max rad	Simulated max rad (Figure 6.26 (b))	Error%
1	0.0267	0.005056 (Figure 6.25)	0.005045	0.22
2	0.0251	0.004986 (Figure 6.15 (b))	0.005045	1.17
3	0.0288	0.005133 (Figure Figure 6.27)	0.005045	1.74

Table 6-10 shows the results from RS optimized value (Table 6-9) and the measured values from the SEM images. The simulated system assumes a level of perfection in both material, combustion pressure and lubrication. Hence variations are recorded between the simulation and experimental data.

As the rotational momentum builds during operation, the highest levels of rotation are recoded in the first 20 radians of the crank rotation. Studies have been noted [4,9,52,53,134] that pistons rings might exhibit a continuous motion. However other work has been presented where little or no rotation has been observed [5,97]. However the validation work presented from the samples suggests that a large action of ration occurs over a small amount of crank rotation.

6.3.5. A study into the effects of with fixed and free rotation

Torque outputs obtained for both simulated and dynamometer tests are reported in Figure 6.28 for the coated ring and in figure 6 for the uncoated ring.

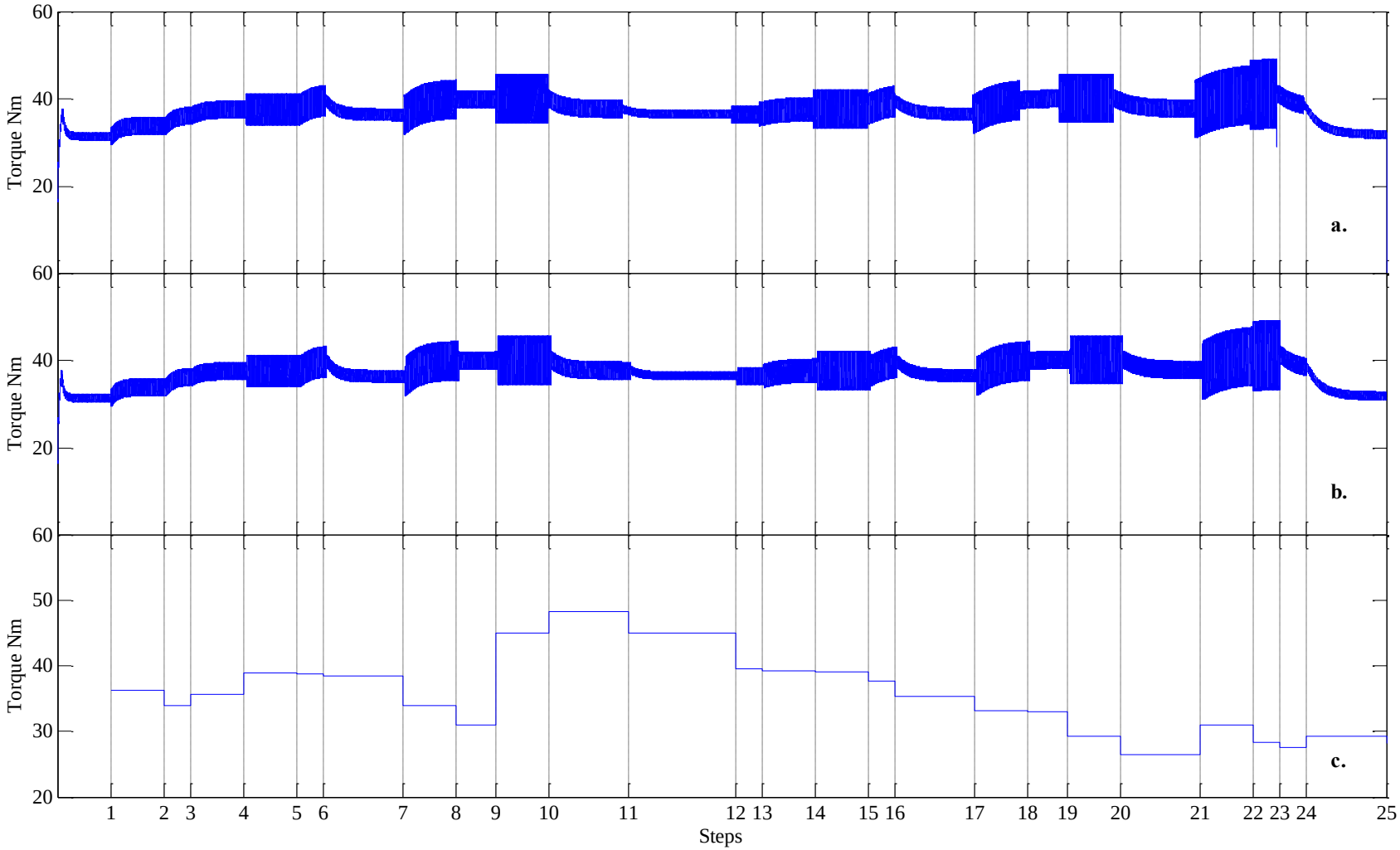

Figure 6.28 - Torque output of coated rings, calculated when ring is free to rotate (a) or fixed (b) or measured in dynamometer test when ring is free to rotate (c)

Table 6-11 - Maximum, mean and standard deviation of torque outputs calculated or measured over the 25 running-in steps for coated rings

	Calculated		**Measured**
	Figure 6.28.a	Figure 6.28.b	Figure 6.28c
Maximum Torque Nm	47.88	48.56	57.10
Mean Torque Nm	35.61	36.23	37.67
Standard deviation	2.85	2.70	6.86

Figure 6.28 and Table 6-12 show maximum, mean and standard deviation of torque outputs calculated or measured over the 25 running-in steps for respectively coated and uncoated rings.

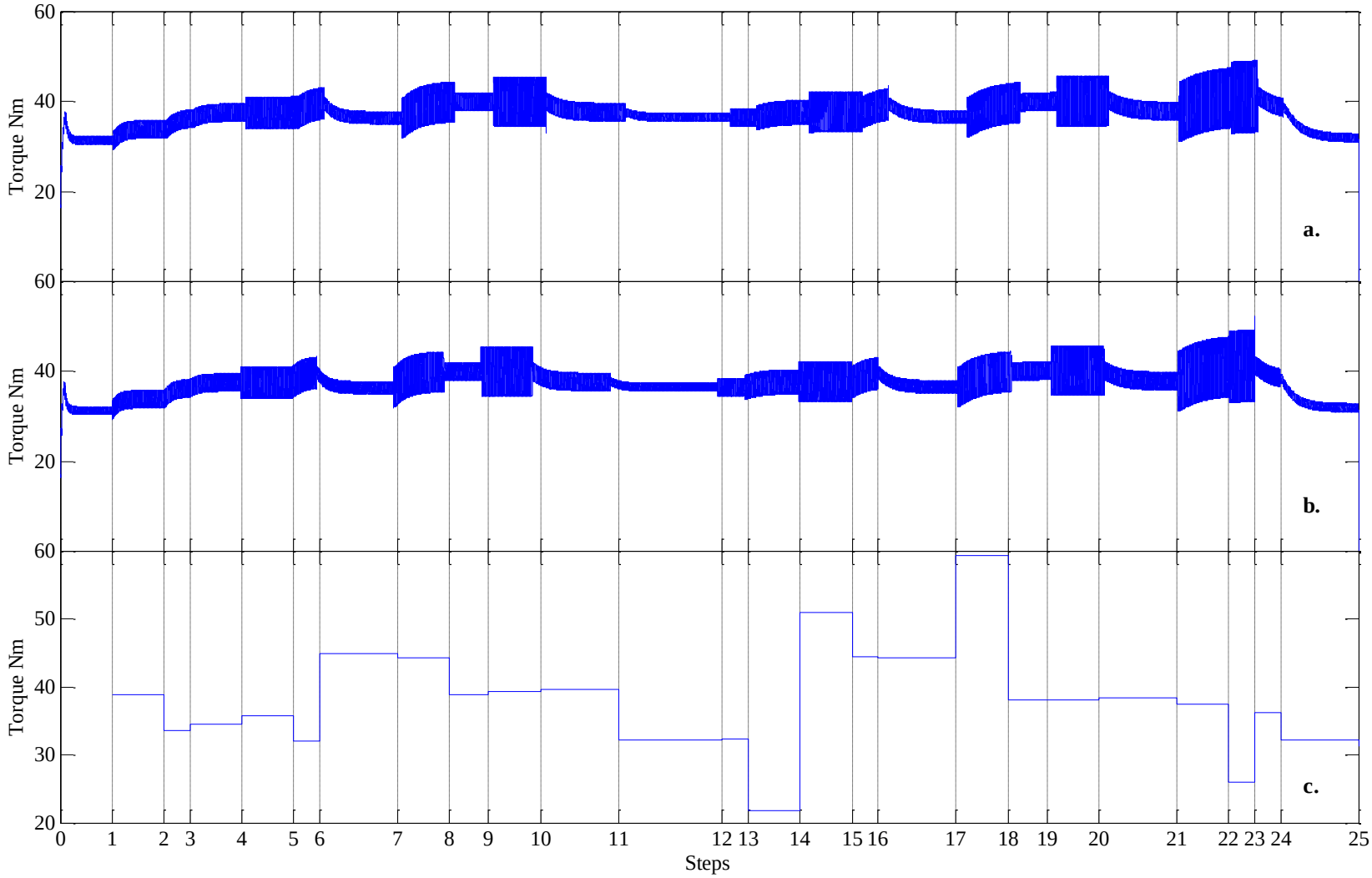

Figure 6.29 - Torque output of uncoated rings, calculated when ring is free to rotate (a) or fixed (b) or measured in dynamometer test when ring is free to rotate (c)

Figure 6.28 and Figure 6.29 show respectively the results from coated and uncoated simulation in free (a) and fixed states (b). The simulated torque outputs are compared with the torque measured at the end of each of the 25 running-in steps.

Table 6-12 - Maximum, mean and standard deviation of torque outputs calculated or measured over the steps running-in steps for coated rings

	Calculated		**Measured**
	Figure 6.29a	Figure 6.29b	Figure 6.29c
Maximum Torque Nm	49.15	49.21	59.30
Mean Torque Nm	37.44	37.45	38.30
Standard deviation	3.18	3.19	7.81

From the simulation results the restrained coated condition performs with a highest operation output, however compared against the dynamometer tests the maximum output is almost 10Nm lower than the simulated, indicating extra effecting phenomena that has not been considered in the model.

Like what was seen in the coated conditions the constrained rotation incurs an increased a performance output. However the results from the dynamometer show the same value difference of almost 10Nm. In restricting ring motion around the crown, torque output is increased. Simulated results obtained with a fixed ring in both coated and uncoated show an increased performance and a higher output in mean average. By constraining the axis around the piston groove performance is increased on all scales.

The dynamometer indicates an extra factor that has not been considered within the model. The sudden change in performance similar to what has been seen has been noted in studies, related to oil burn known as glazing or varnishing [7,146]. The phenomenon is a results of deposits to the cylinder and ring surface creating a varnished effect, this can lead to permeant performance loss. However in the dynamometer results it is assumed

that this is only phase one of this phenomenon and the change in operating conditions deters progression. Considering step 1 and 25 plus also 3 and 13 where the operating conditions of the engine are the same there is a loss in response from the engine, which could be an indication that glazing has more of an impact in the engine than what is normally assumed.

6.4. Conclusion

In this chapter the focus has been to examine the compression ring geometry and through the use of simulation packages offer possible solutions for increased performance of the combustion engine. By offering a reduction in the contact chamfer of the coating applied to the present ISO 622 piston ring contact chamfer design a reduced level of stress constriction was achieved. The design modification to the contact chamfer was validated using the present KTM 520 engine with a grey cast iron compression ring coated with 0.16 mm MoS_2 and a 0.2 mm contact chamfer. The method for modification offered in the work has major impacts in the manufacturing process of the ring. By using this ring, a racing combustion engine would benefit in an extended life cycle of the coated compression ring. However the results presented also could also indicated that the material could have surface damage, in particular around the substrate to coating interface. This indication prompted the work into the effect of ring rotation occurring around the crown of the piston. Also the thermal morphological effect of the coating and compression ring also has an influence on the operation of the compression ring.

During operation the compression ring temperature increases causing the material to deform. This deformation will seal the cylinder to almost meeting the cylinder wall. The heat from the process causes the ring to deform so that there will almost never be continuous rotation. As the mass and dimensions of the ring increase then the effects of

the heat will be reduced and it is possible that a ring on a large engine will continuously rotate. The work has shown the simulated response of the KTM 520 developed using COMSOL software, some element of the system have not been considered. As the engine cycle occurs the piston will go through thermal morphological changes. Therefore the y axis will be slightly offset and also the piston will be encouraged to tilt. The process of thermal morphological change will lead to the compression ring creating a seal, between the piston and the wall. In initial process the compression ring will rotate acting like a second order system. The validating SEM images were taken that do indicate what has been reported in the simulation work. The effects of the heat based of compression ring rotation prompted further work into examining the displacement and thermal strain of the compression ring to coating interface.

During operation the compression ring temperature and pressure will increase and then decrease in the cylinder, which has effects on all components that are working around the cylinder area, this process is with the idea of the ring bedding-in to the cylinder wall to create an ideal seal. In the race car condition this seal is vital to ensure the highest level of performance as possible. As the heat increases the substrate will act against the coating attempting to deform however the coating will restrict the ring, as seen in Figure 6.21 and Figure 6.22 both substrates are interrupted when reaching the point where both coating and substrate meet. The coating will resist the ring leaving and incomplete deformation process, leave a drop in performance.

As noted in work show by Renevier [80] the morphological changes seen in MoS_2 will support the running-in of a component. The results presented in this show the results of restricting the compression ring from rotating in the piston groove. The maximum output torque of the fixed ring shows a greater output than what is seen with the free ring. The

uncoated rings display a higher level of output torque for some time, however it is assumed that due to the characteristics of the compression ring the wear rate will increase. The conformability is increased but only for a small level of time. Depending on the engine application would depend on the method of running the compression ring, for example in conditions where power is vital fixed geometry would give greater performance in both coated and uncoated.

The compared dynamometer test data shows error through most simulations, this has led to the assumption that during the running-in procedure glazing should not be overlooked and considered as a major factor when simulating this stage of the engine life cycle.

The model presented is given with an ideal lubrications system where starvation of the rings has not been considered. Wear does occur however material transfer during running in has not been considered, hence possible oil contamination will not occur in the model presented and should be further examined.

The results have shown that uncoated compression rings have a higher coefficient of friction than what was seen when the ring has a MoS_2 coating. During the running-in large levels of fluctuating Coolant temperatures were recorded (Figure 6.3).

In a study into the effect of MoS_2 coated gears Martins [143] results showed that an MoS_2 coating while in operation would promote decrease in temperature. The experimental results obtained during the running-in of the KTM 520 engine show a similar effect.

To examine the compression ring before and after use the Dickinson Rotating Ring Contact Profiler (DRRCP) was developed to measure the surface roughness of components. A piston ring was used as a test case. To confirm the validity of the developed product results were compared to the standard system and observations using the gage R&R methodology.

Thus, the DRRCP profile is a fast, convenient and simple system for measuring the surface profiles of components with ring profiles such as race car piston rings. The system design does however offer some system modification options. The first point of the present system is that the mount system is unable to acquire for a large range of piston rings, to present the system will only support 90-98 mm rings.

The mounting plates on the DRRCP could be reproduced in a numerous amounts of times to take a range relative to the ring diameter.

Another option to solve this design problem could be to redesign the clamping method. The idea of changing the disk method seems a much more logical approach as at the moment another design flow in the system is that the plate fixing bolts one must be removed for the plate to be removed. During operation of the DRRCP the base arms that mount the plates are fixed into one position, this poses a problem as if the ring is thicker or thinner than 1.1 mm the ring will be loose, hence resulting in results that could be questionable. These design limitations suggest that further development of the fixture is required. The DRRCP allows for full ring surface analyses.

The compression ring when first coated will have a greater roughness, however an uncoated ring will be smoother as post processing is not done. The running-in process shows that both rings will wear to a close value. The results show that the uncoated ring will wear more evenly. The MoS_2 coating will wear almost to the same level as the uncoated. However the results also show that the coating will not wear evenly, thus indicating that the compression ring will not have a permanent state of rotation around the crown of the piston.

From examining the compression ring before and after operation the results have a strong indication that rotation of the component will take effect. However examination of further compression ring sets should be done as to quantify the results seen.

Conclusion

In this chapter the focus has been to examine the compression ring geometry and through the use of simulation packages offer possible solutions for increased performance of the combustion engine. By offering a reduction in the contact chamfer of the coating applied to the present ISO 622 piston ring contact chamfer design a reduced level of stress constriction was achieved. The design modification to the contact chamfer was validated using the present KTM 520 engine with a grey cast iron compression ring coated with 0.16 mm M_oS_2 and a 0.2 mm contact chamfer. The method for modification offered in the work has major impacts in the manufacturing process of the ring. By using this ring, a racing combustion engine would benefit in an extended life cycle of the coated compression ring. However the results presented also could also indicated that the material could have surface damage, in particular around the substrate to coating interface. This indication prompted the work into the effect of ring rotation occurring around the crown of the piston. Also the thermal morphological effect of the coating and compression ring also has an influence on the operation of the compression ring.

During operation the compression ring temperature increases causing the material to deform. This deformation will seal the cylinder to almost meeting the cylinder wall. The heat from the process causes the ring to deform so that there will almost never be continuous rotation. As the mass and dimensions of the ring increase then the effects of the heat will be reduced and it is possible that a ring on a large engine will continuously rotate. The work has shown the simulated response of the KTM 520 developed using COMSOL software, some element of the system have not been considered. As the engine cycle occurs the piston will go through thermal morphological changes. Therefore the y axis will be slightly offset and also the piston will be encouraged to tilt. The process of thermal morphological change will lead to the compression ring creating a seal, between

the piston and the wall. In initial process the compression ring will rotate acting like a second order system. The validating SEM images were taken that do indicate what has been reported in the simulation work. The effects of the heat based of compression ring rotation prompted further work into examining the displacement and thermal strain of the compression ring to coating interface.

During operation the compression ring temperature and pressure will increase and then decrease in the cylinder, which has effects on all components that are working around the cylinder area, this process is with the idea of the ring bedding-in to the cylinder wall to create an ideal seal. In the race car condition this seal is vital to ensure the highest level of performance as possible. As the heat increases the substrate will act against the coating attempting to deform however the coating will restrict the ring, as seen in Figure 29 and Figure 30 both substrates are interrupted when reaching the point where both coating and substrate meet. The coating will resist the ring leaving and incomplete deformation process, leave a drop in performance.

As noted in work show by Renevier [80] the morphological changes seen in MoS_2 will support the running-in of a component. The results presented in this show the results of restricting the compression ring from rotating in the piston groove. The maximum output torque of the fixed ring shows a greater output than what is seen with the free ring. The uncoated rings display a higher level of output torque for some time, however it is assumed that due to the characteristics of the compression ring the wear rate will increase. The conformability is increased but only for a small level of time. Depending on the engine application would depend on the method of running the compression ring, for example in conditions where power is vital fixed geometry would give greater performance in both coated and uncoated.

The compared dynamometer test data shows error through most simulations, this has led to the assumption that during the running-in procedure glazing should not be overlooked and considered as a major factor when simulating this stage of the engine life cycle.
The model presented is given with an ideal lubrications system where starvation of the rings has not been considered. Wear does occur however material transfer during running in has not been considered, hence possible oil contamination will not occur in the model presented and should be further examined.

The results have shown that uncoated compression rings have a higher coefficient of friction than what was seen when the ring has a MoS_2 coating. During the running-in large levels of fluctuating Coolant temperatures were recorded (Figure 6.3).

In a study into the effect of MoS_2 coated gears Martins [143] results showed that an MoS_2 coating while in operation would promote decrease in temperature. The experimental results obtained during the running-in of the KTM 520 engine show a similar effect.

To examine the compression ring before and after use the Dickinson Rotating Ring Contact Profiler (DRRCP) was developed to measure the surface roughness of components. A piston ring was used as a test case. To confirm the validity of the developed product results were compared to the standard system and observations using the gage R&R methodology.

Thus, the DRRCP profile is a fast, convenient and simple system for measuring the surface profiles of components with ring profiles such as race car piston rings. The system design does however offer some system modification options. The first point of the present system is that the mount system is unable to acquire for a large range of piston rings, to present the system will only support 90-98 mm rings.

The mounting plates on the DRRCP could be reproduced in a numerous amounts of times to take a range relative to the ring diameter.

Another option to solve this design problem could be to redesign the clamping method. The idea of changing the disk method seems a much more logical approach as at the moment another design flow in the system is that the plate fixing bolts one must be removed for the plate to be removed. During operation of the DRRCP the base arms that mount the plates are fixed into one position, this poses a problem as if the ring is thicker or thinner than 1.1 mm the ring will be loose, hence resulting in results that could be questionable. These design limitations suggest that further development of the fixture is required. The DRRCP allows for full ring surface analyses.

The compression ring when first coated will have a greater roughness, however an uncoated ring will be smoother as post processing is not done. The running-in process shows that both rings will wear to a close value. The results show that the uncoated ring will wear more evenly. The MoS_2 coating will wear almost to the same level as the uncoated. However the results also show that the coating will not wear evenly, thus indicating that the compression ring will not have a permanent state of rotation around the crown of the piston.

From examining the compression ring before and after operation the results have a strong indication that rotation of the component will take effect. However examination of further compression ring sets should be done as to quantify the results seen.

CHAPTER 7 - CONCLUSIONS AND FURTHER WORK

7.1. Piston assembly modelling results summary

When the engine is in operation the four stroke process will take effect. As the piston travels from BDC to TDC the compression ring will be in contact with the cylinder wall, the torque produced by the crank will travel up through the connecting rod through the piston hence creating a vector. This vector will be transferred from the piston to the piston ring. Results produced in the study into the contact chamfer of the compression ring, used laws first introduced by Love [44].

The results showed that by refining the contact chamfer from 0.2 mm to 0.1 mm, the stress at the interface between coating and substrate can be reduced hence indicating that the operation life of the coating would be increased. The modification of the geometry would not increase any manufacturing costs. To develop the model several assumptions were considered. The assumptions included the method used to calculate the surrounding compression ring pressures, the lubrication pressures where disregarded. The dynamics of the simulation suggested that the ring moved on the same axis of the piston as the force applied on the ring was linearly projected.

The projected vector will also play a large role in rotation of the piston ring. As the piston comes from BDC to TDC the vector and also the ring radius presents the idea behaviour for rotation to occur. The work that was done to examine the rotation of the compression ring showed that as the combustion heat increases the ring will go through its morphological state and the occurring torque will cause the ring to rotate and come to rest. The results offered a solution as to why some who have tested on small 4 stroke engines have found no indication of rotation occurring however larger marine diesel engines do record rotation. However the results shown do imply that the lubrication

conditions are perfect also that the material being studied will only wear and thermal expand perfectly with no interruptions.

Following from this work a study was done examining the piston grove area to study the effect the ring dynamics based on the response surface methodology. By using this method a number of runs where produced resulting in the present industry standard being the optimised solution. However the results did show rotational behaviour which when measured against observations made from the SEM images showed a %error maximum of 1.74 in against μradians. The recorded %error could have been a result of assumption that lubrication would lubricate with no minimum film thickness change.

As the compression ring heat increases the substrate material, in the example of the simulation work presented grey cast iron the material will begin to expand due to the coefficient of thermal expansion also the Mos_2 will go through an expansion stage. Each material according to its specification will expand, hence during the running-in of the ring each will expand at different rates.

By simulating the engine environment this was presented in work where two substrate materials where used to study the deformation of the coating to examine if the coating is restricting the substrate morphological change. The presented results showed that as the engine is in operation the compression ring the thermal change of the coating is interrupted by the displacement of the substrate material, leaving it difficult for coated to deform correctly to the cylinder wall. However the in this study the thermal cooling from the cylinder was not considered as the focus was to examine the relation between the ring and the ring coating. The conclusion of this work is that if the running-in procedure is carefully defined, the efficiency of the combustion engine would be increased. Based on the compression rings ability to seal the cylinder the engine will have a variation of possible torque outputs.

If the ring is coated and free to move around the crown of the piston groove the studies have shown that the ring compression ring will not perform as efficiently as expected.

However if it is uncoated and free to move this could also make a difference in engine operation. But if both examples are fixed this could simply restrict the problem.

The finial study presented examined these problems, by using the same running-in procedure that was used for the physical testing the model was run. In the results of the validity test the physical testing was compared against the modelled response. Analysis of the results showed a behaviour from the physical testing that was not noted in the simulated test. However by restricted the motion around the groove axis it is assumed that the wear rate will increase. Within the results a discrepancy was noted where in some stages the dynamometer stages where the performance will suddenly drop and follow with a spike in performance this behaviour is consistent to what has been seen in the phenomenon known as glazing or cylinder varnishing. This is a direct results of material transfer and also lubrication contaminants as noted in previous work noted in chapter 6.

7.2. Dynamometer results summary

Dynamometer tests have been conducted on the KTM 520 motorcycle engine to torque and temperature outlet during each of the running-in steps. The profiles of the compression rings have been measured using a 3D surface profilometer before and after the full running-in process. A mounting frame has been developed to assess the ring removing the need of destructive testing or acquisition of expensive 5 axis profilometer.

Results from a gauge R&R performed on the mounting frame have shown that the main source of error can be attributed to repeatability. Additional considerations into the manufacturing process of the mount to further reduce errors have been undertaken to ensure that both arm and rotating disc are at 90 degrees, removing the need for further time consuming and bespoke adjustments. Rings have been individually positioned using

markers and a motorised precision positioning would further reduce fitting time. Running-in of the KTM 520 engine performed on the dynamometer using coated and uncoated piston rings have shown that slight higher torque output and a $10^{\circ C}$ increased oil temperature have been obtained with uncoated rings It has been assumed that a greater seal between the cylinder and the ring has been achieved. These results have been broadly confirmed with the simulation model. The discrepancy between the results from dynamometer test and the simulation has been attributed to the lubrication assumptions used in the simulation (fully flooded and contaminant free)

The Y-axis of the contact face examined for all in total 4 compression rings, the results displayed that before operation the Mos_2 coating has small peak values, however after operation in the area of sample 1, 3 and 4 a great peak value can be seen, however on sample 2 the peak value is elevated. This could be an indication that of the thrust face as sample one is the end of the ring, this would imply that because the gap was originally set facing the front of the engine and if the sample 2 is the thrust face area then the ring has moved and come to rest within the area of 45 degrees. As expected because the Grey cast iron material dose not possess the material qualities of MoS_2 the uncoated ring begins with a surface containing high peaks which is assumed to be a result of manufacturing. Samples 1, 2, 3 and 4 have clearly been worn to a greater extent that what is seen on the rest of the samples, the areas are similar to what was seen in the coated ring, at 2 and 3 the surface is much smoother to what is seen in 1, 3 and 4 again this could be an indicator that rotation and then settling has occurred, thus supporting what was resulted in the simulation models. Following from the surface observation where made to examine the surface of the top land of the compression ring to examine the coating and the substrate material. The surface SEM images displayed surface damage to the top land showing wear channels these channels indicate rotation which relates to simulation models presented.

7.3. Main Contributions of the thesis

The research presented in this work has contributed to understanding and knowledge of the running-in procedure in the following ways.

The ISO 6622-1 (Internal combustion engine – piston rings – part 1 – rectangular rings made of cast iron) has been updated several times over the year. A simulation using Love [44] original work applied on the piston ring chamfer has identified that maximum stress was located at the interface between the coating and the cast iron. A new design, that do not require additional manufacturing costs, has been proposed to reduce localised stresses and material loss. While the ISO 6622-1 has not been yet amended the ISO 6622-2 (Internal combustion engine – piston rings – part 1 – rectangular rings made of steel) has been amended in 2013. For many years there has been a controversy on compression ring rotating [53] or not [5] around the piston crown. Computer simulation and dynamometer engine tests have carried out to contribute to the discussion and have been able to support the argument that rings are rotating around the crown. The phenomenon known as glazing process has only been studied on old engines at the end of the engine life cycle. It has been a common belief that once this process has taken place, it is almost irreversible. Dynamometer tests have been conducted showing what could be noted as phase 1 of the glazing phenomenon occurring during the running-in and results have been correlated with the literature available to date.

The running-in of engines included race engines have been very loosely defined and currently no standard process can been openly found. A computer simulation has been developed to study the output performance, thermal deformation, the impact of coatings and ring constraints during the running-in. Simulated results have been validated with dynamometer engine tests. The work has highlighted the benefit in race conditions of fixing the compression ring in the groove over free rings where higher output power can

be achieved. The work has also emphasised the importance of the running-in for piston rings and coatings.

7.4. Recommendations for future work

The running-in of race engine is specialised procedure with many unknowns therefore, further work should consider further simulations using design of experiment in attempt to define universal conditions for the running-in of race engines with consideration of factors such as intervals, number of steps, throttles, speed. The simulation should be validated with dynamometer testing where compression rings are analysed after each running-in steps to account for the full running-in process.

Engine simulation and dynamometer testing during the running-in have both shown a clear difference in performance when compression rings were fixed within the piston groove compared to standard method when the ring free to move. Further work should consider additional modifications to both piston and compression ring to fix the ring in the groove.

Only basic aspects of lubrication have been considered in the present work. The results obtained from dynamometer testing have shown a behaviour consistent with first stages of cylinder polishing (or glazing) which has also been found by Dimkovski [146].

In the results presented on the dynamometer displayed what is presumed to be the first stages of cylinder polishing (or glazing) this initial assumption is supported by work presented Dimkovski [146]. The discrepancy between simulation and dynamometer testing during the running-in of race engine can be attributed to heat degradation of the lubricant during the burning process which generate carbon pollutants and material loss due to friction and wear. The effect of contaminants should be considered in further simulations investigate, so there is a better fit between simulation and dynamometer tests.

REFERENCES

[1] A.Martyr and M.A.Plint, Engine testing: theory and practice (Butterworth-Heinemann, Elsevier Linacre House, Jordon Hill, Oxford, 2007).

[2] W.Pulkrabek, Engineering Fundamentals of the Internal Combustion Engine (Pearson, Prentice Hall, University of Wisconsin, Platteville, 2004).

[3] R.Stone and J.K.Ball, Automotive engineering fundamentals (SAE International, 2004, 2004).

[4] S.C.Tung and Y.Huang, Tribology Transactions 47 (2004) 17-22.

[5] V.Dunaevsky and S.Alexandrov, Tribology Transactions 48 (2005) 108-118.

[6] S.f.M.American, in: Friction, Lubrication, and Wear Technology, Vol. 18, (ASM International, 1992) ch. 3.

[7] G.C.Barber and K.C.Ludema, Wear 118 (1987) 57-75.

[8] P.J.Blau, Tribology International 38 (2005) 1007-1012.

[9] M.Dickinson, N.Renevier, and J.Calderbank. A Study into the Compression Ring Rotation Based on Geometry. SAE 2014 World Congress & Exhibition. 4-1-2014.

[10] A.Guermat, G.Monteil, and M.Bouchetara, in: Damage and Friction Mechanics, eds. T.Boukharouba, M.Elboujdaini, and G.Pluvinage (Springer, Algiers, 2010).

[11] N.W.Bolander, B.D.Steenwyk, F.Sadeghi, and G.R.Gerber, Proceedings of the Institution of Mechanical Engineers Part J-Journal of Engineering Tribology 219 (2005) 19-31.

[12] R.González, A.Hernández Battez, D.Blanco, J.Viesca, and A.Fernández-González, Tribology Letters 40 (2010) 269-277.

[13] M.Priest, D.Dowson, and C.M.Taylor, Wear 231 (1999) 89-101.

[14] M.Priest and C.M.Taylor, Wear 241 (2000) 193-203.

[15] C.Y.Ho and R.E.Taylor, in: Thermal Expansion of Solids, (ASM International, 1998) ch. 1.

[16] M.Puskar, P.Bigos, and P.Puskarova, Measurement 45 (2012) 1067-1076.

[17] M.Puskar and P.Bigos, Measurement 46 (2013) 3389-3400.

[18] M.Puskar, P.Bigos, M.Kelemen, and R.Tonhajzer, Measurement 50 (2014) 203-212.

[19] Z.Anastasios and G.Pantelis, Int Jnl of Struct Integrity 6 (2015) 300-324.

[20] J.Ramsbottom, Proceedings of the Institution of Mechanical Engineers 1847-1982 (vols 1-196) 5 (1854) 70-74.

[21] J.Fu, J.Liu, Y.Wang, B.Deng, Y.Yang, R.Feng, and J.Yang, Applied Energy 113 (2014) 248-257.

[22] A.Gabriel-Buenaventura and B.Azzopardi, Renewable and Sustainable Energy Reviews 41 (2015) 955-964.

[23] T.Wang, Y.Zhang, J.Zhang, Z.Peng, and G.Shu, Energy Conversion and Management 84 (2014) 97-107.

[24] Anon, Ind Lubrication and Tribology 7 (1955) 42-43.

[25] R.I.Taylor, M.A.Brown, and D.M.Thompson, in: Tribology Series
Lubricants and Lubrication - Proceedings of the 21th leeds-Lyon Symposium on Tribology, ed. D.Dowson (Elsevier, 1995).

[26] C.Jun, M.Xianghui, X.Youbai, and L.Wenxiang, Ind Lubrication and Tribology 67 (2015) 468-485.

[27] V.P.Astakhov, in: Machining, (Springer London, 2008).

[28] Y.Wang, C.Yao, G.C.Barber, B.Zhou, and Q.Zou, Wear 259 (2005) 1041-1047.

[29] Y.Wang and S.Tung, Wear 225-229 (1999) 1100-1108.

[30] Z.Ye, C.Zhang, Y.Wang, H.S.Cheng, S.Tung, Q.J.Wang, and X.He, Wear 257 (2004) 8-31.

[31] K.Friedrich, in: Multifunctionality of Polymer Composites, eds. K.Friedrich and U.Breuer (William Andrew Publishing, Oxford, 2015).

[32] A.Gebhard, F.Haupert, and A.K.Schlarb, in: Tribology of Polymeric Nanocomposites (Second Edition), eds. K.Friedrich and A.K.Schlarb (Butterworth-Heinemann, Oxford, 2013).

[33] E.R.Braithwaite, A.B.Greene, and B.M.Train, Ind Lubrication and Tribology 51 (1999) 274-286.

[34] J.L.Hepworth, Ind Lubrication and Tribology 2 (1950) 13-15.

[35] P.C.Nautiyal, S.Singhal, and J.P.Sharma, Tribology International 16 (1983) 43-49.

[36] V.Esfahanian, A.Javaheri, and M.Ghaffarpour, Applied Thermal Engineering 26 (2006) 277-287.

[37] C.Íner, H.Hazar, and M.Nursoy, Materials & Design 30 (2009) 914-920.

[38] H.Scheerer, E.M.Slomski, T.Trobmann, and C.Berger, Surface and Coatings Technology In Press, Corrected Proof (2010).

[39] Anon, Honda model cb550k owners manual (Honda Motor Co. Ltd, 1977).

[40] Anon, Suzuki GS550 Service Manual (Suzuki Motor Co. Ltd, 1978).

[41] Anon, Aprilia SXV/RXV 450 - 550 owers manual (Valley Forge Deca, Ravenna, Modena, Torino, 2006).

[42] P.Mather, KTM EXC Enduros & SX Motocross service & repair manual: 2000 to 2007 (Haynes, 2007).

[43] R.Mittler and A.Mierbach. Understanding the fundamentals of piston ring axial motion and twist and the effetcs on blow-by. Proceedings of the ASME Internal Combustion Engine Division 2009 Spring Technical Conference . 5-6-2009.

[44] A.E.H.Love, Philosophical Transactions of the Royal Society of London. Series A, Containing Papers of a Mathematical or Physical Character 228 (1929) 377-420.

[45] M.GmbH, Pistons and engine testing (Vieweg+Teubner Verlag, 2013).

[46] W.Ritz, Journal fur die Reine und Angewandte Mathematik (1909) 1-61.

[47] R.Courant, K.Friedrichs, and H.Lewy, IBM Journal of Research and Development 11 (1967) 215-234.

[48] G.M.Miller, ARCHIVE: Proceedings of the Institution of Mechanical Engineers 1847-1982 (vols 1-196) 13 (1862) 315-327.

[49] M.J.J.Nunney, Light and Heavy Vehicle Technology (Taylor & Francis, 2012).

[50] R.I.Taylor and P.G.Evans, Proceedings of the Institution of Mechanical Engineers, Part J: Journal of Engineering Tribology 218 (2004) 185-200.

[51] M.J.Neale, in: Tribology Handbook (Second Edition), eds. M.J.Neale, OBE, E.BSc, DIC, FCGI, WhSch, FEng, and FIMechE (Butterworth-Heinemann, Oxford, 1996).

[52] L.J.Brombolich. Structural Mechanics of Piston Rings. 1-34. 1993. St louis, MO, Compu-Tec Engineering, Inc (Internal Report).

[53] R.Mittler. Optimization of Piston Ring Dynamics by direct 3D analysis of dynamic effects. 10-7-2009.

[54] R.Mittler, A.Mierbach, and D.Richardson, ASME Conference Proceedings 2009 (2009) 721-735.

[55] C.Baker, H.Rahnejat , R.Rahmani, and S.Theodossiades. Analytical Evaluation of Fitted Piston Compression Ring: Modal Behaviour and Frictional Assessment. SAE 2011 Noise and Vibrations Conference and Exhibitions . 5-17-2011. SAE International.

[56] J.F.Archard, Journal of Applied Physics 24 (1953) 981-988.

[57] A.Rabinovich, Russian Engineering Research 27 (2007) 169-173.

[58] E.Rabinowicz, L.A.Dunn, and P.G.Russell, Wear 4 (1961) 345-355.

[59] C.Cheng , A.Kharazmi , and H.Schock . Modeling of Piston Ring-Cylinder Bore-Piston Groove Contact. SAE 2015 World Congress & Exhibition. 2015. SAE International.

[60] A.Ganguly , K.Vikas, and T.Santra , SAE Int. J. Engines 8 (2015).

[61] B.Peng, H.Zhang, H.Shao, Y.Xu, X.Zhang, and H.Zhu, arXiv preprint arXiv:1509. 01391 (2015).

[62] H.Shahmohamadi, M.Mohammadpour, R.Rahmani, H.Rahnejat, C.P.Garner, and S.Howell-Smith, Tribology International 90 (2015) 164-174.

[63] M.Gore, M.Theaker, S.Howell-Smith, H.Rahnejat, and P.D.King, 228 (2014) 344-354.

[64] K.Wannatong, S.Chanchaona, and S.Sanitjai, Simulation Modelling Practice and Theory 16 (2008) 127-146.

[65] X.Wang and X.Chen, Measurement 43 (2010) 197-203.

[66] C.Baelden and T.Tian , SAE Int. J. Engines 7 (2014) 156-171.

[67] N.Lam , M.Tuner , P.Tunestal , A.Andersson , S.Lundgren , and B.Johansson , SAE Int. J. Engines 8 (2015).

[68] N.Morris, R.Rahmani, H.Rahnejat, P.D.King, and B.Fitzsimons, Tribology International 59 (2013) 248-258.

[69] P.M.Lee, M.S.Stark, J.J.Wilkinson, M.Priest, J.R.Lindsay Smith, R.I.Taylor, and S.Chung, in: Tribology and Interface Engineering Series
Life Cycle Tribology Proceedings of the 31st Leeds-Lyon Symposium on Tribology Held at Trinity and All Saints College, Horsforth, Leeds, UK 7th 10th September 2004, ed. D.Dowson (Elsevier, 2005).

[70] E.H.Smith, Tribology International 44 (2011) 29-41.

[71] S.C.Tung and H.Gao, Wear 255 (2008) 1276-1285.

[72] C.Lotz Felter, Tribology International 41 (2008) 914-919.

[73] D.Dawson and G.R.Higginson. Elana–hydrodynamic lubrication: rhefimdamemals of rollerand gears lubrication. Pergamon Press, Oxford.

[74] H.Van Der Hortst. Electrolytic process of making piston rings. [2367159]. 1-9-1945. 8-10-1939.

[75] H.C.Barshilia, M.S.Prakash, D.V.Sridhara Rao, and K.S.Rajam, Surface and Coatings Technology 195 (2005) 147-153.

[76] N.J.M.Carvalho, E.Zoestbergen, B.J.Kooi, and J.T.De Hosson, Thin Solid Films 429 (2003) 179-189.

[77] C.Charrier, P.Jacquot, E.Denisse, J.P.Millet, and H.Mazille, Surface and Coatings Technology 90 (1997) 29-34.

[78] D.Hche, G.Rapin, and P.Schaaf, Applied Surface Science 254 (2007) 888-892.

[79] C.Leyens, J.-W.van Liere, M.Peters, and W.A.Kaysser, Surface and Coatings Technology 108-109 (1998) 30-35.

[80] N.M.Renevier, V.C.Fox, D.G.Teer, and J.Hampshire, Materials & Design 21 (2000) 337-343.

[81] Z.M.Wang, MoS2: Materials, Physics, and Devices (Springer International Publishing, 2013).

[82] Y.Yu, C.Li, Y.Liu, L.Su, Y.Zhang, and L.Cao, Scientific reports 3 (2013).

[83] E.P.Becker and K.C.Ludema, Wear 225ΓÇô229, Part 1 (1999) 387-404.

[84] B.I.Chaika, I.M.Fedorchenko, P.N.Lapko, E.I.Ishchenko, V.P.Moldavanov, Y.Beizerman, A.D.Sokolov, A.R.Pikman, and Z.M.Medovoi, Powder Metallurgy and Metal Ceramics 17 (1978) 235-239.

[85] C.Friedrich, G.Berg, E.Broszeit, F.Rick, and J.Holland, Surface and Coatings Technology 97 (1997) 661-668.

[86] P.Hones. Structural and mechanical properties of chromium nitride, molybdenum nitride, and tungsten nitride thin films. Journal of Physics D: Applied Physics 36[8], 1023. 2003.

[87] M.I.Morkhov and K.A.Egorova, Chemical and Petroleum Engineering 1 (1965) 144-145.

[88] W.Wang, P.L.Wong, and F.Guo, Wear 257 (2004) 823-832.

[89] E.Tomanik, SAE 1996 Transactions - Journal of Materials & Manufacturing - V105-5 (1996).

[90] J.C.Maxwell and P.M.Harman, The Scientific Letters and Papers of James Clerk Maxwell: 1846-1862 (Cambridge University Press, 1990).

[91] H.Chang, Y.Zhang, and L.Chen, Applied Thermal Engineering 23 (2003) 2285-2292.

[92] M.Nakada, Tribology International 27 (1994) 3-8.

[93] ASM International.Handbook Committee, ASM handbook (ASM International, 2009).

[94] N.Gifford. Advances in Internal Combustion Piston Design. 250014848. 2001.

[95] L.Carley. Piston design, an evolutionary tale. 1-4-2003.

[96] S.H.Smith. State of the art piston rings. 11-9-2010.

[97] J.Heywood, Internal combustion engine fundamentals (McGraw-Hill, Inc., 1988).

[98] S.Safari and M.Hadfield, Wear 219 (1998) 8-15.

[99] M.Ashby. CES EduPack. 2-20-2015. Cambridge, UK, Granta Design.

[100] J.A.da Cruz Junior and D.B.Santos, Journal of Materials Research and Technology 2 (2013) 93-99.

[101] R.L.Errichello, in: Tribology Data Handbook, (CRC press, New York, 1997) ch. 67.

[102] G.H.Xu, M.Zhu, J.Liu, Z.Zhou, and H.Liang, Wear 255 (2003) 246-252.

[103] L.Su, Y.Zhang, Y.Yu, and L.Cao, Nanoscale (2014).

[104] Q.Peng and S.De, Physical Chemistry Chemical Physics 15 (2013) 19427-19437.

[105] A.E.Musson and E.Robinson, Science and technology in the industrail revolution (University of Manchester at the University Press, 1969).

[106] A.M.Brenneke. Combustion cylinder sleeve or Liner and combustion seal. [3340774]. 9-13-1967.

[107] S.Jacoby. Electrodeposited Coatings of Cylinder Bores for Small Aluminum Engines. 1976. SAE Technical Paper.

[108] A.F.Zimmerman, G.Palumbo, K.T.Aust, and U.Erb, Materials Science and Engineering: A 328 (2002) 137-146.

[109] R.M.Mortier and M.F.Fox, Chemistry and technology of lubricants (Springer, New York, 2010).

[110] A.Beek, Advanced engineering design: lifetime performance and reliability (TU Delft, 2006).

[111] E.R.Booser and Society of Tribologists and Lubrication Engineers, Tribology data handbook (CRC Press, 1997).

[112] D.Jones, T.Childs, C.Taylor, F.Martin, G.Zhu, D.Dowson, R.Chittenden, M.Priest, K.Holmes, and J.Bell, Engine Tribology (Elsevier, 1993).

[113] T.Tian, Proceedings of the Institution of Mechanical Engineers, Part J: Journal of Engineering Tribology 216 (2002) 209-228.

[114] M.T.Ma, I.Sherrington, and E.H.Smith, ARCHIVE: Proceedings of the Institution of Mechanical Engineers, Part J: Journal of Engineering Tribology 1994-1996 (vols 208-210) 210 (1996) 29-44.

[115] B.V.Dollegoorweg. Putoline Nano Tech 10W-50. 5-6-2014. Kroon-Oil. 1-6-0015.

[116] ISO/TC 22. ISO 6622-1:2003 Internal combustion engines. Piston rings. Rectangular rings made of cast iron. [2]. 12-19-0003. BSI.

[117] T.Kazushi, N.Kenichi, T.Masaaki, S.Tsuneo, and Nissan motor Co, JSAE Review 15 (1994) 276.

[118] D.E.Neuenschwander, Emmy Noether's Wonderful Theorem (Johns Hopkins University Press, 2010).

[119] H.Neuber and K.Federhofer, ZAMM - Journal of Applied Mathematics and Mechanics / Zeitschrift fur Angewandte Mathematik und Mechanik 31 (1951) 227.

[120] R.J.Chittenden and M.Priest, in: Tribology Series
Engine Tribology, ed. C.M.Taylor (Elsevier, 1993).

[121] H.I.Kawasaki, Kawasaki KZ550 service, repair and maintenance (Kawasaki Motor Co., 1977).

[122] B.Welghtman and D.Light, Biomaterials 7 (1986) 20-24.

[123] L.H.Tanner, Wear 57 (1979) 81-91.

[124] C.W.Y.Yip, J.P.Y.Ho, D.Nikezic, and K.N.Yu, Radiation Measurements 36 (2003) 245-248.

[125] P.K.Khanna, S.K.Bhatnagar, and W.Gust, Materials Letters 40 (1999) 170-174.

[126] Y.Lu, J.Xu, B.Liu, and J.Kong, Biosensors and Bioelectronics 22 (2007) 1173-1185.

[127] J.K.Norskov, Physica B+C 127 (1984) 193-202.

[128] R.Stewart, L.Li, and R.Isherwood, Optics & Laser Technology 34 (2002) 613-620.

[129] B.V.Cockeram and W.L.Wilson, Surface and Coatings Technology 139 (2001) 161-182.

[130] N.Bacchetta, D.Bisello, F.Broz, M.Catuozzo, Y.Gotra, E.Guschin, A.Lacaita, N.Malakhov, Y.Musienko, P.Nicolosi, A.Paccagnella, E.Pace, D.Pantano, Z.Sadygov, P.Villoresi, and F.Zappa, Nuclear Instruments and Methods in Physics Research Section A: Accelerators, Spectrometers, Detectors and Associated Equipment 387 (1997) 225-230.

[131] T.Kasai, K.Horio, T.Yamazaki, M.Komoda, T.K.Doy, and N.Kubo, Journal of Non-Crystalline Solids 177 (1994) 397-404.

[132] T.Kimura, X.M.Duan, M.Kato, S.Okada, S.Yamada, H.Matsuda, and H.Nakanishi, Polymer 39 (1998) 491-495.

[133] Y.C.Tan and Z.M.Ripin, Tribology International 44 (2011) 592-602.

[134] M.Dickinson, N.Renevier, and W.Ahmed. Optimising Piston Ring Contact Face Chamfer for High Performance Engines. SAE 2013 World Congress & Exhibition. 2013-01-0965. 4-8-2013. SAE. 4-16-2013.

[135] M.Dickinson, N.Renevier, and W.Ahmed. The Refinement of the contact compression ring chamfer for race
engine conditions. Comsol conference 2013. 9-5-2012. Comsol. 9-14-2012.

[136] H.Douglas. Method of Piston Ring Manufacture. [2380654]. 7-31-1945. United States.

[137] N.I.Muskhelishvili, Some Basic Problems of the Mathematical Theory of Elasticity (Noordhoff, 1975).

[138] R.E.Bradley and E.Sandifer, Leonhard Euler: Life, Work and Legacy (Elsevier Science, 2007).

[139] ISO/TC 22. ISO 6621-3:2000 Internal combustion engines. Piston rings. Part 3: Material specifications. [2]. 12-19-0003. BSI.
Ref Type: Online Source

[140] S.H.Mansouri and V.W.Wong, Proceedings of the Institution of Mechanical Engineers, Part J: Journal of Engineering Tribology 219 (2005) 435-449.

[141] M.W.Dickinson, N.M.Renevier, and W.Ahmed, International Journal of Surface Engineering and Interdisciplinary Materials Science 1 (2013) 1-12.

[142] M.W.Dickinson, N.Renevier, and J.Calderbank, SAE International Journal of Passenger Cars - Mechanical Systems (2015).

[143] R.C.Martins, P.S.Moura, and J.O.Seabra, Tribology International 39 (2006) 1686-1697.

[144] R.I.Amaro, R.C.Martins, J.O.Seabra, N.M.Renevier, and D.G.Teer, Tribology International 38 (2005) 423-434.

[145] Y.Gortyshov, A.Druzhinin, V.Gureev, I.Gumerov, and V.Stroganov, Russian Engineering Research 30 (2010) 385-387.

[146] Z.Dimkovski, L.Baath, S.Rosen, R.Ohlsson, and B.G.Rosen, Wear 270 (2011) 247-251.

APPENDIX A.

A Novel System for analysis of surface profiles from 3-D components using the Dickinson Rotating Ring Contact Profiler

Matthew Dickinson, Nathalie Renevier and Waqar Ahmed

Institute of Nanotechnology and Bioengineering, School of Computing, Engineering and Physical Sciences, University of Central Lancashire, Preston PR1 2HE

Abstract

In this paper we present a novel system, the Dickinson Rotating Ring Contact Profiler (DRRCP) for measuring the surface profiles of components with ring profiles. Race car piston rings have been used as a test case to prove the simplicity and validity of the new system. The results obtained from the DRRCP were compared with the standard system and similar values of the mean and standard deviation were obtained, Ra = 0.3±0.05 and Rz = 0.6 ± 0.09 respectively. The system is readily adaptable to other cylindrical components and is predicted to have further applications in other fields/systems.

1. Introduction

Surface profilometery is a common method used in the analysis of surface roughness, shape and waviness of engineering components (Welghtman and Light 20-24;L.H. 81-91). The analysis involves measurement in high resolution along the lateral and vertical axis. It is well known that the performance and life of engineering components is highly dependent on the surface properties (Yip et al. 245-48). For example, wear rates are considerable greater in rough surface compared to smooth surface and components engineered to have a smooth surface have longer lifetimes (Khanna, Bhatnagar, and Gust 170-74). There are a number of methods for measuring the surface roughness of components including optical techniques

such as classical interferometry, holographic interferometry, speckle techniques and white light interferometry (Lu et al. 1173-85;J.K. 193-202;Stewart, Li, and Isherwood 613-20) as well as mechanical techniques (Cockeram and Wilson 161-82). In this paper we focus on the later employing Taylor Hobson Talysurf (Cockeram and Wilson 161-82;Bacchetta et al. 225-30;Kasai et al. 397-404;Kimura et al. 491-95). This instrument employs a mechanical transducer known as the stylus which moves across the x-axis of the surface of a component and its vertical movement is recorded to obtain the surface profile. One of the major disadvantages of this method is that it restricted to horizontal substrates and therefore to obtain profiles of 3-D components such as piston liner to ring contact face is problematic. In this paper we present the design, manufacture and application of a new piston ring mounting system for use in the analysis of surface profiles of the complete piston ring component. The data obtained will give a greater insight into the causes of wear and performance of piston rings in racing engine.

2. Experimental

2.1 Surface Profilometer

The Taylor Hobson instrument employs the movement of a 90^{o} conical diamond stylus with a spherical tip in the range of 6mm which is carried at one end of a beam pivoted at the fulcrum on knife edges. The remote end carries an armature which moves between a pair of coils altering their relative inductance. Special gauges are employed to amplify the signal increasing the resolution ratio from 1000:1 to 64000:1allowing a 0.6nm resolution to be reached for a range of 0.03 mm in the z-direction with a maximum nominal measuring range of 0.8mm. The instrument has a length interval of 120 mm/0.1 mm (Xmax/Xmin). The data sampling interval is 0.25 mm for traverse length to 30 mm and 1 mm for length over 30 mm. Surface texture parameters are obtained from the digitalized signal, for peak parameters with

uncertainty of 2%+4nm. The instrument is controlled by Ultra software incorporating calibration and measurement functions.

2.2 Standard Sample Holder Systems

The standard sample stage system (Figure 1) comprises of a three base plates where the lower base plate is incorporated to allow for fixing to the machine. The mid plate is used to allow the adjustment plate the movement range of 20mm in the Y axis. The adjustment plate is positioned by a micrometer which is mounted to the front of the base plate. Between the two plates an inner rail and outer rail is mounted: these rails allow the adjustment plate to be moved with ease. To allow for precession movements of the adjustment plate, two springs at each side of the adjustment plate are placed parallel with the micrometer which are held by two locator spring pins. For special project mounting holes are placed in the adjustment plate to allow for fixing into position.

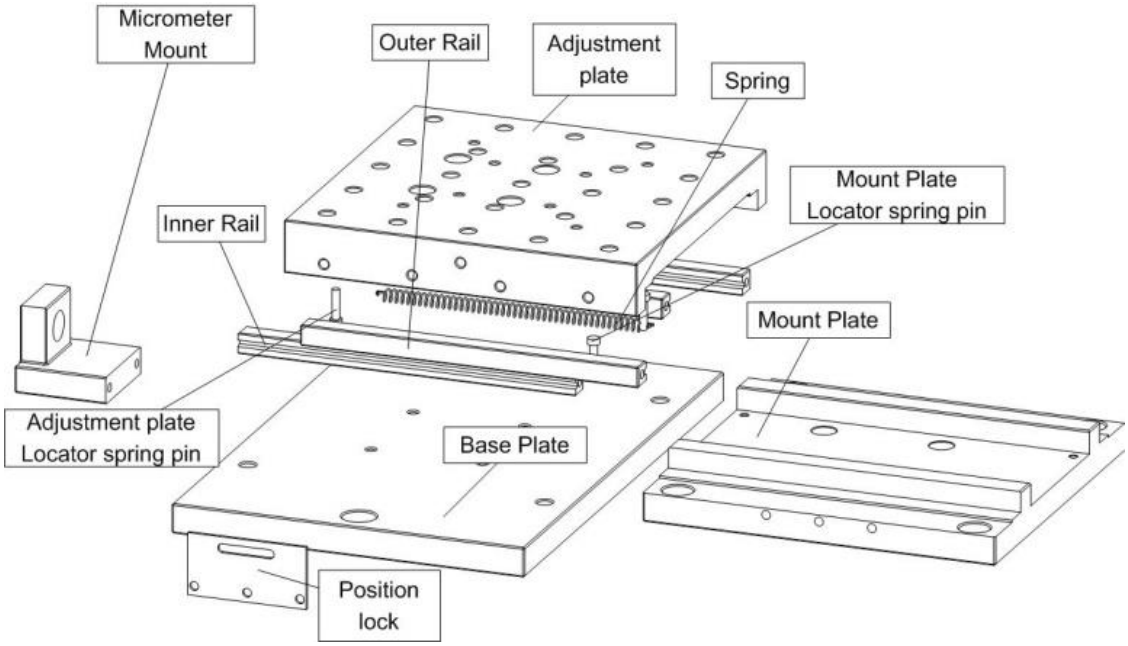

Figure 2 - Exploded View of Mount stage

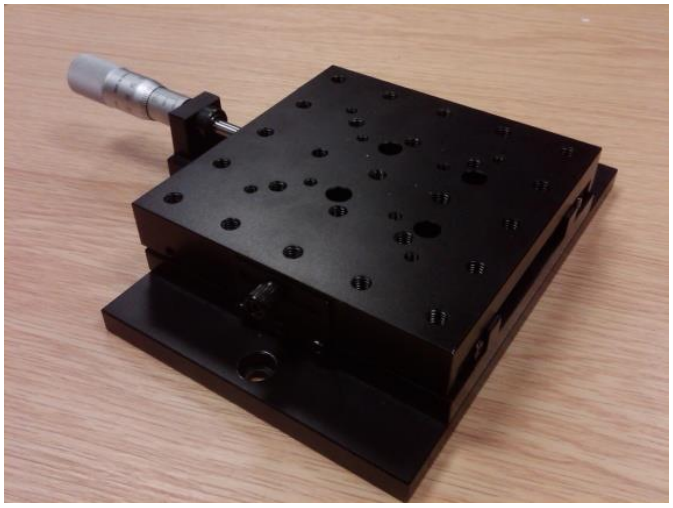

Figure 3 - Mount Stage

2.3 New Piston Ring Mount System

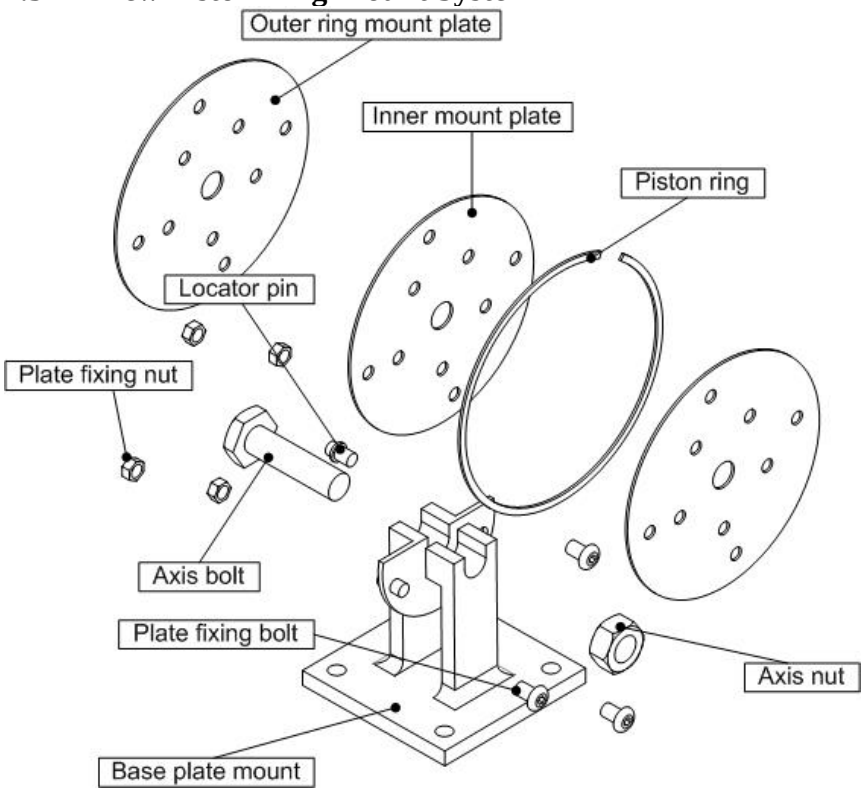

Figure 4 - Exploded RCP jig

Figure 5 - RCP Jig

To overcome the disadvantages of the standard sample holder system (Figure 1), a new piston ring mount system was designed, manufactured and tested in our research laboratories at the University of Central Lancashire (Figure 2). The system consists of three fixing plates made from aluminium held together by four fixing bolts positioned at 90^{o} relative to the base plate mount assembly. The plates can be rotated manually at intervals of 72^{o} for complete analysis of the entire piston ring. The inner mount plate is made from neoprene foam material which enables a soft contact with the piston ring to prevent damage to nano-engineered surfaces of the piston ring. This assembly is mounted to the standard system base plate and the screw is tightened to keep the assembly in the correct position.

2.4 Results and discussion

2.4.1 Piston surface profiles

Figure 6a shows the piston ring used in race engines. It explains the terminologies commonly used including top ring, land, bottom ring land, ring gap and contact face. Figure 6b shows the North, East, South and West directions of the measurements made using the Dickinson Rotating Ring Contact Profiler. Measurements were repeated 10 times to determine the statistical errors in the measurements using the Talysurf. The North direction has been specific at the gap in the piston ring which was rotated 5 times for each position.

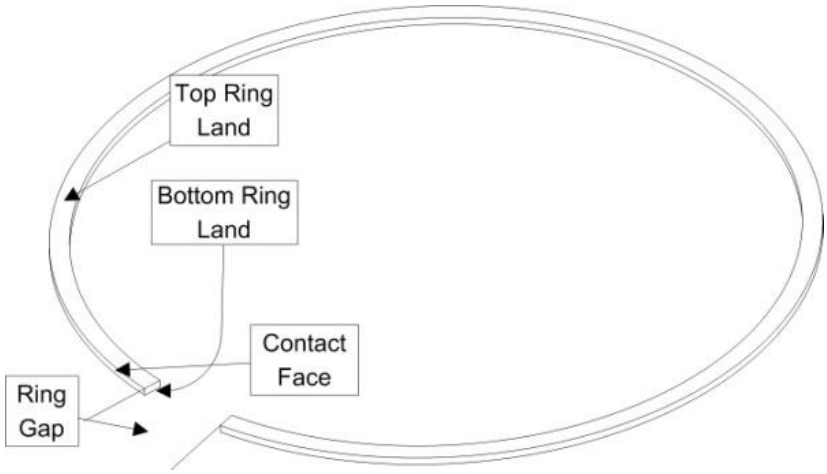

Figure 6a – Race Piston Ring Terminologies

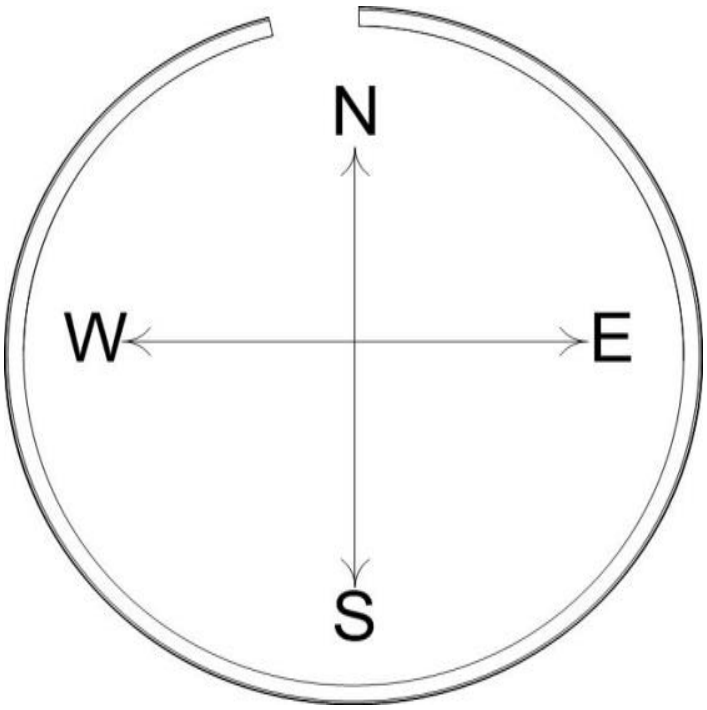

Figure 6b - Test Regions

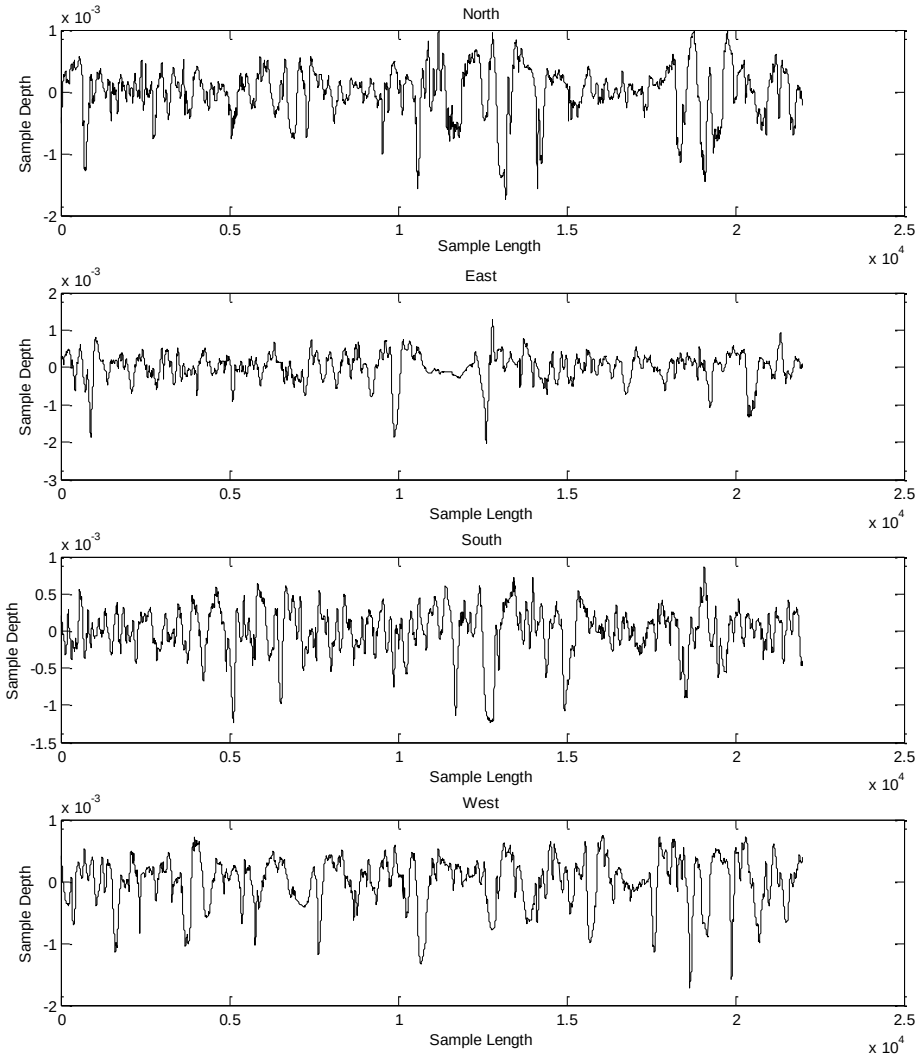

Figure 7 – Surface Profile Measurements

2.4.2 Standard system

Figure 7 shows surface profile measurements carried on the piston ring at four different locations, namely North, East South, and West locations respectively. The measurements of Ra values is one of the most common profile parameters, this parameter gives the average roughness. Ra is typically expressed in μm for engineering components in engines. The average roughness has a significant influence on the performance and lifetime of engine wear parts. In general the lower the Ra values the lower the coefficient of friction determining wear rates, life and performance. This parameter refers to profiles exceeding the roughness profile mean line. The parameter Rz however refers to the average maximum height of

profile. The Rp parameter refers to the maximum profile peak height of the surface. These three parameters allow for a good understanding of the surface profile during analysis hence the reason for selecting these three profiles for comparison.

Repeat Flat ring profile			
Test No.	Ra (um)	Rp (um)	Rz (um)
1	0.3006	0.6696	1.9815
2	0.3002	0.6682	1.9856
3	0.3002	0.6702	1.9966
4	0.3004	0.669	2.0047
5	0.3004	0.6698	1.9935
6	0.3118	0.6797	2.057
7	0.3006	0.6704	2.0053
8	0.3032	0.6704	1.9966
9	0.3009	0.6672	1.9988
10	0.2986	0.6773	2.017
Mean (σ)	0.30169	0.67118	2.00366
Standard deviation $\sqrt{\sigma^2}$	0.0035	0.0038	0.0202

Table 1. Flat ring profiles measurements repeated 10 times on the top land of the ring with mean and standard deviations calculated.

Table 1 shows the 10 measurements made with Ra, Rp and Rz values. The mean and standard deviation were calculated for Ra, Rp and Rz which gave values of 0.30169 and 0.0035; 0.67118 and 0.0038; and 2.00366 and 0.0202 respectively. These values will be used as baseline standard reference to compare subsequent results using the new Dickinson Rotating Ring Contact Profiler.

Rotation Flat ring profile				
Test No.	Ra (um)	Rp (um)	Rz (um)	
1	0.2846	0.7156	1.9033	East
2	0.2843	0.5949	1.5449	
3	0.2621	0.7175	1.7909	
4	0.5304	2.2246	3.392	
5	0.3504	0.6789	1.5842	
Mean (σ)	0.3424	0.9863 (0.6767)	2.0431	
Standard deviation $\sqrt{\sigma^2}$	0.0986	0.6207	0.6872	
1	0.3058	0.6425	1.7349	North
2	0.2415	0.595	1.4546	
3	0.2545	0.5946	1.5713	
4	0.3154	0.6199	1.7461	
5	0.2771	0.6043	1.5704	
Mean (σ)	0.2789	0.6113	1.6155	
Standard deviation $\sqrt{\sigma^2}$	0.0285	0.0181	0.1106	

Rotation Flat ring profile				
Test No.	Ra (um)	Rp (um)	Rz (um)	
1	0.2457	0.5924	1.4032	South
2	0.5075	0.7625	3.4498	
3	0.282	0.7024	1.857	
4	0.2475	0.5642	1.5702	
5	0.3056	0.8559	1.8804	
Mean (σ)	0.3177	0.6955	2.0321	
Standard deviation $\sqrt{\sigma^2}$	0.0975	0.1078	0.7311	
1	0.3101	0.6311	1.7217	West
2	0.3544	0.6159	1.7843	
3	1.1551	2.0771	4.1126	
4	0.3975	1.0255	2.4187	
5	1.0944	1.9858	3.598	
Mean (σ)	0.6623	1.2671 (0.7931125)	2.7271	
Standard deviation $\sqrt{\sigma^2}$	0.3791	0.9606	0.9667	

Table 2. Surface profile measurements in four directions repeated five times with associated mean and standard deviations.

In table 2 the standard system has been employed using flat profile in the four principle directions. Measurements in the North and South gave means and standard deviations for Ra, Rp and Rz which are similar to those used as baseline from repeated tests shown in table 1. However, the East and West measurements for the mean and standard deviation Rp are higher than expected i.e. 0.9863 and 1.2671 for the means and 0.6207 and 0.9606 for the standard deviation respectively. There are several possible reasons for these anomalies. Firstly they may be a result of surface defects present in the piston ring and particulates embedded in the surface. Investigations using scanning electron microscopy are currently being carried out and will be reported in a subsequent paper. However, with these values omitted the mean and standard deviations were as expected.

There are limitations of this current system. Each set of results were only able to be obtained on the flat profile, therefore, to obtain corner profiles of the piston ring and with zero movement the compression ring would need to be divided. In a situation in which ring profiles are needed however dividing the ring into smaller pieces is not an option the standard system is unable to achieve this.

2.4.3 New system – the Dickson Rotating Ring Contact Profiler (DRRCP)

The surface profile measurements were repeated using the Dickinson Rotating Ring Contact Profiler following the same procedures used for the standard system.

Repeat position RCP ring profile			
Test No.	Ra (um)	Rp (um)	Rz (um)
1	0.3148	1.265	2.3214
2	0.3135	1.2278	2.3168
3	0.3099	1.2581	2.321
4	0.3173	1.2394	2.3481
5	0.3177	1.215	2.353
6	0.3187	1.1972	2.361
7	0.3196	1.1948	2.2993
8	0.3201	1.1781	2.2606
9	0.3195	1.1481	2.2443
10	0.3163	1.1291	2.2102
Mean (σ)	0.3167	1.2053	2.3036
Standard deviation $\sqrt{\sigma^2}$	0.0031	0.0426	0.0476

Table 3. Ring profiles measurements repeated 10 times on the top land of the ring with mean and standard deviations calculated using the Dickinson Rotating Ring Contact Profiler.

When the mean and standards deviations of the Ra, Rp and Rz were compared to standard systems the new system gave similar values to the standard system for Ra and Rz. However, the mean Rp values and standard deviation were significantly higher than those obtained for the standard system. The new system mean Rp of 1.2053 and standard deviation of 0.0426 compared to the values obtained from the standard system mean Rp of 0.67118 and standard

deviation of 0.0038. An examination of these means demonstrates that the mean acquired by the DRRCP is almost twice that obtained by the standard values. This suggests that the Rp values are not good indicates of surface roughness in this case possibly because the surface is curved.

Table 3 and 4 results were obtained by placing the ring into the Dickinson Rotating Ring Contact Profiler to analyse the contact face relative to the stylus.

Rotation position RCP ring profile				
Test No.	Ra (um)	Rp (um)	Rz (um)	
1	0.4497	1.6304	2.989	East
2	0.3574	1.2117	2.4293	
3	0.2908	0.99	2.0951	
4	0.3127	1.0876	2.2562	
5	0.3757	1.3468	2.5052	
Mean (σ)	0.3573	1.2533 (0.611)	2.4550	
Standard deviation $\sqrt{\sigma^2}$	0.0553	0.2234	0.3025	
1	0.2498	0.8777	1.8272	North
2	0.2645	0.8306	1.7748	
3	0.2542	0.8386	1.7692	
4	0.4479	1.1017	2.3961	
5	0.3074	1.1588	2.167	
Mean (σ)	0.3048	0.9615 (0.5615)	1.9869	
Standard deviation $\sqrt{\sigma^2}$	0.0744	0.1399	0.2521	

Rotation position RCP ring profile				
Test No.	Ra (um)	Rp (um)	Rz (um)	
1	0.3609	1.154	2.3418	South
2	0.3171	1.1254	2.1745	
3	0.5279	1.4848	3.1277	
4	0.4735	1.1392	2.5536	
5	0.5116	1.4323	3.0539	
Mean (σ)	0.4382	1.2671 (0.66714)	2.6503	
Standard deviation $\sqrt{\sigma^2}$	0.0840	0.1574	0.3799	
1	0.246	0.7615	1.7141	West
2	0.3194	1.0854	2.0918	
3	0.3795	1.6603	2.9039	
4	0.7053	2.3467	4.2752	
5	0.4385	1.8217	3.0529	
Mean (σ)	0.4177	1.5351 (0.7351)	2.8076	
Standard deviation $\sqrt{\sigma^2}$	0.1573	0.8673	0.8867	

Table 4. Surface profile measurements in four directions repeated five times with associated mean and standard deviations using the Dickinson Rotating Ring Contact Profiler.

The new DRRCP has been used to measure the surface roughness profiles in four different directions north, south, west and east (Table 4). As expected the mean values are in the range 0.3±xx and standard deviation of 0.07± xx and this compares favourably with

measurements taken using the standard system. There are deviations in the East and West directions similar to those obtained in the standard system. This indicates the presence of surface defects or particles.

3. Conclusions

In this paper we have presented the design and development of the Dickinson Rotating Ring Contact Profiler (DRRCP) to measure the surface roughness of components. The piston ring was used as a test case. Results were compared to the standard system and observations demonstrate that the performance of the system was similar to the standard system. Thus, the DRRCP profile is a fast, convenient and simple system for measuring the surface profiles of components with ring profiles such as race car piston rings.

Acknowledgements

The authors would like to thank Michael Bodel from the University of Central Lancashire for design and technical support and Rebecca Harris for her recommendations for improvements to this paper.

Reference List

Bacchetta, N., et al. "MRS detectors with high gain for registration of weak visible and UV light fluxes." Nuclear Instruments and Methods in Physics Research Section A: Accelerators, Spectrometers, Detectors and Associated Equipment 387.1GÇô2 (1997): 225-30.

Cockeram, B. V. and W. L. Wilson. "The hardness, adhesion and wear resistance of coatings developed for cobalt-base alloys." Surface and Coatings Technology 139.2GÇô3 (2001): 161-82.

J.K., N+ rskov. "Theory nof chemisorption and heterogeneous catalysis." Physica B+C 127.1GÇô3 (1984): 193-202.

Kasai, Toshio, et al. "Polishing to reveal micro-defects on glass." Journal of Non-Crystalline Solids 177.0 (1994): 397-404.

Khanna, P. K., S. K. Bhatnagar, and W. Gust. "Surface studies of interconnecting zones for selective-area sealing of hybrid microcircuits using isothermal solidification process." Materials Letters 40.4 (1999): 170-74.

Kimura, Tatsumi, et al. "Synthesis and non-linear optical properties of aromatic ester oligomers as chained chromophores." Polymer 39.2 (1998): 491-95.

L.H., Tanner. "A comparison between talysurf 10 and optical measurements of roughness and surface slope." Wear 57.1 (1979): 81-91.

Lu, Yidong, et al. "Photosynthetic reaction center functionalized nano-composite films: Effective strategies for probing and exploiting the photo-induced electron transfer of photosensitive membrane protein." Biosensors and Bioelectronics 22.7 (2007): 1173-85.

Stewart, R., L. Li, and R. Isherwood. "The effect of microscopic features upon the transmissivity of enclosed laser ablated laminated metallised polymer films." Optics & Laser Technology 34.8 (2002): 613-20.

Welghtman, B. and D. Light. "The effect of the surface finish of alumina and stainless steel on the wear rate of UHMW polyethylene." Biomaterials 7.1 (1986): 20-24.

Yip, C. W. Y., et al. "Study of inhomogeneity in thickness of LR 115 detector with SEM and Form Talysurf." Radiation Measurements 36.1GÇô6 (2003): 245-48.

APPENDIX B.

(2013-01-0965)

Optimising piston ring contact face chamfer for high performance engines

Matthew Dickinson[1 2], Nathalie Renevier[1,2] and Waqar Ahmed[1*]

1. Institute of Nanotechnology and Bioengineering, School of Computing, Engineering and Physical Sciences, University of Central Lancashire, Preston PR1 2HE

2. Jost Institute for Tribotechnology, School of Computing, Engineering and Physical Sciences, University of Central Lancashire, Preston PR1 2HE

ABSTRACT

Internal combustion engine components have been a main research interest over many decades [1]. While bulk material and surface engineering developments have improved the resistance to fatigue, reduced the amount of wear and friction during operation, small improvements in race applications designs can increase the engine performance and give a competitive edge to racing engines. Piston rings are designed to create a seal which means that they will suffer large levels of material loss due to wear during operation. The compression ring is the top or closest ring to combustion gases and is exposed to the highest operating temperature. In this paper, the authors propose a design modification to the compression ring coated chamfer which can reduce stress concentration and material loss during operation.

INTRODUCTION

The internal combustion engine has been an area of research for many years. The pioneering work was completed by Rambottom in 1854 [2] with the incorporation of a new type of rings to the piston to create a better seal during engine operation. Miller in 1862 [3] re-examined Rambottom rings design and made further improvements in allowing pressure to build on the back side of the ring. Over many years several design modifications to piston rings, piston and cylinder have been achieved. In an effort to lower the fuel consumption the piston was redesigned to enable the piston ring to sit closer to the crown [4]. Many advancement in engines lubricants have also been made with the introduction of synthetic oils and the incorporation of detergents additives in lubricants. Detergent additives have maintained carbon deposits from burnt fuel in a non-solidified state to prevent carbon to react and harden around the piston ring causing the ring to stick in the grove of the piston. A noted problem over many years was the phenomenon known as corking, this was a result of fuel burning casing carbon emissions depositing on to the piston ring [5].

The chamfer has been one of the piston ring significant design feature incorporated and refined over many years. A.E.H. Love in 1882 [6] suggested that the addition of geometrical features, such as chamfer placed on the top back edge of the ring would result in further improvements.

Some of the first piston rings were used without surface treatment or protective coatings. In an effort to reduce wear in the piston ring, in the 1940's Cr coatings where applied to the outside face of the ring [7]

The design of the piston ring has been the main focus of many studies over decades; the aim of this

work is to focus on a relatively new design feature of the piston ring, the piston ring contact chamfer. The piston act as a reciprocating mass moving from the bottom dead centre position (BDC) to the top dead centre (TDC), the piston ring achieves optimal performance when the ring contact is perpendicular to the cylinder. This is illustrated in Figure 1.

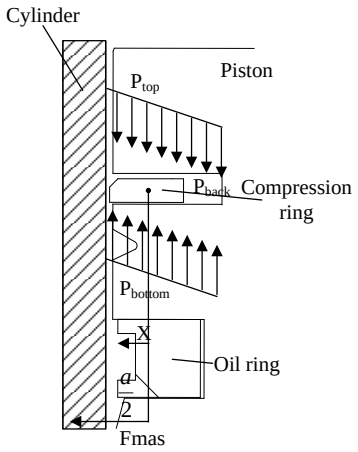

Figure 1 Cross section of the compression ring and oil ring showing with piston running parallel to the length of the cylinder wall.

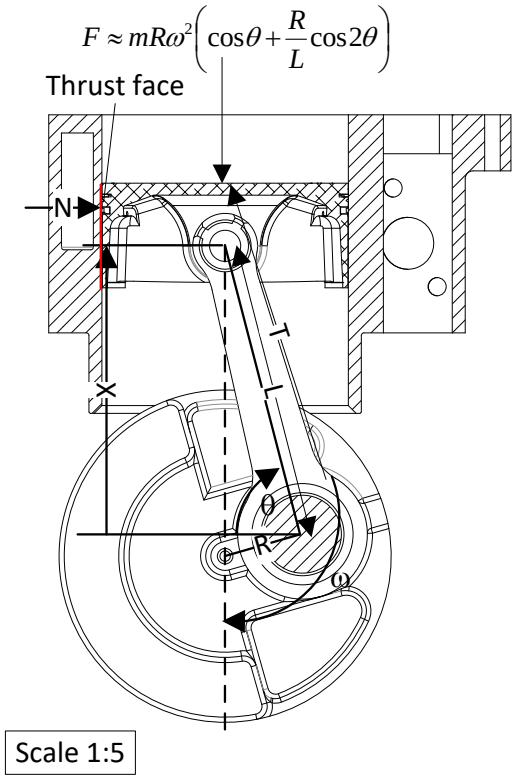

Figure 2. Cylinder, Piston, Piston ring, Connecting rod and Crank configuration

The compression ring been the closest ring to combustion gases is therefore exposed to the highest operating temperature. The compression ring transfers 70% of the combustion chamber heat from the piston to the cylinder wall where heat transfer and thermal elastic deformation phenomena will occur. Cylinder liners have a higher coefficient of expansion than the compression ring and therefore increased clearances must be allowed for, so the piston skirt clearance in the liner is greater than that for piston ring. The skirt transmits the side thrust (N in Figure 2), caused by the varying angularity of the con rod, to the liner. Excessive clearance will cause the piston to tilt. The tilt can cause large levels of stress centred on the ring top edge of the contact face. In an attempt to relieve the concentrated levels of stress, companies have incorporated a small chamfer on the top of the contact face. This work examines the chamfer design feature and suggests an optimal geometrical size.

Reverse Engineering of a KTM 520 engine has been used to develop a 3D Computer Aided Design (CAD) model using SolidWorks that has been further analysed by Finite Element Analysis (FEA) using COMSOL to determine the piston tilt effect on the chamfer stresses. KTM 520 gave us realistic engine geometries and engine operational condition. It has been possible to compare experimental data with data generated by the models.

Over the past 200 years, the piston ring geometric shape has remained rectangular as shown in Figure 1. In the past 50 years the piston ring has been altered [8,9] to incorporate in the ring a torsional twist feature in a form of a contact chamfer on the piston ring face. The thrust (T in Figure 2) coming from the system encourages the piston to tilt as the engine velocity and load increases when the piston reciprocates from bottom dead centre towards the top dead centre.

SYSTEM

KTM 520 engine materials and dimensional characteristics have been reported in Table 1.

Table 1 - Showing component details

Dimension (mm)	Component	Material

95	Compression ring	BS-Grade 400 grey cast iron coated with 0.116mm MoS_2
94.95	Piston	4032-T6 alloy
95	Cylinder	NikaSil

In this study, both primary inertia force ($m\omega^2 R\cos\theta$) and secondary inertia force ($mR\omega^2 \frac{1}{n}\cos 2\theta$) acting on the pistons during operation have been considered [1], where m , ω , R, n , θ are respectively piston weight, angular momentum, crank radius, rod to crank length ratio $\frac{1}{n} = \frac{R}{L}$ and the crankshaft rotation measured from top dead centre.

When calculating the engine cycle, the equation assumes that there is a zero offset from the centre of the crank.

However, in a standard four stroke internal combustion engine, in the cooled state, when the engine is first started, the piston has a cylindrical profile from crown to the bottom of the oil ring, while the piston shape is elliptical from the bottom of the oil ring to the bottom of the skirt. Once the piston is in operation it is assumed that the geometry becomes an almost perfect cylindrical shape on both sides of the oil ring.

The following boundary conditions have been used:

- Continuity in motion and torque in all directions
- Piston shape is assumed to be cylindrical at all time.

In Figure 3, Pythagoras's theorem was employed to calculate the contact angle β between the piston and the cylinder

$$\sin(\beta) = \frac{C_L}{P_L} \qquad (1)$$

where P_L , C_L and B_L are respectively piston length, piston cylinder clearance and cylinder area covered while in operation.

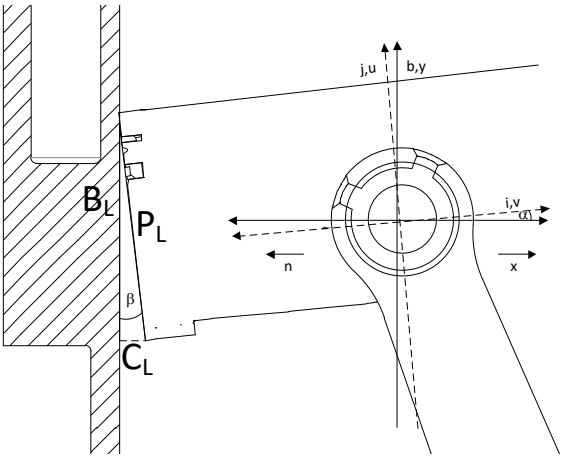

Figure 3 Schematic representation of the piston tilt

Using Love's principles [6], stress generated through torsional twist can be calculated using Euler rotational principles [10].

$$\Delta k_i = -\beta k_j - \frac{d^2 v}{ds^2} \quad ; \qquad \Delta k_j = +\beta k_i + \frac{d^2 v}{ds^2} \quad ;$$
$$\tau = \frac{d(-\beta + k_j u + k_i v)}{ds}; \; ds = r_s d\varphi \qquad (2)$$

where coordinates (u, v) are obtained by rotation of angle α of the coordinates (i, j) as shown in Figure 3 and β, Δκ, τ and ds are respectively the twist angle, change of the curvatures, torsion in the ring and the arc length.

Finally the pressures acting on the piston rings have to be considered. These pressures are calculated using the equations 3-6. The negative pressure direction is calculated in the following equation:

$$p(x) = \frac{1}{2}(P_{bottom} + P_{back})\frac{x}{a} + (P_{bottom} - P_{back}) \qquad (3)$$

The resulting gas pressure acting on the ring contact face gap is calculated using

$$p(x) = -\frac{1}{2}(P_{top} - P_{bottom})\frac{x}{a} - (P_{top} - P_{bottom}) \qquad (4)$$

The gas force in the system can be determined from the pressure of the top and bottom, based on the circumference of the ring thickness a.

$$Gas_F = -\frac{1}{2}a\left(P_{top} - P_{bottom}\right) \quad (5)$$

The presented work assumed the ring being fully flooded with lubricant and R.Mittler & al. approach [11] have been used where the effects of blow-by were studied while considering the geometry of the piston. The lubrication distribution throughout the system has been calculated using B.Deng & al. methodology [12] where trigometric oil film thickness distribution is represented by

$$h_m(\emptyset) = A + B|\sin\emptyset| \quad (6)$$

To calculate the forces applied to the ring, a simple equation is used, $F = \frac{p}{A}$ where F, p and A are respectively the force, pressure and area. The level of deformation of the ring has been calculated using the shear stress equation, to evaluate the stress acting at this point.

$$\tau = \frac{\sigma_1 - \sigma_2}{2} \quad (7)$$

where σ_1 and σ_2 are the major and minor principal stresses respectively.

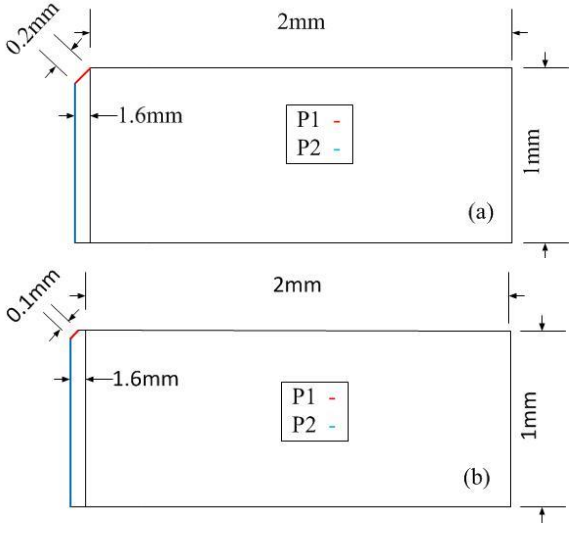

Figure 2 (a) ISO 6622-1 Internal combustion engines cast iron standard ring dimensions based on 90mm diameter. (b) new Dickinson proposed design

To construct an accurate simulation of the ring, the dimensions were taken from the ISO 6622-1 [1] for a ϕ90mm compression ring as shown on Figure (4a) close enough to the ϕ95mm KTN rings used in the study. The proposed design of the ring coated chamfer is shown on Figure 4 (b) with a 0.1mm contact chamfer machined to the upper outside face corner of the piston ring.

The operational engine speed range for the KTM 520 engine was between 6,000-10,000RPM. The boundary conditions incorporated into the simulation allowed for forces, pressures and inertias to be considered. It should be noted that in this paper the description of radial forces and hydrodynamic lubrication of the ring face are not discussed.

RESULTS

Accumulated stresses have been generated during the upward dynamic displacement of the piston (BDC to TDC). This confirms the behaviour previously noted by R.Mittler & al. [11]. The problem investigated in this work refers to the piston ring chamfer concentration stresses found on the contact face of the ring; this is shown in more detail in Figure 4 (a) and (b) marked as P1 and P2 variables respectively.

Inertia forces as a function of RPM have been shown in figure 5. Figure 6 details both the chamfer configurations in the operation range of 6000-10000 rpm.

Simple square ring geometry has been used for the simulation to focus the investigation on the stress concentration created near P2 (Figure 4) when the engine operates in sector 1 (Figure 6).

When the engine operates in sector 1 as shown in Figure 6, where the piston inertia forces will not exert a stress great enough to induce a large level of structural damages, grey cast iron rings can resist against the stress being applied. Studies done on the elastic properties of uncoated piston ring [6,8,9] have shown that a chamfer can relieve some of the concentrated stresses present in the grey cast iron. While the ISO standard [13] recommends for the chamfer to reach the grey cast iron substrate, this has been contradicted by Love [6] works suggesting that the chamfer should remain within the coating thickness, as excessive stresses would

be generated at the grey cast iron/MoS_2 interface causing severe damages to both coating and grey cast iron substrate.

As the engine speed rises in excess of 9,500 rpm and enters Sector 2 as shown in Figure 6, the contact point between the grey cast iron ring and the cylinder wall begins to shear (Sector 2 in Figure 6).

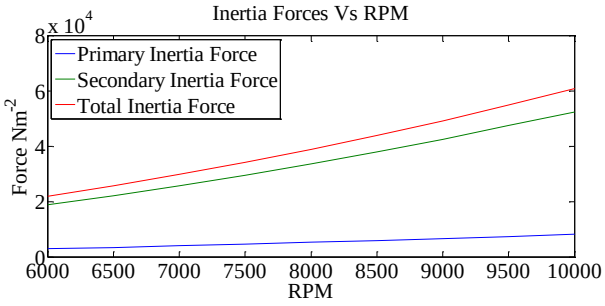

Figure 5. The inertia force and RPM rise.

The grey cast iron ring begins to shear between the operational rpm values of 10,000 – 11,000 rpm (sector 2 of Figure 6), hence it is suggested that engine should refrain from operating in this range.

The standard design of the piston ring chamfer shown in Figure 4 (a) can be modified to half of its original dimension as shown in Figure 4 (b), this conforms to work noted in references [6,8,9]. The contact chamfer on the ring was reduced from the standard size from 0.2mm (Figure 4a) to a new size of 0.1mm (Figure 4b), and results are conformed with Love principles [6]. Both ring designs (Figure 4 (a-b)) were simulated in the same operating conditions. Shearing (Figure 6) present during operation in section 2 can be reduced with the new design (Figure 4 (b)), this would increase life expectancy and failure to fatigue.

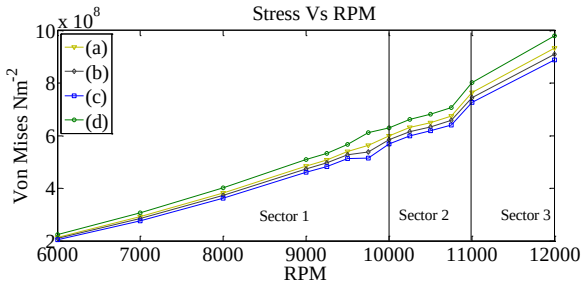

Figure 6: Effect of Shearing as a function of chamfer length (a) 0.2mm recommended in ISO standard,(b) 0.175mm, (c) 0.15mm and (d) 0.1mm

When Love's principles [6] are used to optimise the design and manufacture of the chamfer, reduced stress and improved performances can be obtained. As the rpm increases, the inertia forces also increases when both inertia forces and pressure forces are incorporated in the calculation.

DISCUSSION

When the engine operates in the rpm range of 10,000 to 11,000 shearing becomes especially greater around the operational value of 10,750rpm. During a full cycle of the engine, the piston will move from bottom dead centre to top dead centre, at this point the piston will tilt, the ring contact face will also be set at β, hence shearing may occur.

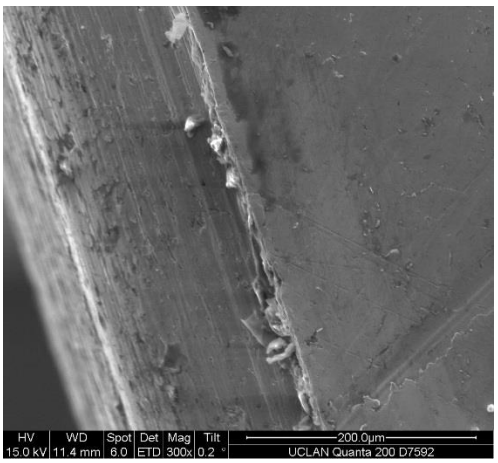

Figure 7 - Grey Cast Iron coated with MoS_2 un-used

A scanning electron microscopy (SEM) image of an un-used KTM piston ring chamfer is shown on Figure 7, while the same ring is presented after 90

minutes of running-in in figure 8. The area highlighted in red presents deep cracks. This paper has examined only race car conditions; hence the combustion pressures that have been given are extremely high compared to what is seen in normal engine output pressures. The work completed references [6,8,11], indicates that by placing a chamfer on the material in such a way will allow the material to deform and have a more even stress distribution during the operation.

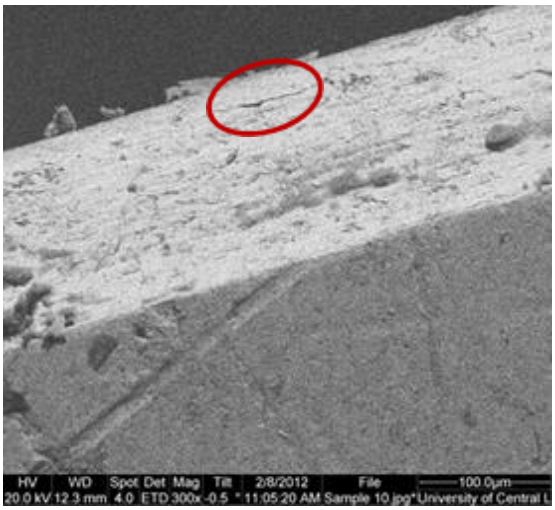

Figure 8 - Grey Cast Iron coated with MoS_2 after a 90 minutes

By taking the material thickness and then dividing the dimension by two, a stress reduction has been recorded [6,7,11]. If a change to the contact chamfer is made, the shear force acting in sector 2 will be reduced as shown in Figure 6. If the engine speed increases, the stress (sector 3 in Figure 6) continues to climb exponentially, however with the geometrical modifications, stress levels can be further reduced.

CONCLUSION

Reduction in level of stress on the contact chamfer has been achieved in modifying the present ISO 6622 piston ring contact chamfer design. The design modification to the chamfer has been validated on a KTM 520 engine with a grey cast iron compression ring coated with 0.2mm MoS_2 and a 0.2mm contact chamfer. This new design has no major impact on the manufacturing process of the ring.

High performance engines would benefit from such alteration to the ring which extended the life cycle of the coated ring.

However the results presented also indicated that material damage would be present on the coated ring coating which has been confirmed through modelling and optical observation. Further work should consider the effect of the rotation along the piston crown [6, 9, 11, 12] which should be complemented by optical observation of the damaged induced to the ring during testing.

REFERENCES

1.R.Stone, J.K.Ball, Automotive engineering fundamentals, SAE International, (2004)
2.J.Ramsbottom, Improved piston for steam-engines, Proceedings of the Institution of Mechanical Engineers, 5 (1854) p.70-74.
3.M J Nunney, Light and Heavy Vehicle Technology, Butterworth-Heinemann Title; 4 edition (2006).
4.G.M.Miller, Proceedings of the Institution of Mechanical Engineers, 13 (1862) p.315-327.
5.M.S. Stark, J.J. Wilkinson,, P.M. Lee, J.R. Lindsay Smith, M. Priest, R.I. Taylor, S. Chung, The degradation of lubricants in gasoline engines: Development of a test procedure to evaluate engine oil degradation and its consequences for rheology, Tribology and Interface Engineering Series, Vol.48 (2005) Pages p.593–602.
6.A.E.H.Love, The Stress Produced in a Semi-Infinite Solid by Pressure on Part of the Boundary, Philosophical Transactions of the Royal Society of London. Series A, Containing Papers of a Mathematical or Physical Character 228 (1929) p.377-420.
7.H.Douglas. Method of Piston Ring Manufacture. [2380654]. 31-7-1945. United States.
8.N.I.Muskhelishvili, Some Basic Problems of the Mathematical Theory of Elasticity (Noordhoff, 1975).
9.H.Neuber, K.Federhofer, Dynamik des Bogentragers und Kreisringes, Zeitschrift fur Angewandte Mathematik und Mechanik 31 (1951) p.227.
10.O.A.Bauchau, Flexible Multibody Dynamics (Springer, 2010).
11.R.Mittler, A.Mierbach, and D.Richardson, Understanding the fundamentals of piston ring axial motion and twist and the effects on blow-by, ASME Conference Proceedings 2009, 2009, p.721-735.
12.B.Deng, J.Yang, J.Fu, S.Chen, and S.Wang., The friction analysis of main bearing on an

internal combustion engine based on multi-body dynamics and elasto-hydrodynamic, Electric Information and Control Engineering (ICEICE), 2011, p.2762-2766
13.ISO 6622-1 Internal combustion engines - Piston rings - Part 1: Rectangular rings made of cast iron.

APPENDIX C.

(2014-01-0932)

A study into the compression ring rotation based on geometry

Matthew Dickinson[1, 2], Nathalie Renevier[1] and John Calderbank[2, 3]

The Jost Institute, School of Computing, Engineering and Physical Sciences, University of Central Lancashire, Preston PR1 2HE

Racing to Research team, School of Computing, Engineering and Physical Sciences, University of Central Lancashire, Preston PR1 2HE

School of Computing, Engineering and Physical Sciences, University of Central Lancashire, Preston PR1 2HE

ABSTRACT

Internal combustion engine components have been a main research interest over many decades [1]. The structural mechanics and dynamics of the piston rings has been a large focus of work in order to gain a greater understanding of the how the piston ring dynamics affect the piston ring. Piston rings are designed to create a seal which means that they will suffer large levels of material loss due to wear during operation. To further the understanding of the ring allows for a more accurate estimate of its behaviour.

INTRODUCTION

For over a century there has been considerable interest in the behaviour of piston rings in the combustion environment [1-4]. The engine for this study is the KTM 520, the engine is a four stroke internal combustion engine. This engine is used as a motor cycle engine, hence making this engine an ideal choose for the research in racing environments. To simulate the environment of running condition, the engine speed of 9,000 rpm was selected [5]. This paper presents simulation results from COMSOL to show how the compression ring performs. In this work the standard air cycle was employed, hence the ideal gas was used, which allowed for a cycle pressure plot. A thermal and dynamic analysis was carried out to enable an accurate behaviour to represent the ring during operation.

SYSTEM

The KTM 520 engine dimensions and material features (defined as typical KTM Spec) have been reported in Table 1.

Table 1 - showing component details

Dimension [mm]	Component	Material
95	Compression ring	BS-Grade 400 grey
94.95	Piston	4032-T6 alloy
95	Cylinder	Nikasil

115	Connecting Rod	UNS C67400
31	Crank	EN-30B Alloy Steel

In this study an ideal gas was used to predict the pressure output from the piston. The air standard Otto cycle was applied, to generate a pressure output, which in turn created a pressure output.

To calculate the pressure output the displacement of the piston during one cycle is calculated using the equation noted by Stone [1,6]. By using both methods for pressure calculation a 'look up' table containing pressures at different positions for use within simulations.

$$\mathbf{x \approx R\left\{cos\emptyset + \frac{L}{R}\left[1 - \frac{1}{2}\left(\frac{R}{L}\right)^2\left(\frac{1}{2} - \frac{1}{2}cos2\emptyset\right)\right]\right\}} \quad (1)$$

Where R, L and $\emptyset$ are the crank radius, the connecting rod length and the crank rotation respectively. Using numerical integration produces the piston velocity and, once again, to produce the piston acceleration [1]. The primary inertia force $(m\omega^2 R cos\theta)$ and the secondary inertia force $(mR\omega^2 \frac{1}{n} cos2\theta)$ acting on the piston have been considered.

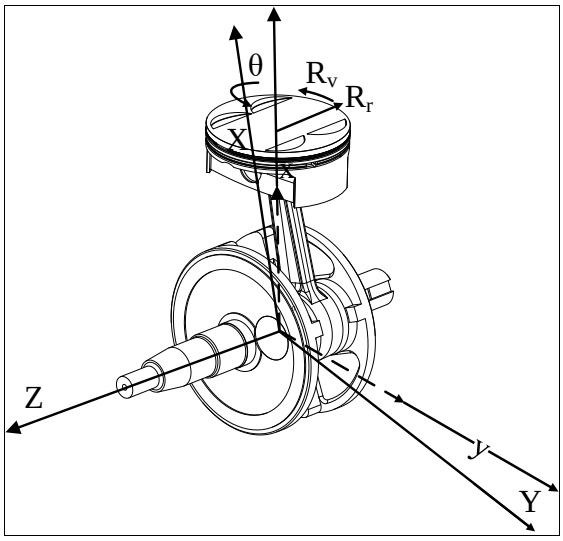

Figure 1 - Euler rotation on KTM system

Figure 1 is showing the system diagram for predicting the ring rotation. By using methods of Euler and Noether, the rotation of the piston ring is calculated [7,8]:

$$\mathbf{x = Xcos(\theta) + Ysin(\theta)} \quad (2a)$$

$$y = -Xsin(\theta) + Ysin(\theta) \quad (2b)$$

Where θ is the singular axis of rotation [7]. With these values the integration of the conservation is permitted.

$$\mathbf{L = R_r R_v R_m} \quad (3)$$

Where L, R_r, R_v, and R_m are the conservation of angular momentum, ring radius, ring velocity and ring mass respectively [8]. This will now allow for the ring to fully rotate around the cylinder during operation. The final factor in the system is heat, as the engine operates the heat will cause the ring to deform. A method to represent the thermal expansion of the ring is to calculate the thermal strain[9].

$$\Delta_l = \propto \Delta \mathbf{T} \quad (4)$$

Where Δ_l, $\propto$ and c are the thermal strain, linear coefficient of thermal expansion and temperature rise respectively. By including the thermal expansion the ring shown in Figure 2, will begin to oscillate and after expansion come to almost rest position.

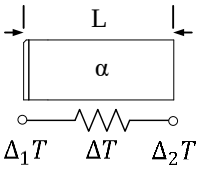

Figure 2 Thermal expansion diagram

In the four stroke internal combustion engine in the cooled state, the piston has a cylindrical profile from the crown to the bottom of the oil ring. The piston shape is elliptical from the bottom of the oil ring to the bottom of the skirt. Once the piston is in operation it assumed that the geometry becomes an almost cylindrical [10,11].

In this work it is assumed that the piston is of cylindrical profile.

RESULTS

By using the standard air cycle, a pressure was simulated Figure 3 which shows one cycle output.

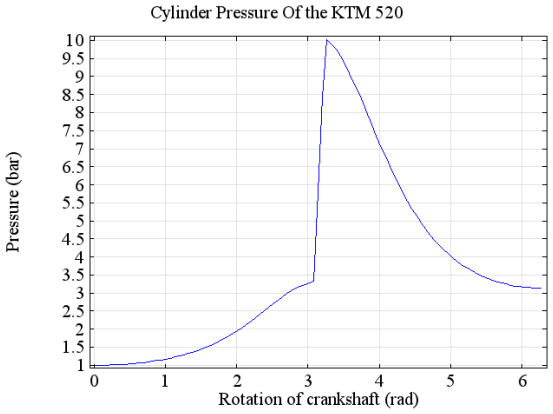

Figure 3 - showing the results from the KTM pressure

The inertia forces were simulated for a range of speeds from 6000 to 12000 rpm. The values of the forces used in the simulation are shown in Figure 4.

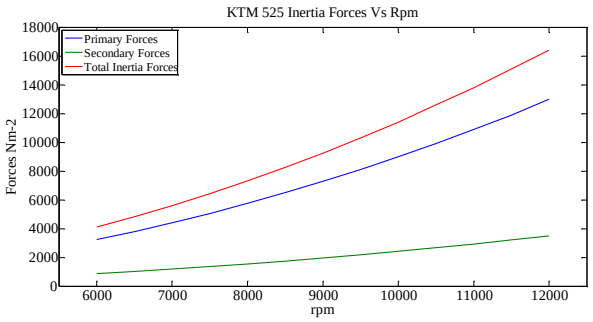

Figure 4 - Showing the force's output

Several ring widths were used to show displacement of the rings while operating at 9,000rpm. Figure 5 shows the oscillation output obtained with several ring widths including the recommended 1 mm from the 6622 ISO standard. A further 3 more variations have been examined.

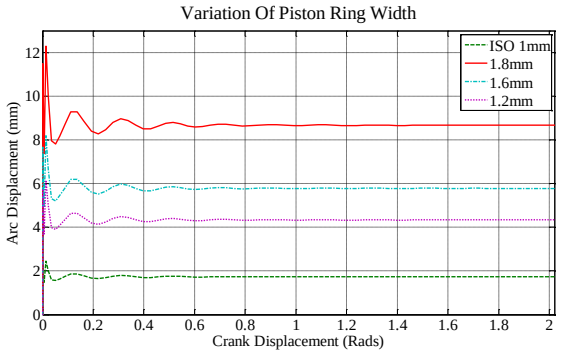

Figure 5 - showing total ring displacement around the z axis

Figure 5 with a number of ring thicknesses and indicates increased steady state offset with ring thickness. The values presented are for the dimensions of a KTM engine running at 9000rpm. The piston rings have a low cross-sectional dimensions.

DISCUSSION

As the rotational momentum builds during operation, each width change shows a great distance move from the origin, indicating mass of the ring is one of the significant parameters during this process. It has been noted [2,12,13] that pistons rings might exhibit a continuous motion. Other work [14-16] indicates little or no motion. The increasing steady-state offset in the rotation around the z-axis indicates that the system is dependent on the bedding-in process The simulation indicate motion is dependent upon the geometry and radius of curvature of a piston ring.

CONCLUSION

During operation the ring temperature increases causing the material to deform. This deformation will seal the cylinder to almost meeting the cylinder wall.

The heat from the process causes the ring to deform so that there will almost never be continuous rotation. As the mass and dimensions of the ring increase then the effects of the heat will be reduced and it is possible that a ring on a large engine will continuously rotate.

Further work will include a study of maximum stress found in the ring during operation, a full investigation on how uncoated and coated compression rings deform during the heat cycle and if this deformation could indicate a methodology for bedding the compression ring into the cylinder.

Acknowledgements

I would like to thank Daniel Marfiewicz for his input and assistance on this paper.

REFERENCES

1. R.Stone and J.K.Ball, Automotive engineering fundamentals (SAE International, 2004).
2. R.Mittler. Optimization of Piston Ring Dynamics by direct 3D analysis of dynamic effects. 7-10-2009.
3. Y.C.Tan and Z.M.Ripin, Tribology International 44 (2011) 592-602.
4. R.I.Taylor and P.G.Evans, Proceedings of the Institution of Mechanical Engineers, Part J: Journal of Engineering Tribology 218 (2004) 185-200.
5. P.Mather, KTM EXC Enduros & SX Motocross service & repair manual: 2000 to 2007 (Haynes, 2007).
6. M.Dickinson, N.Renevier, and W.Ahmed. Optimising Piston Ring Contact Face Chamfer for High Performance Engines. SAE 2013 World Congress & Exhibition. 2013-01-0965. 8-4-2013. SAE. 16-4-2013.
7. R.E.Bradley and E.Sandifer, Leonhard Euler: Life, Work and Legacy (Elsevier Science, 2007).
8. D.E.Neuenschwander, Emmy Noether's Wonderful Theorem (Johns Hopkins University Press, 2010).
9. C.Y.Ho and R.E.Taylor, Thermal Expansion of Solids (ASM International, 1998).
10. S.H.Mansouri and V.W.Wong, Proceedings of the Institution of Mechanical Engineers, Part J: Journal of Engineering Tribology 219 (2005) 435-449.
11. V.Esfahanian, A.Javaheri, and M.Ghaffarpour, Applied Thermal Engineering 26 (2006) 277-287.
12. L.J.Brombolich. Structural Mechanics of Piston Rings. 1-34. 1993. St louis, MO, Compu-Tec Engineering, Inc (Internal Report).
13. S.C.Tung and Y.Huang, Tribology Transactions 47 (2004) 17-22.
14. V.Dunaevsky and S.Alexandrov, Tribology Transactions 48 (2005) 108-118.
15. Y.Gortyshov, A.Druzhinin, V.Gureev, I.Gumerov, and V.Stroganov, Russian Engineering Research 30 (2010) 385-387.
16. J.Heywood, Internal combustion engine fundamentals (McGraw-Hill, Inc., 1988).

APPENDIX D.

(2015-01-1335)

A study into compression ring dynamics using response surface methodology

Matthew Dickinson[1, 2], Nathalie Renevier[1] and John Calderbank[2, 3]

The Jost Institute, School of Computing, Engineering and Physical Sciences, University of Central Lancashire, Preston PR1 2HE

Racing to Research team, School of Computing, Engineering and Physical Sciences, University of Central Lancashire, Preston PR1 2HE

School of Computing, Engineering and Physical Sciences, University of Central Lancashire, Preston PR1 2HE

ABSTRACT

For decades the operational dynamics of the compression ring during operation, have been subject to debate [1-7]. A complex computer simulation, using Design Of Experiments (DOE) methodology, was developed to study the effect of the compression ring rotation during running-in stages. Response Surface (RS) has been used to optimize ring displacement, as function of ring mass, width and radius. The optimised surface response has been compared to used compression rings and has shown a 2% variation between calculated and measured values.

INTRODUCTION

For almost two century's since the introduction of the split ring, there has been a considerable interest in the mechanics and dynamics of the piston rings in the combustion conditions [8-12]. The four stroke engine that has been used for this study is a KTM 520. As this engine is a motorcycle engine this means, a high level of RPM can be obtained, this makes this an ideal selection for race condition research. To simulate the environment of running-in conditions the recommended running-in operational speed has been selected of 7,000 rpm [13]. This paper presents simulation results from MatLab to display how the compression ring behaviours. In this work the ideal gas was used, a thermal and dynamic analysis was performed to enable an accurate behaviour representation. 3 sample sets of KTM BS-grade compression rings with MoS2 coatings were analysed after 60mins of operation. Each ring was checked using a Quanta FEI Scanning Electron Microscope (SEM). Each image was cross analysed using open source software Gwyddion.

SYSTEM

The KTM 520 engine dimensions and material features have been reported in Table 1.

Table 1 - showing component details

Dimension [mm]	Component	Material
95	Compression ring	BS-Grade 400 grey
94.95	Piston	4032-T6 alloy

95	Cylinder	Nikasil
115	Connecting Rod	UNS C67400
31	Crank	EN-30B Alloy Steel

To calculate pressure and displacement of the piston during operation, equations noted by Stone were used [11]. Further modelling methods were used from work noted by Dickinson [4].

To reduce the number of simulations, a centre composite, 3 factorial RS has been used to optimise the compression ring displacement. Factors such as radius, cross sectional width and the ring overall mass were studied.

Table 2 – Factors for RS

Ring Width mm	Ring Rad mm	Ring Mass g
1 - 5	30 – 50	0.2 - 1.2

Table 2 shows the factors used in the RS. This produced a surface based on 20 runs, generating the RS graph.

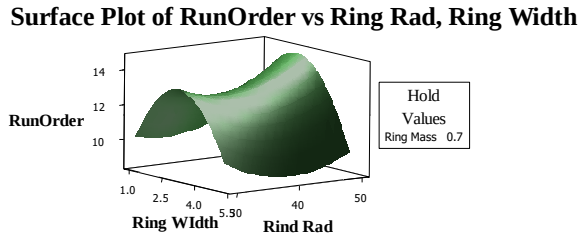

Figure 1 - RS plot

Figure 1 shows the RS plot defined through the factorial set-up.

The defined variables are introduced into a Matlab/SimMechanics model. Each engine component is reengineered and defined within the SimMechanics system. The system is a G-Graphical interface to keep the system organised, where each major components are created with their own sub program (Figure 2).

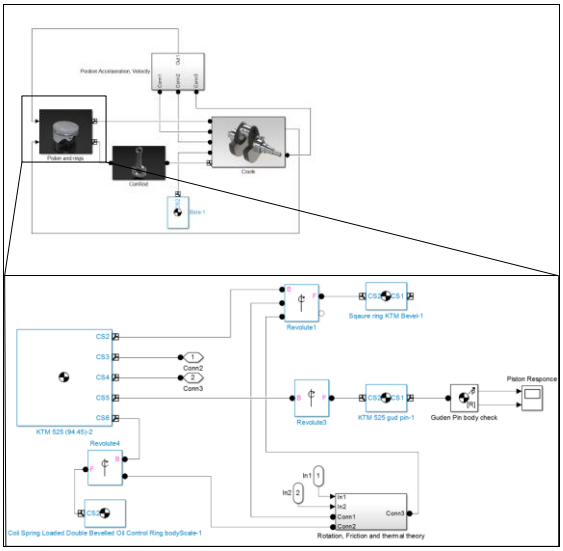

Figure 2 - MatLab/SimMechanics model

Figure 2 shows the SimMechanics model used. The methodology used has been previously described [2-4].

To validate the simulation results, SEM images were taken of the top face of the compression ring to examine for scratches on the surface that would indicate ring rotation. The displacement angle indicating ring displacement has been calculated using:

$$x = tan^{-1}\left(\frac{L}{R_{rad}}\right) \quad (1)$$

$$R_{rad} = R - D \quad (2)$$

Where L is the length of the measured scratch, R is the piston ring radius, D is the SEM observed image position from the outer radius of the ring.

RESULTS

Post processing of the data generated by the RS DOE shows a good correlation in the running order, as seen in Figure 3.

Figure 3 - running order results best fit

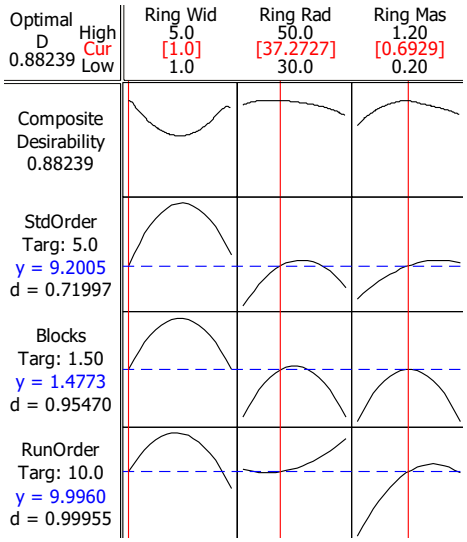

Figure 4 - Running order of the optimised solution

The running order of the optimised solution (Table 3) is presented in Figure 4.

Table 3 - Optimised solution

Ring Width (RW) mm	**Ring Rad (RR) mm**	**Ring Mass (RM) g**
1	37.27	0.69239

Each goal for the StdOrder = 5, Blocks = 1.5 and Runorder = 10. The composite desirability is 0.88239.

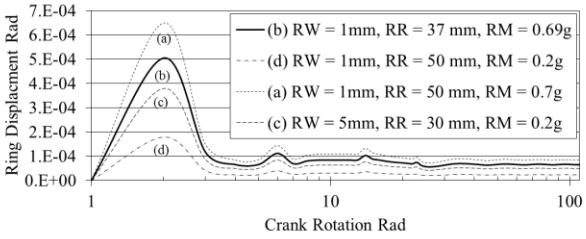

Figure 5 – Ring displacement radius (b)

Figure 5 shows four representatives RS ring displacement radius outputs. Large oscillations are found below 10 radians of the crank rotation, with the factors defined, a second order system behaviour is seen. For the optimised solution (Table 3), the ring will rotate by a maximum of 0.005 rads. The result also indicates a resting time reached after 50 rads.

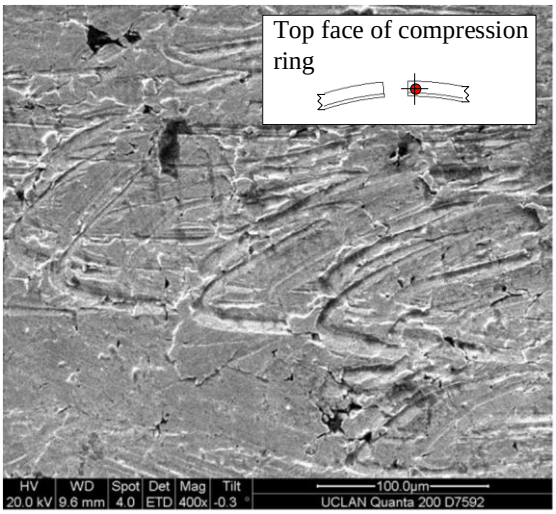

Figure 6 - KTM 520 sample 1 top face

Figure 6 shows one of three samples images taken with SEM of the run-in KTM piston rings. Each image was measured for the maximum arc size relative to the ring radius.

Table 4 - Simulated against sample results

Sample No.	Sample length	Sample max rad	Figure 5 max rad (b)	Variation %
1	0.0267	0.005656	0.005045	0.22
2	0.0251	0.004986	0.005045	1.17

3	0.0288	0.005133	0.005045	1.74

Table 4 shows the results from RS optimized value (Table 3) and the measured values from the SEM images. The simulated system assumes a level of perfection in both material, combustion pressure and lubrication. Hence variations are recorded between the simulation and experimental data.

DISCUSSION

As the rotational momentum builds during operation, the highest levels of rotation are recorded in the first 20 radians of the crank rotation. Studies have been noted [1,3,4,14,15] that pistons rings might exhibit a continuous motion. However other work has been presented where little or no rotation has been observed [16,17]. However the validation work presented from the samples suggests that a large action of ration occurs over a small amount of crank rotation.

CONCLUSION

The compression ring will initially rotate and behave as a second order system. There is a good correlation between the experimental and the simulated results.

In an effort to optimise the rotation of the compression ring, it was originally thought that no rational would be the optimised value however results indicate that the must rotate regardless of the range of factors studied.

Further work will consider the effect of lubrication and also study the depths of the scratches.

Acknowledgements

I would like to thank Daniel Marfiewicz-Dickinson for suggestions of how to improve the paper.

REFERENCES

[1] L.J.Brombolich. Structural Mechanics of Piston Rings. 1-34. 1993. St louis, MO, Compu-Tec Engineering, Inc (Internal Report).

[2] M.Dickinson, N.Renevier, and W.Ahmed. The Refinement of the contact compression ring chamfer for race engine conditions. Comsol conference 2013. 5-9-2012

[3] M.Dickinson, N.Renevier, and W.Ahmed. Optimising Piston Ring Contact Face Chamfer for High Performance Engines. SAE 2013 World Congress & Exhibition. 2013-01-0965. 8-4-2013. SAE. 16-4-2013.

[4] M.Dickinson, N.Renevier, and J.Calderbank. A Study into the Compression Ring Rotation Based on Geometry. 1-4-2014.

[5] D.Dowson, International Journal of Mechanical Sciences 4 (2003) 159-170.

[6] R.Mittler, A.Mierbach, and D.Richardson, ASME Conference Proceedings 2009 (2009) 721-735.

[7] M.Priest and C.M.Taylor, Wear 241 (2000) 193-203.

[8] G.M.Miller, Proceedings of the Institution of Mechanical Engineers 1847-1982 (vols 1-196) 13 (1862) 315-327.

[9] J.Ramsbottom, ARCHIVE: Proceedings of the Institution of Mechanical Engineers 1847-1982 (vols 1-196) 5 (1854) 70-74.

[10] E.H.Smith and R.D.Arnell, Tribol Lett 55 (2014) 315-328.

[11] R.Stone and J.K.Ball, Automotive engineering fundamentals (SAE International, 2004).

[12] R.I.Taylor, M.A.Brown, and D.M.Thompson, in: Tribology Series Lubricants and Lubrication - Proceedings of the 21th leeds-Lyon Symposium on Tribology, ed. D.Dowson (Elsevier, 1995).

[13] P.Mather, KTM EXC Enduros & SX Motocross service & repair manual: 2000 to 2007 (Haynes, 2007).

[14] J.Heywood, Internal combustion engine fundamentals (McGraw-Hill, Inc., 1988).

15] S.C.Tung and Y.Huang, Tribology Transactions 47 (2004) 17-22.

[16]V.Dunaevsky and S.Alexandrov, Tribology Transactions 48 (2005) 108-118.

[17]J.Heywood, Internal combustion engine fundamentals (McGraw-Hill, Inc., 1988).

APPENDIX E.

Conformability study into restricted displacement of coated and uncoated compression rings

Matthew Dickinson[1, 2], Nathalie Renevier[1] and John Calderbank[2, 3]

The Jost Institute, School of Computing, Engineering and Physical Sciences, University of Central Lancashire, Preston PR1 2HE

Racing to Research team, School of Computing, Engineering and Physical Sciences, University of Central Lancashire, Preston PR1 2HE

School of Computing, Engineering and Physical Sciences, University of Central Lancashire, Preston PR1 2HE

ABSTRACT

Engine technology has been the main interest of many studies during the past two centuries. A complex computer model has been developed to study the effects of coated and uncoated compression rings on the output torque effect during running-in when the ring is free to rotate around the piston groove or fixed in the groove.

INTRODUCTION

The main role of the compression ring is to seal the combustion area during operation. This has been the centre of much debate and progresses for the past two hundred years [1-4]. However running-in procedures, presented in the manufacturer's manual of new engines, had limited development over the years [5-8]. During the first operational stages many factors including ring composition or surface treatment applied on contact face will affect the way a compression ring will run-in with the cylinder wall. A KTM 520 four stroke motorcycle engine has been used to achieve racing operating conditions with high rpm values. The running-in procedure used was defined using the KTM user manual [8]. This paper examines the behaviour of simulated results from MatLab to those obtained from dynamometer experimental testing. Both dynamic and thermal effects have been included in this work. Coated and uncoated compression rings were simulated in two separate states where the ring was fixed in position within the groove of the piston or free to move around the piston groove (Figure 1).

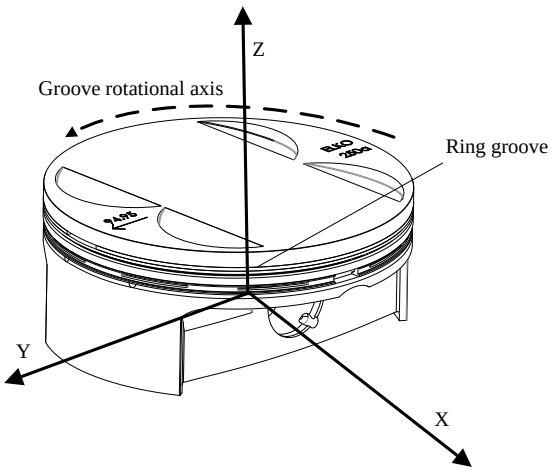

Figure 1 - Piston, compression ring and oil ring assembly

SYSTEM

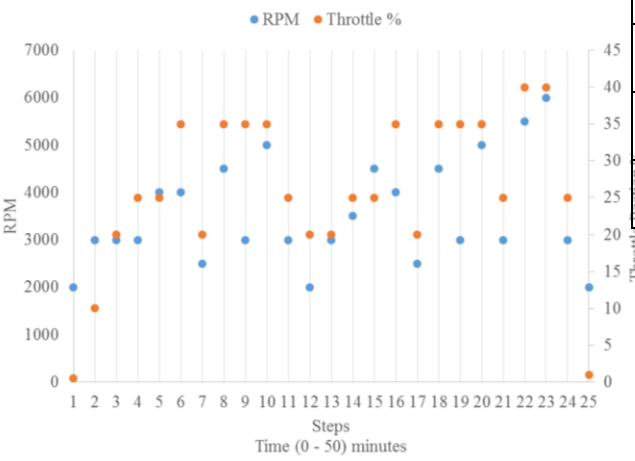

Figure 2 – Rpm and Throttle position used in each of the 25 steps of the Running-in process [8]

KTM 520 engine material and dimensions are noted in *Table 1*.

Figure 2 shows the running-in procedure used based on the KTM manual recommended method for running a new engine developed to study both simulated and dynamometer work. The factors considered for this study were RPM, throttle position and time intervals as shown in Figure 2.

Table 1 - Components dimensions and composition

Component	Dimension	Material
Compression ring	95	BS-Grade 400 grey cast iron
Piston	94.95	4032-T6 alloy
Cylinder	95	Nikasil
Connecting Rod	115	UNS C67400
Crank	31	EN-30B Alloy Steel

The method used to calculate pressure and displacement of the piston during operation has been previously presented [9-12]. Cylinder conformability has been added in this study using Tomanik work. Tomanik noted that if $\emptyset$ is the angular position, Δr is the radial deformation, A_n, B_n are the Fourier co-efficient and n is the order of deformation then the displacement can be mathematically represented as a Fourier series[13].

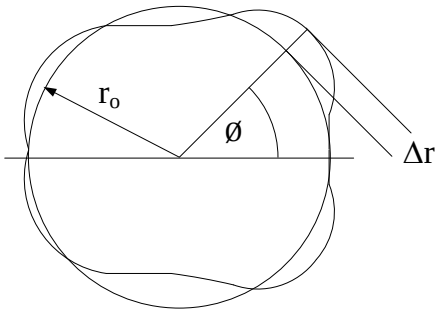

Figure 3 - Cylinder deformation noting phase angle

Equation 1 - Fourier series deformation

$$\Delta r = A_0 + A_1 \cos(\emptyset) + A_2 \cos(2\emptyset) + \cdots + A_n \cos(n\emptyset) + B_1 s + B_n \sin(n\emptyset)$$

The maximum cylinder deformation u_{bn} was calculated at each phase angle $\emptyset_{bn}$ and each n^{th} order term the maximum cylinder deformation u_{bn} was calculated using Equation 1 and is represented in Equation 2 as:

Equation 2 - Cylinder phase angle

$$\emptyset_{bn} = \left(\frac{1}{n}\right) arctangent \left(\frac{B_n}{A_n}\right)$$

Equation 3 - Cylinder maximum deformation

$$U_{bn} = 2\sqrt{(A_n^2 + B_n^2)}$$

To simulate the response of the system, the variables were placed into a Matlab/SimMechanics model. Each engine component was reengineered and defined accurately within the SimMechanics software package. SimMechnics is a G-Programming method where component blocks are used to represent each engine part (Figure 4).

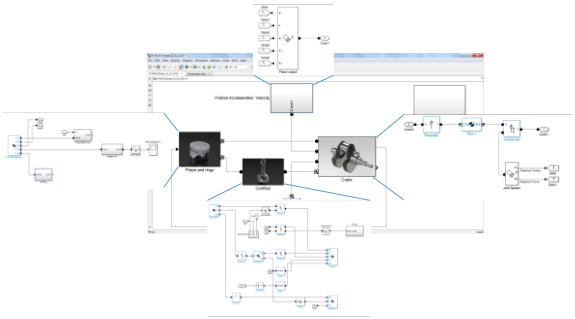

Figure 4 - Matlab/SimMechanics model

RESULTS

Torque outputs obtained for both simulated and dynamometer tests are reported in figure 5 for the coated ring and in figure 6 for the uncoated ring.

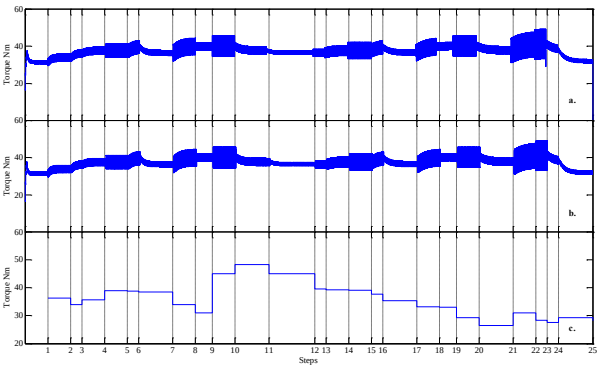

Figure 5 - Torque output of coated rings, calculated when ring is free to rotate (a) or fixed (b) or measured in dynamometer test when ring is free to rotate (c)

Table 2 – Maximum, mean and standard deviation of torque outputs calculated or measured over the 25 running-in steps for coated rings

	Calculated		Measured
	Figure 5a	Figure 5b	Figure 5c
Maximum Torque Nm	47.88	48.56	57.10
Mean Torque Nm	35.61	36.23	37.67
Standard deviation	2.85	2.70	6.86

Table 2 and Table 3 show maximum, mean and standard deviation of torque outputs calculated or measured over the 25 running-in steps for respectively coated and uncoated rings.

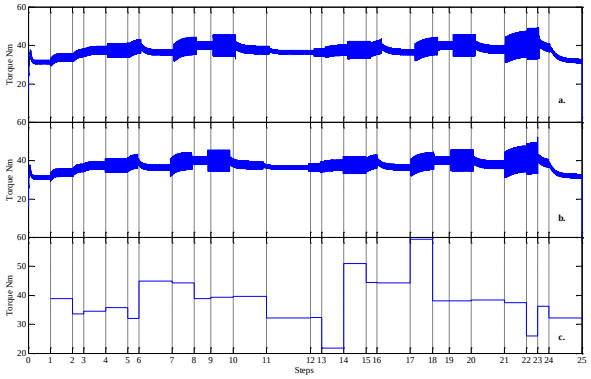

Figure 6 - Torque output of uncoated rings, calculated when ring is free to rotate (a) or fixed (b) or measured in dynamometer test when ring is free to rotate (c)

Figure 5 and Figure 6 show respectively the results from coated and uncoated simulation in free (a) and fixed states (b). The simulated torque outputs are compared with the torque measured at the end of each of the 25 running-in steps.

Table 3- Maximum, mean and standard deviation of torque outputs calculated or measured over the steps running-in steps for coated rings

	Calculated	Measured

	Figure 6a	Figure 6b	Figure 6c
Maximum Torque Nm	49.15	49.21	59.30
Mean Torque Nm	37.44	37.45	38.30
Standard deviation	3.18	3.19	7.81

Figure 7: Calculated temperature during the running-in

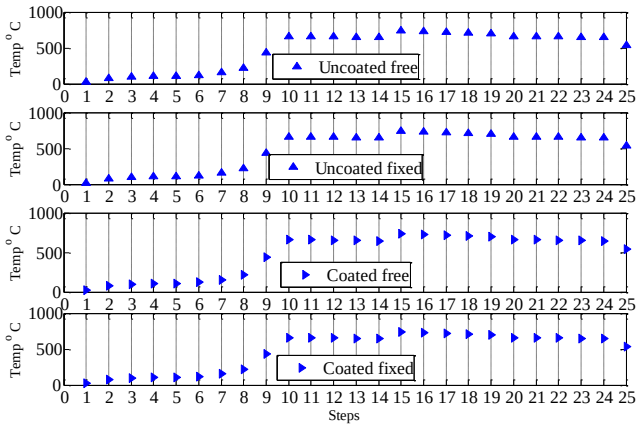

Figure 7 - show the calculated temperature inside the combustion chamber during running-in.

DISCUSSION

In restricting ring motion around the crown, torque output is increased. Simulated results obtained with a fixed ring for both coated and uncoated rings show an increased performance and a higher torque output in mean average.

By constraining the axis around the piston groove performance is increased on all scales. However it is assumed that due to the characteristics of the compression ring the wear rate will increase In restricting compression ring from rotating in the piston groove, the maximum output torque can be increased overall. Uncoated rings display higher level of torque output compared to coated rings. However due to the characteristics of the compression ring the wear rate will increase and therefore conformability would only increase for a limited time beyond the running-in.

Fixing ring in the groove would give greater performances to both coated and uncoated rings in race engine operating conditions where torque outputs are critical.

Discrepancy between calculated and measured torque outputs can be imputed to additional phenomenon such as glazing, currently not accounted for in the present running-in. Glazing should not be overlooked and should be considered as a major factor when simulating this stage of the engine life cycle. Therefore conformability would only increase for a limited duration beyond the running-in.

However, torque outputs obtained with dynamometer tests are almost 10Nm higher than the simulated one indicating that additional factors have not been considered in the current model.

Sudden drops in performance are consistent to oil burn known as glazing or varnishing [14,15]. The phenomenon is the result of deposits onto the cylinder wall and ring surface, creating a varnished effect, leading to permanent performance loss. However in the dynamometer results, it is assumed that only partial glazing phenomenon is taking place and changes in rpm and throttle position during the running-in process deter further glazing progression.

Despite steps 1 and 25 having the same rpm and throttle position, torque outputs are very different. The difference in torque output could be attributed to glazing taking place when the engine has reached several hundred degrees.

A similar observation can be made for step 3 and 13. Glazing cannot take place in step 1 and 3 where temperatures are too low for the

phenomenon to occur. Glazing has more of an impact in the engine than what is normally assumed.

CONCLUSION

In restricting compression ring from rotating in the piston groove, the maximum output torque can be increased overall. Uncoated rings display higher level of torque output compared to coated rings. However due to the characteristics of the compression ring the wear rate will increase and therefore conformability would only increase for a limited time beyond the running-in.

Fixing ring in the groove would give greater performances to both coated and uncoated rings in race engine operating conditions where torque outputs are critical.

Discrepancy between calculated and measured torque outputs can be imputed to additional phenomenon such as glazing, currently not accounted for in the present running-in. Glazing should not be overlooked and should be considered as a major factor when simulating this stage of the engine life cycle.

The current model assumes ideal lubrications system where starvation, abnormal behaviour, oil contamination due to wear debris have not been considered in this paper.

Acknowledgements

The authors would like to thanks Mick Bodill for his technical support during dynamometer testing.

REFERENCES

[1] D.Dowson, International Journal of Mechanical Sciences 4 (2003) 159-170.
[2] G.M.Miller, ARCHIVE: Proceedings of the Institution of Mechanical Engineers 1847-1982 (vols 1-196) 13 (1862) 315-327.
[3] M.Priest and C.M.Taylor, Wear 241 (2000) 193-203.
[4] J.Ramsbottom, ARCHIVE: Proceedings of the Institution of Mechanical Engineers 1847-1982 (vols 1-196) 5 (1854) 70-74.
[5] Honda model cb550k owner's manual (Honda Motor Co. Ltd, 1977).
[6] Suzuki GS550 Service Manual (Suzuki Motor Co. Ltd, 1978).
[7] Aprilia SXV/RXV 450 - 550 owers manual (Valley Forge Deca, Ravenna, Modena, Torino, 2006).
[8] P.Mather, KTM EXC Enduros & SX Motocross service & repair manual: 2000 to 2007 (Haynes, 2007).
[9] M.Dickinson, N.Renevier, and W.Ahmed. The Refinement of the contact compression ring chamfer for race
[10] M.Dickinson, N.Renevier, and W.Ahmed. Optimising Piston Ring Contact Face Chamfer for High Performance Engines. SAE 2013 World Congress & Exhibition. 2013-01-0965. 8-4-2013. SAE. 16-4-2013.
[11] M.Dickinson, N.Renevier, and J.Calderbank. A Study into the Compression Ring Rotation Based on Geometry. 1-4-2014.
[12] M.W.Dickinson, N.Renevier, and J.Calderbank. A study into compression ring dynamics using response surface methodology. 2015. SAE Technical Paper.
[13] E.Tomanik. Piston Ring Conformability in a Distorted Bore. SAE International Congress & Exposition. 1-2-1996. SAE. 17-1-2014.
[14] G.C.Barber and K.C.Ludema, Wear 118 (1987) 57-75.
[15] Z.Dimkovski, L.BÑÑth, S.Rosn, R.Ohlsson, and B.G.Rosn, Wear 270 (2011) 247-251.
[16] R.Stone and J.K.Ball, Automotive engineering fundamentals (SAE International, 2004).